Université de Montreal

Time-Resolved Phosphoproteomics Unravel the Dynamics of Intracellular Signaling

par
Peter Kubiniok

Département de Chimie
Faculté des Arts et des Sciences

Thèse présentée à la Faculté des études supérieures et postdoctorales
en vue de l'obtention du grade de
Philsosophiæ Doctor (Ph.D.)
en chimie

Mai 2018

Resumé

La phosphorylation des protéines est une modification post-traductionnelle très abondante qui cible les acides aminés sérine, thréonine et tyrosine. Les groupements phosphates sont ajoutés aux protéines par les kinases et retirés par les phosphatases. La phosphorylation d'une protéine régule sa conformation structurelle; ce qui modifie ses fonctions. C'est un vecteur de signalisation intracellulaire, impliqué notamment dans la régulation des interactions protéine-protéine et de l'activité des enzymes. La prolifération, la différenciation et la morphologie cellulaires sont autant de processus régulés par des événements de phosphorylation. Une meilleure compréhension des voies de phosphorylation est ainsi importante pour faire avancer la recherche contre le cancer. L'étude de la phosphorylation des protéines a grandement bénéficié de l'amélioration des techniques de protéomique basées sur la spectrométrie de masse, qui permettent d'analyser en quelques heures des milliers de sites de phosphorylation. Les expériences de spectrométrie de masse permettent habituellement d'étudier les effets de stimuli extracellulaires sur le phosphoprotéome en prenant des mesures à un seul temps post-stimulation donné. Ce type d'analyse ne permet toutefois pas de suivre les changements de phosphorylation dans le temps, ce qui serait utile pour comprendre le fonctionnement des voies de signalisation. La présente thèse décrit le développement et l'application de nouvelles techniques de phosphoprotéomique permettant de mesurer la phosphorylation avec une grande résolution temporelle. Cette approche a permis d'identifier de nouvelles voies de signalisation dépendantes de stimuli et de mieux caractériser certains réseaux de phosphorylation déjà connus.

Tout d'abord, une analyse temporelle du phosphoprotéome a été effectuée pour déterminer les effets de stress thermiques sur *Saccharomyces cerevisiae* dans les 30 minutes post-stimulation. 15 profils cinétiques différents ont été identifiés. Ces profils de phosphorylation ont permis de mieux définir des interactions kinase-substrat. L'information temporelle a notamment permis de caractériser les réseaux de signalisation des kinases Cdc28 et PKA suite à un choc thermique. De grands changements d'état de phosphorylation ont été observés pour des protéines impliquées dans la transcription, le repliement des protéines et la progression du cycle cellulaire.

Dans une seconde étude, des cellules humaines de cancer du côlon contenant des mutations somatiques de BRAF ou KRAS ont été traitées avec un inhibiteur de BRAF, le Vermurafenib. L'utilisation de la phosphoprotéomique temporelle a permis d'identifier de nouveaux substrats de la voie BRAF-RAS-ERK. De fait, il a été démontré que les facteurs de transcription MKL1/2 et TEAD3 sont des cibles directes de la kinase ERK.

Enfin, les effets sur le phosphoprotéome de petites molécules activatrices de la protéine phosphatase 2 A (PP2A) ont été étudiés. Des cellules hématopoïétiques murines ont été traitées avec les sphingolipides anti-oncogéniques C2-ceramide et SH-BC-893 ainsi qu'avec l'inhibiteur spécifique de PP2A, le LB-100. Les sphingolipides utilisés sont des activateurs connus de PP2A qui causent la mort cellulaire en privant les cellules de nutriments. De fait, les deux sphingolipides causent la perte de transporteurs de nutriments. SH-BC-893 mène en plus à la formation de vacuoles, un phénotype lié à la mobilisation de nutriments. La dynamique du phosphoprotéome a été suivie pendant les 60 minutes suivant le traitement, révélant une activation différentielle de PP2A en présence des sphingolipides. En comparant ces réponses avec le phosphoprotéome de cellules traitées avec le LB-100, il a été possible d'identifier des sites de PP2A sur de nombreuses GTPases et protéines du cytosquelette d'actine, notamment Arhgef2 et Paxilin. De plus, la privation de nutriments s'est avérée être partiellement dépendante de la polymérisation de l'actine induite par les sphingolipides. Finalement, les phosphoprotéines lysosomales associées au kinase AKT et impliquées dans le recyclage des endosomes sont régulées différent par SH-BC-893 et C2-ceramide, ce qui explique partiellement pourquoi C2-ceramide ne cause pas la formation de vacuoles.

Somme toute, l'analyse temporelle du phosphoprotéome a permis d'étudier différents processus plus en profondeur que ce que permettent les techniques de phosphoprotéomique traditionnelles. Elles ont permis d'élucider des mécanismes biologiques d'importance pour la recherche contre le cancer.

Mots clés: Phosphoprotéomique, Signalisation intracellulaire, Spectrométrie de Masse, Cancer, Petites Molécules médicamenteuses.

Abstract

Protein phosphorylation is a highly abundant post translational modification primarily observed on the amino acids Serine, Threonine and Tyrosine. Phosphate residues are transferred through kinases and are removed by protein phosphatases. Phosphorylation regulates the structural conformation of proteins, therefore modifying their function. It functions as an intracellular signaling mediator that regulates key processes such as protein-protein interactions and the activity of enzymes. Cell proliferation, differentiation and morphology are some of the most important cellular machineries regulated through phosphorylation signaling. Knowledge about phosphorylation pathways therefore is of high importance for cancer research. The study of protein phosphorylation has greatly benefited from the implementation of mass spectrometry based proteomics techniques that allows for the profiling of thousands of protein phosphorylation sites in a matter of hours. When investigating the effects of extracellular stimulations on the phosphoproteome, mass spectrometry experiments are typically designed by taking a snapshot of the phosphoproteome at a given time post stimulation. This type of analysis, however, does not allow to follow the temporal characteristics of phosphorylation that could explain the functioning of signaling pathways. This thesis describes the development and application of phosphoproteomics techniques that monitor phosphorylation signaling at high temporal resolution. This approach allowed the discovery of stimulation dependent signaling pathways and aided the refinement of already characterized phosphorylation networks.

At first, temporal profiling of the phosphoproteome was applied to study the effects of heat and cold stress on *Saccharomyces cerevisiae* within the first 30 minutes post stimulation. Fifteen different kinetic trends were discovered. Kinase-substrate interactions could be unraveled based on kinetic patterns of phosphorylation. In more detail, temporal information allowed the characterization of the signaling network of the kinases Cdc28 and PKA following temperature stress. These responses were associated with extensive changes in phosphorylation on proteins involved in transcription, protein folding and cell cycle progression.

In a second study, human colon cancer cells harboring somatic BRAF or KRAS mutations were subjected to treatments with the BRAF kinase inhibitor Vemurafenib. Temporally resolved

phosphoprotoemics aided the discovery of novel targets of the BRAF-RAS-ERK signaling pathway. The transcription factors MKL1/2 and TEAD3 were found to be direct target of the kinase ERK. ERK mediated phosphorylation of MKL1/2 could be associated to actin binding, regulating their activity.

Third, a study investigating the effects of protein phosphatase 2 A (PP2A) small molecule activators on the phosphoprotoeme is described. Hematopoietic mouse cells were treated with the anti-oncogenic sphingolipids C2-ceramide and SH-BC-893 as well as the specific PP2A inhibitor LB-100. The investigated sphingolipids are known activators of PP2A that starve cancer cells to death. Both sphingolipids cause nutrient transporter loss, leading to cell starvation. In addition, SH-BC-893 causes vacuolation, a phenotype that is linked to nutrient mobilization. Phosphoprotoeme dynamics were monitored within 60 minutes post stimulation and unraveled differential activation of PP2A with sphingolipids. Comparison of sphingolipid response to the LB-100 perturbed phosphoprotoeme revealed PP2A directed phosphorylation on numerous GTPase and actin cytoskeletal proteins including Arhgef2 and Paxilin. Cell starvation was found to be partially dependent on sphingolipid induced actin polymerization. Lysosomal phosphoproteins affiliated with the kinase AKT and endosome recycling were differentially regulated by SH-BC-893 and C2-ceramide, partially explaining why C2-ceramide does not induce vacuolation.

Overall, temporal profiling of the phosphoproteome improved the depth of knowledge gained from phosphoproteomics experiments compared to conventional studies, and lead to the discovery of yet unknown biological mechanisms that are of importance to cancer research.

Keywords: Phosphoproteomics, Intracellular signaling, Mass spectrometry, Cancer, Small Molecule Drugs.

Table of Contents

List of Tables

List of Figures

List of Abbreviations

μM	micromolar
ACN	Acetonitrile
ATP	Adenosine triphosphate
C18	Octadecyl carbon chain
Cdc28	Cyclin-dependent kinase 1
CFC	Cardio-Facio-Cutaneous syndrome (CFC)
CID	Collision induced dissociation
DAPI	4',6-diamidino-2-phenylindole
DDA	Data dependent acquisition
DMEM	Dulbecco modified Eagle's minimal essential medium
DNA	Deoxyribonucleic acid
EGFR	Epidermal Growth Factor Receptor
EMT	Epithelial-Mesenchymal Transition
ERK	Extracellular signal-regulated kianse
ESI	Electrospray ionisation
ETS	E26 Transformation-Specific transcription factor family
FA	Formic acid
FBS	Fetal bovine serum
FDA	Food and drug administration
FDR	False Discovery Rate
FL5.12	Fetal liver clone 5.12 cell line
GAP	GTPase activator
GDP	Guanylyl diphosphate
GEF	Guanylyl exchange factor
GO	Gene Ontology
GTPase	Guanine nucleotide exchange factor
GTPase	Guanylyl triphosphate hydrolysing enzyme
HCD	Higher energy collision induced fragmentation
HeLa	Henrietta Lacks cervical cancer cell line
HPLC	High performance liquid chromatography

IAA	Iodo Acetamide
KIM	Kinase Interaction Motif
LC	Liquid chromatography
LC-MS	Liquid chromatography mass spectrometry
LIT	Linear ion trap
m/z	Mass to charge
MAPK	Mitogen activated protein kinase
MAPK1/3	Mitogen Activated Kinase 1 and 3
MEK	Mitogen activated protein kinase kinase
MKL1/2	Myocardin-like protein 1 and 2
mM	millimolar
MS	Mass spectrometry
MS/MS	Tandem mass spectrometry
NPC	Nuclear Pore Complex
NS	Noonan Syndrome
NTA	Nitriloacetic acid
PAK	p21 Activated Kinase
PBS	Phosphate buffered saline
PKA	Protein Kinase A
PM	Plasma Membrane
PP2A	Protein phosphatase 2 A
PSM	Peptide spectrum match
RAF	Rapidly Accelerated Fibrosarcoma
RAS	Rat sarcoma kinase
RP	Reverse phase
RPMI	Roswell Park Memorial Institute medium
RPS6KA1/2/3	Ribosomal Protein S6 Kinase A 1/2/3
RSK	Ribosomal s6 kinase
RT	Room temperature
RTK	Receptor Tyrosine Kinase
SCX	Strong cation exchange

SDC	Sodium deoxycholate
SILAC	Stable isotope labeling of amino acids in cell culture
SPE	Solid phase extraction
TB	Terrific Broth
TEAD	TEA Domain transcription factors
TFs	Transcription Factors
TOF	Time of flight
WT	Wild Type

Acknowledgements

The time it took to generate the knowledge of this thesis was accompanied by the enlightening experience of living abroad from my home country Germany. An experience that was filled with cultural and scientific novelty. This would not have been possible without my supervisor, co-workers, friends and family that all have supported me during the course of this thesis.

At first, I would like to express my gratitude to my PhD supervisor Dr. Pierre Thibault to accept me as one of his doctoral students and for his continuing support throughout my thesis. Working together with one of the leading Canadian scientists in mass spectrometry and proteomics research has greatly benefited the way I understand nature. Pierre has shared the depth of his knowledge with me and has introduced me to cancer research, a field that appeared out of reach for someone with a background in pure chemistry. Only with this acquired knowledge it was possible for me to perform cutting edge research in the field of oncology and analytical chemistry. Pierre gave me the freedom I needed to build my own niche of scientific expertise and generously introduced me to experts in the field of drug discovery and cancer biology.

Moreover, I would like to express my deepest appreciation to Dr. Hugo Lavoie and his mentor Dr. Marc Therrien, for teaching me the art of scientific expertise and for the great work we published together.

Dr. Aimee Edinger from the Univeristy of California, Irvine (USA) and Dr. Stephen Hanessian from the University of Montreal (Canada), both receive my greatest respect and gratitude for the outstanding scientific collaboration that we built during the last two years of my doctoral studies. I consider myself very fortunate to have worked together with these great scientists and their laboratory members, including Alison McCracken, Tricia Nguyen and Lorenzo Sernissi.

I would also like to thank the members of my thesis committee, Dr. Mike Tyers and Dr. Pierre Chaurand for the supporting comments and discussions provided during the committee meetings and beyond.

Furthermore, I would like to thank all of my co-workers from the laboratories of Dr. Pierre Thibault for having worked together with me smoothly. Especially I would like to thank Evgeny Kanshin who has trained me in mass spectrometry and who has always answered my questions. I am very glad for the good work atmosphere that had developed with Sibylle Pfammatter, Chongyang Li, Francis McManus and Mirela Pascariu. From the neighboring laboratories at the institute for research in immunology and cancer, I would like to thank Kevin Leguay, Marjorie Lapouge, Marine Diennet and Virginie Mondin for the good times spent inside and outside the laboratories, and for patiently teaching me French. A special thank you also goes to Myreille Larouche for having introduced me so well to the Quebecois culture and for all the times spent together! Thank you also to Celine Laumont for being a good friend, and for all the very interesting conversations we had about science – you really helped me to understand biology.

Aside from the people that directly supported me at the work place, I would like to express a big thanks to David Haberl and Timon Geib, who both have become close friends during the years that I have lived in Montreal, and who have always been by my side. Thank you David and Timon!

Finally, I would like to thank the Canadian government for the generous support in the form of a Vanier scholarship.

It is possible to fly without motors,

but not without knowledge and skill.

— Wilbur Wright

Chapter 1

Introduction

1.1 Intracellular Signaling

Intracellular signaling is the process in which information is transferred within the cell. In the natural habitat of cells, intracellular signaling begins outside the cell through a stimulation or stress and is transduced inside the cell causing a reaction. In cell biology, intracellular signaling is defined as "A chain of reactions that transmits chemical signals from the cell surface to their intracellular targets" [1]. These chemical signals often originate from receptor proteins at the cell surface that recognize changes in the extracellular space. Receptor proteins are usually large proteins that are embedded into the lipid bilayer membrane and stick out at both the intracellular and extracellular sides of the cell membrane. Translation of an extracellular stress into an intracellular response mostly happens through conformational changes of the intracellular protein domain on the receptor protein. This, in turn, allows for the receptor protein to interact with an abnormal set of intracellular proteins or enzymes. Once these intracellular proteins interact with the receptor, their activity changes and induces a cascade of chemical signals.

1.1.1 Stress response and signaling

Research over the past two decades has found that extracellular stress often activates intracellular signaling cascades through G-protein coupled receptors [2]. The binding of a ligand to the extracellular part of a G-protein coupled receptor can change the conformation of the intracellular domains that are linked to G-proteins. G-proteins are guanine nucleotide binding proteins acting as molecular switches through hydrolysis of guanosine triphosphate (GTP – ON state) to guanosine diphosphate (GDP – OFF state). Upon ligand binding to a receptor, the GDP bound to the G-protein is phosphorylated to GTP and, in turn, can induce the activation of various signaling cascades [3, 4]. Depending on the type of stress, distinct receptors are activated, leading to the activation of stress-specific signaling pathways [5]. An obvious, day-to-

day example of intracellular signaling is receptor-mediated activation of nerve cells through light and heat [6]. Due to the large diversity of cells in the body, different cell types contain different receptors that are prone to react to specific types of stimuli. In addition to the activation of signaling cascades through extracellular stresses and receptors, when enzymes that normally mediate the chemical signals within a cell are impaired, they can cause similar perturbations to signal transduction mimicking stress or growth conditions. These can be induced through activity-changing mutations on proteins or through treatment with exoogenous chemicals, such as chemotherapeutics, which bind to target proteins with the intent to induce cytotoxic signaling events. All signaling cascades are of extremely high complexity and do not occur in a linear fashion. Accordingly, the impacts from impaired and altered signaling cascades on the biological system can vary from allergic reactions and the perception of pain to the growth of tumors. Thus, it is important to understand disease-associated signaling events in great detail in order to decipher those that can be targeted for treatments. This thesis is focused on studying targeted and general stress responses in yeast, a model organism, as well as signalling in mammalian tumor cells, with the aim of gaining knowledge on cancer-specific cell signaling.

1.1.2 Types of intracellular signaling

Intracellular signaling can be mediated through numerous classes of chemicals. Here, we will discuss the classes that are most important for intracellular signaling. Accordingly, hormones, cytokines and growth factors, which are all signaling molecules of the endocrine (extracellular) system, will not be discussed.

Intracellular signaling molecules transform stimulations into biochemical chains of action. These signalling cascades can be carried out through post-translational modification (PTM) of proteins. Chemical modifications of proteins occur through the covalent addition of functional groups or small proteins. Acetylation, glycosylation, methylation, ubiquitination, sumoylation, phosphorylation, and proteolysis, the enzymatic cleavage of proteins, are amongst the most important chemical modifications to proteins [7-9]. These post-translational modifications can change the activity and chemical properties of modified proteins. The change in activity of one protein affects the activity of the downstream interactor of the protein and thus, results in the

spread of a signal. One of the most abundant types of post-translational modification is phosphorylation, which is highly involved in the regulation of protein cascades that regulate cellular processes including proliferation, differentiation, and cell death [10].

1.1.3 Occurrence and mediation of protein phosphorylation

Protein phosphorylation is a post-translational modification that occurs mostly through the phosphorylation of the amino acids Serine (Ser) and Threonine (Thr), which make up an estimated 79.3% and 16.9% of all phosphosites found, respectively. Less commonly found is Tyrosine (Tyr) phosphorylation, at 3.8% [11]. Studies also suggest that non-canonical phosphorylation occurs on Histidine (His), Aspartic acid (Asp), Glutamic acid (Glu), Lysine (Lys) and Arginine (Arg), but these are far less studied due to the thermal instability of the respective phosphor ester bonds [12]. The insertion of a phosphogroup into a protein causes an increase in negative charge and a concomitant decrease in hydrophobicity, which, in turn, can alter the conformation, and thus the activity, of the protein [13]. Phosphorylation can simultaneously occur at different places within a protein and often affects the three-dimensional conformation of a protein in various ways [14]. Recent studies suggest that there are about 20,000 protein encoding genes in human cells (5,400 in yeast), of which about 13,000 (3,000 in yeast) are regulated through phosphorylation [15]. Most phosphoproteins can be phosphorylated at multiple amino acid residues, creating a large pool of ~230,000 (~40,000 in yeast) estimated phosphorylation sites [15]. At present, scientists can unravel key stress response pathways within this large pool of possible phosphorylation patterns that are causes and results of major diseases, including cancer [16]. Phosphorylation is performed by protein kinases that are bound to adenosine triphosphate (ATP), which can transfer one phosphogroup to either of the aforementioned amino acids on a protein. Most kinases are specific to phosphorylation of either Ser/Thr or Tyr [17, 18]; they are thus said to harbour serine-threonine-kinase or tyrosine-kinase activity although some outlier kinases display both activities and are said to be dual-specificity kinases. The transfer of phosphogroups from a kinase to its substrate happens in the active site of protein kinases, and is schematically depicted in Figure 1.1 [19].

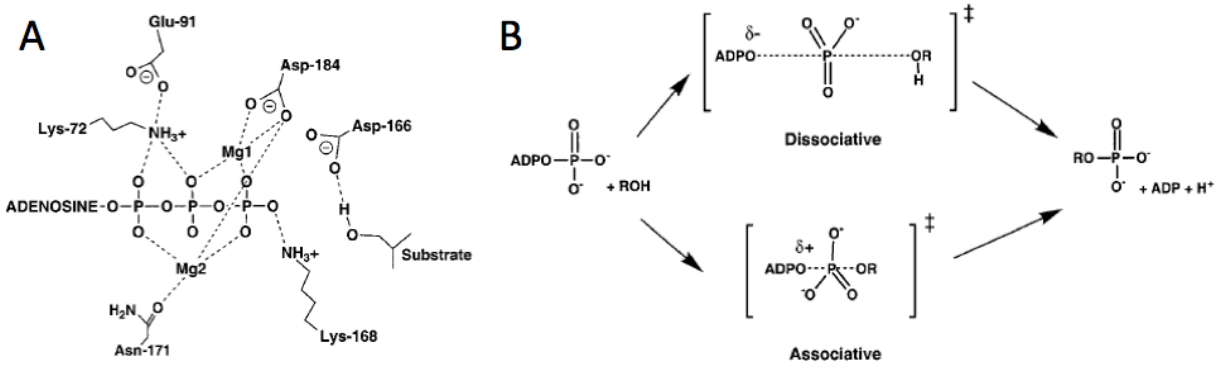

Figure 1.1. The transfer of phosphogroups by protein kinases.

A) Key residues interactions in the active site of protein kinase A (PKA). B) Associative and dissociative reaction transition states for protein kinases. Figure adapted from reference [19].

The process of protein-catalyzed transfer of phosphorylation was first discovered in 1954 by Eugene P. Kennedy [20], while the breakthrough in understanding the biological relevance of reversible protein phosphorylation occurred in the late 1980s and early 1990 through the purification of JAK kinases [21]. Since then, kinases have been found to phosphorylate specific substrate proteins through different types of recognition mechanisms. Initially identified was the recognition of substrates via amino acid motifs that increases the affinity to the catalytic pocket of the kinase [22]. Kinase recognition motifs were found in close proximity to the phosphorylation site and are specific for certain types of kinases. Early research on this topic found that the kinases CDK2, ERK2, PKA, twitchin and casein kinase each phosphorylate peptides with distinct amino acid sequences [23]. Songyang *et al.* (1996) found that the acidity, basicity and hydrophobicity of the amino acids surrounding the phosphorylation sites are of great importance for substrate recognition. Recognition motifs are generally well-conserved and thus, phosphorylation sites surrounded by conserved motifs are more likely to be important for protein functionality [24, 25]. In addition to kinase recognition by amino acid motifs near the phosphorylation site, recurring strings of amino acids have been found on protein substrates that increase the kinase-substrate affinity and thus, the likelihood of phosphorylation. This second type of kinase-substrate recognition motif does not necessarily occur close to the phosphorylation site and these motifs are referred to as "docking motifs". A well-investigated example are the "Kinase Interaction Motif" (KIM) docking motifs of mitogen-activated protein (MAP) kinases, which significantly increase the kinase-to-substrate affinity [26]. The two

combined recognition mechanisms guide the phosphorylation landscape of kinases and thus explain the specificity by which intracellular signaling is mediated. Differential regulation of kinases alters the abundance of phospho-sites on a specific population of proteins, which can, in turn, affect the proportion of active cellular machineries. Kinase-induced signals typically result in a snowball effect, spreading information within the cell, and are termed signaling cascades [27]. A general example of such a cascade is a system where protein kinase A phosphorylates protein kinase B, which in turn phosphorylates protein C. Each of these protein kinases can have several substrates and thus, a simple stimulation can result in complex signaling cascades [28]. Initial studies were performed on the cyclic AMP-dependent protein kinase, which mediates receptor-induced signaling [29]. At present, 518 kinases, of which 90 are Tyrosine and 428 are Serine/Threonine protein kinases, have been mapped in the human proteome [30]. Amongst these, 13 kinases with dual specificity have been identified. With the combined information about protein kinases, mass spectrometry based proteomics can be utilized to investigate stress response pathways regulated by certain kinases and assess their association with major diseases, including cancer [16].

1.1.4 Protein de-phosphorylation

Kinases regulate cellular processes through the transfer of phosphate residues to proteins with regulatory functions. The reverse reaction, the de-phosphorylation of amino acid residues, is accomplished by protein phosphatases through hydrolysis of the phosphate ester bonds. Accordingly, phosphatases are integral to signaling cascades in a similar fashion to kinases. The mechanism of de-phosphorylation was discovered by Cori and Green in 1943, about a decade before the discovery of kinases [31]. However, the biological significance of phosphatases was studied much later, when techniques became available that allowed the cloning of proteins in model organisms, such as yeast [32, 33]. Further investigations manifested that phosphatases can be grouped into three different classes based on the mechanism by which the phosphor ester bond is hydrolysed. The first class of phosphatases requires magnesium ions and an aspartate residue in close proximity to the catalytic cleft and these are referred to as phosphatases of the Fcp/Scp family. These phosphatases are mostly single protein phosphatases that do not contain other protein subunits. The second family of phosphatases depends on metal-catalyzed

hydrolysis mediated through either Mg^{2+} or Mn^{2+} ions that dephosphorylate Ser/Thr residues. These are further sub-classified into mostly single subunit phosphatases (PPM) and the multi-subunit protein phosphatases (PPP) family. These PPP's regulate most of the Ser/Thr-directed de-phosphorylation, which makes up about 80% of the phosphosites in the proteome. The third group is the protein tyrosine phosphatases (PTPs), which regulate mostly Tyrosine phosphorylation. The catalytic mechanisms are summarized in Figure 1.2 [34].

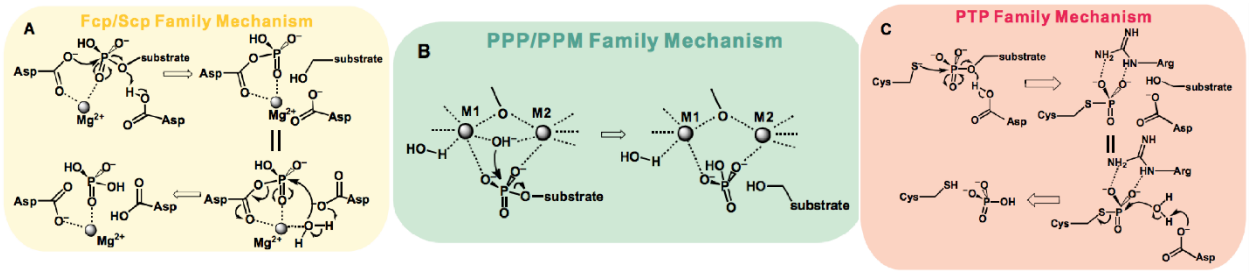

Figure 1.2. Catalytic mechanisms of protein phosphatases.

A) Mechanism of the Fcp/Scp family phosphatases. B) Mechanisms of the PPP/PPM family phosphatases. M1 and M2 depict Mg^{2+} ions. C) Catalytic mechanism of PTP phosphatases. Figure adapted from reference [34].

In the human genome, there are 107 PTPs [35] and around 30 Serine and Threonine protein phosphatases (PPP and PPM family) [36] that counteract the activity of 90 Tyrosine and 428 Serine/Threonine protein kinases [30]. The dichotomy in number of Ser/Thr kinases versus Ser/Thr phosphatases is explained through the mechanism by which the phosphatases become substrate specific. The most important Ser/Thr phosphatases (PPP family) are multimeric, comprising of a catalytic subunit (the phosphatase itself), as well as regulatory subunits that determine the substrate specificity. Accordingly, numerous regulatory subunits generate different substrate specificities for the same protein phosphatase. At present, these multimeric phosphatases are well studied and have been found to regulate major phosphorylation pathways involved in cell proliferation, cell cycle regulation, and nutrient transport processes involved in diseases such as cancer. The most prominent of the multimeric PPP family phosphatases is the protein phosphatase 2 A (PP2A) [37].

1.2 Cancer and protein phosphorylation

1.2.1 Causes of cancer

Simply put, cancer is the uncontrolled proliferation of cells [38]. Uncontrolled cell proliferation often is a result of mutations in genes that regulate signaling pathways involved in cell growth. Genomic mutations can be inherited or are acquired during the life cycle of cells through factors such as tobacco, viruses or ultraviolet radiation from the sun [39]. Random errors during cell division can also cause genetic mutations [40]. Usually, cancers are formed in the presence of multiple mutations that, in combination, activate the proliferation machinery and deactivate cellular defense and repair mechanisms [41]. Cellular defense mechanisms induce cell death (apoptosis) in malfunctioning cells to prevent the outgrowth of unhealthy cells. In the case of mutational deactivation of these defense mechanisms, combined with constitutively activated proliferation machineries, the growth of tumor cells is likely to occur [42]. Researchers found that cancer contains, on average, 60 gene mutations, of which only a few are relevant to cancer growth [43, 44]. At present, genomic screens can identify at least 125 cancer-driving mutations amongst 3,284 tumor genomes [45]. Several of these mutations have been studied intrinsically with the aim to unravel target genes and affiliated pathways that could be chemically blocked. Noteworthy examples of mutations often found in malignant cancers are amino acid substitutions in active regions of the small GTPase Ras and the kinase Raf, as well as the tumor suppressor proteins PTEN and p53. Intriguingly, Ras and Raf are activators of phosphorylation-mediated signaling pathways that induce proliferation [46] while PTEN negatively regulates the cell cycle through its lipid phosphatase activity. In more detail, PTEN prevents cells from proliferating by reducing the amount of a phosphorylated lipid (phosphatidylinositol-3,4,5-trisphosphate), which is an activator of the proliferation-inducing kinases Akt/PKB [47]. The protein p53 is a tumor suppressor found to be altered in over 50% of cancers [48], and the functional deactivation of p53, through either mutation or phosphorylation, is most likely to support tumor growth [49, 50]. Together, these findings depict how mutations in the signal transduction machinery, which is strongly regulated by phosphorylation, can result in unchecked cell growth and the development of cancer. In fact, several researchers state that cancer does not only arise from genetic mutations, but also from epigenetic changes that induce defects in the signal transduction

machinery [51]. Thus, the study of signaling pathways that are dysregulated in cancers is of crucial importance for the development of novel therapeutic strategies that target cancers.

1.2.2 Mitogen activated kinase (MAPK) pathway

Mutations in kinases that impact enzymatic activity can lead to constitutively active or inactive signaling pathways. Kinases harboring such mutations have been found through genetic screenings of cancer cells [52]. At present, several kinases and associated signaling pathways that are evolutionary conserved amongst biological species have been identified to be the cause of several cancers. One of the most frequently studied kinase pathways involved in cancer is the mitogen-activated protein kinase (MAPK) pathway. In healthy cells, the MAPK pathway regulates cell proliferation through receptor-mediated communication with the cell's immediate environment. Receptor proteins such as receptor tyrosine kinases (RTKs) can recognize tissue injuries, and other factors that require healthy tissues to grow, and, in turn, activate the MAPK pathway to induce cell proliferation [53]. The activation of receptors through the binding of extracellular ligands then leads to the activation of Ras-type guanylyl exchange factors which, in turn, activate Raf kinases through the support of several co-factors [54]. Following the activation of Raf, the signal proceeds through a phosphorylation cascade transmitted to the downstream kinases MEK1/2, followed by extracellular signal-regulated kinase 1 and 2 (ERK1/2). The latter kinases have been found to positively regulate cell proliferation through the phosphorylation of several cellular effectors including nuclear transcription factors such as TCF and ELK1 (Figure 1.3) [55].

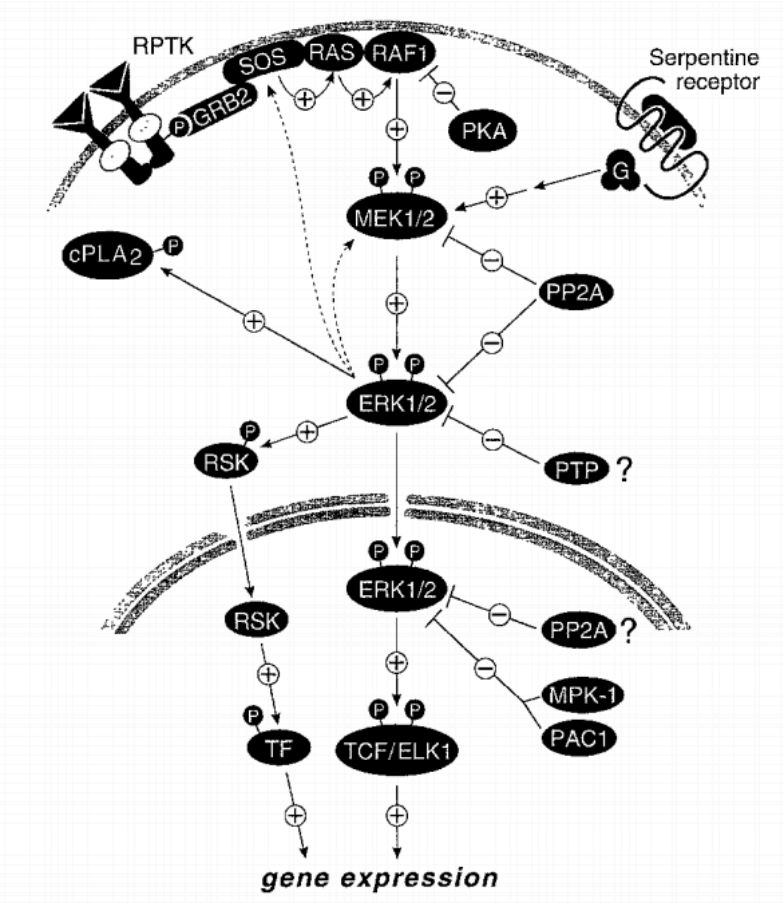

Figure 1.3. The mitogen activated kinase (MAPK) pathway.

Figure adapted from reference [10].

In addition, ERK1/2 has been found to indirectly activate additional transcription factors by activation of ribosomal s6 kinase (RSK). The activation of these transcription factors induces cell proliferation programs and inhibits apoptotic cell death [56]. In healthy cells, the proliferation stops with a decrease in receptor activity when the extracellular stimulation stalls. In cancer cells, however, mutations in MAP kinase pathway genes constitutively activate signaling, resulting in uncontrolled proliferation of cells. Across all tumor types, the most frequent genetic lesions leading to constitutive MAP kinase pathway signalling occur in the BRAF gene (the most common being BRAF V600E; substitution of valine 600 to glutamic acid) and in the KRAS gene (the most frequent being G12D and G13D substitutions; mutations of glycine 12 or glycine 13 to aspartic acid) [57-59]. The clear causal relationship between MAPK pathway activation and cancer development and progression has raised scientific and clinical interest in understanding the mechanisms by which this pathway affects tumor growth.

1.2.2.1 The kinase ERK

The MAP kinases ERK 1/2 (extracellular signal-regulated kinase 1 and 2) are the key distributors of intracellular information that arrives through the MAPK pathway. Numerous scientific studies have found that ERK1/2 regulate the proliferative and survival machineries of cells [60]. It has been found that ERK1/2 primarily phosphorylate Ser/Thr [61] residues in close proximity to proline, and that docking sites on ERK1/2 substrates, referred to as the KIM docking motifs, confer increased substrate specificity [26]. Upon activation through MAPKs, ERKs activate the proliferative machinery through activation of cytoplasmic RSK as well as through the phosphorylation of a battery of transcription factors in the nucleus. Nuclear translocation of ERK1/2 commences upon phosphorylation at Thr202/Tyr204 by MEK [62, 63]. A portion of activated ERK1/2 then translocate to the nucleus, where they remain during the completion of cell division [64, 65]. It has been found that nuclear ERKs are necessary for cell division and proliferation due to their role in activating the phosphorylation of several growth-stimulating kinases and transcription factors. For example, nuclear ERKs activate mitogen- and stress-activated protein kinases (MSKs) that have been shown to positively regulate gene translation by directly phosphorylating Histone H3 Ser10 and Ser28 [66]. Amongst the best characterized transcription factors activated by ERKs are the ternary complex factors (TCFs), of which Elk-1 is amongst the best studied, as well as the proto oncogene c-Myc. The Elk-1 transcription factor is activated upon phosphorylation of Ser383 by ERK1 or ERK2 [67] and, in turn, it increases the expression of mitogen-inducible genes. The proto oncogene c-Myc can be activated through ERKs by phosphorylation on Ser62, leading to the expression of growth regulating genes [68]. In addition to the stimulation of the proliferative machinery through the MAPK pathway, ERK has been found to positively regulate cell survival through the inactivation of components of the cell death machinery and through deactivation of tumor supressing transcription factors of the FOXO transcription complex [69]. Altogether, the ERK kinases activate cellular proliferation and concomitantly dysregulate tumor supressing machineries, explaining their involvement in the cause of malignant cancers. At present, tumors treated with chemotherapeutic agents targeting MAPK to prevent unchecked cell growth through activated ERK consistently become resistant to the inhibition of MAPK [70, 71]. There is a therefore urgent clinical need for a better

understanding of these mechanisms, as well as the identification of downstream ERK targets that could be targeted for treatment. This could, to some extent, be achieved through a more detailed profiling of ERK-dependent signaling in different types of cancer cells.

1.2.3 Tumor-supressing phosphatases

Kinases regulate cellular processes through the transfer of phosphate residues to proteins. Dynamic regulation of these biochemical reactions is assured through protein phosphatases, which invert phosphorylation reactions through hydrolysis of phosphate ester bonds. Phopshatases are therefore involved in regulating the same mechanisms as kinases, making them key regulators of cancers, in a similar fashion to kinases. As described in the chapter "Protein De-phosphorylation", the family of Ser/Thr phosphatases (PPPs and PPMs) regulates the majority of protein phosphorylation sites within the cell [34]. Aberrant activity of several members of these Ser/Thr phosphatases has been linked to several diseases, such as diabetes, cancer, and Alzheimer's [72-74], making them promising targets for treatment of these conditions. Of high interest for drug design are the multimeric Ser/Thr phosphatases (PPPs) that regulate key processes in the cell cycle [37]. Amongst the highly regulatory phosphatases of this group are protein phosphatase 1 (PP1), PP2A, PP2B, PP4, PP5, PP6 and PP7, which all exhibit high sequence homology [37, 72]. Amongst these phosphatases, PP2A is arguably the most studied tumor supressing phosphatase and has been proposed to be a potential therapeutic target to treat cancer [75, 76].

1.2.3.1 The phosphatase PP2A

In mammalian cells, the enzyme PP2A is present as a heterotrimer comprised of scaffold, regulatory and catalytic subunits, each of which exist in various isoforms depending on the taxonomy. In the human genome, PP2A can be assembled by a combination of 2 catalytic subunits (C-subunits), 2 scaffold subunits (A-subunits) and 12 regulatory subunits (B-subunits) [77, 78]. The PP2A holoenzyme is held together by the scaffold subunits, and substrate de-phopshorylation is catalyzed through the C (catalytic) subunit [79] (Figure 1.4).

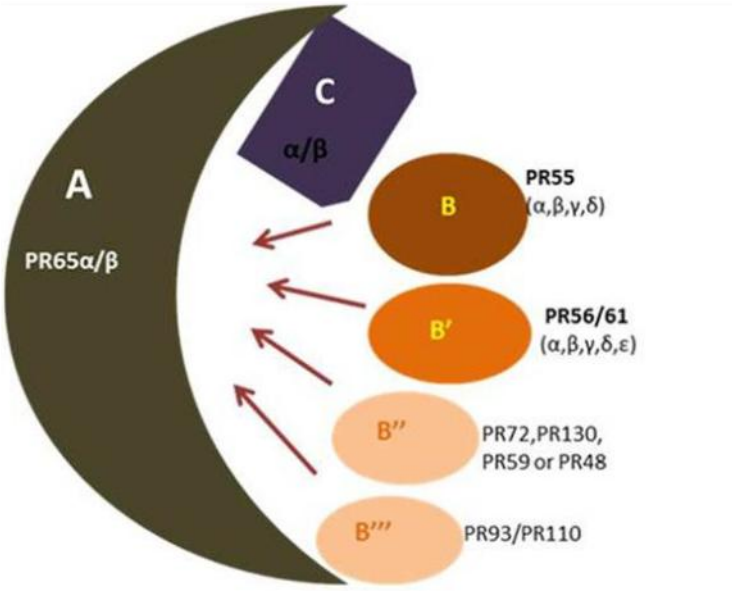

Figure 1.4. All subunits and corresponding isoforms of the protein phosphatase 2 A (PP2A).

A represents the scaffold, C the catalytic and B the regulatory subunits. Figure adapted from reference [79].

The regulatory subunits (B subunits) play a crucial roles in substrate specificity [80]. Enzymatic activity and *in vivo* targets thus depend on the assembly of the protein phosphatase trimer, which leads to a variety of complexly-regulated functions. PP2A has been found to regulate several signaling cascades involved in cell cycle regulation and proliferation. PP2A-dependent signaling cascades affect MAPK [81], the growth controlling mTOR (mechanistic target of rapmycin) pathway [82-84], and the Wnt signaling pathways, which regulate proliferation and cell polarity [85, 86]. PP2A has been found to be the key regulator of cell cycle progression and mitosis, making it the master regulator of the cell cycle [37]. Most of the molecular functions

corresponding to cell cycle progression are negatively regulated by PP2A and, accordingly, increased activity has been associated with cell cycle arrest, resulting in reduced proliferation. The negative regulation of the proliferative and growth machinery makes PP2A an important tumor suppressor [87]. In line with these findings, PP2A is underrepresented, or partially deactivated, in various cancers. These include prostate cancer, lung cancer, and leukemia [88-90]. Intriguingly, cell cycle regulation does not seem to be the only mechanism by which PP2A affects tumor growth, as recent studies show strong evidence for PP2A involvement in cellular nutrient supply wagons [91, 92]. Scientists have linked this finding to PP2A activation and found associated inhibition of tumor growth [93]. From this standpoint on, activation of PP2A has emerged as a potential treatment for cancer [94]. Suggested approaches to activate PP2A include the inhibition of PP2A-specific inhibitor proteins, such as Set and CIP2A and small molecules such as sphingolipids [95-97]. The mechanisms by which PP2A activation could be achieved and how PP2A activation leads to reduced tumor growth, however, are not yet fully understood. New molecular machineries by which PP2A influences tumors are still emerging. In-depth investigation of PP2A-activating compounds, associated signaling events, and phenotypes could be strategic approaches to unravel the potential of PP2A as an anti-oncogenic target.

1.2.4 Small molecule regulators of kinases and phosphatases

As discussed in the earlier chapters, phosphorylation is highly involved in the formation of cancer. The proteins that administer the abundance of phosphorylation on other regulatory proteins are kinases and phosphatases. Dysregulation of both classes of enzymes is found in cancers, and targeted adjustment of their activities through chemicals has been used to inhibit tumor growth [98]. At present, a large number of kinase inhibitors targeting altered signaling pathways in cancer cells are on the market. Kinases typically are tumor inducers due to their positive regulation of cell growth, leading most chemotherapeutic drugs to be designed as kinase inhibitors [99]. Notable examples are inhibitors of Raf proteins, an important family of kinases that act as molecular switches to regulate cell signaling, primarily through the stimulation of the MAPK pathway [100]. Raf inhibition subsequently blocks downstream effectors that control key cellular processes such as actin cytoskeletal integrity, cell proliferation and differentiation, and apoptosis. Furthermore, numerous kinase inhibitors targeting the cell growth inducer mTOR

[101, 102], the mTOR activator kinases of the PI3K class [103], or the receptor tyrosine kinases (RTKs) [104] are in clinical use to combat cancer. As there are a large number of kinases present in the human genome, the specificity of kinase inhibitors is important, so as not to cause side effects. At present, most clinically-used kinase inhibitors are of high specificity and are often applied only to a specific cancer genotype, for example, those that harbor somatic mutations on genes, such as BRAF [105]. The main problem encountered when treating cancer cells by specifically inhibiting kinases is that the stall of the tumor proceeds slower than cells can establish resistance mechanisms, causing prolonged life of patients but not a complete cure [106, 107]. A better understanding of signalling events may lead to the development of some potential inhibitors that target resistant cancers, but no definite cure can be achieved using such medicines [108]. As occurrences of resistance and the transient effects of kinase inhibitors accumulate, more suggestions to treat cancer from different angles are being discussed [109]. Enzymes such as phosphatases are of increasing interest for the development of chemotherapeutics due to their pleiotropic effect on the cell cycle [110, 111]. Given that phosphatases of the PP2A class are categorized as tumor suppressors, their inhibition by agents like Calyculin A and Okadaic acid, is highly carcinogenic. This suggests that conversely, PP2A-activating chemicals could inhibit tumor growth [112, 113]. Within the last decade, ceramides, a class of naturally occurring sphingolipids, were discovered to activate PP2A and to drastically diminish cell proliferation [75]. Since then, synthetic analogues of ceramides have been found to reduce cancer growth. A noteworthy example is FTY720, a synthetic sphingolipid which activates PP2A and, in turn, causes cancer cells to die through cell cycle arrest and nutrient deprivation [114, 115]. Nonetheless, the development of PP2A-activating small molecules is still in its early stages, as only a few compounds with PP2A-activating properties are known, making a complete understanding of these medicines crucial for further advancements.

1.2.4.1 Vemurafenib (PLX4032)

Vemurafenib, or PLX4032, is an FDA-approved kinase inhibitor used to treat metastatic melanoma harboring the BRAF V600E somatic mutation, which causes consecutive activation of the MAPK pathway [116]. Vemurafenib specifically inhibits the kinase activity of the BRAF V600E gene through ATP-competitive binding, a mechanism by which the kinase is deprived of the transferable phosphor group provided by ATP, making it kinase-dead [117]. Vemurafenib efficiently inhibits the kinase activity of BRAF V600E at nanomolar concentrations, while the inhibition of wild-type BRAF kinase occurs only at higher dosages, a phenomenon that originates from the BRAF gene to form active kinase dimers [118]. RAS-dependent dimerization of the wild-type (wt) BRAF kinase is required for its activity, while the mutated BRAF V600E is kinase-active in the monomeric conformation, making Vemurafenib a highly specific inhibitor of the BRAF V600E monomer. Vemurafenib and related kinase inhibitors, including Dabrafenib, favor wt BRAF to form dimers, resulting in paradoxical activation of MAPK in wt BRAF cells [119-121]. Inhibition of wt BRAF through dimer-inducing compounds is only observed with excessive dosages of the kinase inhibitor, limiting its use for the treatment of cancers harboring the BRAF V600E mutation [122] (Figure 1.5). Such dosages, however, are not applicable for treatment and, therefore, Vemurafenib is used only to treat the BRAF V600E melanoma genotype. Thus, treatments with Vemurafenib require genomic sequencing prior to treatment [123]. In turn, dimer dependency of the wt BRAF gene causes melanomas not harboring the BRAF V600E mutation to worsen when treated with Vemurafenib, a phenomenon referred to as paradoxical activation [124]. These occurrences are of high clinical significance, as several melanomas and other types of cancers, including colon cancer, often harbor somatic KRAS mutations (G13D or V14D), which lead to BRAF/MEK/ERK activation, but that cannot be treated with Vemurafenib [125]. Furthermore, the off target effects of Vemurafenib has been found to lead to the accumulation of side effects and the cause of cancers, including cystic lesions and basal cell carcinomas [126]. Interestingly, the efficacy of BRAF V600E inhibition leads to several primary and secondary resistances that are not yet fully understood. Primary resistance refers to the lack of response to Vemurafenib in cancers with elevated epidermal growth factor (EGFR) signaling, as has been observed in metastatic colon rectal cancer, requiring discontinuation of treatment [127]. Furthermore, Vemurafenib treatments remain

efficient only up to one year from the first dosage, due to acquired resistance that can result from re-activated MAP kinases [128]. Several underlying mechanisms, such as the overexpression of various RAF isoforms [129, 130] or feedback phosphorylation events that lead to internal MAPK activation [131], have been studied, but the underlying signaling events leading to these types of resistance require further investigations.

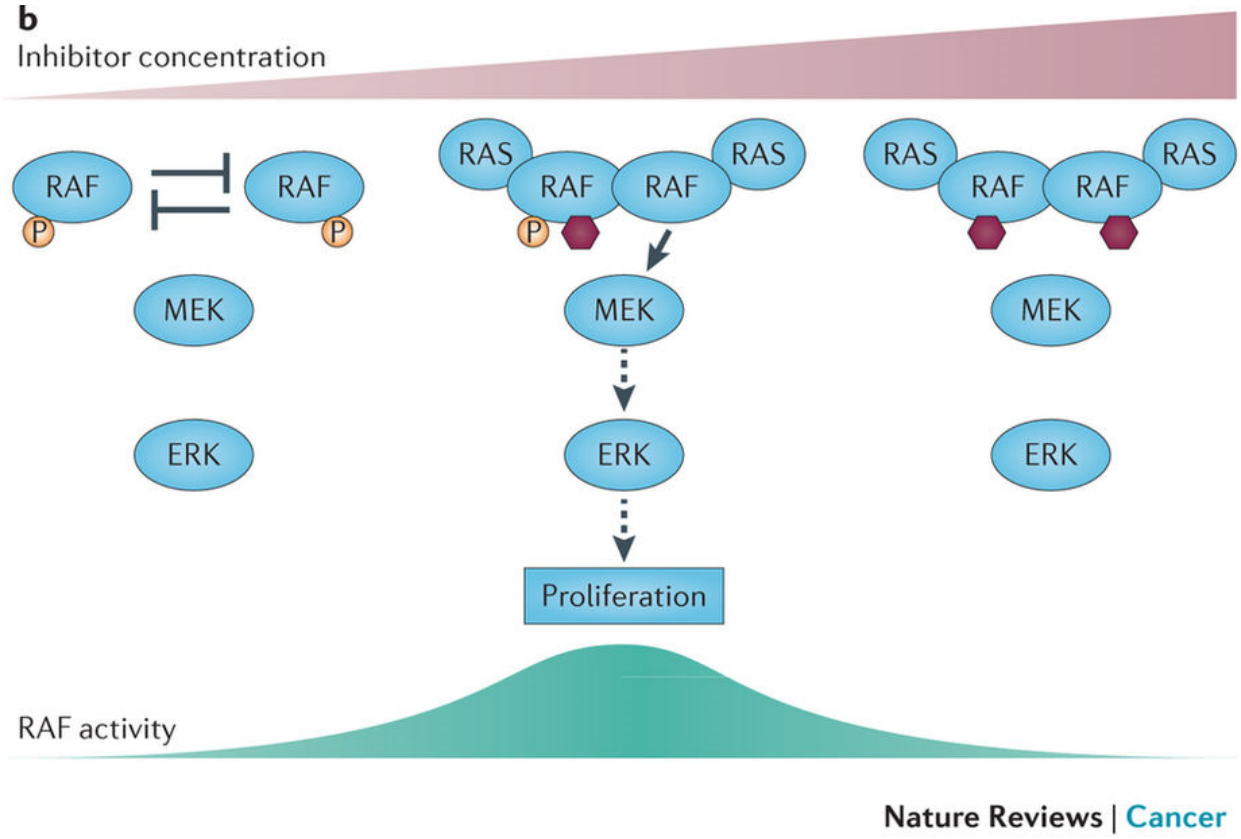

Figure 1.5. Activation of the RAF kinases in dependence of inhibitor concentration.

Wild-type RAF proteins exist largely in an auto-inhibited state. In the context of activated RAS, RAF inhibitors stimulate MEK activation at sub-saturating inhibitor concentrations by relieving auto-phosphorylation (P) of wild-type RAF, promoting RAF dimerization and association with RAS. Saturating inhibitor concentrations prevent MEK phosphorylation by blocking all RAF catalysis.

Figure adapted from reference [132].

The impact of cell type, genotype and time of treatment on the efficiency by which MAPK inhibitors, such as Vemurafenib, inhibit the growth of tumors raises strong interest in the generation of a complete picture of the phosphorylation-dependent signaling that spreads from BRAF kinases. In line with the interest in phospho-dependent signaling that is extensively discussed in this thesis, the study of global phosphorylation events triggered by Vemurafenib in

different cancer genotypes is studied with the aim of gaining additional knowledge on potential resistance mechanisms and of generating a more complete picture of MAPK signaling.

1.2.4.2 Sphingolipids and SH-BC-893

Sphingolipids are lipid-like molecules that are present in mammalian cells, as well as in single cellular microorganisms, such as yeast [133, 134]. Noteworthy sphingolipids with proven biological activity are: phytosphingosine, which is widely expressed in yeast; ceramide, with variable fatty acid chain lengths; as well as sphingomyelin and glucosylceramide (Figure 1.6).

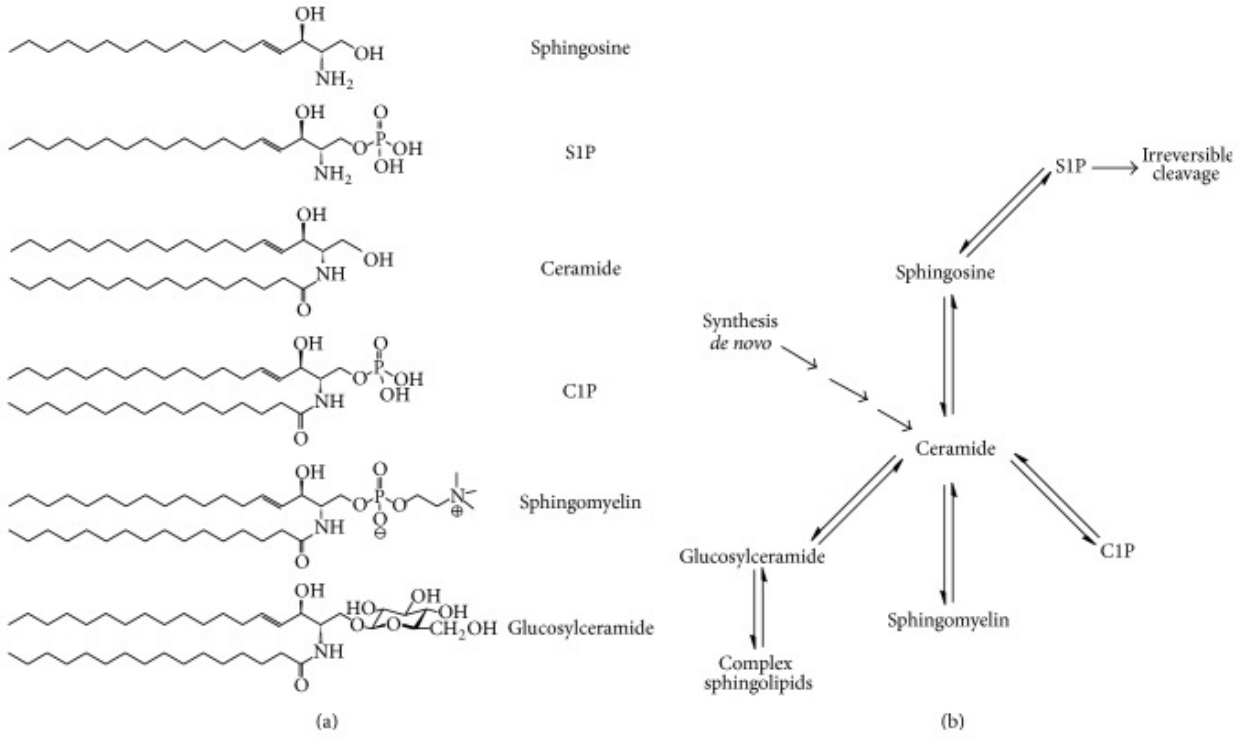

Figure 1.6. Most important sphingolipids.

From left to right: Sphingolipid structures, corresponding names, placement within the metabolic pathway of sphingolipids. Figure adapted from reference [135].

In vivo synthesis of sphingolipids is evolutionary conserved and the expression of various sphingosine metabolites is known to regulate membrane homeostasis and a variety of intracellular signaling events that balance physiological cues and stresses [136]. It has been found that membrane homeostasis is mediated through the regulation of proteins involved in endocytosis and intracellular trafficking [137]. Ceramides, a subclass of sphingolipids, have been

named tumor suppressor lipids due to their impact on cell proliferation, death, migration, and senescence, making them of special interest as medicines [138-141]. Furthermore, researchers found that sphingolipid treatment elicits PP2A activation *in vivo* and *in vitro* through an unknown biochemical mechanism [75, 142], and may be associated with nutrient suppression and subsequent death of cancer cells [143]. Activation of PP2A causes deprivation of cells from extracellular nutrients through blockage of endocytosis and lysosomal fusion, mechanisms known to be sphingolipid-dependent [144, 145]. Importantly, such nutrient deprivation is specifically deadly to cancerous tissues, which depend on extracellular amino acids and glucose due to altered self-supply mechanisms, while healthy cells are able to adapt to starvation [146]. Commonly known as the Warburg effect, tumor cells require high amounts of extracellular nutrients because of impaired metabolic pathways and, thus, are sensitive to suppressed nutrient influx. C2-ceramide and a structurally related FDA-approved compound FTY720 (Fingolimod), which is used to treat multiple sclerosis by targeting sphingosine 1 phosphate receptors (S1P), have been shown to limit nutrient access to cells by activating PP2A, causing death of tumor cells [147, 148]. As these findings made sphingolipids potential candidates for a universal treatment of cancer, synthetic analogues of such compounds with optimized chemical properties were recently synthesized by researchers at the University of Montreal. Taking the presently-studied and FDA-approved multiple sclerosis drug FTY720, which harbors anti-oncogenic properties, as a starting point, *Chen et al.* (2015) designed compounds that have higher potency to disrupt nutrient access than FTY720 [149]. Compound SH-BC-893, the most potent constrain of a series of FTY720-like molecules, has proven to specifically starve cancer cells, similar to C2-ceramide and FTY720 [150]. Importantly, SH-BC-893 does not induce bradycardia, which is a side effect that occurs at high doses of FTY720, and does not affect the survival of mice [149]. As of now, phenotypes observed upon treatment with synthetic (FTY720 and SHBC893) and natural sphingolipids (C2-ceramide and phytosphingosine) are the internalization of nutrient transporters, including the amino acid transporter 4F2HC, possibly through activated endocytosis [93, 151]. *Kim et al.* (2016) show that these starvation phenotypes caused by SH-BC-893 and ceramide are consistently reversed using PP2A inhibitors, such as the non-specific Calyculin A, suggesting PP2A as a direct or indirect target of compound SH-BC-893 and ceramides. As PP2A is one of the major phosphatases in the cell, it is of high clinical and scientific interest to unravel the intracellular signaling by which sphingolipid-activated protein phosphatase induces death of

cancer cells.

1.3 Phosphoproteomics to understand intracellular signaling

The signaling machineries that comprise thousands of phosphorylation sites are highly complex and require high throughput technologies to be analyzed on a system-wide level [152]. At present, there are a few high and low throughput techniques that allow the assessment of the abundance of phosphorylation sites on proteins. The most commonly known technique is the antibody based western blot profiling of phosphorylation sites [153]. In this low throughput technique, protein extracts from cells that are either stimulated or unstimulated are separated by sodium-dodecyl-sulfate polyacrylamide gel electrophoresis (SDS-PAGE) and are subsequently transferred to a nitrocellulose membrane. Incubation of this membrane with antibodies that were raised against specific phosphorylation sites on the protein of interest allow chemoluminescence-based detection and approximate quantification of protein phosphorylation [154]. This approach is not applicable to the study of signaling systems since only one or a handful of phosphorylation sites can be profiled at a time. In addition, each analysis requires time-consuming optimization of experimental procedures. At present, systems-wide analysis of the phosphoproteome is achieved using mass spectrometry-based proteomics [155]. Mass spectrometry-based proteomics is a branch of proteomics in which the analysis of proteins and their modifications is achieved using mass spectrometry. In brief, mass spectrometry-based proteomics can be compared with genomics, as both fields make use of technology that is capable of screening the whole cellular system at once. The difference is that genomics profiles the genome (DNA and RNA), while, in proteomics, the proteome (proteins and their modifications) is investigated in whole [156]. With the use of specialized mass spectrometry, which will be discussed in greater detail in the next section, protein systems including the phosphorylated proteome, can be profiled within days of sample preparation. The field of systems biology has greatly benefited from the use of mass spectrometry-based proteomics and has substantially advanced the knowledge of signaling machineries through systems wide investigation of post translational modifications [157, 158]. Therefore, the use of mass spectrometry is the preferred methodology to profile the effects of stimulations on biological systems in a systems wide manner. Nonetheless, the complexity of these systems brings analytical challenges that need to be addressed in order to disentangle the

vast amount of information gained from high throughput mass spectrometry-based proteomics. The theory of mass spectrometry based proteomics and challenges arising from the profiling of signaling networks are described in the following section.

1.4 Mass spectrometry-based proteomics

Proteomics is the study of the entire variety of proteins in a biological system, termed the proteome, and, over the last two decades, has become an emerging technology in pharmaceutical sciences and molecular biology [159]. In contrast to genomics, in which the entire genome is studied, proteomics focuses on the set of proteins that is produced from the genome under certain conditions [160]. Contrary to genetic material, which is more or less constant over time and in a variety of environmental conditions, proteins are highly dynamic in terms of abundance, cellular localization, and post-translational modification, including protein phosphorylation [161]. These factors greatly increase the level of complexity of proteomic analyses and require analytical strategies to study parts of the proteome that are of main interest to the researcher. Proteomics can be understood as the science of proteins that investigates their biochemical reactions in a biological context and, accordingly, is applicable to studies of changes arising from diseases, stresses or chemicals. The development of mass spectrometry (MS) techniques that allow ionization and sequencing of peptides and proteins has allowed the performance of system-wide analyses of almost the entire array of proteins and their post-translational modifications [162, 163]. As of now, proteomics has become a widely used technique for the development of diagnostics, drugs and chemotherapeutics, as well as concepts in basic sciences [164-166]. Analytical strategies to extract and enrich the proteome of interest, as well as mass spectrometry-based analysis, form the base of proteomics and require optimized workflows to generate reliable and robust data. Different workflows that study proteins at different molecular stages have been developed, the one used throughout this thesis is termed shotgun proteomics. In shotgun proteomics, all proteins in a sample are enzymatically digested into peptides and are analyzed by mass spectrometry [167]. Generic sample preparation techniques to extract and analyze the proteome have been developed during the last two decades of shotgun proteomics research and those used in this thesis are summarized in Figure 1.7. The key elements are sample collection and the preparation of protein extracts from biological samples (1). Protein digestion into

peptides and optional enrichment of peptides harboring post-translational modifications (2). Peptide analysis by liquid chromatography (LC) coupled to MS, often abbreviated as LC-MS and pre-fractionation methods can be applied to reduce sample complexity and increase the coverage of the proteome (3). Bio-informatics analysis follows to extract information about protein identification and quantification (4).

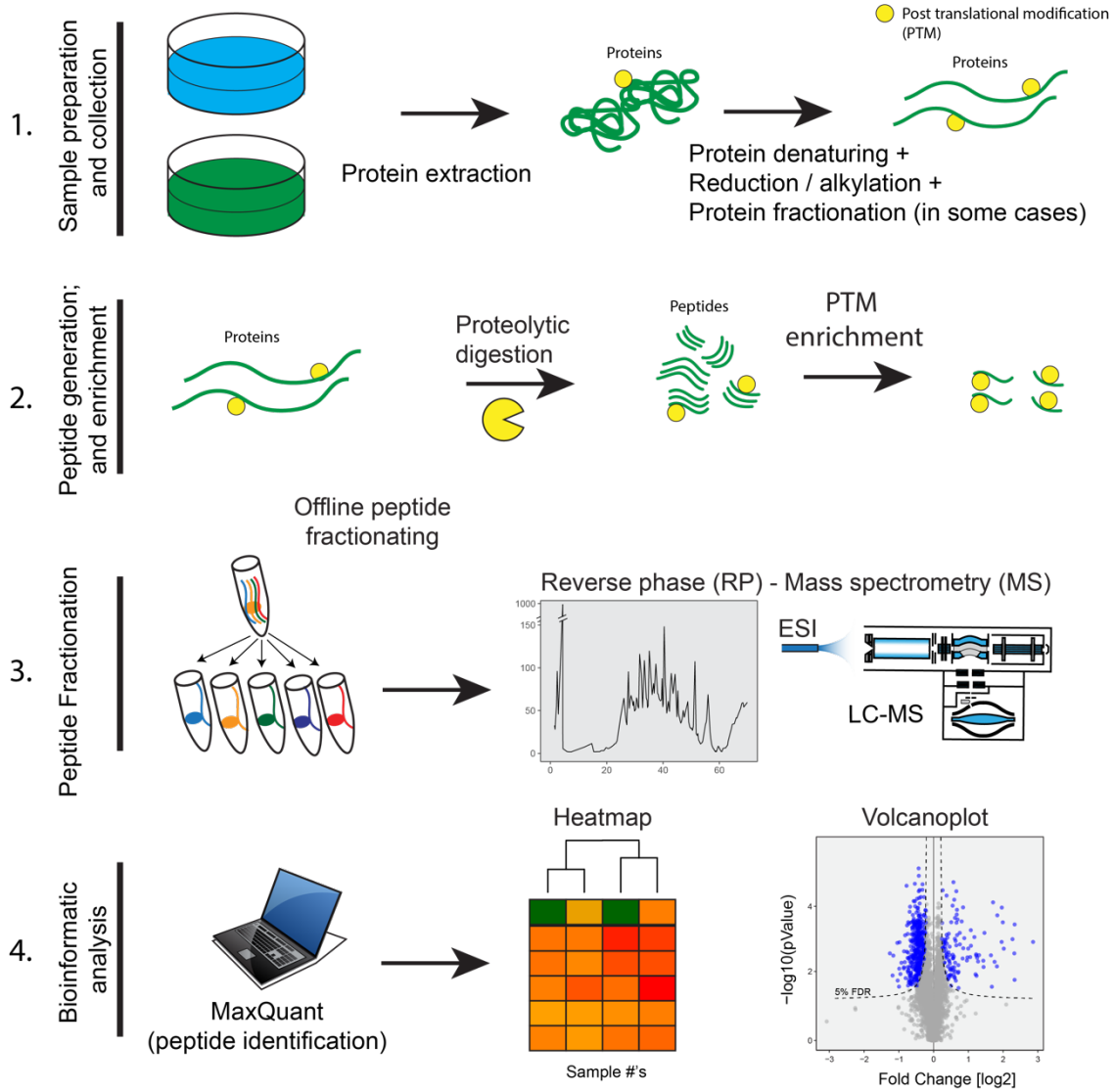

Figure 1.7. Schematic illustration of the shotgun proteomics workflow.

1.4.1 Sample preparation

Samples for proteomic analyses can be provided in the form of tissues or cells that have been subjected to a stimulation such as drug treatment or temperature shocks. In this thesis, yeast or mammalian cells were used to study changes in the phosphoproteome through stable isotope labeling of amino acids in cell culture (SILAC). Stable isotope labeling of amino acids is a technique in which cells are grown in the presence of isotopically labeled amino acids that incorporate into the proteome and, thus, greatly enhance the relative quantification of peptides and proteins by mass spectrometry. Of importance to sample preparation when using SILAC is the growth of cells in appropriate media for at least 7 cell doublings prior to stimulation and mass spectrometry-based analysis [168]. Technical details about the metabolic labeling technique used in this study will be explained in the section "Protein quantification". Cells typically grow suspended in media or adhered to petri dishes that are filled with growth media, culture collection can be achieved through centrifugation of cell solutions or through scraping cells off of the growing surfaces. After cell collection, cells are washed with isotonic buffers, such as phosphate buffered saline (PBS), to remove any extracellular proteins that could contaminate the mass spectrometry-based analysis. Due to the dynamic nature of proteins and the biochemical system of a cell, specific care is necessary when handling biological samples during these steps. Biological material are kept at low temperatures to minimize biochemical reactions that are unrelated to the stimulation; furthermore, the time of any sample preparation are kept to a minimum to avoid peptide/phosphopeptide degradation through hydrolysis [169].

1.4.2 Extraction, quantification and digestion of proteins

Protein extraction from cells or tissues is generally performed using lysis buffers that contain detergents, glass beads or similar reagents that break the cell walls [170-172]. Extraction of proteins from cells, is achieved by mixing collected cells with a lysis buffer. Lysis buffers should contain detergents that lyse the cellular membrane and solubilize proteins, be of physiological pH (7-8) and should contain inhibitors of enzymes, such as proteases and phosphatases, which can induce changes in proteome dynamics after sample collection. Detergents, the most important ingredient of lysis buffers, also have a denaturing effect and can thus inactivate protein

functions, a process that preserves the dynamic state of the proteome at the time of cell lysis. Denaturing of proteins further linearizes the protein structure, which, in turn, facilitates proteolytic digestion into peptides [173]. A commonly-used detergent applicable to mass spectrometry-based proteomics is sodium deoxycholate (SDC) in the class of ionic detergents. Urea is often used to replace SDC due to its chaotropic properties that promote protein denaturation, solubilisation and cell lysis. Non-ionic detergents are not applicable to mass spectrometry, as these cannot be removed from samples through reverse phase purification prior to mass spectrometry analysis. Importantly, removal of detergents prior to mass spectrometry analysis is necessary, as detergents are of high ionization efficiency and are well-retained on reverse phase stationary chromatography phases, resulting in detector saturating signals that mask peptides and changes in the chromatographic properties of separation columns [174]. In addition to detergents, further aid to extract and solubilize proteins can be achieved with acoustic sonication of samples following cell lysis [168, 175].

Once protein extraction from cells through lysis buffers and sonication is achieved, insoluble debris-containing lipid membranes are separated from the protein-containing solution using centrifugation. Determining the concentration of proteins is a crucial step on which all subsequent calculations of the amounts of proteolytic enzyme used, and the peptides loaded onto separation phases and the LC-MS system, are based. In order to have a standardized method, the commercially-available pierce BCA kit was used throughout all proteomic analyses in this thesis [176].

Following protein quantification, the remaining sample is subjected to proteolytic digestion. Numerous enzymes are used for proteolytic digestion to generate a full array of possible peptides for mass spectrometry analysis. The most commonly used enzymes are trypsin, followed by Lys-C, chymotrypsine, Glu-C and pepsin [177]. More than 80% of all mass spectrometry-based analyses are carried out using trypsin to generate peptides, mainly due to the improved sequencing properties of tryptic peptides, arising from cleavage at the basic amino acids Lysine (Lys) and Arginine (Arg) [178]. Peptides containing a basic C-term comprising of either Lys or Arg and a basic N-terminus amine are most likely to be doubly charged during MS analysis and generate fragment ions from both the N- and C-termini of the peptide, greatly enhancing the

sequencing capabilities of mass spectrometers [179]. Details of these effects on peptide sequencing will be discussed later on in the section “Peptide sequencing”. Trypsin allows the identification of most proteins and post-translational modification sites within the proteome and was thus used in this thesis to profile the phosphoproteome of cells subjected to different stimulations. Proteolytic digestion using trypsin is sensitive to excess detergents/chaotropes and physiological pH, requiring careful choice of lysis buffers. In a shotgun proteomics workflow, as was used throughout this thesis, tryptic digestion of proteins is performed in SDC or urea-containing lysis buffers and twelve hours of reaction time.

For the majority of analytical chromatography techniques and mass spectrometry-based analysis, it is of great importance that samples are free of contaminants, such as salts or detergents, which are present in lysis buffers. For this, solid phase extraction (SPE) of peptides from proteolytic digests is required. SPE is a simple technique based on chromatographic separation that is used to separate hydrophilic salts or other small, charged molecules from the more hydrophobic peptides [180]. Accordingly, hydrophobic stationary phases, commercially available in the form of cartridges, are commonly used to extract peptides from more complex matrices. In brief, solvents can be run through cartridges using a pressure gradient generated by a vacuum pump, and application of peptide samples and washes to remove hydrophilic compounds is achieved using aqueous solvents with low pH (~2). Elution of peptides into clean tubes is subsequently performed with aqueous solutions containing up to 50% of organic solvents such as methanol or acetonitrile [181]. The evaporation of solvents with vacuum systems is further used to generate lyophilized peptide samples that are ready to use in LC-MS or further sample preparation. In cases where scientists are interested in a specific part of the proteome, such as the phosphoproteome, enrichment of phosphorylated peptides is a must, due to the low abundance of phosphorylation, which makes up only around 1% of the protein material [182]. A noteworthy comment to the reader is that the enrichment of PTM’s on the peptide level is preferred, as enrichment of proteins harboring the PTM’s of interest would result in the generation of mostly unmodified peptides upon digestion of the enriched proteins.

1.4.3 Large scale phosphopeptide enrichment

Serine, threonine and tyrosine protein phosphorylations are the most commonly found phosphorylation sites and are the only ones investigated in this thesis. The negative charge of the phosphate group allows for specific enrichment of phosphopeptides using affinity chromatography media. As of now, several materials have been found to bind phosphorylated peptides and proteins with high affinity, including the metal oxide titanium dioxide and positively-charged metals such as Fe(3+), Ga(3+), Al(3+), Zr(4+) and Ti(4+) [183]. Titanium dioxide is easy to handle as it is commercial available as nanoparticles, while metal species have to be immobilized on stationary chromatography phases that contain chelating groups, such as nitriloacetic acid (NTA) [184]. Specific enrichment of phosphopeptides likely occurs due to the electrostatic interactions of positively charged metals and negatively charged phosphate groups, as unwanted enrichment of very acidic peptides is often observed in phosphopeptide samples [185]. The exact mechanisms by which the above-mentioned stationary phases enrich phosphate-containing peptides and why they perform much better than other commonly used anion exchange materials are not fully elucidated but likely rely on the formation of metal chelate complexes [186]. In addition to the enrichment of phosphopeptides based on physical/chemical properties, antibodies to enrich for selected phosphopeptides, such as the low-abundant tyrosine phosphorylation sites, have been developed [187] and are frequently used to study phospho tyrosine signalling [188, 189]. This thesis, however, aims to monitor time-dependent dynamics of the general population of phosphorylation sites and, thus, the more complicated and less reproducible use of antibodies has been avoided. Furthermore, studying the spread of phosphosignaling over time requires the analysis of numerous samples (time points) in parallel, making the implication of high throughput techniques mandatory. Workflows capable of processing phosphopeptide enrichments of numerous samples need to be reproducible, applicable to parallelisation and simple. The aforementioned immobilized metal affinity chromatography (IMAC) has been found to be a good means to enrich a general population of phosphopeptides similar to titanium dioxide nano-particles [190]. However, handling the IMAC stationary phases requires careful adjustment of salt and pH conditions, which are not needed when operating titanium dioxide nanoparticles.

As stated earlier, all of the following high throughput studies are aimed at the analysis of system-wide perturbations of the phosphoproteome, making the use of titanium dioxide nanoparticles logical. Accordingly, all phosphopeptide enrichments prepared in the scope of this thesis use titanium dioxide beads. As up to 14 samples needed to be processed for a single experiment, an experimental design allowing for parallel enrichment had to be developed. Commonly-used methods were assessed and adjusted to properly match the aim of parallelized phosphopeptide enrichment, and the use of spin tip columns was determined to be the most suitable [191]. In-house spin tips for parallel enrichment of phosphoproteomes were prepared as described in the following paragraph, and are based on publicatons by *Liu et al.* (2016) and *Kanshin et al.* (2012 & 2013) [185, 191, 192]. The main advantage of spin tip columns over high performance liquid chromatography systems (HPLC) is that they can be used in centrifuges and allow parallel processing of samples. Preparation of spin tip columns is shown in Figure 1.8.

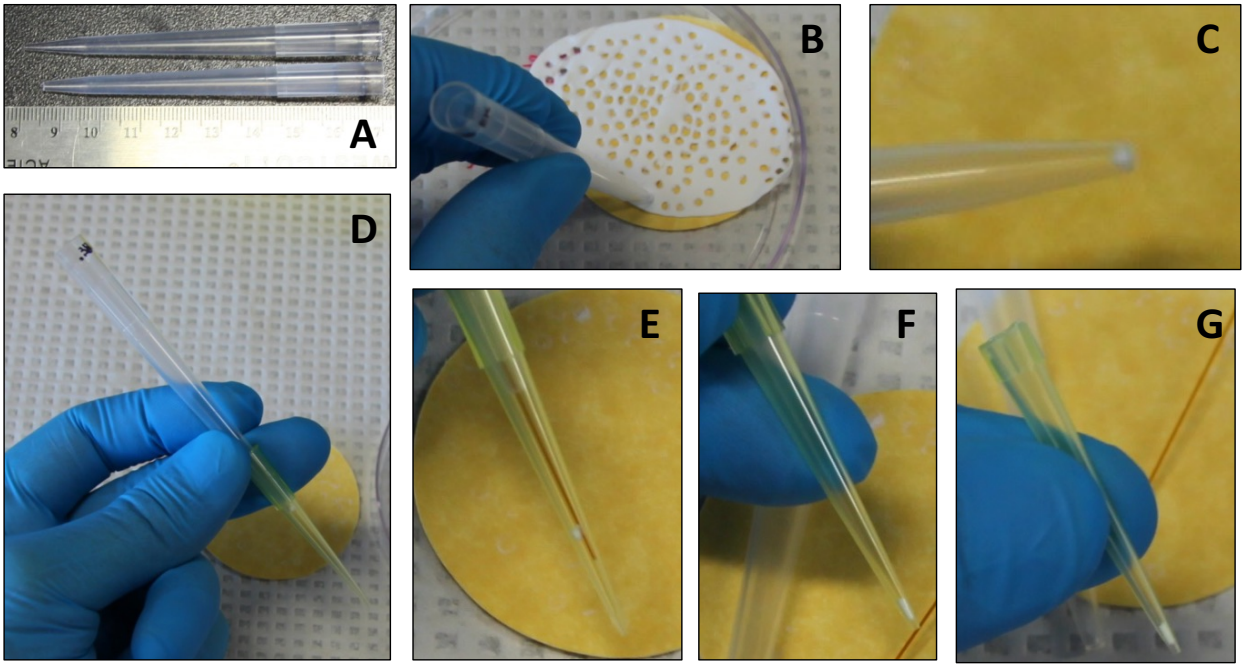

Figure 1.8. Preparation of spin tip columns.

A-G) depicts the workflow to insert extraction disks into 200uL pipette tips. A) 1mL pipette tips have to be cut by 5mm to enlarge orifice. B) Cut 1mL tips are used to take up extraction disk. C-G) Insertion of extraction disk from the 1mL tip to the 200uL tip with the help of a capillary.

Spin tip columns are made from pipette tips filled with small polymer-based frits to allow loading of stationary phases, such as titanium dioxide nanoparticles. In this workflow, these frits are made of a hydrophobic material, such as C18-coated extraction disks, which retain

phosphopeptides after elution from titanium dioxide [193]. Purified phosphopeptides can then be recovered from the same spin tip after desalting and elution with a hydrophobic liquid phase (a strong organic solvent containing acetonitrile or methanol). Titration of the frit capacity is done prior to each analysis in order to assure no loss of phosphopeptides. Insertion of these frits into each spin column requires manual precision work and is depicted in Figure 1.8 A-G. Following the insertion of these frits, titanium dioxide is loaded onto the spin tip by placing each tip, to which a frit has been added into an Eppendorf tube, as depicted in Figure 1.9 H. Equal amounts of titanium dioxide are loaded by pipetting the metal oxide homogenate into the spin columns (Figure 1.9 steps J&K). Elution of the solvent through the column is achieved through centrifugal force, deployed during centrifugation. Preparation of sufficient amounts of phosphopeptide enrichment tips can be done within a few hours and allows the processing of up to 24 samples (depending on the number of positions in the rotor) in parallel.

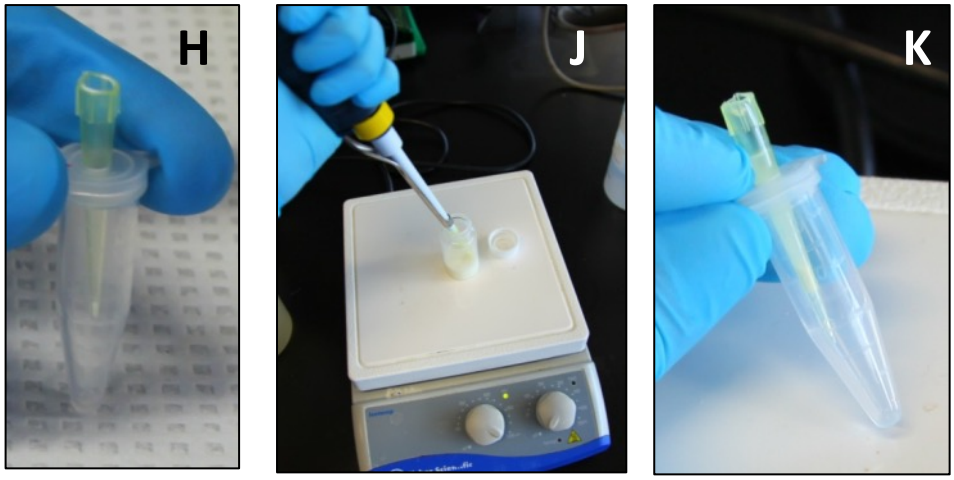

Figure 1.9. *Loading of spin tip with titanium dioxide beads for phosphopeptide enrichment.*

H) Placment of the spin tip containing one extraction disc into 1.7mL Eppendorf tubes. J-K) Pipetting of titanium dioxide homogenate into the spin tip.

Following the preparation of spin tip columns, conditioning of the stationary phase with the mobile phase used throughout the enrichment procedure is necessary, as for most chromatographic applications. Generally, the mobile phase contains 50% acetonitrile, 2% formic acid (FA), and lactic acid, which prevents the binding of nonspecific, negatively charged peptides [194]. After phosphopeptide binding and several wash steps, elution of phosphorylated peptides is achieved with an aqueous solution of neutral pH containing excess free phosphate molecules that simply replace the phosphopeptides on the metal oxide phase. These

phosphopeptides are subsequently retained by the hydrophobic frit at the bottom end of the spin column, which allows for desalting and recovery of the phosphoproteome. Enriching phosphopeptides on micro-scale columns requires consistent amounts of material loaded onto the stationary phase in order to not overload the metal oxide material, which could result in the loss of low affinity binders such as mono-phosphorylated peptides or phosphopeptides of basic nature. Considering that around 1% of the protein material is phosphorylated, 5mg of protein would result in an amount of phosphopeptides that is equivalent to 50µg of protein material, sufficient for further sample preparation prior to mass spectrometry analysis. All amounts of peptides are referred to as equivalents to protein material, as the quantification of such small amounts of peptides prior to LC-MS analysis would result in the loss of a large proportion of the sample and, therefore, is not feasible. Empiric experience has shown that the injection of roughly 1µg of peptides (equivalent to 1µg of proteins) is best for mass spectrometry-based analysis of highly complex samples. Accordingly, 2-5mg of starting material is the standard amount of protein that is used for the affinity enrichment of phosphopeptides throughout the studies presented later on. Excess amounts of phosphopeptides had to be generated as the enriched phosphoproteome samples still are of extremely high complexity and need further fractionation to increase the depth of analysis.

1.4.4 Chromatographic separation of peptides

Chromatographic separation of chemical species is a technique discovered in the late nineteenth century when Schoenbein and Goppelsroeder experimented with the separation of dye mixtures into their pure forms on filter papers [195]. In chromatography, mixtures are dissolved in a fluid phase (mobile phase) and are separated by being flushed over columns of a solid phase (stationary phase). Unique physical properties of different chemical species lead to different travel times over the stationary phase, resulting in separation of the components of a mixture [196]. Such separation can be used to identify or purify one or more chemical species for analytical or practical purposes. Chromatography has much advanced since its first application to separate dyes from plants [197], and, at present, is widely used to aid the identification and quantification of trace materials in various samples such as soils, blood or food [198, 199] and

the purification of larger quantities of molecules, such as insulin, which is used to treat diabetes [200].

In a shotgun proteomics workflow, chromatography is used for the separation of the vast number of peptides present in the proteome digest and has been found to be of great help in decomplexifying samples [201]. Decomplexification of samples, in other words, the presence of less chemical species at the time the sample enters a detector, allows for better analytical performance of mass spectrometers that are highly limited in the number of analytes (peptides) they can analyze at a given time [202]. Different types of stationary and mobile phases can be used to separate peptides or proteins by different types of chemical properties. In laboratory practice, two types of chromatography have emerged for peptide separation – reverse phase chromatography and ion exchange chromatography. In reverse phase chromatography, peptides are separated based on hydrophobicity [203, 204] while, in ion exchange chromatography, separation occurs based on the peptide charge state [205, 206]. As both physicochemical properties are of very different nature, the two separation technologies can be considered orthogonal and thus, are applicable to combination [207]. In a shotgun proteomics workflow, ion exchange chromatography is often performed using cation exchange materials to fractionate peptide samples into several fractions prior to their injection onto a reverse phase liquid chromatography system which operates in hyphenation to a mass spectrometer [208]. This exact setup is used in all studies of this thesis and its application is expanded upon in the following paragraphs.

1.4.4.1 Offline strong cationic fractionation

For shotgun based proteomics, where up to hundreds of thousands of different peptides are generated, efforts must be made to reduce sample complexity. Indeed, the identification of low abundance peptides or proteins is amongst the biggest challenges in proteomics research, making the sensitivity and speed by which mass spectrometers sequence peptides the major limitation [167]. Nonetheless, advances in peptide identification through the use of chromatographic separation, which de-complexifies samples prior to LC-MS analysis improve the depth of the proteome [201]. This so-called offline fractionation of samples increases the number of low abundant peptides identified in highly complex peptide mixtures while drastically increasing the

time of analysis. Accordingly, offline pre-fractionation is of high demand in studies that aim for the systems-wide analysis of proteomes [208].

As described by *Lenz and Urlaub* (2014), offline fractionation is nothing more than chromatographic separation of all peptides present in a sample and successive collection of sample fractions that each contain their unique pool of peptides. The analysis of a smaller pool of peptides per LC-MS run grants more time to the mass spectrometer to sequence low abundant peptides and results in higher sensitivity [209]. In this thesis, cation exchange chromatography was used for the separation of peptide and phosphopeptide samples prior to LC-MS analysis. To allow for maximum sample throughput, parallelisation of fractionation was achieved by using spin tip columns, similar to the ones used for the enrichment of phosphopeptides. Spin tips were packed with strong cation exchange (SCX) material and peptides were bound to the stationary phase under acidic conditions. This SCX material contains highly acidic sulfonyl groups, which are deprotonated even under acidic conditions (pH>0) and allow for electrostatic binding of positively charged peptides [210]. Separate fractions are generated through step-wise elution of peptides with buffers of increasing ionic strength, resulting in the elution of negatively charged peptides prior to neutral and more positively charged species. Buffers are applied onto the stationary phase and are flushed through the column during centrifugation, making each fraction the result of a single centrifugation step. Individual fractions are collected and dried under a vacuum. Importantly, phosphopeptides are especially well suited for separation by SCX due to the negative charge added by each phospho group, resulting in a larger variability of charges amongst the pool of tryptic peptides compared to a set of unmodified peptides [211]. In practice, the resolution of spin tip columns is sufficient enough to generate more than 6 fractions for each peptide sample, permitting the analysis of a large dynamic range of peptides [212].

1.4.4.2 Reverse phase chromatography prior to mass spectrometry analysis

Reverse phase (RP) chromatography coupled with mass spectrometry is widely established for the identification and quantification of peptide species. The terminology ‘reverse phase’ implies that peptides are separated based on hydrophobicity using a hydrophobic stationary phase. The mobile phases used are binary mixtures of water and organic solvent, each containing small amounts of organic acid to protonate peptides [213, 214]. Combining reverse phase separation and mass spectrometry maximizes the number of peptides that can be identified by minimizing the number of species the mass spectrometer has to sequence at a given time. Separation of peptides prior to analysis by MS is performed to 1) not oversaturate the detector and 2) provide more time to accumulate and sequence a given peptide [214]. Accordingly, the quality of reverse phase separation is of high importance. Physicochemical parameters that influence separation performance are longitudinal diffusion of particles, mass transfer kinetics between the stationary and mobile phases, as well as pathways molecules can follow within the column [215]. As chromatographic separation can be imagined as multiple extractions, the performance of chromatographic columns is measured in plate heights, describing the number of theoretical extractions occurring during the length (or height) of a column. Smaller plate heights imply better separation and strongly depend on the flow rate of the mobile phase, which directly influences longitudinal diffusion and mass transfer kinetics. Channeling of molecules through the column packing, a factor that negatively influences plate height, is determined only by the properties of the packing material, such as its porosity and particle size [198]. The relationship of plate height and flow rate is well described by the van Deemter equation and is of importance for practical optimization of chromatography parameters (Figure 1.10) [216].

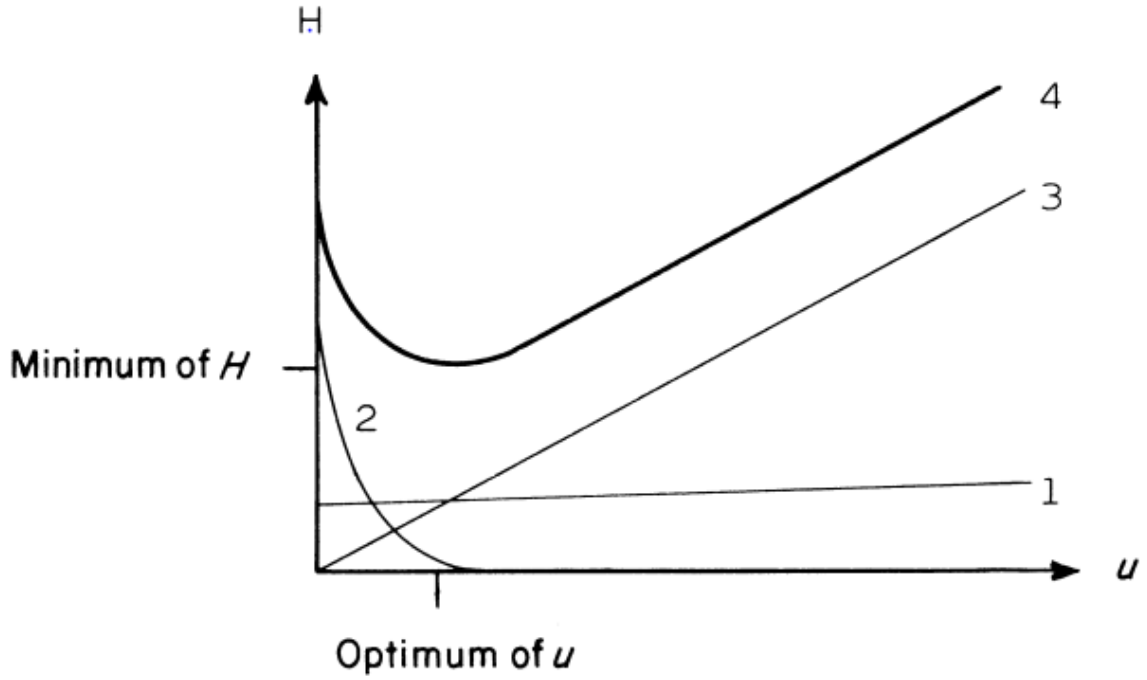

Figure 1.10. Van Deemter curve.

1. Flow channel distribution coefficient. 2. Longitudinal diffusion coefficient. 3. Mass transfer component. 4. Resulting theoretical Van Deemter curve. Figure adapted from reference [217].

Accordingly, the use of smaller particles and optimized flow rates is beneficial, but results in increased backpressure, requiring compatible high performance liquid chromatography (HPLC) systems [218]. As reverse phase stationary and mobile phases are widely used for peptide analysis, high quality chromatography systems are cost effective to operate and easy to implement. Furthermore, reverse phase chromatography is perfectly suited for mass spectrometry, as volatile mobile phases cause minimal interferences with the mass spectrometer [213, 214]. Noteworthy, however, is the strong correlation between peptide length (mass) and hydrophobicity, making the mass spectrometer (separator and detector) and reverse phase chromatography not be perfectly orthogonal, resulting in co-elution of peptides with similar masses [219]. Nonetheless, reverse phase LC is universally used for peptide separation prior to mass spectrometry analysis and has proven to generate high quality separation of analytes. To guarantee high performance chromatography under constant flow, nano-HPLC systems that operate at nano-liter flow rates are used. Low flow rates increase sensitivity and minimize the limit of detection/quantification of peptides, by increasing the proportion of eluting molecules

that can be ionized [220]. Details about the ionization of analytes for mass spectrometry and the corresponding liquid-gas interface are discussed later on, in the section ‘Ionisation’.

Reverse phase columns suited for LC-MS can be prepared in house by packing capillaries of lengths between 15 and 20cm with octadecyl carbon chain (C18)-coated silica particles [221]. Piston pump HPLC systems used to operate these columns are best to generate reliable flow rates and stable operation of mass spectrometers [222]. In laboratory practice, peptides are dissolved in water under acidic conditions, injected onto the column and are successively eluted with a gradient of increased organic mobile phase. During the course of multiple injections of samples from cohering experiments, variations in elution profiles and retention times of peptides constantly have to be evaluated with peptide standards to assure maximum performing liquid chromatography [223]. Due to the high sample complexity, injection times of shotgun proteomics samples generally vary between 70 and 250 minutes, depending on the depth of peptide coverage demanded. Gradient times of around 120 minutes are found to provide optimal balance between average peak width of a peptide elution peak, number of co-eluting peptides and feasible analysis time, resulting in acceptable coverage of the proteome [224]. Altogether, optimized RP chromatography parameters and a stably operating system are of key importance for a successful large-scale shotgun proteomics experiment [225].

1.4.5 Mass spectrometry

Mass spectrometry analysis is the determination of mass to charge ratios (m/z) of gas phase ions [226]. Any aperture capable of measuring mass to charge ratios is comprised of a sample inlet, an interface at which gas phase ions form, the mass analyzer, in which ions are separated depending on m/z, and a detector that detects gas phase ions [227]. Mass spectrometric data are processed with the aid of a computer and sophisticated analysis software. Data are typically visualized in the form of mass spectra. A general scheme describing mass spectrometry analysis is presented in Figure 1.11.

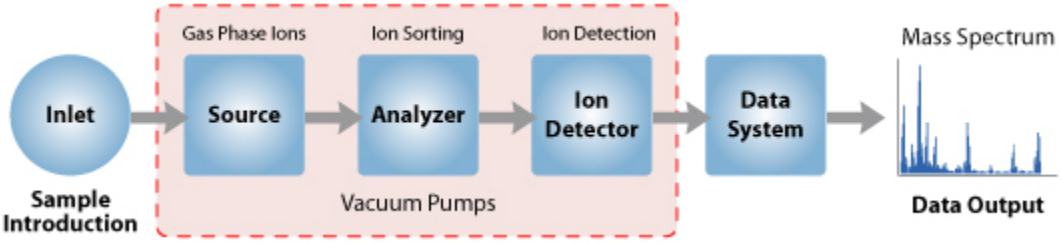

Figure 1.11. *General scheme of a mass analyzer.*

Figure adapted from reference [227].

Mass spectrometry was born in the late nineteenth century when, in 1899, Wilhelm Wien constructed a device that separated anode rays based on their mass to charge ratio [228]. Judith Jarvis Thompson and Francis Aston successively improved mass spectrometers and built the fundamentals of today's mass analysis [226, 229]. The following sections describe the general principles of mass spectrometry, including brief historical reviews, and mainly exemplify the newest mass spectrometry technology used for proteomics analyses.

1.4.5.1 Ionisation techniques

In mass spectrometry, the mass to charge ratio of gas phase ions is measured. Molecules are charged and dispersed into the gas phase in the ion source of a mass spectrometer, where gas phase ionization occurs. Three major ionization techniques have emerged during the development of modern mass spectrometry, atmospheric pressure chemical ionization (APCI), electrospray ionization (ESI) and matrix-assisted laser desorption ionization (MALDI). ESI and MALDI are soft ionization techniques [230], whilst ionization in APCI sources occurs during harsher conditions, leading to higher chances for fragmentation of labile molecules [231]. Soft ionization is preferred for the analysis of labile molecules and complex mixtures, as in source fragment ions, interfere with sample components. Furthermore, peptide and protein sequencing are based on controlled fragmentation, prohibiting the use of harsh ionization conditions, in most cases. MALDI and ESI, the most frequently used ionization techniques in proteomics, both have unique areas of application. MALDI is used for the analysis of mostly crystallized stationary samples with a light-absorbing matrix, while ESI is best suited to generate ions at the liquid gas phase interface, as present in liquid chromatography mass spectrometry (LC-MS) [230]. During this study, ESI has been used exclusively and is described in detail below.

Electrospray generates gas phase ions after electrisation of the eluting liquid stream from the chromatographic column. At the end of a chromatographic column, a voltage varying between 500 and 4500 V, depending on the diameter and composition of the eluting liquid stream, is applied and induces the formation of ions [232]. At the liquid to gas transition zone, the formation of a fine spray with cone geometry represents the presence of charged droplets, as described by Goeffrey Taylor [233]. If flow rates greater than 5uL/minute are used for chromatography, a nebulizing gas can feed into the solvent flow to aid the formation of the electrospray. While the electrospray mist travels towards the mass spectrometer, charge concentration gradually increases inside the liquid droplets due to solvent evaporation. Native gas phase ions have been suggested to then form due to sequential fission of droplets, caused either by successive evaporation of the solvent, as proposed by Dole [163], or the explosion of highly charged droplets due to the increasing electric field, as suggested by Thomson and Irbarne [234, 235]. In both cases, naked charged ions are formed at atmospheric pressure and, as a result

of their electric potential, are accelerated to the mass analyzer. A graphical illustration of these processes occurring during electrospray ionization is given in Figure 1.12 [198].

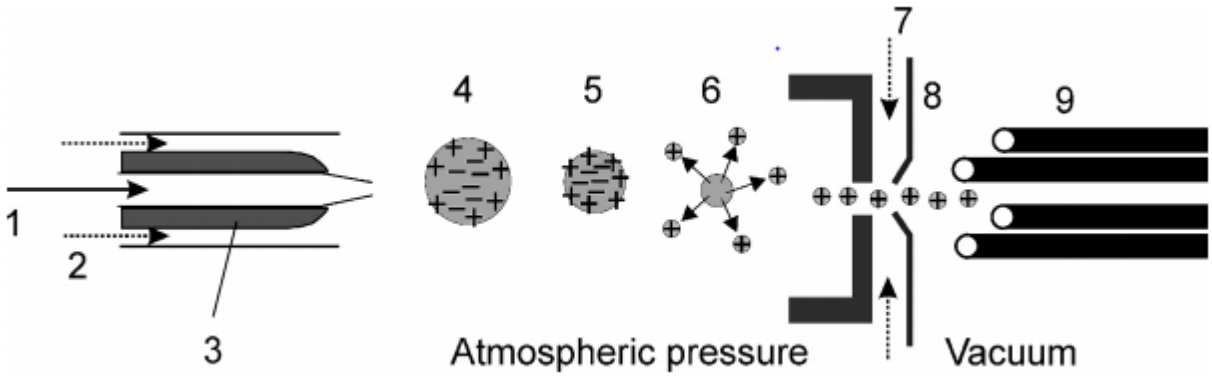

Figure 1.12. HPLC-MS interface for ESI.

1. HPLC column; 2. Nebulizing gas; 3. High voltage; 4. Charged droplet (drawn too large); 5. Evaporation; 6. Coulomb explosion; 7. Drying gas; 8. Skimmer; 9. Quadrupole. Figure adapted from reference [217].

Most commonly used for the analysis of peptides is electrospray ionization in positive mode, where a positive voltage that is applied at the liquid phase causes the formation of protons [236]. Protons then protonate eluting molecules at basic sites, resulting in charged species that can be described with the general formula $[M+nH]^{n+}$. As anticipated from this formula, ions formed in an electrospray source can be multiply charged, depending on the number of basic sites present on the analyte. This allows for the analysis of large molecules at low mass to charge ratios in mass spectrometers with limited m/z scan ranges. Proteomics analyses have greatly benefited from the generation of multiply charged ions by electrospray ionization and are of utmost importance for peptide sequencing in tandem with mass spectrometry analyses [237, 238].

1.4.5.2 Tandem mass analysis (MS/MS)

Tandem mass analysis is a technique used to resolve the molecular structure of analytes. In tandem mass analysis, mass spectra of ions and their fragmentation products are sequentially acquired. This can take place in several hyphenated mass analysers, or, for the case of ion trapping devices, in a single mass analyzer [239]. Most frequently, a mass spectrum of non-fragmented ions, the parent ion spectrum, is acquired first. The ion of interest is subsequently selected, fragmented and analyzed in a second mass spectrum, generating a spectrum of product

ions [240]. The subsequent acquisition of parent and product ion spectra is referred to as MS/MS acquisition. Acquisition of n time fragmentation of fragments is referred to as MS^n and can be executed in ion trap devices. MS^n is used in rare cases when detailed structural information is required or background contamination needs to be filtered out for increased quantification quality [241]. MS/MS acquisition is primarily used for peptide analysis. It is performed by first scanning all co-eluting ions in a full MS (MS^1) scan, the selecting ion species of interest and fragmenting them into product ions, from which the peptide sequence can be determined. The product ion spectrum is referred to as the MS^2 or the MS/MS spectrum [242]. Ions can be selected in a data-dependent (DDA) or data-independent (DIA) format. In DDA, ion species of interest are selected for MS/MS acquisition from the MS^1 scan. In between the acquisition of MS^1 spectra, a pre-defined number of the most abundant ions in the MS^1 spectra that show peptide characteristics are selected for fragmentation [243]. This type of data collection is termed "Top-n", as n peaks are selected for fragmentation prior to the next full MS measurement. Time-constricted exclusion lists of already fragmented ions are further generated to limit re-fragmentation of ions. In contrary to DDA, DIA of parent ions is performed by step-wise fragmentation of all ions eluting at a given time and is commonly used if highly reproducible data are required [244]. Each of these methods, DDA and DIA accommodate their unique advantages, whilst DDA is the most frequently used data acquisition method for discovery proteomics studies. Peptide and phosphopeptide data in this thesis have all been collected using data-dependent acquisition, mostly because the Orbitrap mass analyzers used throughout all experiments appear to be best suited for DDA.

1.4.5.2 Ion fragmentation

Peptide sequence information can be obtained through ancient methods, such as the Edman degradation, which is very time consuming, or within milliseconds from product ion spectra. To gain structural information about the amino acid sequence of a peptide using tandem mass spectrometry, controlled dissociation of peptides must occur at the peptide bonds to be able to read off the peptide sequence from the fragment ions in the MS/MS spectrum. The two most frequently used fragmentation methodologies are collision-induced dissociation (CID) and higher energy collisional dissociation (HCD). In both cases, fragmentation occurs due to

collision of ions with a carrier gas at low pressure [245, 246]. While CID fragmentation is based on ion trap instruments, HCD-induced fragmentation is performed in specifically designed trap cells that allow for later identification of ions in high resolution Orbitrap mass analyzers. It has been observed that HCD fragmentation generates better defined product ion spectra, especially in the case of peptides harboring labile modifications, such as phosphorylation. While HCD had a slow start due to longer fragmentation times, it has emerged as the primary method of fragmentation for Orbitrap-based peptide analysis [247].

1.4.5.3 Peptide sequencing

Peptide sequence information is retrieved from the mass to charge values of fragment ions resulting from peptide backbone fragmentation. Dissociation of covalent bonds through collisions with gas molecules can occur at amide bonds, as depicted in Figure 1.13 [248]. Peptide sequences are depicted from the N-terminal, on the left hand side, to the C-terminal, on the right hand side. Fragment ions that are generated correspond to either the C-terminal end of the peptide, termed as x, y and z ions, or the N-terminal end, termed as a, b and c ions [249]. Ions are numerated based on their distance, measured in numbers of amino acids, from either the C-terminus or N-terminus for the respective ion species. Identification and assignment of these ion species in a mass spectra is the primary information needed to obtain the peptide sequence [250].

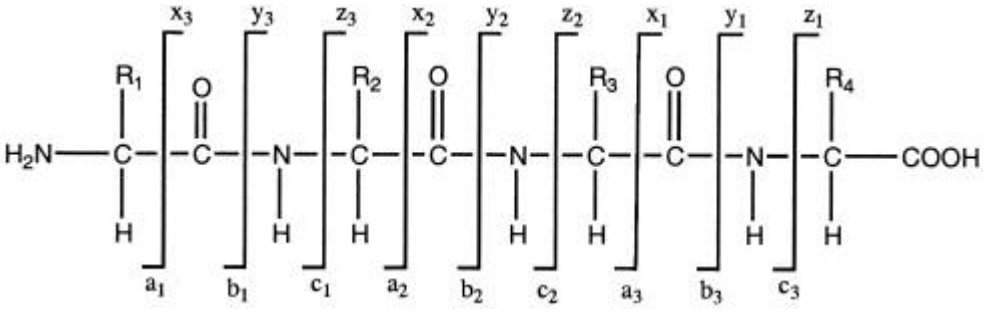

Figure 1.13. Peptide fragment ion nomenclature.

Figure adapted from reference [248].

Upon HCD and CID collision, acylium ions (b) and ammonium ions (y) are the mostly frequently observed ion species. Many other ions species, including neutral losses and

fragmentation of amino acids themselves, can be observed, depending on the collision energy used [251]. Thus, collisional energy has to be optimized for every mass spectrometer to obtain the highest proportion of peptide backbone fragmentation. As the exact mass of the parent (precursor) ion is known for a given MS/MS ion spectrum, mass resolution for tandem mass analysis is of less importance as for the acquisition of MS^1 spectra. Fragmentation spectra, therefore, are acquired in most types of mass analysers including the Orbitrap, Ion trap and time of flight (TOF) mass analyzer.

1.4.5.4 Localizing and identifying phosphosites

Phosphate residues add +80Da to the total mass of the corresponding non-phosphorylated peptide, making the determination of the number of phosphorylation sites on a peptide fairly easy through collation of parent ion masses with theoretical peptide masses from in silico digestions of appropriate proteomes [252]. Phosphopeptides are sequenced in the same way non-modified peptides are sequenced, mostly by HCD and CID fragmentation [253]. A typical phosphopeptide product ion spectra is depicted in Figure 1.14 [254]. The localization of phosphopeptides on the peptide backbone requires the presence of fragment ions containing phosphate groups. Unfortunately, the labile phosphor ester bond tends to fragment during gas phase reactions, resulting in neutral loss of phosphate, suppressing the abundance of phosphate-containing product ions [255]. Several approaches have been suggested to improve phosphopeptide localization confidence, including the creation of spectral databases and a combination of different fragmentation techniques [247, 256-258].

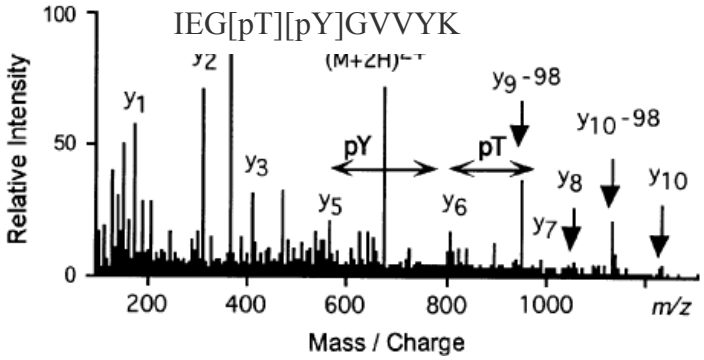

Figure 1.14. Example of a phosphopeptide product ion spectra.

Spectra depicts fragments that correspond to the phosphorylated ions. Figure adapted from reference [254].

At present, however, the acquisition of phosphoprotoemics data does not differ much from that of other proteomics data, mostly because the gain in spectral information from improved fragmentation methods would result in a decrease in the number of identified peptides, due to longer acquisition times [259]. Still, up to 50,000 phosphopeptides have been mapped in the scope of large-scale phosphoproteomics experiments conducted with conventional HCD fragmentation, showing that the quality of phosphoproteomics data acquisition has reached that of regular proteomics studies [260].

1.4.5.5 Mass analysers

Mass analyzers are the modules of a mass spectrometer that are capable of assigning charged ions to their mass to charge value [261]. Several types of mass analyzers have been developed, of which the most frequently used for proteomics analysis are the Quadrupole (Q) and Linear Ion Trap (LIT), the Time of Flight (TOF) analyzer, Fourier-Transform Ion Cyclotron Resonance (FT-ICR)-based instruments and the Orbitrap [262]. The most important parameters defining the characteristics of mass analyzers are resolution, sensitivity, mass to charge range, mass range, dynamic range and scanning speed. Resolution (R) is defined as the ratio of the measured mass (m) and the peak width (Δm) at 50% of the maximum peak height and can be written as $m/\Delta m$ [263]. Higher resolution allows for better resolving power of adjacent peaks at a given mass, making the resolution capabilities of a mass analyzer a primary characteristic of high importance for the definition of molecular species. Also, the trend curve by which resolution decreases with increasing mass is an important factor to consider if the analysis of high m/z species is anticipated [264, 265]. Sensitivity is the amount of ions detectable whereas mass to charge range is the range over which m/z values can be reported [263]. Mass range is simply the range of masses of molecular species detectable. Dynamic range is the ratio of the smallest to the largest detectable signal [263]. Scanning speed, which is one of the more important parameter for the analysis of proteomics samples, is the number of scans the analyzer can acquire in a given time and is usually reported as a frequency in Hz [266].

For the analysis of complex peptide samples, high resolution to accurately define ion species, a large dynamic range to detect low and highly abundant peptides simultaneously and a high scanning speed to analyze as many peptides per time window as possible are the main factors that determine the suitability of a given mass analyzer [262, 267]. Orbitrap mass analysers and linear ion traps, which can be coupled with Orbitraps through Quadrupoles, have been used throughout this thesis and are described in more detail in the following sections.

1.4.5.5.1 Quadrupole

The Quadrupole is an ion filtering device that comprises of a square array of four conduction rods and is placed between an ion source and an ion detector [268]. Ions are separated based on their m/z-dependent, stable trajectories through oscillating electric fields. Oscillating electric fields are generated by concomitantly applying radio frequency (RF) and direct current (DC) potentials to opposing pairs of rods. The resulting potentials are $-(U+V_0\cos(\Omega t))$ and $+(U+V_0\cos(\Omega t))$, where U is the DC, and $V_0\cos(\Omega t)$ is the RF component, as illustrated in Figure 1.15 [269].

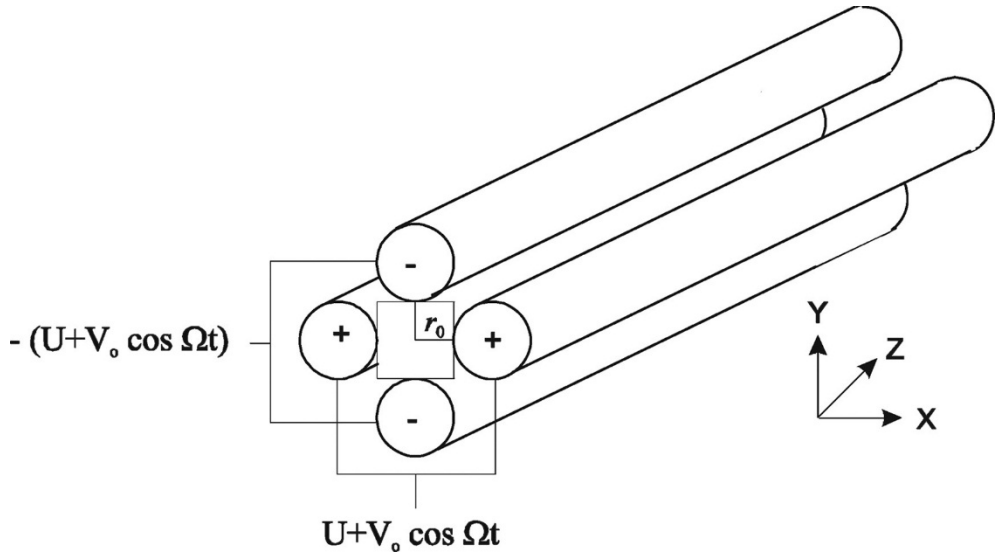

Figure 1.15. Schematic presentation of a Quadrupole mass filter.

Figure adapted from reference [269].

The corresponding electric fields influence the trajectories of ions that travel through the quadrupole, letting only ions with a specific m/z value pass through the quadrupole. Ions that are not traveling on stable trajectories are neutralized on the conduction rods, leaving only those that pass the ion filter to reach the detector. Variation of the electric potentials allows for scanning of ions with different m/z values. The m/z selectivity can be controlled by adjusting the DC/RF ratio, but is limited to resolutions of around ~3000, defining Quadrupoles as low resolution instruments [270]. An advantage of these instruments is that the duty cycle is nearly 100%, as no delay or dead times occur when scanning through the same or different m/z ranges. This allows for high scan rates at minimal loss of ions, making Quadrupoles the basis of very sensitive and fast mass analyzers [271]. Accordingly, Quadrupoles are well suited for the analysis of samples with low complexity, and as ion transmission tubes that are capable of guiding specific subsets of ions through the mass spectrometer. The latter finds unprecedented use in tandem mass analysis, where only ions with selected m/z are intended to be fragmented and analyzed in an MS/MS spectrum [272]. For the latter purpose, Quadrupoles are combined with other mass analyzers including Orbitraps and Ion traps [273, 274].

1.4.5.5.2 Linear Ion Trap (LIT)

Linear ion traps are devices capable of trapping, accumulating and sequentially releasing ions to a detector. Quadrupole rods focus the ions radially while a static electric potential confines ions axially, allowing for injection and accumulation of ions [275]. Ions can be sequentially ejected from the trap by varying the RF frequency [276]. Furthermore, ion traps are capable of fragmenting ions of desired m/z values by ejecting all but the desired ions and subsequently increasing their kinetic energy. The kinetic energy of ions within the trap is increased through the application of a resonance voltage, inducing strong radial oscillation of ions. The higher kinetic energy of ions then results in fragmentation due to collisions with carrier gas molecules inside the ion traps [277]. The most frequently used gas is nitrogen. A fragment ion spectrum (MS/MS) can then be acquired by successive ejection of ions and detection by high voltage dynodes. While a single linear ion trap is capable of performing MS^n experiments in which ion species can be sequentially selected and fragmented, their use in proteomics is often coupled to high resolution

mass analysers that allow for parallel acquisition of high resolution MS^1 spectra and low resolution MS/MS spectra [278].

1.4.5.5.3 Orbitrap

The Orbitrap mass analyzer is the latest addition to the set of high performance mass analyzers and has been commercially available since 2005. It has been developed with the motivation to build a high performance mass analyzer that is more accurate than ion traps, more sensitive than time-of-flight instruments and faster and more compact compared to conventional FT-ICR instruments [273]. Orbitraps are ion trapping devices in which ions oscillate around an inner electrode within an electric field generated by two symmetrical outer electrodes. The discovery that trapped ions can orbit around linear inner electrodes on stable trajectories dates back to 1923, when KH Kingdon first described a cylindrical aperture with a centered wire, capable of trapping ions [279]. *RH Perry et al. (1981)* picked up on Kingdon's studies and developed devices that can successfully trap laser-generated ions [280, 281]. The breakthrough was achieved later by *Makarov et al. (2000)*, who described Orbitrap cells with spindle shaped inner electrodes and symmetrical outer electrodes, as depicted in Figure 1.16 [282]. This cell was shown to allow for successful trapping of ESI-generated ions that were injected from a bend Quadrupole trap [283]. Makarov further described the generation of m/z resolved spectra by fast Fourier transformation. Mass to charge resolved spectra can be acquired in Orbitrap cells, as ions with the same m/z isochronally oscillate along the curved inner electrode. This results in the separation of ions with similar m/z, allowing for the detection of an image current on the outer electrodes, which can be transformed into a mass spectrum through Fourier transformation [284]. This allows for fast acquisition of high resolution mass spectra with high mass accuracy, good sensitivity and dynamic range. However, as for all trapping devices, the number of ions that can be injected into the trap is limited. Therefore, careful control of the size of ion packages injected into the Orbitrap analyser is necessary and can be achieved with the curved RF-only Quadrupole trap, named C-trap [285].

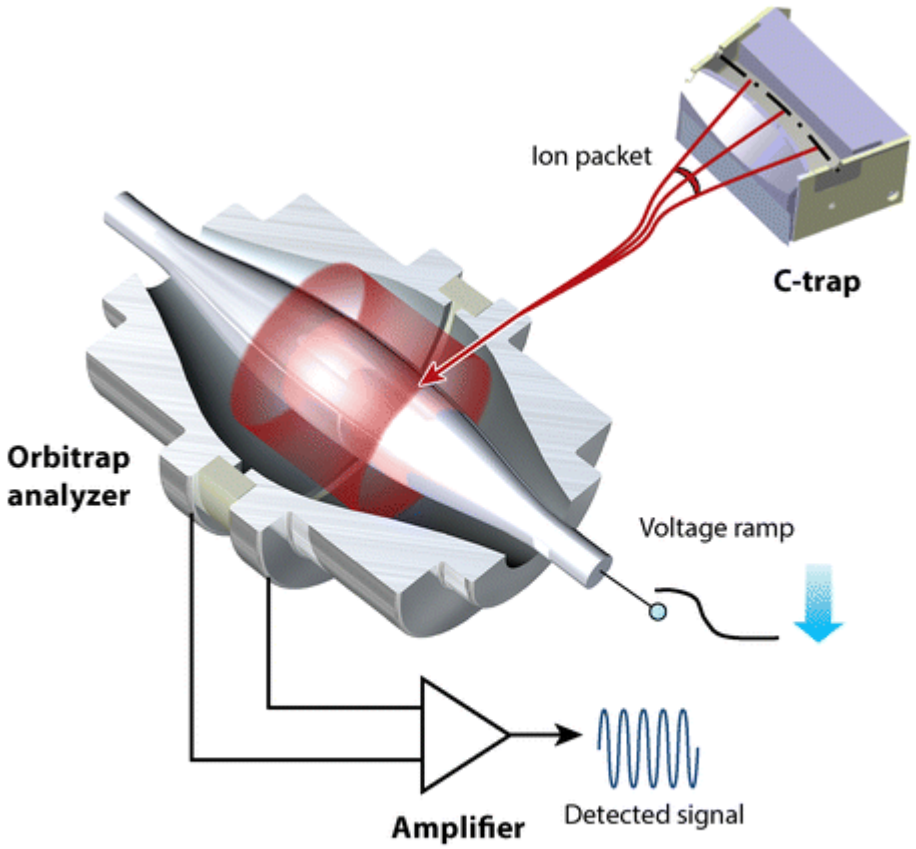

Figure 1.16. Schematic presentation of a bent linear ion trap (C-trap) hyphenated to an Orbitrap mass analyzer. Figure adapted from reference [273].

As the Orbitrap mass analyzer is dependent on the injection of ions, the duty cycle of these instruments is determined by the time necessary to trap and inject ions and the time it takes to acquire a spectrum. It is of importance to know that higher resolution mass spectra require longer acquisition times because spatial separation of ions with similar m/z is time dependent [285]. This characteristic has been a major limitation of early Orbitrap instruments used for discovery proteomics and metabolomics, as highly complex mixtures require long duty cycles. However, recent developments have enabled Orbitrap-based instruments to acquire mass spectra at up to 23 Hz and faster at resolutions ranging from 15,000 to 60,000 (at m/z = 200) [286]. Two Orbitrap instruments, the Thermo Fisher Orbitrap Q-Exactive and the Thermo Fisher Orbitrap Fusion, were exclusively used for proteomics analysis in this thesis and are described in more detail below.

1.4.5.5.4 Thermo Fisher Q-Exactive

The Q-Exactive is a benchtop mass spectrometer with a standalone Orbitrap mass analyzer. It is available with a standard or ultra-high field Orbitrap. The newer version of the instrument, with a ultra-high field Orbitrap, is referred to as Q-Exactive HF. The Q-Exactive series of Orbitrap instruments can be coupled to ion sources compatible with Nano and micro flow liquid chromatography systems. Ions are funneled in an S-lens and are guided through a Quadrupole mass filter into a higher energy collision induced dissociation (HCD) cell, where peptides can be fragmented. Injection into the Orbitrap is carried out from the C-trap [286]. An illustration of the geometry of the Q-Exactive mass spectrometer is shown in Figure 1.17 a.

Hybridisation of a Quadrupole and an Orbitrap enables tandem mass analysis, where either all co-eluting ions pass the Quadrupole prior to the acquisition of a MS^1 spectrum or a specific ion with a set m/z is filtered by the Quadrupole, fragmented in the HCD cell and subsequently analyzed in an Orbitrap MS/MS scan. This setup allows for the generation of high resolution MS^1 spectra and lower resolution MS/MS spectra, both from the Orbitrap cell. The scanning speed has been maximised by allocating most of the duty cycle time to the accumulation and fragmentation of ions parallel to the acquisition of mass spectra. As depicted in Figure 1.17 b, the Orbitrap mass analyser is almost constantly acquiring mass spectra, with very short transition times needed for injecting ions [287]. Full MS (MS^1) spectra, which typically are measured at high resolution, require much longer analysis times compared to MS/MS data generation, making the acquisition of 10-20 MS/MS spectra per full MS scan necessary to maximise the number of peptides identifiable from complex mixtures. In a regular peptide sequencing experiment, the Q-Exactive instruments achieve up to 12 Hz at resolving powers of 17,500 (corresponding to a peak at m/z = 400) for MS/MS and around 1Hz at resolving powers of 70,000 for MS^1 spectra [288]. The improved Q-Exactive-HF is able to acquire peptide sequencing data at up to 23Hz at resolving powers of 15,000, allowing for the identification of 4400 proteins from cell digests within one hour of analysis time [287].

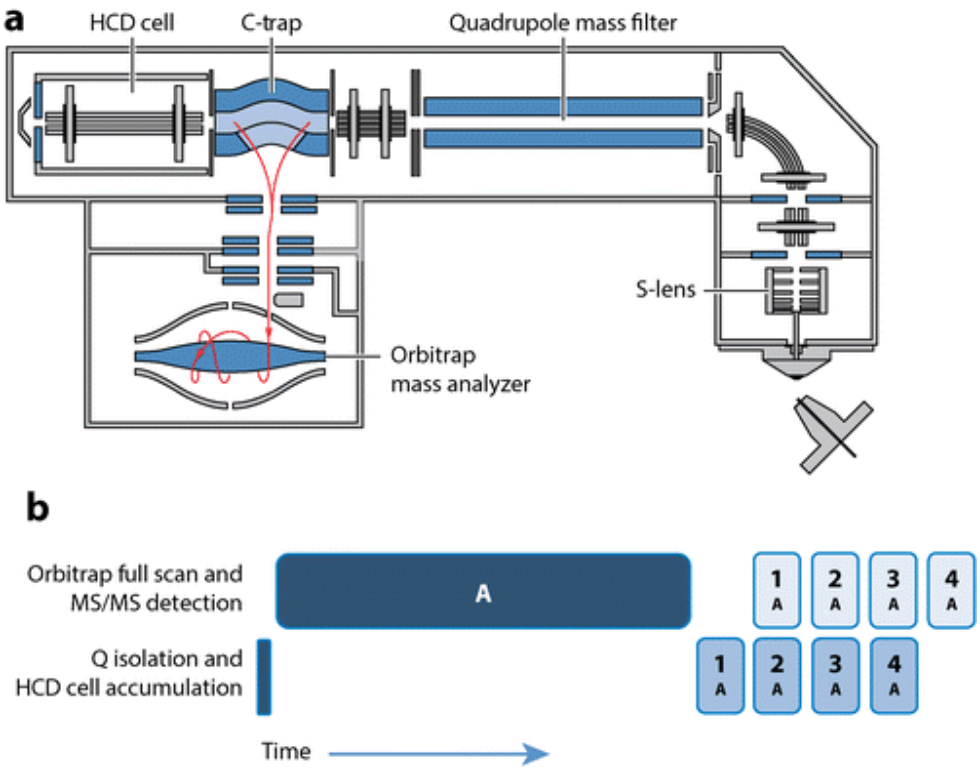

Figure 1.17. *The Orbitrap Q-Exactive.*

a) Geometry of the Orbitrap Q-Exactive. b) Diagram of parallel data acquisition. Figure adapted from reference [273].

While Q-Exactive instruments are generally designed for peptide analysis, small intact proteins can be analyzed as well [289]. This type of Orbitrap instrumentation is also frequently used in metabolomics research [290]. In the scope of this thesis, the Orbitrap Q-Exactive and Q-Exactive-HF have been used for the analysis of phosphoprotoemics and proteomics samples. Data acquisition methods were based on the above-described methodologies.

1.4.5.5.5 Thermo Fisher LTQ Orbitrap Fusion

The Orbitrap Fusion instrument is one of the most recent generations of Orbitrap-based hybrid mass spectrometers. The Orbitrap Fusion combines a Quadrupole mass filter, an Orbitrap and a Linear Ion Trap, enabling fully parallelized data acquisition [291]. As depicted in Figure 1.18 a, the Orbitrap Fusion contains the Quadrupole mass filter before the C-trap, which is orthogonally coupled with the Orbitrap mass analyzer, similar to the arrangement in the Q-Exactive instruments. In line with the C-trap, an HCD fragmentation-compatible ion routing multipole is

coupled to a LIT cell. Precursor selection can be performed in either the Quadrupole mass filter or at any MS^n level in the Ion Trap. Fragmentation can be done using CID in the Ion Trap, HCD, or with electron transfer dissociation (ETD), a technique mostly applied for the fragmentation of larger, highly charged molecules, such as proteins [292]. The instrument's geometry allows for highly diverse types of MS data acquisition that go far beyond regular shotgun proteomics applications. Of benefit for shotgun proteomics is the greatly improved duty cycle rate at which peptides can be sequenced, as HCD-type fragments can be measured in the ion trap parallel to the acquisition of high resolution MS^1 scans. This type of parallelized data acquisition, as depicted in Figure 1.18 b, becomes most handy when time-consuming high-resolution spectra (R>120.000 @ 200m/z) are intended to be acquired.

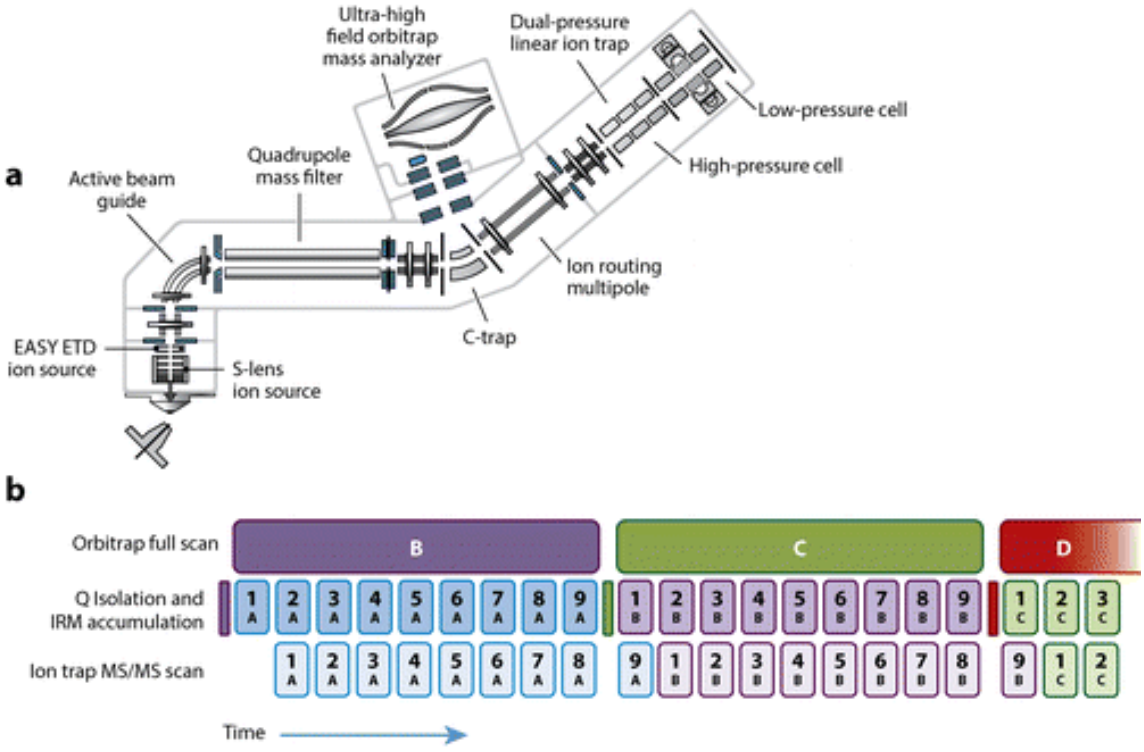

Figure 1.18. The LTQ Orbitrap Fusion

a) Geometry of the LTQ Orbitrap Fusion. b) Diagram of parallel data acquisition. Figure adapted from reference [273].

Despite the outstanding flexibility of the Orbitrap Fusion mass spectrometer, practice has shown that both the Orbitrap Fusion and the Orbitrap Q-Exactive perform equally well for regular shotgun proteomics approaches [288, 291]. Nonetheless, the Orbitrap Fusion is of great benefit for experimental designs, where specific quantification strategies, such as tandem mass tag

(TMT) labeling [293] or neutron encoded stable isotope labeling, are in use [294]. As mostly standard MS^1 quantification methodologies were applied in the studies published as part of this work, the Orbitrap Fusion and the Orbitrap Q-Exactive have been used in a similar fashion and were considered to collect data of equal quality.

1.4.5.6 Quantification of proteins and peptides

Accurate and precise quantification of proteins and peptides has become of major importance for the understanding of complex biological systems. Small changes in the abundance of proteins or post-translational peptide modifications can cause drastic changes in cell and tissue dynamics. At present, the largest number of quantifiable proteins is achieved using shotgun proteomics approaches [295]. Thus, peptide abundance is the currency of protein and peptide quantification, requiring their accurate determination. The study of biological systems is mostly achieved by comparison of stimulated and non-stimulated systems where, in the best case, many stimulations can be compared in a single mass LC-MS run.

Quantification methodologies are grouped into four different classes: metabolic labeling, chemical labeling, spiked in peptides and label-free approaches [296]. Corresponding workflows are depicted in Figure 1.19. As highlighted in this illustration, samples are combined at different points within the sample processing workflow, leaving room to introduce technical errors where samples from different conditions are not yet combined. Accordingly, each labeling strategy bears its own advantages and disadvantages, requiring their careful evaluation before designing a proteomics experiment. Due to the importance and complementarity of each labeling technique, detailed descriptions of these strategies are elucidated below.

Label-free quantification is the measurement of peptide abundances measured by a mass spectrometer within an LC run [297]. In shotgun proteomics, measurements can be recorded in spectral counts, e.g. the number of times a given peptide has been observed, or in the form of MS^1 intensities of peptide parent ions. The corresponding values are then used to compare relative protein and peptide abundances across different experiments. The disadvantage of label

free quantification is low sample throughput and the absence of internal standards, resulting in less accurate and reproducible quantification.

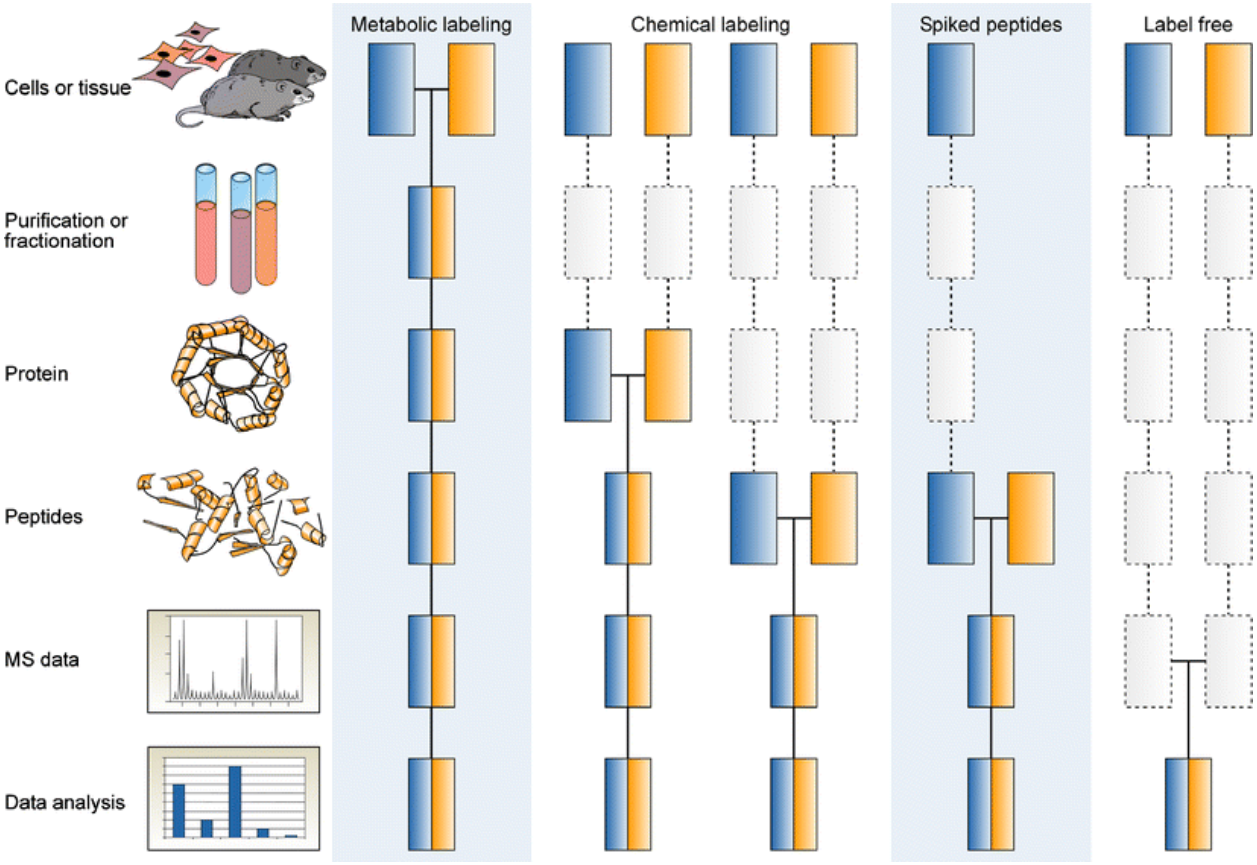

Figure 1.19. Overview of labeling technologies in mass spectrometry.

Figure adapted from reference [296].

To permit higher throughput of proteomics samples, techniques enabling multiplexed analysis of up to ten stimulations within a given LC-MS run have been developed. At present, the methodology granting the highest sample throughput is tandem mass tag (TMT) labeling, where peptides are chemically labeled with up to ten different isobaric mass tags [298]. Once peptides functionalized with a tandem mass tag are fragmented, the isobaric tags dissociate into reporter ions with distinct masses. Relative abundances of these reporter ions can be read out from MS/MS spectra with allocated software, providing relative peptide abundances for each of the investigated conditions. The disadvantages are signal dilution for highly multiplexed

experiments, ratio suppression due to increased background signals in the low m/z range where TMT-reporter ion intensities are measured [299], as well as high operational costs.

One more affordable technique to chemically label peptides is the insertion of isotopically-labeled dimethyl groups at basic amine residues on peptides [300]. This technique, termed dimethyl labeling, allows for the comparison of up to three conditions within one LC-MS injection, and significantly improves the quantification accuracy of peptides and proteins in comparison to label-free quantification. Peptides are labeled with either unlabeled (+28Da), deuterated (+32Da) or deuterated and ^{13}C labeled (+36) methyl groups in an amine reductive reaction [300]. MS^1 intensities of co-eluting isotopic clusters from the same peptide species are reported and used for relative quantification of peptides and proteins. Chemical modification of peptides, however, results in lower identification rates and does not account for sample handling errors introduced prior to peptide digestions. The latter reduces the accuracy of quantification, as errors arising from sample processing contribute to the variation in measured peptide intensities, as illustrated in Figure 1.19 [296]. However, sample processing-based errors can be ruled out by metabolically labeling proteomes, as described below.

Stable isotope labeling of amino acids in cell culture (SILAC) is a labeling technology developed by Mathias Mann and is extensively used for the analysis of proteomics samples [168]. In SILAC, the isotopically-labeled amino acids Arginine (Arg or R) and Lysine (Lys or K) are fed to either cells or animals such as mice or flies, resulting in metabolic incorporation of isotopes into the proteome after several cell divisions [301]. Once complete incorporation of amino acids into the proteome has been achieved, up to three experimental conditions can be compared in one mass spectrometry experiment. Each condition is allocated to one isotopic channel, labeled with either ^{0}Lys, ^{0}Arg (Light), ^{4}Lys, ^{6}Arg (Medium) or ^{8}Lys, ^{10}Arg (Heavy) [302]. As for dimethyl labeling and label-free quantification, SILAC quantification is based on precursor ion intensities reported in the MS^1 spectra [303]. SILAC is especially well-suited for the analysis of post-translational modifications, as this method allows for the accurate quantification of single peptides while not perturbing sequence information through chemical additions to the peptides. Finally, sample errors are minimized, as samples can be combined immediately after the

stimulation of cell cultures (Refer to Figure 1.19). However, human tissue extracts cannot be labeled with SILAC and require the use of different labeling strategies.

1.4.5.7 Bioinformatics analysis

Numerous software is available to analyze mass spectrometry-based proteomics data. The one mostly used in the scope of this thesis is MaxQuant and the implemented search engine Andromeda, which are freeware software developed by Jürgen Cox et al. within the workgroup of Matthias Mann at the Max Planck Institute for Biochemistry in Munich, Germany [303, 304]. MaxQuant has been specifically designed to quantify metabolically-labeled peptides and proteins and can be used for the majority of quantification methods [305]. The search engine Andromeda performs peptide spectral matching (PSM) of peptides with variable post-translational modifications and is extremely user-friendly [304].

Similar to the majority of peptide search engines, PSM in MaxQuant is performed with the help of proteome databases that are provided in the fasta format [306]. Databases can be downloaded from websites such as Uniprot.org, where genomic information that are translated into proteomes is made available for various taxonomies [307]. Once raw files and proteomics databases are linked to the search engine, peptides are in silico digested with the protease specified. Masses of the theoretical (tryptic) peptides can then be collated to parent ion peaks from the raw LC-MS files to reduce the peptide database created from in silico digestion of the proteome. This reduced peptide database is then matched with observed MS/MS spectra from raw proteomics files, and peptide identifications are scored based on binomial distribution probabilities [304]. In order to guarantee high confidence of matched peptide sequences, a false database is created by reverting or randomizing the original peptide database used [308]. Peptides are then matched to this false database and are assigned scores. These matches are referred to as false positives. False positive scores are further used to determine a score cut-off at which a minimum of 1% of peptides are false positives, assuring that, theoretically, 99% of all peptides with scores higher than the cut-off score are true positive identifications [309]. This approach has proven to be well-suited for large-scale proteomics data where not all peptides are anticipated to be detected. In addition to

PSM, peptides and proteins can optionally be quantified. Quantification of SILAC shotgun proteomics data by MaxQuant is briefly elucidated in the following paragraph.

MS^1 intensities of SILAC isotope clusters are extracted from raw files based on the specific mass shifts observed from Light, Medium or Heavy Lysine and Arginine residues in each tryptic peptide. Intensities of SILAC pairs/triplets are extracted over the elution profile of a peptide and are plotted against each other, regressed with a linear model and the slope of the regression line is reported as the fold change. It is noteworthy that MaxQuant also realigns isotope-induced retention time shifts, which are mostly observed on amino acids labeled with deuterium, as is the case for ^{4}Lys. Protein fold changes are reported as the median of all peptide fold changes. A more detailed description of the quantification procedures can be found in the supplementary material of the publication by Cox et al. (2009) [310].

At present, numerous other peptide search and quantification software are available that can be used in a very similar fashion to MaxQuant. The most frequently used are Peaks [311], Mascot [312] and OpenMS [313]. However, with the aim to make the data analysis reproducible, only data from MaxQuant are discussed and depicted in the studies of this thesis. The programming language R (http://www.R-project.org/) has almost exclusively been implemented in bioinformatics workflows to analyze and visualize MaxQuant outputs.

1.5 Time-resolved phosphoproteomics

Knowledge about signalling cascades builds the foundation of many disease treatments. Most cellular biology studies aiming to understand signaling pathways are based on already known interactions, not allowing for unbiased assessment of systems-wide cellular responses. The era of mass spectrometry-based proteomics has allowed researchers to address this issue with large-scale studies monitoring post-translational modifications in an unbiased manner. Phosphoproteomics has emerged as a powerful tool to understand phosphorylation pathways linked to specific kinases [314, 315], to unravel signaling cascades associated with extracellular stresses [316] and has been used to identify molecular events linked to cancer [317]. In addition to these few highlighted examples, phosphoproteomics has been the foundation of numerous

studies aiding our current knowledge about intracellular signaling. Few studies, however, have focused on monitoring the phosphoproteome in a time-dependent manner, even though the depth of information gained from phosphoproteome screenings at single time points have a limited scope. Those that have attempted to study the temporally-resolved proteome remarked that temporal resolution of signaling events benefits the definition of signaling cascades. One of the most interesting studies prior to the debut of this thesis was a publication by Jesper V. Olsen *et al.* (2006), who demonstrated insights into EGF signaling dynamics using five timepoints at 0, 1, 5, 10 and 20 minutes post-stimulation with epidermal growth factor [318]. This dynamics study found kinetic trends to correlate with functionally related phosphorylation events and, based on the large number of identified phosphorylation sites, re-defined the EGF signaling pathway. In a similar approach, Thiago Verano-Brag *et al.* investigated the Angiotensin-dependent phosphoproteome in a time-dependent manner. Based on this experimental approach, a clear signaling network of Angiotensin was defined and its anti-oncogenic activities were found to correlate with phosphorylation-dependent delocalization of the forkhead box protein O1 (FOXO1) [319]. Another publication by Rochelle D'Suza *et al.* used temporally-resolved phosphoproteomics to dissect the early signaling events triggered by the transforming growth factor-β (TGF- β) and showed that rapid changes in phosphorylation occur primarily on transcription-independent molecular machineries [320].

Altogether, the aforementioned studies consistently highlight that dynamic profiling of the phosphoproteome bears the potential to more precisely define the current knowledge on signaling cascades through continuous observation of molecular mechanisms. Nonetheless, these previous studies faced limitations due to the low number of timepoints monitored, allowing for only hypothetical correlations between phosphoproteome dynamics and signaling networks. A lack in the number of phosphorylation sites monitored over time further restricted systems-wide assessments of signaling events.

1.6 Biochemical approaches to assess the functionality of protein phosphorylation

Phosphoproteomics screens provide massive amounts of data that depict stimulation-specific changes. Hundreds and even thousands of phosphorylation sites with altered abundances can arise from changing environmental conditions of cell cultures, making the interpretation of systems-wide-acquired data a challenge. Whilst statistical and bio-informatics analyses allow for the assessment of perturbed molecular mechanisms, no exact information about the functionality of phosphorylation sites in biochemical pathways can be extracted from proteomics data. Additional techniques are required to clearly understand some of the interesting signaling events monitored during phosphoproteomics screens. These techniques include point-directed mutagenesis of phosphorylated amino acids into their inactive equivalents to perform functional assays and the use of immunofluorescence to link observed changes in the phosphoproteome to molecular mechanisms. These techniques however, are, by no means, applicable to a large-scale assessment of phosphosites, making the choice of investigated phosphorylation events often biased towards the interests of researchers or journal editors. Nonetheless, functional assessment of phosphorylation sites is crucial for the understanding of signaling networks and their relevance in biochemical processes.

1.6.1 Site-directed mutagenesis

Site-directed mutagenesis is a molecular biology technique used to study the effect of one or several proteogenic amino acid substitutions on cell biology. This technique is frequently used to assess the functionality of phosphorylation of the amino acids Ser, Thr, and Tyr, through substitution with non-phosphorylatable amino acids, such as alanine, or with phosphorylation-mimicking amino acids such as Aspartic acid and Glutamic acid. Aspartic and Glutamic acid have been found to mimic the chemical properties of a phosphorylation group [321], while alanine has the opposite effect as it does not contain a phosphorylatable residue [322]. Carrying out mutagenesis to mimic either of the phosphorylation states of an amino acid helps to understand the effects of changes is phosphorylation abundances, as measured in phosphoproteomics screens. Point mutations are generated with genomic techniques in which DNA plasmids of the protein of interest are produced with or without the mutations. Protocols

explaining the exact procedures to synthesize plasmids with the help of polymerases can be found in references [323-325]. After genetic cloning, the corresponding proteins can be expressed either in the cellular system being studied or in bacterial cells for later purification of proteins. *In vivo* expression of mutated proteins in the investigated cell cultures is often performed to test for phosphorylation-dependent changes, including the appearance of phenotypes, the viability of cell cultures, and many more. On the other hand, expression of mutated proteins in bacterial cultures is used to generate larger amounts of the proteins for their purification, which are required for *in vitro* functional assays. One prominent application where purified proteins are needed is the investigation of kinase substrate relationships with radioactive phosphor probes. This technique, commonly known as "*in-vitro* kinase assay", determines the affinity of a kinase to a specific phosphorylation site and requires the expression and purification of kinase and the substrate of interest [326, 327]. Point mutations in the phosphorylation sites on substrates are necessary to prove that no other phosphorylation site on the substrate is phosphorylated by the kinase, as radioactive detection of phosphorous cannot resolve for the exact amino acid residue that is phosphorylated. Both *in vivo* and *in vitro* assays are widely applied to pinpoint the functionalities of specific phosphorylation sites discovered in large-scale phosphoproteomics studies.

1.6.2 Immunofluorescence

Immunofluorescence is a technique applied to microbiological samples that uses the specificity of antibodies to their antigens to assign fluorescent dyes to proteins of interest [328]. Fluorescence can be visualized with a fluorescence-sensitive microscope. Immunofluorescence is widely used to assess changes in cellular morphology and specific molecular processes, such as actin polymerization, upon stimulation or the expression of exogenously expressed proteins[329].

1.7 Research outline

This thesis is aimed at the development of mass spectrometry-based techniques to characterize the temporal diffusion of phosphorylation-mediated intracellular signaling and to study the biological effects of signaling using functional assays. Primarily, the phosphoproteomics screens conducted in this thesis focus on:

1. The development of mass spectrometry-based techniques to monitor the phosphoproteome with high temporal precision upon extracellular stimulation.
2. Defining the BRAF-RAS-MEK-ERK signaling cascade and attributed cellular events in colon cancer.
3. Characterizing the effect of the kinase inhibitor Vemurafenib (PLX4032) on the phosphoproteome of colon rectal cancers.
4. Gathering comprehensive information about mechanistic details by which the anti-oncogenic sphingolipids SH-BC-893 and C2-ceramide starve cancer cells to death through activation of protein phosphatase 2 A (PP2A).

Unraveling phosphorylation signaling cascades has mostly been approached through the observation of changes in the phosphoproteome at a given time post-stimulation. However, assessment of the dynamics of the molecular mechanisms is only possible when also observing what happens from the beginning of a stimulation until the observed response. Accordingly, the main focus of this thesis is dedicated to the development of a workflow that uses mass spectrometry-based proteomics techniques to monitor phosphorylation signaling at high temporal resolution and subsequently, the application of such a workflow to understand cell signaling and mechanisms by which small molecule drugs target cancerous cells.

To begin with, the model organism yeast was subjected to temperature shocks, leading to a high degree of anticipated dynamic changes in phosphorylation signaling. This experimental setup was motivated by its simplicity, as temperature shock can be timed easily and yeast cells are relatively simple to handle. Also, excessive changes in the phosphoproteome are expected and there has been a long-lasting interest in characterizing temperature stress response in yeast.

Accordingly, this approach appeared to be well-suited to conduct a systems biology study and, at the same time, to develop a technically challenging workflow with a simple model organism. Intriguingly, this approach enabled precise dynamic profiling of more than 3000 phosphorylation sites, of which around 600 sites drastically changed in abundance with time. Furthermore, we observed an intense variability in different phosphorylation kinetics and were able to define kinase targets based on kinetic information.

Upon successful development of a workflow that allows for temporal deconvolution of intracellular signaling, we applied this technique to gain further insights into cancer treatment with kinase inhibitors. We focussed on two genotypes of colon cancer that paradoxically respond to treatment with the kinase inhibitor Vemurafenib (PLX4032). While treatment of KRAS G13D mutated cancer with Vemurafenib results in activation and thus, growth of cancer cells, colon cancer cells harboring the BRAF V600E mutation respond well to the drug that efficiently inactivates the BRAF kinase activity. While this phenomenon has been well studied from a mechanistic point of view, we intended to unravel the underlying signaling events with the aid of temporally-resolved phosphoprotoemics. The resulting study presents a remarkably deep profiling of the phosphoproteome and offers extensive knowledge on MAPK pathway signaling. Furthermore, we unraveled novel targets of the kinase ERK and connected actin polymerization to the activation of the transcription factors MKL1/2.

The third study was motivated by the recent discovery of a potential protein phosphatase 2 A (PP2A)-activating anti-oncogenic sphingolipid, named SH-BC-893. This molecule, developed in the workgroup of Dr. Stephen Hanessian at the University of Montreal and characterized by the cancer biology laboratories of Dr. Aimee Edinger at University of California in Irvine, required further investigation regarding its PP2A-activating properties. Scientists in the Edinger laboratory discovered that SH-BC-893 starves cancer cells to death through the activation of protein phosphatase 2 A. However, the underlying signaling events that lead to starvation had to be resolved in order to refine the mechanistic details of its tumor-inhibiting properties. It has been reported that starvation of cells occurs after the formation of vacuoles and the internalization of nutrient transporters. Both phenotypes can be reversed with PP2A inhibitors such as LB-100, while, interestingly, the natural analogue of SH-BC-893, C2-ceramide, keeps its

tumor-killing activity without inducing vacuolation. Accordingly, we set out to compare the effects of SH-BC-893 on the phosphoproteome to the PP2A inhibitor LB-100 and C2-ceramide in a phosphoproteomics screen to decipher the impact of each of the molecules on signaling dynamics. These experiments enabled us to conclude that guanylyl exchange factors (GTPases) are major drivers of PP2A-directed cell starvation and that SH-BC-893 activates a specific subset of the heterotrimeric protein phosphatase 2 A.

In conclusion, this thesis presents the development of a phosphoprotoemics workflow capable of monitoring phosphorylation dynamics at minute-scale temporal resolution using metabolic labeling techniques. Refined data analysis workflows have been developed and have helped us to gain a deeper understanding of the dynamics of cellular signaling, as well as the effects that anti-oncogenic drugs exert on mammalian cancer cells.

1.8 Thesis overview

The first chapter of my doctoral thesis represents the literature review of cell biology relevant for the thematic of the conducted studies. A detailed description of the analytical techniques, focused on mass spectrometry-based proteomics, is also presented. This introductory chapter covers the most relevant literature and has been composed in accordance with the contents of this thesis.

The second chapter presents my first article describing the “Phosphoproteome dynamics of *Saccharomyces Cerevisiae* under heat shock and cold stress”, published in **Molecular Systems Biology** [330]. This publication focuses on the development of phosphoprotemics techniques to reproducibly monitor the phosphoproteome in cells with high temporal precision using metabolic labeling techniques. Experiments were carried out on the model organism yeast that were subjected to either heat or cold stress. The dynamics of the phosphoprotome were successively monitored from 0 until 28 minutes post-stimulation, resulting in interesting insights into cellular signaling.

In the third chapter, my second publication, entitled “Time-Resolved phosphoproteome analysis of paradoxical RAF activation reveals novel targets of ERK”, published in **Molecular and Cellular Proteomics,** is presented [331]. In this scientific work, we applied the techniques developed as part of the first publication to study the dissipation of phosphorylation-mediated signaling in colon cancer cells treated with the FDA-approved kinase inhibitor Vemurafenib (PLX4032).

Chapter four represents the third and last article of my thesis that is submitted to **Molecular and Cellular Proteomics**. This study, entitled “Dynamic phosphoproteomics uncovers signaling pathways modulated by anti-oncogenic sphingolipid analogs” builds on using temporally-resolving phosphoproteomics to characterize the effects of the novel anti-oncogenic inhibitor SH-BC-893 on phosphorylation signaling. In more detail, SH-BC-893 stimulation was compared to a specific inhibitor of protein phosphatase 2 A (PP2A), LB-100 and one of its natural analogues, C2-ceramide, to unravel its PP2A-activating and cancer-killing properties.

Chapter five highlights the main findings from all three articles and contains a critical discussion of the results from each article. Furthermore, future perspectives and suggestions are stated.

1.9 References

1. Alberts, B., *Molecular Biology of the Cell*. 2017: CRC Press.
2. Cooper, G.M., *The cell : a molecular approach*. 2000, Washington, D.C.; Sunderland, Mass.: ASM Press ; Sinauer Associates.
3. Lavoie, H. and M. Therrien, *Regulation of RAF protein kinases in ERK signalling.* Nat Rev Mol Cell Biol, 2015. **16**(5): p. 281-98.
4. Aoki, Y., et al., *Recent advances in RASopathies.* J Hum Genet, 2016. **61**(1): p. 33-9.
5. De Araujo, C.P., *[An individual philosophy on nursing].* Rev Enferm Nov Dimens, 1976. **2**(4): p. 197-9.
6. Malmberg, A.B. and K.R. Bley, *Turning up the Heat on Pain: TRPV1 Receptors in Pain and Inflammation*. 2006: Birkhäuser Basel.
7. Ulrich, H.D., *Two-way communications between ubiquitin-like modifiers and DNA.* Nat Struct Mol Biol, 2014. **21**(4): p. 317-24.
8. Flotho, A. and F. Melchior, *Sumoylation: a regulatory protein modification in health and disease.* Annu Rev Biochem, 2013. **82**: p. 357-85.
9. Deribe, Y.L., T. Pawson, and I. Dikic, *Post-translational modifications in signal integration.* Nat Struct Mol Biol, 2010. **17**(6): p. 666-72.
10. Hunter, T., *Protein kinases and phosphatases: the yin and yang of protein phosphorylation and signaling.* Cell, 1995. **80**(2): p. 225-36.
11. Olsen, J.V., et al., *Global, in vivo, and site-specific phosphorylation dynamics in signaling networks.* Cell, 2006. **127**(3): p. 635-48.
12. Hardman, G., et al., *Extensive non-canonical phosphorylation in human cells revealed using strong-anion exchange-mediated phosphoproteomics.* bioRxiv, 2017.
13. Johnson, L.N., *The regulation of protein phosphorylation.* Biochem Soc Trans, 2009. **37**(Pt 4): p. 627-41.
14. Nishi, H., K. Hashimoto, and Anna R. Panchenko, *Phosphorylation in Protein-Protein Binding: Effect on Stability and Function.* Structure, 2011. **19**(12): p. 1807-1815.
15. Vlastaridis, P., et al., *Estimating the total number of phosphoproteins and phosphorylation sites in eukaryotic proteomes.* Gigascience, 2017. **6**(2): p. 1-11.
16. Singh, V., et al., *Phosphorylation: Implications in Cancer.* Protein J, 2017. **36**(1): p. 1-6.
17. Capra, M., et al., *Frequent alterations in the expression of serine/threonine kinases in human cancers.* Cancer Res, 2006. **66**(16): p. 8147-54.
18. Hunter, T. and B.M. Sefton, *Transforming gene product of Rous sarcoma virus phosphorylates tyrosine.* Proc Natl Acad Sci U S A, 1980. **77**(3): p. 1311-5.
19. Adams, J.A., *Kinetic and catalytic mechanisms of protein kinases.* Chem Rev, 2001. **101**(8): p. 2271-90.
20. Burnett, G. and E.P. Kennedy, *The enzymatic phosphorylation of proteins.* J Biol Chem, 1954. **211**(2): p. 969-80.
21. Cohen, P., *The origins of protein phosphorylation.* Nat Cell Biol, 2002. **4**(5): p. E127-30.
22. Good, M.F., A. Saul, and P.M. Graves, *Malaria vaccines.* Biotechnology, 1992. **20**: p. 69-98.
23. Songyang, Z., et al., *A structural basis for substrate specificities of protein Ser/Thr kinases: primary sequence preference of casein kinases I and II, NIMA, phosphorylase*

kinase, calmodulin-dependent kinase II, CDK5, and Erk1. Mol Cell Biol, 1996. **16**(11): p. 6486-93.
24. Levy, E.D., S.W. Michnick, and C.R. Landry, *Protein abundance is key to distinguish promiscuous from functional phosphorylation based on evolutionary information.* Philos Trans R Soc Lond B Biol Sci, 2012. **367**(1602): p. 2594-606.
25. Lai, A.C., A.N. Nguyen Ba, and A.M. Moses, *Predicting kinase substrates using conservation of local motif density.* Bioinformatics, 2012. **28**(7): p. 962-9.
26. Tanoue, T., et al., *A conserved docking motif in MAP kinases common to substrates, activators and regulators.* Nat Cell Biol, 2000. **2**(2): p. 110-6.
27. Papin, J.A., et al., *Reconstruction of cellular signalling networks and analysis of their properties.* Nat Rev Mol Cell Biol, 2005. **6**(2): p. 99-111.
28. Kemp, B.E., et al., *Substrate specificity of the cyclic AMP-dependent protein kinase.* Proc Natl Acad Sci U S A, 1975. **72**(9): p. 3448-52.
29. Walsh, D.A., J.P. Perkins, and E.G. Krebs, *An adenosine 3',5'-monophosphate-dependant protein kinase from rabbit skeletal muscle.* J Biol Chem, 1968. **243**(13): p. 3763-5.
30. Manning, G., et al., *The protein kinase complement of the human genome.* Science, 2002. **298**(5600): p. 1912-34.
31. Cori, G.T. and A.A. Green, *CRYSTALLINE MUSCLE PHOSPHORYLASE: II. PROSTHETIC GROUP.* Journal of Biological Chemistry, 1943. **151**(1): p. 31-38.
32. Ohkura, H., et al., *The fission yeast dis2+ gene required for chromosome disjoining encodes one of two putative type 1 protein phosphatases.* Cell, 1989. **57**(6): p. 997-1007.
33. Arino, J., et al., *Human liver phosphatase 2A: cDNA and amino acid sequence of two catalytic subunit isotypes.* Proc Natl Acad Sci U S A, 1988. **85**(12): p. 4252-6.
34. Zhang, M., et al., *Viewing serine/threonine protein phosphatases through the eyes of drug designers.* FEBS J, 2013. **280**(19): p. 4739-60.
35. Alonso, A., et al., *Protein tyrosine phosphatases in the human genome.* Cell, 2004. **117**(6): p. 699-711.
36. Shi, Y., *Serine/threonine phosphatases: mechanism through structure.* Cell, 2009. **139**(3): p. 468-84.
37. Wlodarchak, N. and Y. Xing, *PP2A as a master regulator of the cell cycle.* Crit Rev Biochem Mol Biol, 2016. **51**(3): p. 162-84.
38. Alberts, B., et al., *Essential Cell Biology, Fourth Edition*. 2013: Taylor & Francis Group.
39. Blackadar, C.B., *Historical review of the causes of cancer.* World J Clin Oncol, 2016. **7**(1): p. 54-86.
40. Tomasetti, C. and B. Vogelstein, *Variation in cancer risk among tissues can be explained by the number of stem cell divisions.* Science, 2015. **347**(6217): p. 78-81.
41. Loeb, K.R. and L.A. Loeb, *Significance of multiple mutations in cancer.* Carcinogenesis, 2000. **21**(3): p. 379-85.
42. Vogelstein, B. and K.W. Kinzler, *Cancer genes and the pathways they control.* Nat Med, 2004. **10**(8): p. 789-99.
43. Ikediobi, O.N., et al., *Mutation analysis of 24 known cancer genes in the NCI-60 cell line set.* Mol Cancer Ther, 2006. **5**(11): p. 2606-12.
44. Futreal, P.A., et al., *A census of human cancer genes.* Nat Rev Cancer, 2004. **4**(3): p. 177-83.
45. Vogelstein, B., et al., *Cancer genome landscapes.* Science, 2013. **339**(6127): p. 1546-58.

46. Hilger, R.A., M.E. Scheulen, and D. Strumberg, *The Ras-Raf-MEK-ERK pathway in the treatment of cancer.* Onkologie, 2002. **25**(6): p. 511-8.
47. Jain, M.V., et al., *Inhibition of miR301 enhances Akt-mediated cell proliferation by accumulation of PTEN in nucleus and its effects on cell-cycle regulatory proteins.* Oncotarget, 2016. **7**(15): p. 20953-65.
48. Baker, S.J., et al., *Chromosome 17 deletions and p53 gene mutations in colorectal carcinomas.* Science, 1989. **244**(4901): p. 217-21.
49. Nigro, J.M., et al., *Mutations in the p53 gene occur in diverse human tumour types.* Nature, 1989. **342**(6250): p. 705-8.
50. Pise-Masison, C.A., et al., *Phosphorylation of p53: a novel pathway for p53 inactivation in human T-cell lymphotropic virus type 1-transformed cells.* J Virol, 1998. **72**(8): p. 6348-55.
51. Harsha, H.C. and A. Pandey, *Phosphoproteomics in cancer.* Mol Oncol, 2010. **4**(6): p. 482-95.
52. Torkamani, A., G. Verkhivker, and N.J. Schork, *Cancer driver mutations in protein kinase genes.* Cancer Lett, 2009. **281**(2): p. 117-27.
53. Marshall, C.J., *Specificity of receptor tyrosine kinase signaling: transient versus sustained extracellular signal-regulated kinase activation.* Cell, 1995. **80**(2): p. 179-85.
54. Naor, Z., O. Benard, and R. Seger, *Activation of MAPK cascades by G-protein-coupled receptors: the case of gonadotropin-releasing hormone receptor.* Trends Endocrinol Metab, 2000. **11**(3): p. 91-9.
55. Hill, C.S. and R. Treisman, *Transcriptional regulation by extracellular signals: mechanisms and specificity.* Cell, 1995. **80**(2): p. 199-211.
56. Vickers, E.R., et al., *Ternary complex factor-serum response factor complex-regulated gene activity is required for cellular proliferation and inhibition of apoptotic cell death.* Mol Cell Biol, 2004. **24**(23): p. 10340-51.
57. Sclafani, F., et al., *KRAS and BRAF mutations in circulating tumour DNA from locally advanced rectal cancer.* Sci Rep, 2018. **8**(1): p. 1445.
58. Serup-Hansen, E., et al., *KRAS and BRAF mutations in anal carcinoma.* APMIS, 2015. **123**(1): p. 53-9.
59. Xing, M., *BRAF mutation in papillary thyroid cancer: pathogenic role, molecular bases, and clinical implications.* Endocr Rev, 2007. **28**(7): p. 742-62.
60. Mebratu, Y. and Y. Tesfaigzi, *How ERK1/2 activation controls cell proliferation and cell death: Is subcellular localization the answer?* Cell Cycle, 2009. **8**(8): p. 1168-75.
61. Roskoski, R., Jr., *ERK1/2 MAP kinases: structure, function, and regulation.* Pharmacol Res, 2012. **66**(2): p. 105-43.
62. Brunet, A., et al., *Nuclear translocation of p42/p44 mitogen-activated protein kinase is required for growth factor-induced gene expression and cell cycle entry.* EMBO J, 1999. **18**(3): p. 664-74.
63. Ferrell, J.E., Jr. and R.R. Bhatt, *Mechanistic studies of the dual phosphorylation of mitogen-activated protein kinase.* J Biol Chem, 1997. **272**(30): p. 19008-16.
64. Fukuda, M., Y. Gotoh, and E. Nishida, *Interaction of MAP kinase with MAP kinase kinase: its possible role in the control of nucleocytoplasmic transport of MAP kinase.* EMBO J, 1997. **16**(8): p. 1901-8.
65. Reszka, A.A., et al., *Association of mitogen-activated protein kinase with the microtubule cytoskeleton.* Proc Natl Acad Sci U S A, 1995. **92**(19): p. 8881-5.

66. Soloaga, A., et al., *MSK2 and MSK1 mediate the mitogen- and stress-induced phosphorylation of histone H3 and HMG-14.* EMBO J, 2003. **22**(11): p. 2788-97.
67. Marais, R., J. Wynne, and R. Treisman, *The SRF accessory protein Elk-1 contains a growth factor-regulated transcriptional activation domain.* Cell, 1993. **73**(2): p. 381-93.
68. Sears, R., et al., *Multiple Ras-dependent phosphorylation pathways regulate Myc protein stability.* Genes Dev, 2000. **14**(19): p. 2501-14.
69. Yang, J.Y., et al., *ERK promotes tumorigenesis by inhibiting FOXO3a via MDM2-mediated degradation.* Nat Cell Biol, 2008. **10**(2): p. 138-48.
70. Flaherty, K.T., et al., *Inhibition of mutated, activated BRAF in metastatic melanoma.* N Engl J Med, 2010. **363**(9): p. 809-19.
71. Slamon, D.J., et al., *Use of chemotherapy plus a monoclonal antibody against HER2 for metastatic breast cancer that overexpresses HER2.* N Engl J Med, 2001. **344**(11): p. 783-92.
72. Parameswara, V.K., A.J. Sule, and V. Esser, *Have we overlooked the importance of serine/threonine protein phosphatases in pancreatic beta-cells? Role played by protein phosphatase 2A in insulin secretion.* JOP, 2005. **6**(4): p. 303-15.
73. Arroyo, J.D. and W.C. Hahn, *Involvement of PP2A in viral and cellular transformation.* Oncogene, 2005. **24**(52): p. 7746-55.
74. Tian, Q. and J. Wang, *Role of serine/threonine protein phosphatase in Alzheimer's disease.* Neurosignals, 2002. **11**(5): p. 262-9.
75. Dobrowsky, R.T., et al., *Ceramide activates heterotrimeric protein phosphatase 2A.* J Biol Chem, 1993. **268**(21): p. 15523-30.
76. Bialojan, C. and A. Takai, *Inhibitory effect of a marine-sponge toxin, okadaic acid, on protein phosphatases. Specificity and kinetics.* Biochem J, 1988. **256**(1): p. 283-90.
77. Seshacharyulu, P., et al., *Phosphatase: PP2A structural importance, regulation and its aberrant expression in cancer.* Cancer Lett, 2013. **335**(1): p. 9-18.
78. Kamibayashi, C., et al., *Comparison of heterotrimeric protein phosphatase 2A containing different B subunits.* J Biol Chem, 1994. **269**(31): p. 20139-48.
79. Mayer-Jaekel, R.E. and B.A. Hemmings, *Protein phosphatase 2A--a 'menage a trois'.* Trends Cell Biol, 1994. **4**(8): p. 287-91.
80. Eichhorn, P.J., M.P. Creyghton, and R. Bernards, *Protein phosphatase 2A regulatory subunits and cancer.* Biochim Biophys Acta, 2009. **1795**(1): p. 1-15.
81. Letourneux, C., G. Rocher, and F. Porteu, *B56-containing PP2A dephosphorylate ERK and their activity is controlled by the early gene IEX-1 and ERK.* EMBO J, 2006. **25**(4): p. 727-38.
82. Peterson, R.T., et al., *Protein phosphatase 2A interacts with the 70-kDa S6 kinase and is activated by inhibition of FKBP12-rapamycinassociated protein.* Proc Natl Acad Sci U S A, 1999. **96**(8): p. 4438-42.
83. Kuo, Y.C., et al., *Regulation of phosphorylation of Thr-308 of Akt, cell proliferation, and survival by the B55alpha regulatory subunit targeting of the protein phosphatase 2A holoenzyme to Akt.* J Biol Chem, 2008. **283**(4): p. 1882-92.
84. Laplante, M. and D.M. Sabatini, *mTOR signaling in growth control and disease.* Cell, 2012. **149**(2): p. 274-93.
85. Zhang, W., et al., *PR55 alpha, a regulatory subunit of PP2A, specifically regulates PP2A-mediated beta-catenin dephosphorylation.* J Biol Chem, 2009. **284**(34): p. 22649-56.

86. He, T.C., et al., *Identification of c-MYC as a target of the APC pathway.* Science, 1998. **281**(5382): p. 1509-12.
87. Perrotti, D. and P. Neviani, *Protein phosphatase 2A: a target for anticancer therapy.* Lancet Oncol, 2013. **14**(6): p. e229-38.
88. Ruvolo, P.P., et al., *Low expression of PP2A regulatory subunit B55alpha is associated with T308 phosphorylation of AKT and shorter complete remission duration in acute myeloid leukemia patients.* Leukemia, 2011. **25**(11): p. 1711-7.
89. Shouse, G.P., Y. Nobumori, and X. Liu, *A B56gamma mutation in lung cancer disrupts the p53-dependent tumor-suppressor function of protein phosphatase 2A.* Oncogene, 2010. **29**(27): p. 3933-41.
90. Cheng, Y., et al., *Evaluation of PPP2R2A as a prostate cancer susceptibility gene: a comprehensive germline and somatic study.* Cancer Genet, 2011. **204**(7): p. 375-81.
91. Guenther, G.G. and A.L. Edinger, *A new take on ceramide: starving cells by cutting off the nutrient supply.* Cell Cycle, 2009. **8**(8): p. 1122-6.
92. McCracken, A.N. and A.L. Edinger, *Nutrient transporters: the Achilles' heel of anabolism.* Trends Endocrinol Metab, 2013. **24**(4): p. 200-8.
93. Kim, S.M., et al., *Targeting cancer metabolism by simultaneously disrupting parallel nutrient access pathways.* J Clin Invest, 2016. **126**(11): p. 4088-4102.
94. Cristobal, I., et al., *Activation of the Tumor Suppressor PP2A Emerges as a Potential Therapeutic Strategy for Treating Prostate Cancer.* Mar Drugs, 2015. **13**(6): p. 3276-86.
95. Sangodkar, J., et al., *All roads lead to PP2A: exploiting the therapeutic potential of this phosphatase.* FEBS J, 2016. **283**(6): p. 1004-24.
96. Junttila, M.R., et al., *CIP2A Inhibits PP2A in Human Malignancies.* Cell, 2007. **130**(1): p. 51-62.
97. Corcoran, N.M., et al., *Open-label, phase I dose-escalation study of sodium selenate, a novel activator of PP2A, in patients with castration-resistant prostate cancer.* Br J Cancer, 2010. **103**(4): p. 462-8.
98. Knight, Z.A., H. Lin, and K.M. Shokat, *Targeting the cancer kinome through polypharmacology.* Nat Rev Cancer, 2010. **10**(2): p. 130-7.
99. Pillai, P., et al., *Cancer Kinases and its Novel Inhibitors: Past, Present and Future Challenges.* Curr Drug Targets, 2015. **16**(11): p. 1233-45.
100. Leicht, D.T., et al., *Raf kinases: function, regulation and role in human cancer.* Biochim Biophys Acta, 2007. **1773**(8): p. 1196-212.
101. Huang, K. and D.C. Fingar, *Growing knowledge of the mTOR signaling network.* Semin Cell Dev Biol, 2014. **36**: p. 79-90.
102. Husseinzadeh, N. and H.D. Husseinzadeh, *mTOR inhibitors and their clinical application in cervical, endometrial and ovarian cancers: a critical review.* Gynecol Oncol, 2014. **133**(2): p. 375-81.
103. Fruman, D.A. and C. Rommel, *PI3K and cancer: lessons, challenges and opportunities.* Nat Rev Drug Discov, 2014. **13**(2): p. 140-56.
104. Mirshafiey, A., et al., *Receptor Tyrosine Kinase and Tyrosine Kinase Inhibitors: New Hope for Success in Multiple Sclerosis Therapy.* Innov Clin Neurosci, 2014. **11**(7-8): p. 23-36.
105. Thomas, N.E., *BRAF somatic mutations in malignant melanoma and melanocytic naevi.* Melanoma Res, 2006. **16**(2): p. 97-103.

106. Sale, M.J. and S.J. Cook, *Intrinsic and acquired resistance to MEK1/2 inhibitors in cancer.* Biochem Soc Trans, 2014. **42**(4): p. 776-83.
107. Lamontanara, A.J., et al., *Mechanisms of resistance to BCR-ABL and other kinase inhibitors.* Biochim Biophys Acta, 2013. **1834**(7): p. 1449-59.
108. Morris, E.J., et al., *Discovery of a novel ERK inhibitor with activity in models of acquired resistance to BRAF and MEK inhibitors.* Cancer Discov, 2013. **3**(7): p. 742-50.
109. Chen, D.H. and X.S. Zhang, *Targeted therapy: resistance and re-sensitization.* Chin J Cancer, 2015. **34**(11): p. 496-501.
110. Chen, W., et al., *PP2A-Mediated Anticancer Therapy.* Gastroenterol Res Pract, 2013. **2013**: p. 675429.
111. Switzer, C.H., et al., *Targeting SET/I(2)PP2A oncoprotein functions as a multi-pathway strategy for cancer therapy.* Oncogene, 2011. **30**(22): p. 2504-13.
112. Suganuma, M., et al., *Calyculin A, an inhibitor of protein phosphatases, a potent tumor promoter on CD-1 mouse skin.* Cancer Res, 1990. **50**(12): p. 3521-5.
113. Dounay, A.B. and C.J. Forsyth, *Okadaic acid: the archetypal serine/threonine protein phosphatase inhibitor.* Curr Med Chem, 2002. **9**(22): p. 1939-80.
114. Romero Rosales, K., et al., *Sphingolipid-based drugs selectively kill cancer cells by down-regulating nutrient transporter proteins.* Biochem J, 2011. **439**(2): p. 299-311.
115. Zhang, L., et al., *FTY720 for cancer therapy (Review).* Oncol Rep, 2013. **30**(6): p. 2571-8.
116. Shaw, H.M. and P.D. Nathan, *Vemurafenib in melanoma.* Expert Rev Anticancer Ther, 2013. **13**(5): p. 513-22.
117. Knight, Z.A. and K.M. Shokat, *Features of selective kinase inhibitors.* Chem Biol, 2005. **12**(6): p. 621-37.
118. Tsai, J., et al., *Discovery of a selective inhibitor of oncogenic B-Raf kinase with potent antimelanoma activity.* Proc Natl Acad Sci U S A, 2008. **105**(8): p. 3041-6.
119. Poulikakos, P.I., et al., *RAF inhibitors transactivate RAF dimers and ERK signalling in cells with wild-type BRAF.* Nature, 2010. **464**(7287): p. 427-30.
120. Hatzivassiliou, G., et al., *RAF inhibitors prime wild-type RAF to activate the MAPK pathway and enhance growth.* Nature, 2010. **464**(7287): p. 431-5.
121. Heidorn, S.J., et al., *Kinase-dead BRAF and oncogenic RAS cooperate to drive tumor progression through CRAF.* Cell, 2010. **140**(2): p. 209-21.
122. Ascierto, P.A., et al., *Phase II trial (BREAK-2) of the BRAF inhibitor dabrafenib (GSK2118436) in patients with metastatic melanoma.* J Clin Oncol, 2013. **31**(26): p. 3205-11.
123. Harding, J.J., et al., *A Retrospective Evaluation of Vemurafenib as Treatment for BRAF-Mutant Melanoma Brain Metastases.* Oncologist, 2015. **20**(7): p. 789-97.
124. Chapman, P.B., et al., *Improved survival with vemurafenib in melanoma with BRAF V600E mutation.* N Engl J Med, 2011. **364**(26): p. 2507-16.
125. Grey, A., et al., *Progression of KRAS mutant pancreatic adenocarcinoma during vemurafenib treatment in a patient with metastatic melanoma.* Intern Med J, 2014. **44**(6): p. 597-600.
126. Anforth, R., P. Fernandez-Penas, and G.V. Long, *Cutaneous toxicities of RAF inhibitors.* Lancet Oncol, 2013. **14**(1): p. e11-8.
127. Kopetz, S., et al., *Phase II Pilot Study of Vemurafenib in Patients With Metastatic BRAF-Mutated Colorectal Cancer.* J Clin Oncol, 2015. **33**(34): p. 4032-8.

128. Nazarian, R., et al., *Melanomas acquire resistance to B-RAF(V600E) inhibition by RTK or N-RAS upregulation.* Nature, 2010. **468**(7326): p. 973-7.
129. Karreth, F.A., et al., *C-Raf inhibits MAPK activation and transformation by B-Raf(V600E).* Mol Cell, 2009. **36**(3): p. 477-86.
130. Shi, H., et al., *Melanoma whole-exome sequencing identifies (V600E)B-RAF amplification-mediated acquired B-RAF inhibitor resistance.* Nat Commun, 2012. **3**: p. 724.
131. Lito, P., et al., *Relief of profound feedback inhibition of mitogenic signaling by RAF inhibitors attenuates their activity in BRAFV600E melanomas.* Cancer Cell, 2012. **22**(5): p. 668-82.
132. Holderfield, M., et al., *Targeting RAF kinases for cancer therapy: BRAF-mutated melanoma and beyond.* Nat Rev Cancer, 2014. **14**(7): p. 455-67.
133. Montefusco, D.J., N. Matmati, and Y.A. Hannun, *The yeast sphingolipid signaling landscape.* Chem Phys Lipids, 2014. **177**: p. 26-40.
134. Kosinska, M.K., et al., *Sphingolipids in human synovial fluid--a lipidomic study.* PLoS One, 2014. **9**(3): p. e91769.
135. Bryan, P.F., et al., *Sphingolipids as Mediators in the Crosstalk between Microbiota and Intestinal Cells: Implications for Inflammatory Bowel Disease.* Mediators Inflamm, 2016. **2016**: p. 9890141.
136. Breslow, D.K. and J.S. Weissman, *Membranes in balance: mechanisms of sphingolipid homeostasis.* Mol Cell, 2010. **40**(2): p. 267-79.
137. Lippincott-Schwartz, J. and R.D. Phair, *Lipids and cholesterol as regulators of traffic in the endomembrane system.* Annu Rev Biophys, 2010. **39**: p. 559-78.
138. Peralta, E.R. and A.L. Edinger, *Ceramide-induced starvation triggers homeostatic autophagy.* Autophagy, 2009. **5**(3): p. 407-9.
139. Young, M.M., M. Kester, and H.G. Wang, *Sphingolipids: regulators of crosstalk between apoptosis and autophagy.* J Lipid Res, 2013. **54**(1): p. 5-19.
140. Jafurulla, M. and A. Chattopadhyay, *Sphingolipids in the function of G protein-coupled receptors.* Eur J Pharmacol, 2015. **763**(Pt B): p. 241-6.
141. Saddoughi, S.A. and B. Ogretmen, *Diverse functions of ceramide in cancer cell death and proliferation.* Adv Cancer Res, 2013. **117**: p. 37-58.
142. Oaks, J. and B. Ogretmen, *Regulation of PP2A by Sphingolipid Metabolism and Signaling.* Front Oncol, 2014. **4**: p. 388.
143. Edinger, A.L., *Starvation in the midst of plenty: making sense of ceramide-induced autophagy by analysing nutrient transporter expression.* Biochem Soc Trans, 2009. **37**(Pt 1): p. 253-8.
144. Guenther, G.G., et al., *Ceramide starves cells to death by downregulating nutrient transporter proteins.* Proc Natl Acad Sci U S A, 2008. **105**(45): p. 17402-7.
145. Teixeira, V., et al., *Ceramide signaling targets the PP2A-like protein phosphatase Sit4p to impair vacuolar function, vesicular trafficking and autophagy in Isc1p deficient cells.* Biochim Biophys Acta, 2016. **1861**(1): p. 21-33.
146. McCracken, A.N. and A.L. Edinger, *Targeting cancer metabolism at the plasma membrane by limiting amino acid access through SLC6A14.* Biochem J, 2015. **470**(3): p. e17-9.
147. Lee, T.K., et al., *FTY720: a promising agent for treatment of metastatic hepatocellular carcinoma.* Clin Cancer Res, 2005. **11**(23): p. 8458-66.

148. McCracken, A.N., et al., *Phosphorylation of a constrained azacyclic FTY720 analog enhances anti-leukemic activity without inducing S1P receptor activation.* Leukemia, 2017. **31**(3): p. 669-677.
149. Chen, B., et al., *Azacyclic FTY720 Analogues That Limit Nutrient Transporter Expression but Lack S1P Receptor Activity and Negative Chronotropic Effects Offer a Novel and Effective Strategy to Kill Cancer Cells in Vivo.* ACS Chem Biol, 2016. **11**(2): p. 409-14.
150. Perryman, M.S., et al., *Effects of stereochemistry, saturation, and hydrocarbon chain length on the ability of synthetic constrained azacyclic sphingolipids to trigger nutrient transporter down-regulation, vacuolation, and cell death.* Bioorg Med Chem, 2016. **24**(18): p. 4390-4397.
151. Selwan, E.M., et al., *Attacking the supply wagons to starve cancer cells to death.* FEBS Lett, 2016. **590**(7): p. 885-907.
152. Margineanu, D.G., *Systems biology, complexity, and the impact on antiepileptic drug discovery.* Epilepsy Behav, 2014. **38**: p. 131-42.
153. Renart, J., J. Reiser, and G.R. Stark, *Transfer of proteins from gels to diazobenzyloxymethyl-paper and detection with antisera: a method for studying antibody specificity and antigen structure.* Proc Natl Acad Sci U S A, 1979. **76**(7): p. 3116-20.
154. Towbin, H., T. Staehelin, and J. Gordon, *Electrophoretic transfer of proteins from polyacrylamide gels to nitrocellulose sheets: procedure and some applications. 1979.* Biotechnology, 1992. **24**: p. 145-9.
155. Karas, M., et al., *Matrix-assisted ultraviolet laser desorption of non-volatile compounds.* International Journal of Mass Spectrometry and Ion Processes, 1987. **78**: p. 53-68.
156. Webb-Robertson, B.J. and W.R. Cannon, *Current trends in computational inference from mass spectrometry-based proteomics.* Brief Bioinform, 2007. **8**(5): p. 304-17.
157. Zhou, H., et al., *Toward a comprehensive characterization of a human cancer cell phosphoproteome.* J Proteome Res, 2013. **12**(1): p. 260-71.
158. Jimenez, C.R. and H.M. Verheul, *Mass spectrometry-based proteomics: from cancer biology to protein biomarkers, drug targets, and clinical applications.* Am Soc Clin Oncol Educ Book, 2014: p. e504-10.
159. Anderson, N.L. and N.G. Anderson, *Proteome and proteomics: new technologies, new concepts, and new words.* Electrophoresis, 1998. **19**(11): p. 1853-61.
160. James, P., *Protein identification in the post-genome era: the rapid rise of proteomics.* Q Rev Biophys, 1997. **30**(4): p. 279-331.
161. Anderson, J.D., et al., *Comprehensive Proteomic Analysis of Mesenchymal Stem Cell Exosomes Reveals Modulation of Angiogenesis via Nuclear Factor-KappaB Signaling.* Stem Cells, 2016. **34**(3): p. 601-13.
162. Yamashita, M. and J.B. Fenn, *Electrospray ion source. Another variation on the free-jet theme.* The Journal of Physical Chemistry, 1984. **88**(20): p. 4451-4459.
163. Clegg, G.A. and M. Dole, *Molecular beams of macroions. 3. Zein and polyvinylpyrrolidone.* Biopolymers, 1971. **10**(5): p. 821-6.
164. Ebhardt, H.A., et al., *Applications of targeted proteomics in systems biology and translational medicine.* Proteomics, 2015. **15**(18): p. 3193-208.
165. Jay, N.L. and M. Gillies, *Proteomic analysis of ophthalmic disease.* Clin Exp Ophthalmol, 2012. **40**(7): p. 755-63.

166. Lao, Y., et al., *Application of proteomics to determine the mechanism of action of traditional Chinese medicine remedies.* J Ethnopharmacol, 2014. **155**(1): p. 1-8.
167. Michalski, A., J. Cox, and M. Mann, *More than 100,000 detectable peptide species elute in single shotgun proteomics runs but the majority is inaccessible to data-dependent LC-MS/MS.* J Proteome Res, 2011. **10**(4): p. 1785-93.
168. Ong, S.E., et al., *Stable isotope labeling by amino acids in cell culture, SILAC, as a simple and accurate approach to expression proteomics.* Mol Cell Proteomics, 2002. **1**(5): p. 376-86.
169. Lygirou, V., M. Makridakis, and A. Vlahou, *Biological sample collection for clinical proteomics: existing SOPs.* Methods Mol Biol, 2015. **1243**: p. 3-27.
170. Schuster, M., et al., *Short cut of protein purification by integration of cell-disrupture and affinity extraction.* Bioseparation, 2000. **9**(2): p. 59-67.
171. Ericsson, C. and M. Nister, *Protein extraction from solid tissue.* Methods Mol Biol, 2011. **675**: p. 307-12.
172. Sajic, T., et al., *Comparison of three detergent-free protein extraction protocols for white adipose tissue.* Anal Biochem, 2011. **415**(2): p. 215-7.
173. Leon, I.R., et al., *Quantitative assessment of in-solution digestion efficiency identifies optimal protocols for unbiased protein analysis.* Mol Cell Proteomics, 2013. **12**(10): p. 2992-3005.
174. Rey, M., et al., *Effective removal of nonionic detergents in protein mass spectrometry, hydrogen/deuterium exchange, and proteomics.* Anal Chem, 2010. **82**(12): p. 5107-16.
175. Blonder, J., et al., *Proteomic analysis of detergent-resistant membrane rafts.* Electrophoresis, 2004. **25**(9): p. 1307-18.
176. Smith, P.K., et al., *Measurement of protein using bicinchoninic acid.* Anal Biochem, 1985. **150**(1): p. 76-85.
177. Tsiatsiani, L. and A.J. Heck, *Proteomics beyond trypsin.* FEBS J, 2015. **282**(14): p. 2612-26.
178. Pan, Y., et al., *Quantitative proteomics reveals the kinetics of trypsin-catalyzed protein digestion.* Anal Bioanal Chem, 2014. **406**(25): p. 6247-56.
179. Paizs, B. and S. Suhai, *Fragmentation pathways of protonated peptides.* Mass Spectrom Rev, 2005. **24**(4): p. 508-48.
180. Guo, X. and B.S. Kristal, *The use of underloaded C(18) solid-phase extraction plates increases reproducibility of analysis of tryptic peptides from unfractionated human plasma.* Anal Biochem, 2012. **426**(1): p. 86-90.
181. Weston, L.A., K.M. Bauer, and A.B. Hummon, *Comparison of bottom-up proteomic approaches for LC-MS analysis of complex proteomes.* Anal Methods, 2013. **5**(18).
182. Tsai, C.F., et al., *Large-scale determination of absolute phosphorylation stoichiometries in human cells by motif-targeting quantitative proteomics.* Nat Commun, 2015. **6**: p. 6622.
183. Fila, J. and D. Honys, *Enrichment techniques employed in phosphoproteomics.* Amino Acids, 2012. **43**(3): p. 1025-47.
184. Thingholm, T.E. and M.R. Larsen, *Phosphopeptide Enrichment by Immobilized Metal Affinity Chromatography.* Methods Mol Biol, 2016. **1355**: p. 123-33.
185. Kanshin, E., S.W. Michnick, and P. Thibault, *Displacement of N/Q-rich peptides on TiO2 beads enhances the depth and coverage of yeast phosphoproteome analyses.* J Proteome Res, 2013. **12**(6): p. 2905-13.

186. Rogers, L.D. and L.J. Foster, *Phosphoproteomics--finally fulfilling the promise?* Mol Biosyst, 2009. **5**(10): p. 1122-9.
187. Lind, S.B., K.A. Artemenko, and U. Pettersson, *A strategy for identification of protein tyrosine phosphorylation.* Methods, 2012. **56**(2): p. 275-83.
188. Storvold, G.L., et al., *Quantitative profiling of tyrosine phosphorylation revealed changes in the activity of the T cell receptor signaling pathway upon cisplatin-induced apoptosis.* J Proteomics, 2013. **91**: p. 344-57.
189. Grossmann, A., et al., *Phospho-tyrosine dependent protein-protein interaction network.* Mol Syst Biol, 2015. **11**(3): p. 794.
190. Yue, X., A. Schunter, and A.B. Hummon, *Comparing multistep immobilized metal affinity chromatography and multistep TiO2 methods for phosphopeptide enrichment.* Anal Chem, 2015. **87**(17): p. 8837-44.
191. Liu, F., et al., *Preparation of Polypropylene Spin Tips Filled with Immobilized Titanium(IV) Ion Monolithic Adsorbent for Robust Phosphoproteome Analysis.* Anal Chem, 2016. **88**(10): p. 5058-64.
192. Kanshin, E., S. Michnick, and P. Thibault, *Sample preparation and analytical strategies for large-scale phosphoproteomics experiments.* Semin Cell Dev Biol, 2012. **23**(8): p. 843-53.
193. Rappsilber, J., M. Mann, and Y. Ishihama, *Protocol for micro-purification, enrichment, pre-fractionation and storage of peptides for proteomics using StageTips.* Nat Protoc, 2007. **2**(8): p. 1896-906.
194. Sugiyama, N., et al., *Phosphopeptide enrichment by aliphatic hydroxy acid-modified metal oxide chromatography for nano-LC-MS/MS in proteomics applications.* Mol Cell Proteomics, 2007. **6**(6): p. 1103-9.
195. Goppelsroeder, F., *Capillaranalyse: beruhend auf capillaritäts-und Adsorptionserscheinungen mit dem Schlusskapitel: das Emporsteigen der Farbstoffe in den Pflanzen*. 1901: E. Birkhauser.
196. McMurry, J., *Organic chemistry with biological applications*. 2nd ed. 2011, Belmont, Calif.: Brooks/Cole Cengage Learning. xxiii, 1044, 53, 30 p.
197. Gesellschaft, D.B., *Berichte der Deutschen Botanischen Gesellschaft*. 1906: Gebrüder Borntræger.
198. Meyer, V.R., *Practical High-Performance Liquid Chromatography*. 2013: Wiley.
199. Snyder, L.R., J.J. Kirkland, and J.W. Dolan, *Introduction to Modern Liquid Chromatography*. 2011: Wiley.
200. Elamin, B.A., et al., *Purification and functional characterization of pancreatic insulin from camel (Camelus dromedarius).* Saudi J Biol Sci, 2014. **21**(6): p. 574-81.
201. Dowell, J.A., et al., *Comparison of two-dimensional fractionation techniques for shotgun proteomics.* Anal Chem, 2008. **80**(17): p. 6715-23.
202. Batth, T.S. and J.V. Olsen, *Offline High pH Reversed-Phase Peptide Fractionation for Deep Phosphoproteome Coverage.* Methods Mol Biol, 2016. **1355**: p. 179-92.
203. Crombie, W.M., R. Comber, and S.G. Boatman, *The estimation of unsaturated fatty acids by reversed-phase partition chromatography.* Biochem J, 1955. **59**(2): p. 309-16.
204. Howard, G.A. and A.J. Martin, *The separation of the C12-C18 fatty acids by reversed-phase partition chromatography.* Biochem J, 1950. **46**(5): p. 532-8.

205. Partridge, S.M. and R.G. Westall, *Displacement chromatography on synthetic ion-exchange resins. 1. Separation of organic bases and amino-acids using cation-exchange resins.* Biochem J, 1949. **44**(4): p. 418-28.
206. Applezweig, N., *Ion-exchange absorbents as laboratory tools.* Ann N Y Acad Sci, 1948. **49**(Art 2): p. 295-314.
207. Law, H.C., et al., *A versatile reversed phase-strong cation exchange-reversed phase (RP-SCX-RP) multidimensional liquid chromatography platform for qualitative and quantitative shotgun proteomics.* Analyst, 2015. **140**(4): p. 1237-52.
208. Lenz, C. and H. Urlaub, *Separation methodology to improve proteome coverage depth.* Expert Rev Proteomics, 2014. **11**(4): p. 409-14.
209. Lau, E., et al., *Combinatorial use of offline SCX and online RP-RP liquid chromatography for iTRAQ-based quantitative proteomics applications.* Mol Biosyst, 2011. **7**(5): p. 1399-408.
210. Chan, K.C. and H.J. Issaq, *Fractionation of peptides by strong cation-exchange liquid chromatography.* Methods Mol Biol, 2013. **1002**: p. 311-5.
211. Olsen, J.V., et al., *Quantitative phosphoproteomics reveals widespread full phosphorylation site occupancy during mitosis.* Sci Signal, 2010. **3**(104): p. ra3.
212. Ishihama, Y., J. Rappsilber, and M. Mann, *Modular stop and go extraction tips with stacked disks for parallel and multidimensional Peptide fractionation in proteomics.* J Proteome Res, 2006. **5**(4): p. 988-94.
213. Niessen, W.M.A., *Liquid Chromatography-Mass Spectrometry, Third Edition*. 2006: Taylor & Francis.
214. Pitt, J.J., *Principles and applications of liquid chromatography-mass spectrometry in clinical biochemistry.* Clin Biochem Rev, 2009. **30**(1): p. 19-34.
215. Gritti, F. and G. Guiochon, *The van Deemter equation: assumptions, limits, and adjustment to modern high performance liquid chromatography.* J Chromatogr A, 2013. **1302**: p. 1-13.
216. J.J. van Deemter, F.J.Z., A. Klinkenberg,, *Longitudinal diffusion and resistance to mass transfer as causes of nonideality in chromatography,*
Chemical Engineering Science. Chemical Engineering Science, 1956. **Volume 5**(Issue 6): p. Pages 271-289.
217. Meyer, V.R., *Practical High-Performance Liquid Chromatography*. 2004: Wiley.
218. Carr, P.W., X. Wang, and D.R. Stoll, *Effect of pressure, particle size, and time on optimizing performance in liquid chromatography.* Anal Chem, 2009. **81**(13): p. 5342-53.
219. Dass, C., *Fundamentals of Contemporary Mass Spectrometry*. 2007: Wiley.
220. Mitulovic, G. and K. Mechtler, *HPLC techniques for proteomics analysis--a short overview of latest developments.* Brief Funct Genomic Proteomic, 2006. **5**(4): p. 249-60.
221. Berg, H.S., et al., *Self-packed core shell nano liquid chromatography columns and silica-based monolithic trap columns for targeted proteomics.* J Chromatogr A, 2017. **1498**: p. 111-119.
222. Erni, F. and R.W. Frei, *A low-cost gradient system for high-performance liquid chromatography. Quantitation of complex pharmaceutical raw materials.* J Chromatogr, 1976. **125**(1): p. 265-74.
223. Beasley-Green, A., et al., *A proteomics performance standard to support measurement quality in proteomics.* Proteomics, 2012. **12**(7): p. 923-31.

224. Moruz, L., et al., *Optimized nonlinear gradients for reversed-phase liquid chromatography in shotgun proteomics.* Anal Chem, 2013. **85**(16): p. 7777-85.
225. Shishkova, E., A.S. Hebert, and J.J. Coon, *Now, More Than Ever, Proteomics Needs Better Chromatography.* Cell Syst, 2016. **3**(4): p. 321-324.
226. Thomson, S.J.J., *Bakerian Lecture:—Rays of positive electricity.* Proceedings of the Royal Society of London. Series A, 1913. **89**(607): p. 1-20.
227. Baghel, U.S., et al., *Application of Mass Spectroscopy in Pharmaceutical and Biomedical Analysis*. 2017.
228. Rüchardt, E., *Zur Entdeckung der Kanalstrahlen vor fünfzig Jahren.* Naturwissenschaften, 1936. **24**(30): p. 465-467.
229. Downard, K.M., *Historical account: Francis William Aston: the man behind the mass spectrograph.* Eur J Mass Spectrom (Chichester), 2007. **13**(3): p. 177-90.
230. Nadler, W.M., et al., *MALDI versus ESI: The Impact of the Ion Source on Peptide Identification.* J Proteome Res, 2017. **16**(3): p. 1207-1215.
231. Bruins, A.P., *Atmospheric-pressure-ionization mass spectrometry: II. Applications in pharmacy, biochemistry and general chemistry.* TrAC Trends in Analytical Chemistry, 1994. **13**(2): p. 81-90.
232. Glish, G.L. and R.W. Vachet, *The basics of mass spectrometry in the twenty-first century.* Nature Reviews Drug Discovery, 2003. **2**: p. 140.
233. Taylor, S.G., *Disintegration of water drops in an electric field.* Proceedings of the Royal Society of London. Series A. Mathematical and Physical Sciences, 1964. **280**(1382): p. 383-397.
234. Thomson, B.A. and J.V. Iribarne, *Field induced ion evaporation from liquid surfaces at atmospheric pressure.* The Journal of Chemical Physics, 1979. **71**(11): p. 4451-4463.
235. Iribarne, J.V. and B.A. Thomson, *On the evaporation of small ions from charged droplets.* The Journal of Chemical Physics, 1976. **64**(6): p. 2287-2294.
236. Cech, N.B. and C.G. Enke, *Practical implications of some recent studies in electrospray ionization fundamentals.* Mass Spectrometry Reviews, 2001. **20**(6): p. 362-387.
237. Angel, T.E., et al., *Mass spectrometry-based proteomics: existing capabilities and future directions.* Chem Soc Rev, 2012. **41**(10): p. 3912-28.
238. Milne, G.L. and J.D. Morrow, *Chapter 5 - Measurement of Biological Materials*, in *Clinical and Translational Science*. 2009, Academic Press: San Diego. p. 69-86.
239. Paul, W., *Electromagnetic traps for charged and neutral particles.* Reviews of Modern Physics, 1990. **62**(3): p. 531-540.
240. Todd, J.F.J., *Recommendations for nomenclature and symbolism for mass spectroscopy (including an appendix of terms used in vacuum technology). (Recommendations 1991)*, in *Pure and Applied Chemistry*. 1991. p. 1541.
241. Glish, G.L., *Multiple stage mass spectrometry: the next generation tandem mass spectrometry experiment.* Analyst, 1994. **119**(4): p. 533-537.
242. Niessen, W.M.A. and R.A.C. C, *Interpretation of MS-MS Mass Spectra of Drugs and Pesticides*. 2017: Wiley.
243. Mann, M., R.C. Hendrickson, and A. Pandey, *Analysis of Proteins and Proteomes by Mass Spectrometry.* Annual Review of Biochemistry, 2001. **70**(1): p. 437-473.
244. Gillet, L.C., et al., *Targeted data extraction of the MS/MS spectra generated by data-independent acquisition: a new concept for consistent and accurate proteome analysis.* Mol Cell Proteomics, 2012. **11**(6): p. O111 016717.

245. Olsen, J.V., et al., *Higher-energy C-trap dissociation for peptide modification analysis.* Nat Methods, 2007. **4**(9): p. 709-12.
246. Wells, J.M. and S.A. McLuckey, *Collision-induced dissociation (CID) of peptides and proteins.* Methods Enzymol, 2005. **402**: p. 148-85.
247. Jedrychowski, M.P., et al., *Evaluation of HCD- and CID-type fragmentation within their respective detection platforms for murine phosphoproteomics.* Mol Cell Proteomics, 2011. **10**(12): p. M111 009910.
248. Graves, P.R. and T.A. Haystead, *Molecular biologist's guide to proteomics.* Microbiol Mol Biol Rev, 2002. **66**(1): p. 39-63; table of contents.
249. Roepstorff, P. and J. Fohlman, *Proposal for a common nomenclature for sequence ions in mass spectra of peptides.* Biomed Mass Spectrom, 1984. **11**(11): p. 601.
250. Biemann, K., *Contributions of mass spectrometry to peptide and protein structure.* Biomed Environ Mass Spectrom, 1988. **16**(1-12): p. 99-111.
251. Steen, H. and M. Mann, *The abc's (and xyz's) of peptide sequencing.* Nature Reviews Molecular Cell Biology, 2004. **5**: p. 699.
252. McLachlin, D.T. and B.T. Chait, *Analysis of phosphorylated proteins and peptides by mass spectrometry.* Curr Opin Chem Biol, 2001. **5**(5): p. 591-602.
253. Aebersold, R. and D.R. Goodlett, *Mass spectrometry in proteomics.* Chem Rev, 2001. **101**(2): p. 269-95.
254. Köcher, T., G. Allmaier, and M. Wilm, *Nanoelectrospray-based detection and sequencing of substoichiometric amounts of phosphopeptides in complex mixtures.* Journal of Mass Spectrometry, 2003. **38**(2): p. 131-137.
255. Brown, R., et al., *Large-Scale Examination of Factors Influencing Phosphopeptide Neutral Loss during Collision Induced Dissociation.* J Am Soc Mass Spectrom, 2015. **26**(7): p. 1128-42.
256. Wiese, H., et al., *Comparison of Alternative MS/MS and Bioinformatics Approaches for Confident Phosphorylation Site Localization.* Journal of Proteome Research, 2014. **13**(2): p. 1128-1137.
257. Wiese, H., et al., *Comparison of alternative MS/MS and bioinformatics approaches for confident phosphorylation site localization.* J Proteome Res, 2014. **13**(2): p. 1128-37.
258. Marx, H., et al., *A large synthetic peptide and phosphopeptide reference library for mass spectrometry–based proteomics.* Nature Biotechnology, 2013. **31**: p. 557.
259. Zhang, Y., et al., *Optimized Orbitrap HCD for Quantitative Analysis of Phosphopeptides.* Journal of the American Society for Mass Spectrometry, 2009. **20**(8): p. 1425-1434.
260. Sharma, K., et al., *Ultradeep human phosphoproteome reveals a distinct regulatory nature of Tyr and Ser/Thr-based signaling.* Cell Rep, 2014. **8**(5): p. 1583-94.
261. Skoog, D.A., F.J. Holler, and S.R. Crouch, *Principles of Instrumental Analysis*. 2007: Thomson Brooks/Cole.
262. Domon, B. and R. Aebersold, *Options and considerations when selecting a quantitative proteomics strategy.* Nature Biotechnology, 2010. **28**: p. 710.
263. Murray Kermit, K., et al., *Definitions of terms relating to mass spectrometry (IUPAC Recommendations 2013)*, in *Pure and Applied Chemistry*. 2013. p. 1515.
264. Lee, J. and P.T. Reilly, *Limitation of time-of-flight resolution in the ultra high mass range.* Anal Chem, 2011. **83**(15): p. 5831-3.
265. Perry, R.H., R.G. Cooks, and R.J. Noll, *Orbitrap mass spectrometry: instrumentation, ion motion and applications.* Mass Spectrom Rev, 2008. **27**(6): p. 661-99.

266. Kalli, A., et al., *Evaluation and optimization of mass spectrometric settings during data-dependent acquisition mode: focus on LTQ-Orbitrap mass analyzers.* J Proteome Res, 2013. **12**(7): p. 3071-86.
267. Scigelova, M. and A. Makarov, *Orbitrap mass analyzer--overview and applications in proteomics.* Proteomics, 2006. **6 Suppl 2**: p. 16-21.
268. Nier, K.A., A.L. Yergey, and P.J. Gale, *The Encyclopedia of Mass Spectrometry: Volume 9: Historical Perspectives, Part B: Notable People in Mass Spectrometry*. 2015: Elsevier Science.
269. March, R.E. and J.F.J. Todd, *Radio frequency quadrupole technology: Evolution and contributions to mass spectrometry.* International Journal of Mass Spectrometry, 2015. **377**: p. 316-328.
270. Douglas, D.J. and N.V. Konenkov, *Mass resolution of linear quadrupole ion traps with round rods.* Rapid Commun Mass Spectrom, 2014. **28**(21): p. 2252-8.
271. Choi, B.K., et al., *Comparison of Quadrupole, Time-of-Flight, and Fourier Transform Mass Analyzers for LC-MS Applications.*
272. Lindon, J.C., *Encyclopedia of Spectroscopy and Spectrometry*. 2010: Elsevier Science.
273. Eliuk, S. and A. Makarov, *Evolution of Orbitrap Mass Spectrometry Instrumentation.* Annu Rev Anal Chem (Palo Alto Calif), 2015. **8**: p. 61-80.
274. Senko, M.W., et al., *Novel parallelized quadrupole/linear ion trap/Orbitrap tribrid mass spectrometer improving proteome coverage and peptide identification rates.* Anal Chem, 2013. **85**(24): p. 11710-4.
275. Douglas, D.J., A.J. Frank, and D. Mao, *Linear ion traps in mass spectrometry.* Mass Spectrom Rev, 2005. **24**(1): p. 1-29.
276. Schwartz, J.C., M.W. Senko, and J.E. Syka, *A two-dimensional quadrupole ion trap mass spectrometer.* J Am Soc Mass Spectrom, 2002. **13**(6): p. 659-69.
277. March, R.E., *Quadrupole ion trap mass spectrometry: a view at the turn of the century.* International Journal of Mass Spectrometry, 2000. **200**(1): p. 285-312.
278. March, R.E., R.J. Hughes, and J.F.J. Todd, *Quadrupole Storage Mass Spectrometry*. 1989: Wiley.
279. Kingdon, K.H., *A Method for the Neutralization of Electron Space Charge by Positive Ionization at Very Low Gas Pressures.* Physical Review, 1923. **21**(4): p. 408-418.
280. Knight, R.D., *Storage of ions from laser-produced plasmas.* Applied Physics Letters, 1981. **38**(4): p. 221-223.
281. Perry Richard, H., R.G. Cooks, and J. Noll Robert, *Orbitrap mass spectrometry: Instrumentation, ion motion and applications.* Mass Spectrometry Reviews, 2008. **27**(6): p. 661-699.
282. Makarov, A., *Electrostatic axially harmonic orbital trapping: a high-performance technique of mass analysis.* Anal Chem, 2000. **72**(6): p. 1156-62.
283. Hardman, M. and A.A. Makarov, *Interfacing the orbitrap mass analyzer to an electrospray ion source.* Anal Chem, 2003. **75**(7): p. 1699-705.
284. Hu, Q., et al., *The Orbitrap: a new mass spectrometer.* J Mass Spectrom, 2005. **40**(4): p. 430-43.
285. Makarov, A., et al., *Performance evaluation of a hybrid linear ion trap/orbitrap mass spectrometer.* Anal Chem, 2006. **78**(7): p. 2113-20.

286. Scheltema, R.A., et al., *The Q Exactive HF, a Benchtop mass spectrometer with a pre-filter, high-performance quadrupole and an ultra-high-field Orbitrap analyzer.* Mol Cell Proteomics, 2014. **13**(12): p. 3698-708.
287. Kelstrup, C.D., et al., *Rapid and Deep Proteomes by Faster Sequencing on a Benchtop Quadrupole Ultra-High-Field Orbitrap Mass Spectrometer.* Journal of Proteome Research, 2014. **13**(12): p. 6187-6195.
288. Michalski, A., et al., *Mass spectrometry-based proteomics using Q Exactive, a high-performance benchtop quadrupole Orbitrap mass spectrometer.* Mol Cell Proteomics, 2011. **10**(9): p. M111 011015.
289. Scheffler, K., R. Viner, and E. Damoc, *High resolution top-down experimental strategies on the Orbitrap platform.* J Proteomics, 2018. **175**: p. 42-55.
290. Shen, G., et al., *Di(2-ethylhexyl)phthalate Alters the Synthesis and beta-Oxidation of Fatty Acids and Hinders ATP Supply in Mouse Testes via UPLC-Q-Exactive Orbitrap MS-Based Metabonomics Study.* J Agric Food Chem, 2017. **65**(24): p. 5056-5063.
291. Senko, M.W., et al., *Novel Parallelized Quadrupole/Linear Ion Trap/Orbitrap Tribrid Mass Spectrometer Improving Proteome Coverage and Peptide Identification Rates.* Analytical Chemistry, 2013. **85**(24): p. 11710-11714.
292. Riley, N.M., et al., *Enhanced Dissociation of Intact Proteins with High Capacity Electron Transfer Dissociation.* J Am Soc Mass Spectrom, 2016. **27**(3): p. 520-31.
293. Ting, L., et al., *MS3 eliminates ratio distortion in isobaric multiplexed quantitative proteomics.* Nat Methods, 2011. **8**(11): p. 937-40.
294. Overmyer, K.A., et al., *Multiplexed proteome analysis with neutron-encoded stable isotope labeling in cells and mice.* Nat Protoc, 2018. **13**(1): p. 293-306.
295. Resing, K.A. and N.G. Ahn, *Proteomics strategies for protein identification.* FEBS Letters, 2005. **579**(4): p. 885-889.
296. Bantscheff, M., et al., *Quantitative mass spectrometry in proteomics: a critical review.* Analytical and Bioanalytical Chemistry, 2007. **389**(4): p. 1017-1031.
297. Al Shweiki, M.R., et al., *Assessment of Label-Free Quantification in Discovery Proteomics and Impact of Technological Factors and Natural Variability of Protein Abundance.* J Proteome Res, 2017. **16**(4): p. 1410-1424.
298. McAlister, G.C., et al., *Increasing the multiplexing capacity of TMTs using reporter ion isotopologues with isobaric masses.* Anal Chem, 2012. **84**(17): p. 7469-78.
299. Megger, D.A., et al., *Comparison of label-free and label-based strategies for proteome analysis of hepatoma cell lines.* Biochim Biophys Acta, 2014. **1844**(5): p. 967-76.
300. Boersema, P.J., et al., *Multiplex peptide stable isotope dimethyl labeling for quantitative proteomics.* Nature Protocols, 2009. **4**: p. 484.
301. Rigbolt, K.T. and B. Blagoev, *Proteome-wide quantitation by SILAC.* Methods Mol Biol, 2010. **658**: p. 187-204.
302. Hilger, M. and M. Mann, *Triple SILAC to determine stimulus specific interactions in the Wnt pathway.* J Proteome Res, 2012. **11**(2): p. 982-94.
303. Cox, J. and M. Mann, *MaxQuant enables high peptide identification rates, individualized p.p.b.-range mass accuracies and proteome-wide protein quantification.* Nat Biotechnol, 2008. **26**(12): p. 1367-72.
304. Cox, J., et al., *Andromeda: a peptide search engine integrated into the MaxQuant environment.* J Proteome Res, 2011. **10**(4): p. 1794-805.

305. Tyanova, S., T. Temu, and J. Cox, *The MaxQuant computational platform for mass spectrometry-based shotgun proteomics.* Nature Protocols, 2016. **11**: p. 2301.
306. National Center for Biotechnology Information (U.S.), *The NCBI handbook*. 2013, National Center for Biotechnology Information (US),: Bethesda (MD). p. 1 online resource.
307. UniProt, C., *UniProt: a hub for protein information.* Nucleic Acids Res, 2015. **43**(Database issue): p. D204-12.
308. Wang, G., et al., *Decoy methods for assessing false positives and false discovery rates in shotgun proteomics.* Anal Chem, 2009. **81**(1): p. 146-59.
309. Goloborodko, A.A., et al., *Empirical approach to false discovery rate estimation in shotgun proteomics.* Rapid Commun Mass Spectrom, 2010. **24**(4): p. 454-62.
310. Cox, J., et al., *A practical guide to the MaxQuant computational platform for SILAC-based quantitative proteomics.* Nature Protocols, 2009. **4**: p. 698.
311. Zhang, J., et al., *PEAKS DB: de novo sequencing assisted database search for sensitive and accurate peptide identification.* Mol Cell Proteomics, 2012. **11**(4): p. M111 010587.
312. Koenig, T., et al., *Robust prediction of the MASCOT score for an improved quality assessment in mass spectrometric proteomics.* J Proteome Res, 2008. **7**(9): p. 3708-17.
313. Rost, H.L., et al., *OpenMS: a flexible open-source software platform for mass spectrometry data analysis.* Nat Methods, 2016. **13**(9): p. 741-8.
314. Grosstessner-Hain, K., et al., *Quantitative phospho-proteomics to investigate the polo-like kinase 1-dependent phospho-proteome.* Mol Cell Proteomics, 2011. **10**(11): p. M111 008540.
315. Jastrzebski, K., et al., *A phospho-proteomic screen identifies novel S6K1 and mTORC1 substrates revealing additional complexity in the signaling network regulating cell growth.* Cell Signal, 2011. **23**(8): p. 1338-47.
316. Soufi, B., et al., *Global analysis of the yeast osmotic stress response by quantitative proteomics.* Mol Biosyst, 2009. **5**(11): p. 1337-46.
317. Britton, D., et al., *Quantification of pancreatic cancer proteome and phosphorylome: indicates molecular events likely contributing to cancer and activity of drug targets.* PLoS One, 2014. **9**(3): p. e90948.
318. Olsen, J.V., et al., *Global, In Vivo, and Site-Specific Phosphorylation Dynamics in Signaling Networks.* Cell, 2006. **127**(3): p. 635-648.
319. Verano-Braga, T., et al., *Time-Resolved Quantitative Phosphoproteomics: New Insights into Angiotensin-(1–7) Signaling Networks in Human Endothelial Cells.* Journal of Proteome Research, 2012. **11**(6): p. 3370-3381.
320. J. D'Souza, R.C., et al., *Time-resolved dissection of early phosphoproteome and ensuing proteome changes in response to TGF-β.* Science Signaling, 2014. **7**(335): p. rs5-rs5.
321. Konson, A., et al., *Pigment epithelium-derived factor and its phosphomimetic mutant induce JNK-dependent apoptosis and p38-mediated migration arrest.* J Biol Chem, 2011. **286**(5): p. 3540-51.
322. Zhao, Y., et al., *Site-directed mutagenesis of phosphorylation sites of the branched chain alpha-ketoacid dehydrogenase complex.* J Biol Chem, 1994. **269**(28): p. 18583-7.
323. Ho, S.N., et al., *Site-directed mutagenesis by overlap extension using the polymerase chain reaction.* Gene, 1989. **77**(1): p. 51-9.
324. Reikofski, J. and B.Y. Tao, *Polymerase chain reaction (PCR) techniques for site-directed mutagenesis.* Biotechnol Adv, 1992. **10**(4): p. 535-47.

325. Zoller, M.J., *New molecular biology methods for protein engineering.* Curr Opin Biotechnol, 1991. **2**(4): p. 526-31.
326. Jia, Y., et al., *Current in vitro kinase assay technologies: the quest for a universal format.* Curr Drug Discov Technol, 2008. **5**(1): p. 59-69.
327. Lewis, P.A., *Assaying the kinase activity of LRRK2 in vitro.* J Vis Exp, 2012(59).
328. Kawamura, A. and Y. Aoyama, *Immunofluorescence in Medical Science*. 1983: University of Tokyo Press.
329. Franke, W.W., et al., *Different intermediate-sized filaments distinguished by immunofluorescence microscopy.* Proc Natl Acad Sci U S A, 1978. **75**(10): p. 5034-8.
330. Kanshin, E., et al., *Phosphoproteome dynamics of Saccharomyces cerevisiae under heat shock and cold stress.* Mol Syst Biol, 2015. **11**(6): p. 813.
331. Kubiniok, P., et al., *Time-resolved Phosphoproteome Analysis of Paradoxical RAF Activation Reveals Novel Targets of ERK.* Mol Cell Proteomics, 2017. **16**(4): p. 663-679.

Chapter 2

Phosphoproteome dynamics of *Saccharomyces cerevisiae* under heat shock and cold stress

Evgeny Kanshin[1,5], Peter Kubiniok[1,2,5], Yogitha Thattikota[1,3], Damien D'Amours[1,3] and Pierre Thibault[1,2,4]*

[1]Institute for Research in Immunology and Cancer, Université de Montréal, C.P. 6128, Succursale centre-ville, Montréal, Québec, H3C 3J7, Canada.
[2] Department of Chemistry, Université de Montréal, C.P. 6128, Succursale centre-ville, Montréal, Québec, H3C 3J7, Canada.
[3] Department of Pathology and Cell Biology, Université de Montréal, C.P. 6128, Succursale centre-ville, Montréal, Québec, H3C 3J7, Canada.
[4] Department of Biochemistry, Université de Montréal, C.P. 6128, Succursale centre-ville, Montréal, Québec, H3C 3J7, Canada.
[5] These authors contributed equally to this work

Manuscript: Published (June 3 2015 in Molecular Systems Biology, 11(6):813)

Authors Contribution

All authors designed and participated in the study concept. P.K. conducted all phosphoproteomics experiments after training by E.K., data analysis was performed by P.K. and E.K. together. E.K., P.K. and P.T. interpreted phosphoproteomics data. D.D. and Y.T. designed and contributed biological follow up experiments. E.K., P.K. and P.T. contributed to the preparation and writing of the manuscript with close support from D.D. and Y.T..

2.1 Abstract

The ability of cells and organisms to survive and function through changes of temperature evolved from their specific adaptations to non-optimal growth conditions. Responses to elevated temperatures have been studied in yeast and other model organisms using transcriptome profiling, and provided valuable biological insights on molecular mechanisms involved in stress tolerance and adaptation to adverse environment. In contrast, little is known about rapid signaling events associated with changes in temperature. To gain a better understanding of global changes in protein phosphorylation in response to heat and cold, we developed a high temporal resolution phosphoproteomics protocol to study cell signaling in *Saccharomyces cerevisiae*. The method allowed for quantitative analysis of phosphodynamics on 2,777 phosphosites from 1,228 proteins. The correlation of kinetic profiles between kinases and their substrates provided a predictive tool to identify new putative substrates for kinases such as Cdc28 and PKA. Cell cycle analyses revealed that the increased phosphorylation of Cdc28 at its inhibitory site Y19 during heat shock is an adaptive response that delays cell cycle progression under stress conditions. The cellular responses to heat and cold were associated with extensive changes in phosphorylation on proteins implicated in transcription, protein folding and degradation, cell cycle regulation and morphogenesis.

2.2 Introduction

Single cell organisms such as yeast are regularly exposed to environmental changes that required the development of adaptation mechanisms for survival in sub-optimal growth conditions. Variation in temperature is a common stress experienced by yeast cells, a condition for which evolutionary changes favored organisms that developed appropriate responses to heat shock and cold stress. For example, *S. cerevisiae* have evolved protective transcriptional programs in response to elevated temperature (> 37℃) that result in physiological changes affecting carbohydrate flux, cytoskeleton dynamics and protein folding [1, 2]. The molecular basis of the response to different stresses including heat shock has been well documented in *S. cerevisiae*, and genome-wide transcriptional profiling studies identified important regulators of environmental stress response (ESR) [3, 4]. A large proportion of induced ESR genes target different cellular processes, including carbohydrate metabolism, protein folding and degradation, autophagy, cytoskeletal reorganization and DNA damage repair. In contrast, ESR genes with repressed expression are involved in protein synthesis, ribosome synthesis and processing, RNA polymerase-dependent transcription and protein translation.

Short-term exposure to moderate heat shock has been reported to induce a complx cellular response culminating in a transient cell cycle arrest at G1/S transition in both yeast and mammalian cells [5]. This response appears to be associated with the activity threshold of cyclin-dependent kinases [5], and overexpression of G1 cyclins in yeast has been shown to overcome the transient arrest induced by heat shock [6]. Moreover, Ste20, Cla4, and Skm1, all members of the p21-activated kinase (PAK) family, are also activated upon changes in temperature, and play important roles in the regulation of osmosensing, filamentous growth and septin ring assembly [7-10]. Interestingly, decreased levels of the molecular chaperone Hsp90 or its kinase-specific chaperone Cdc37 are known to affect Cdc28 and Cla4 stability [11], a condition that favors a subset of cells to switch to a filamentous form in response to hostile environment [12].

While a large body of literature exists on the molecular basis of heat shock in yeast, mechanisms associated with the response to cold stress are still poorly understood [13]. Experimental evidences suggest that changes in membrane fluidity functions as a cold sensor to trigger subsequent signal transduction [14]. Exposure to low temperature induces the accumulation of trehalose, glycerol, and heat shock proteins to protect yeast cells against freeze injury [15]. Both

heat shock and cold stress appear to be regulated by classical stress pathways involving the high-osmolarity glycerol mitogen activated protein kinase Hog1, and the transcriptional factors Msn2 and Msn4 [16]. Aside from the classical stress pathways in which Hog1 is playing a central role, little is known about the signaling events resulting from changes in temperature.

To gain further insights on the dynamic changes in protein phosphorylation associated with heat shock and cold stress, we performed a large-scale phosphoproteomics study on *S. cerevisiae*. Yeast represents one of the most intensively studied eukaryotic cell model organism with a relatively simple genome consisting of approximately 6,500 genes. The introduction of sensitive mass spectrometry (MS) instrumentation and affinity media for phosphopeptide enrichment have paved the way to comprehensive phosphoproteome analysis that significantly expanded the repertoire of protein phosphorylation identified in yeast and other model organisms. Several large-scale quantitative phosphoproteomics studies conducted on yeast cells have already described changes in protein phosphorylation in response to different stimuli including pheromone [17], DNA damage [18], fatty acid and peroxisome induction [19], and kinase inhibition [20]. Other large-scale studies using stable isotope labeling in cell culture (SILAC) highlighted the regulation of protein phosphorylation in yeast during the cell cycle [21], and as a function of ploidy [22]. While MS-based phosphoproteomics enables the profiling of thousands of phosphopeptides from microgram amounts of sample, the identification of the phosphosites that are specific to the stimulus remains a challenge, due to prevalence of promiscuous phosphorylation events arising from random encounters of kinases with abundant neighboring proteins [23]. The identification of differentially regulated phosphoproteins by conventional data analysis approaches typically rely on fold change (FC) in phosphopeptide abundances taken at different time points shortly after the onset of the stimulus. However, dynamic changes in protein phosphorylation are difficult to establish based on FC measurements obtained from a limited number of time points. We reasoned that the acquisition of high resolution kinetic profiles could provide valuable information on phosphoproteome dynamics to further understand how temporal changes in kinase and phosphatase activities are reflected on downstream substrates in response to environmental stress.

Accordingly, we performed quantitative phosphoproteomics analyses using SILAC [24] and profiled changes in protein phosphorylation for the first 28 min upon temperature stress with a temporal resolution of 2 min. The ability to determine kinetic changes in protein

phosphorylation with high resolution enabled the identification of 5,554 high quality profiles (≥ 10 measurements out of 15), including dynamic phosphorylation profiles of low amplitude that typically elude conventional phosphoproteomics approaches based on FC alone. We identified 391 phosphosites that showed distinct changes in phosphorylation upon either heat shock or cold stress. Detailed clustering analyses of dynamic profiles distinguished different types of patterns such as monotonous and adaptation-like responses. Also, we observed that kinases shared similar kinetic profiles with known substrates, a correlation that facilitated the identification of other putative substrates. Phosphosites exhibited notable differences of dynamic patterns in response to cold and heat, underlining the complexity of signaling rewiring essential for cell adaptation and survival. The ability to profile phosphoproteome dynamics and identify stimulus-specific phosphosites may provide additional insights on the regulation of protein phosphorylation in a wide variety of cellular processes.

2.3 Materials and methods

2.3.1 Cell culture

Yeast strain S288C (LYS1Δ::kanMX; ARG4Δ::kanMX - a generous gift of Ole Jensen, University of Southern Denmark) was grown in Synthetic Dextrose (0.17% yeast nitrogen base without amino acids, 0.5% ammonium sulfate, 2% glucose, and appropriate amino acids) supplemented with either light (Lys0/Arg0), medium (Lys4/Arg6) or heavy (Lys8/Arg10) lysine (30 mg/L) and arginine (20 mg/L) (Cambridge Isotope Laboratories). The temperature was monitored throughout all experiments. The temperature of all SILAC cultures was 30^{o}C (+/-1^{o}C) prior to heat or cold shock. Temperature stress experiments were achieved by adding 280 ml of fresh media at 30^{o}C (control, light), 0^{o}C (cold stress, medium) and 60^{o}C (heat shock, heavy) to 175 ml of cell cultures maintained at 30^{o}C to bring the final temperature at 30, 18 and 42^{o}C, respectively. Flasks with cultures were immediately placed into temperature-controlled water bathes. Aliquots of 42 ml from each culture were collected every 2 min and combined in 700 ml of cold 95% ethanol (-80^{o}C).

Yeast cells with an analog-sensitive mutant (*cdc28-as1*) were grown in the same media until OD_{600}=0.7. Inhibition was performed by adding the pharmacological inhibitor 1NM-PP1 to a final concentration of 10 μM whereas control cells were treated with vehicle (DMSO). After 15

min, TCA was added to final concentration 10% and cells were collected by centrifugation (2,000 x g, 10 min) and washed with ice-cold PBS. Proteins were extracted and digested as described below.

2.3.2 Yeast mutant construction

To construct the *cdc28-as1* strain used for SILAC analysis, mutations resulting in the F88G change were introduced at the *CDC28* locus in strain YAL6B. The strain was transformed with a F88G–encoding PCR product amplified from plasmid p575, which carries the *CDC28::Tadh1::HIS3MX6* selection cassette [25]. The presence of the F88G mutation (and absence of secondary mutations) was confirmed by sequencing the entire *CDC28* open reading frame on chromosome 2 in strain D4485. To construct the *cdc28-af* mutant strain, plasmid p1288 was digested with PvuII, SalI and XhoI to release its *cdc28-T18A-Y19F::Tadh1::HIS3MX6* insert and transformed in strain YAL6B. Proper integration of *cdc28-af* mutations at the genomic locus was confirmed by selection on SC-HIS medium, PCR amplicon size analysis, and sequencing the entire *CDC28* open reading frame in strain D4591.

2.3.3 Protein extraction and enzymatic digestion

Cells were pelleted by centrifugation (2,000 x g, 10 min) and ethanol was discarded. Cell pellets were washed twice with 35 ml of cold (0^{o}C) PBS and lysed by bead beating for 10 min in lysis buffer (8 M urea, 50 mM Tris pH 8.0, supplemented with HALT phosphatase inhibitor cocktail, Pierce). Samples were centrifuged at 40,000 x g for 10 min, and the supernatants were transferred into clean tubes prior to determination of protein concentrations by BCA assay (Thermo Fisher Scientific). Disulfide bridges were reduced by adding dithiothreitol to a final concentration of 5 mM and samples were incubated at 56 °C for 30 minutes. Reduced cysteines were alkylated by adding iodoacetamide to 15 mM and incubating for 30 minutes in the dark at room temperature. Alkylation was quenched with 5 mM dithiothreitol for 15 minutes. Samples were diluted 6-fold with 20 mM TRIS, pH 8 containing 1 mM $CaCl_2$ prior to overnight digestion at 37^{o}C with trypsin (Sigma-Aldrich) using an enzyme to substrate ratio of 1:50 (w/w). Tryptic digests were acidified with 1% formic acid (FA), centrifuged (20,000 x g 10 min) and desalted

on Oasis HLB cartridges (Waters). Peptide eluates were snap-frozen in liquid nitrogen, lyophilized in a speedvac centrifuge and stored at -80^{o}C.

2.3.4 Phosphopeptide isolation and fractionation

Tryptic digests were subjected to the TiO_2 enrichment as described previously [26]. Sample loading, washing, and elution steps were performed using custom spin columns [27, 28] made from 200 µl pipette tip containing a SDB-XC membrane (3M) frit and filled with TiO_2 beads. We equilibrate TiO_2 material in 250 mM lactic acid in 70% ACN 3% TFA, the same buffer was used for sample loading. Phosphopeptides were displaced from TiO_2 with 500 mM phosphate buffer at pH=7. Peptides were desalted in 50 µl of 1% FA and subsequently eluted from spin columns using 50 µl of 50% acetonitrile (ACN) 0.5% FA. Eluates were dried in a speedvac and stored at -80^{o}C. To increase phosphoproteome coverage prior to MS analysis, phosphopeptides were fractionated offline by SCX chromatography. Peptides were solubilized in 100 µl of loading buffer (0.2% FA 10% ACN) and loaded onto StageTips containing 15 mg of Poly-sulfoethyl-A SCX phase (5 µm 300A, Canada Life Science). Columns were washed with 50 µl of loading buffer and peptides were eluted in 6 separate 100 µl salt steps of 15, 25, 50, 80, 150 and 1000 mM NaCl. Fractions were collected, dried in a speedvac, resuspended in 15 µl of 4% FA prior to MS analysis.

2.3.5 Offline PGC fractionation of nonphosphorylated peptides

Peptides not retained on TiO_2 resin (nonphosphorylated peptides) we diluted with water to reduce ACN concentration to 2% and subsequently desalted on Oasis HLB cartridges. Eluates were dried on a speedvac. Approximately 100 ug of peptides were fractionated offline on a PGC column (*Hypercarb™ Porous Graphitic Carbon,* 50 x 21 mm) using a 80 min ACN gradient from 0 to 80% in 10 mM ammonium formate, pH=10 with a constant flow rate of 200 uL/min. Fractions were collected every 2 min and lyophilized on a speedvac. Peptides were resuspended in 50 uL of 4% FA and 10 uL were used for LC-MS/MS analyses.

2.3.6 Mass spectrometry

Enriched phosphopeptide extracts were analyzed by LC-MS/MS using a Proxeon nanoflow HPLC system coupled to a Q-Exactive mass spectrometer (Thermo Fisher Scientific). Each sample was loaded on a reverse-phase precolumn (5 mm length, 360 µm i.d.) and separated on a reverse-phase analytical column (18 cm length, 150 µm i.d.) (Jupiter C_{18}, 3µm, 300 Å, Phenomenex). Both columns were packed manually. LC separations were performed at a flow rate of 0.6 µL/min using a linear gradient of 5-40 % aqueous ACN (0.2% FA) in 150 minutes. MS spectra were acquired with a resolution of 70,000 using a lock mass (m/z: 445.120025) followed by up to 10 MS/MS data dependent scans on the most intense ions using high energy dissociation (HCD). AGC target values for MS and MS/MS scans were set to 1e6 (max fill time 500 ms) and 1e6 (max fill time 120 ms), respectively. The precursor isolation window was set to m/z 2 with a HCD normalized collision energy of 25. The dynamic exclusion window was set to 30s.

2.3.7 Data processing and analysis

MS data were analyzed using MaxQuant [29, 30] software version 1.3.0.3 and searched against the SwissProt subset of the *S. cerevisiae* uniprot database (http://www.uniprot.org/) containing 6,630 entries. A list of 248 common laboratory contaminants included in MaxQuant was also added to the database as well as reversed versions of all sequences. The enzyme specificity was set to trypsin with a maximum number of missed cleavages set to 2. The precursor mass tolerance was set to 20 ppm for the first search (used for non-linear mass re-calibration [31] and then to 6 ppm for the main search. Phosphorylation of serine, threonine and tyrosine residues was searched as variable modification; carbamidomethylation of cysteines was searched as a fixed modification. The false discovery rate (FDR) for peptide, protein, and site identification was set to 1%, the minimum peptide length was set to 6, and the ‘peptide requantification’ function was enabled. The option match between runs (1 min time tolerance) was enabled to correlate identification and quantitation results across different runs. MaxQuant parameters.txt and experimentalDesign.txt files used in this study are listed in Supplementary Table S2-9. The

mass spectrometry data from this publication have been submitted to the Peptide Atlas database (http://www.peptideatlas.org/) and assigned the identifier PASS00536.

In addition to an FDR of 1% set for peptide, protein and phosphosite identification levels, we used additional criteria to increase data quality. First we considered only peptides for which abundance ratios (FC=Stimulus/Control) were measured in at least 10 out of 15 time points. Then we set a cut-off for average phosphosite localization confidence across experiments (time points) to 0.75. Final selection of dynamic profiles was achieved by fitting all temporal curves to a polynomial model and filtering out fits those with a regression coefficient $R^2<0.9$. (Supplementary Figure S2.3 and Supplementary Table S2-2). Based on these criteria we obtained 5554 high confidence profiles, of which 2777 represented dynamic phosphosite profiles (Supplementary Table S2-1).

2.3.8 Clustering of kinetic profiles, NetworKIN, GO and PPI network analysis

We used fuzzy C-means algorithm to cluster all dynamic profiles [32]. Analysis and visualization were performed in the R environment (http://www.r-project.org/) with the Mfuzz package[33]. Optimal setting of the "fuzzifier" parameter was 1.235 as estimated with the "mestimate" function. In order to find the optimal number of clusters, we performed Repeated soft clustering for cluster numbers ranging from 6 to 30 were performed to calculate the minimum centroid distance (minimum distance between two cluster centers produced by c-means clustering)[34]. Prediction of kinase-substrate relationships were achieve using KinomeXplorer with default thresholding criteria [35] (http://networkin.info/). Gene ontology enrichment analyses were performed against whole *S. cerevisiae* proteome as background using DAVID bioinformatics resources for proteins containing dynamic phosphosites. [36, 37] A protein-protein interaction network was built in STRING for all proteins containing dynamic phosphosites [38]. All interaction predictions were based on experimental evidences with the minimal confidence score of 0.9 (considered as a "highest confidence" filter in STRING). Results were visualized in Cytoscape network visualization and analysis [39-41].

2.3.9 Yeast cell cycle analyses

Synchronization of cells in G1 was carried out using α-factor treatment (50 ng/ml for 120 min). Cells were released from the arrest by filtration and resuspension in fresh medium at the indicated temperatures. Samples were taken at 15 min intervals and processed to monitor bud formation and mitotic spindle morphology by indirect immunofluorescence, as previously described [42]. Spindle images were acquired on a DeltaVision microscope using the softWoRx software (Applied Precision). Conditions for serial dilution assays are as described previously [42].

2.4 Results

2.4.1 High temporal resolution of the *S. cerevisiae* phosphoproteome dynamics in response to heat and cold

We designed an experimental workflow to measure phosphoproteome dynamics with 2 min temporal resolution, and monitor changes associated with heat shock and cold stress in *S. cerevisiae*. Briefly, cells were grown at 30^{o}C in media containing light (^{0}Lys, ^{0}Arg), medium (^{4}Lys, ^{6}Arg) or heavy (^{8}Lys, ^{10}Arg) isotopic forms of lysine and arginine. Cell cultures were mixed with either cold or hot fresh media and maintained in a thermostated water bath to induce a rapid shift of temperature to 18 ^{o}C (cold stress), 42 ^{o}C (heat shock) or 30 ^{o}C (control) (Figure 2.1A). Aliquots from each culture were collected every 2 min and pooled together in cold (-80^{o}C) ethanol to prevent protein degradation and changes in phosphorylation. After centrifugation, cells were lysed by bead beating in urea buffer, and proteins were digested into peptides with trypsin. Phosphopeptides were enriched on TiO_2 affinity resin, and fractionated offline into 6 SCX salt fractions prior to LC-MS/MS analysis. Phosphopeptide identification and quantification was performed using MaxQuant [29, 30] and further analyses were achieved using R (http://www.r-project.org/), Perl (www.perl.org) and bioinformatics tools such as KinomeXplorer [35] and STRING [38] (Figure 2.1B and Materials and Methods). We identified a total of 9,357 unique phosphosites on 2,344 proteins, of which approximately 70% were localized with high confidence (6,553 phosphosites). The abundance of phosphopeptides was profiled across time, and only those quantified in at least 10 out of 15 time points were retained

for further analysis. Accordingly, we identified 5,554 high quality profiles corresponding to 2,777 phosphosites (1,228 proteins) (Supplementary Figure S2.1 and Supplementary Table S2-1). A pairwise comparison of phosphopeptide abundance across time points is provided as Supplementary data (Supplementary Figure S2.2).

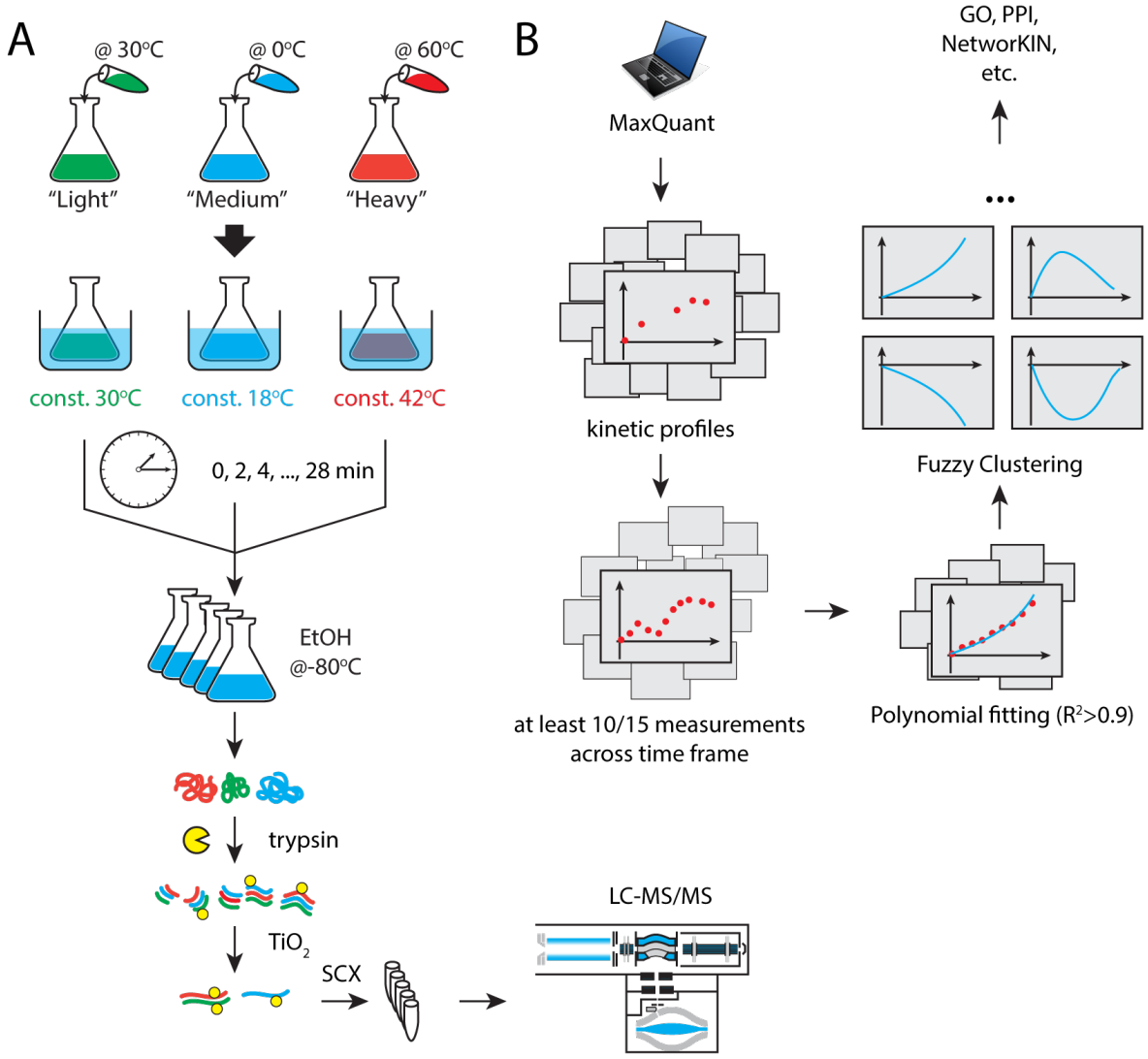

Figure 2.1. Experimental design and data analysis workflow.

A) Temperature shifts are initiated by adding either hot (60°C) or cold (0°C) media to cell cultures. The temperature of cultures is maintained in thermostated water bathes throughout the duration of the experiments. Samples are collected every 2 min by mixing yeast cultures in cold ethanol to immediately preserve protein phosphorylation. Yeast cells are centrifuged and lysed under denaturing conditions, and extracted proteins are digested with trypsin. Phosphopeptides are purified on TiO2 beads and fractionated offline on SCX spin columns prior to LC-MS/MS analyses. B) Phosphopeptide identification and quantitation is performed using MaxQuant, and only kinetic profiles containing at least 10 time measurements were selected for further analysis. Polynomial fitting was used to define regulated phosphosites. Sites with R2 > 0.9 were selected and used for fuzzy c-means clustering and subsequent analyses.

To determine the overall changes in phosphoproteome in response to heat shock or cold stress, we used fold change (FC) ratio of peptide abundance between conditions as a proxy for biological variability induced by the stimulus (Figure 2.2A). Global effects of the treatment (heat or cold) on the phosphoproteome was evaluated from the width of the $\log_2$ FC distribution of all phosphopeptides for a given time point. The width of this distribution is represented as the interquartile range (IQR). If the treatment produces global changes in phosphorylation this will be reflected by a widening of the FC distribution. We plotted the interquartile ranges (IQR) for $\log_2$(FC) distributions of phosphopeptides to monitor the global changes of the phosphoproteome upon heat and cold stress (Figure 2.2B). The IQR values of nonphosphorylated peptides retained on TiO_2 in a nonspecific manner are also shown for comparison. At the onset, (T=0 min), no significant differences were observed in IQR values for all three conditions, and coefficient of variation for abundance measurements were within +/- 0.29 for all quantified peptides. A progressive increase in FC ratio of phosphopeptides was observed during the first 10 min upon heat shock and cold stress while the abundance of non phosphorylated peptides remained relatively constant over the entire time period of the experiment. It is noteworthy that changes in phosphorylation were markedly different between stimuli, suggesting that exposure to elevated temperature has more pronounced effects on the phosphoproteome of *S. cerevisiae* with FC ratios typically 4 times higher on average for heat shock compared to cold stress. Protein phosphorylation reached a plateau around 20 min upon stimulation, possibly reflecting a gradual adaptation of yeast cells to the environmental condition.

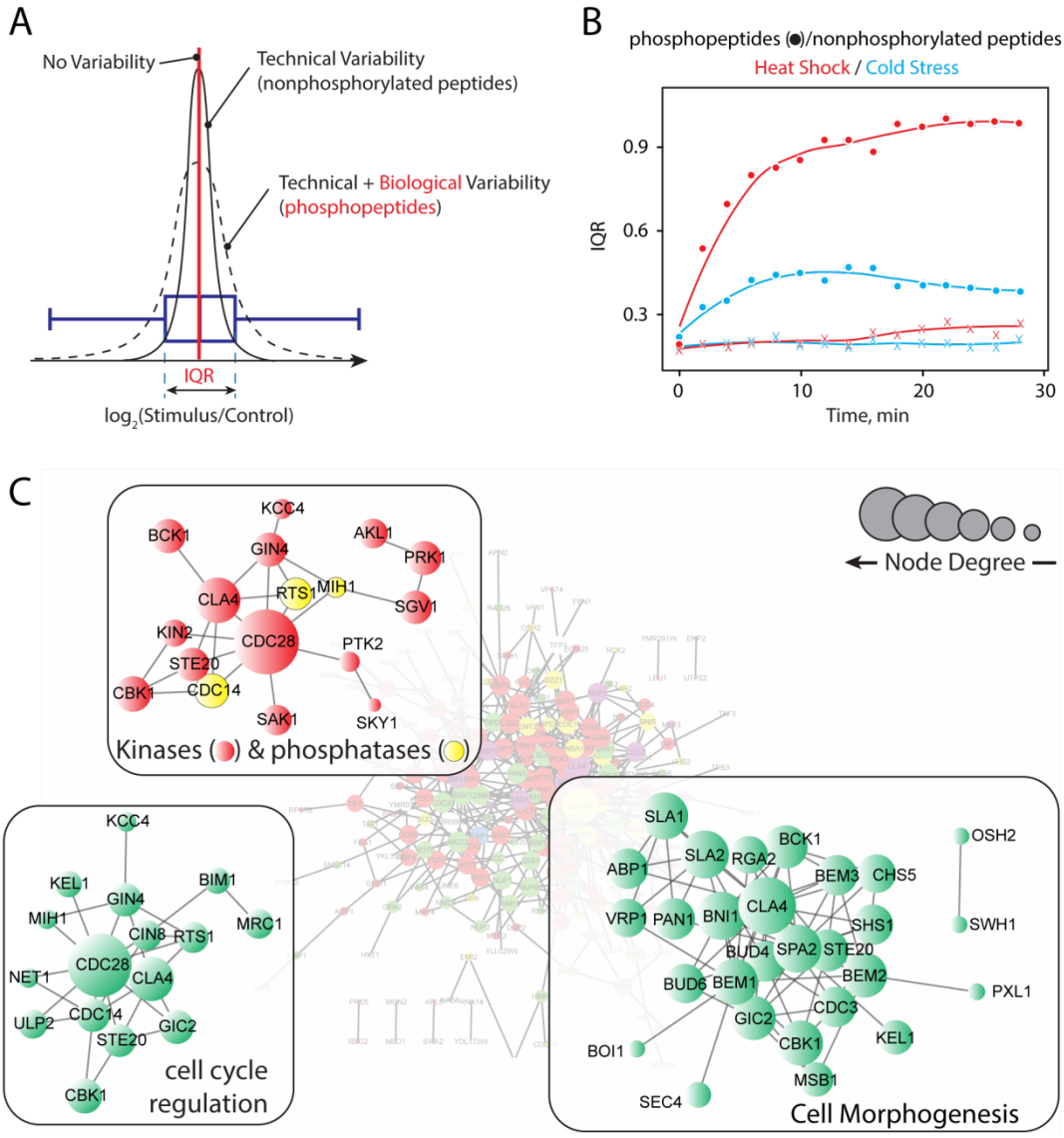

Figure 2.2. Proteome-wide effects of temperature.

A) Width of FC distribution is used to define biological variability associated with a particular stimulus. No significant changes in the abundance of nonphosphorylated peptides were observed during the experiment, and the corresponding coefficient of variation was used to determine technical variability (sample processing and LC-MS/MS analysis). The FC distribution of phosphopeptides corresponds to the sum of technical variability and stimulus-associated changes. B) Phosphopeptides exhibited a progressive increase in IQR with time, reflecting the global effects of temperature on the phosphoproteome. Notably, heat shock produced more pronounced effects compared to cold stress. The distribution of FC for nonphosphorylated peptides remained largely unaffected. C) Proteins that displayed changes in phosphorylation upon temperature shifts were used to build interaction network using the STRING database (http://string-db.org/), and selecting high stringency (score > 0.7) interactions inferred from experimental data. Node degree is the number of interacting partners in the network. These analyses revealed that responses to heat shock and cold stress are complex and involved the activation of many kinases and phosphatases that affect downstream substrates with wide range of cellular functions, including cell cycle regulation and cell morphogenesis.

In order to define biologically regulated phosphosites in the dataset, we first performed fitting of all kinetic profiles with a polynomial model, selecting only those with $R^2 > 0.9$ (Figure 2.1B and

Supplementary Figure S2.3). This analysis does not depend on the absolute ratios of abundance measurements or fold change (FC), rather it is based on the shape and low variance (i.e. low RSD values of SILAC measurements) of kinetic profiles. Profiles with high RSD do not generally provide meaningful R^2 values, and are not considered for subsequent analyses. It is noteworthy that FC values do not reflect actual stoichiometry of phosphorylation. For example, a FC value of 10 might indicate a change in phosphorylation from 1 to 10% whereas a FC value of 2 could correspond to full protein phosphorylation (from 50 to 100%). Since biological relevance of phosphosite cannot be based on FC measurements alone, profiles with low amplitude (small FC) could be as important as profiles with high amplitude (high FC). In this study, we assign significance based on the shape of kinetic profiles rather than absolute values of the corresponding FC values. Therefore, this approach enabled the selection of profiles of low amplitude that could elude conventional quantitative phosphoproteomic methods based on FC alone. We performed fuzzy clustering of these profiles and selected only profiles with cluster membership value higher than 0.7 for subsequent analyses. We identified 388 phosphosites from 271 proteins that showed distinct changes in phosphorylation (increase or decrease) with time for at least one stimulus (Supplementary Table S2-2). For convenience, we hereafter defined these phosphosites as "dynamic" to distinguish them from remaining "static" phosphosites. Dynamic sites showed significant changes in phosphorylation where max $|\log_2 FC|$ measurements were typically 2-fold higher than static sites (Supplementary Figure S2.4). To account for the possibility that changes in protein abundance might affect the interpretation of regulated phosphosites, we performed experiments on flow through fractions containing nonphosphorylated peptides from TiO_2 enrichment experiments. Samples were desalted and fractionated on a PGC column into 40 fractions prior to LC-MS/MS analyses. These experiments enabled the quantitation of ~85% of all dynamic phosphoproteins reported in Supplementary Table S2-2. We observed that only 2 proteins showed FC values higher than 2 over the entire time period of the experiment. Accordingly, Hsp42 ($\log_2$FC: 2.06) and Zeo1 ($\log_2$FC: 1.33) were excluded from the list of dynamic phosphoproteins. The list of quantified proteins and their corresponding changes in protein abundance is reported in Supplementary Table S2-3.

To find relationships among dynamic phosphoproteins that contained at least one dynamic phosphosite, we integrated our identification into protein-protein interaction (PPI) network (Figure 2.2C), and performed GO enrichment analysis [36] (Supplementary Figure S2.5 and

Supplementary Table S2-4). Cell response to changes in temperature appears to be complex, and comprised a network of interacting proteins involved in cytokinesis, cell morphogenesis and cell cycle regulation. Changes in phosphorylation are consistent with a kinase-phosphatase network associated with the response to temperature stress, and we observed that about 15% (20/129) of all kinases and 7% (2/30) of all phosphatases also comprised dynamic sites (Figure 2.2C and Supplementary Table S2-6). Several of these kinases including Rck2 and Hog1 are also regulated upon environmental stress including osmotic shock [43].

2.4.2 Temporal phosphorylation profiles identify potential kinase substrates in response to heat shock and cold stress

To gain further insights on kinetic profiles shared among dynamic phosphosites, we analyzed our dataset using fuzzy c-means clustering, and selected only clusters with membership >0.7 (Figure 2.1B, and Figure 2.3A). These analyses enabled the separation of 388 dynamic phosphosites from 271 proteins into 15 different clusters with unimodal distributions showing monotonous (clusters 5, 6 and 9-12) and adaptation-like (clusters 1-4, 7, 8 and 13, 14) profiles (Supplementary Table S2-2). With the exception of clusters 9-12, the temporal variation in FC (increase or decrease) of several profiles reached a maximum value within 20 min upon temperature shift. Several profiles showed changes in phosphorylation that returned to their original status within 30 min post stimulation. For example, this is the case for the kinase Hog1, and the transcriptional factors Msn2 and Msn4 that were previously reported to be regulated by changes in temperature [16]. It is noteworthy that phosphosites from the same protein can exhibit different profiles, and that individual phosphosite often showed different behaviors in response to heat and cold. For example, we identified 5 dynamic sites on trehalose synthase complex regulatory subunit, Tsl1 (S53, S73/S77, S147 and S161), of which 2 sites (S147 and S161) showed opposite trends upon heat shock and cold stress. Tsl1 is a regulatory subunit of the trehalose synthesis protein (TSP) complex that catalyses the production of trehalose from glucose-6-phosphate and UDP-glucose, an activity mediated by heat shock [44]. Changes in the phosphorylation status of Tsl1 may regulate its association with the TSP complex under stress condition (Supplementary Figure S2.6).

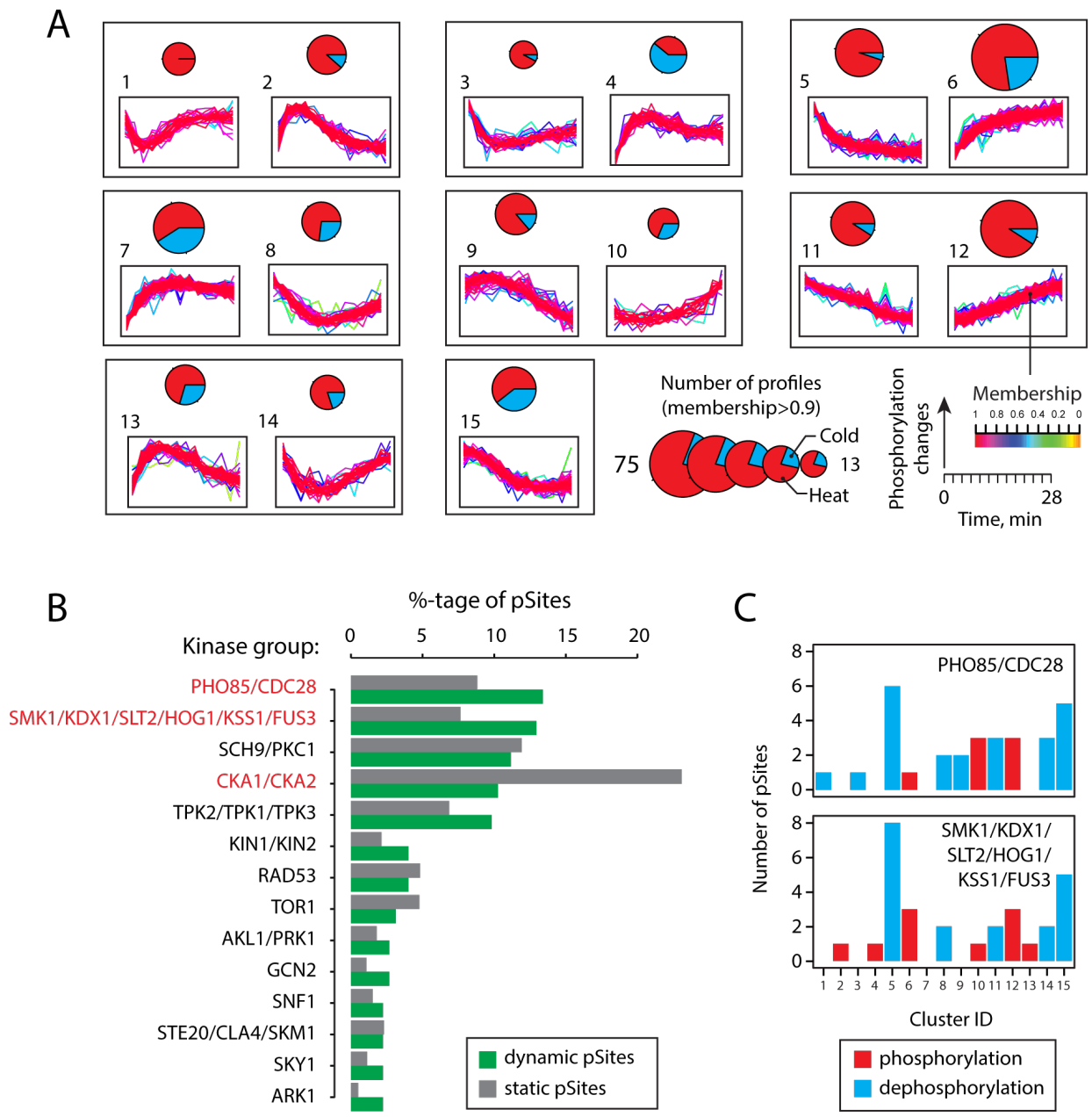

Figure 2.3. *Types of dynamic behavior and kinases involved in response to heat and cold stresses.*

A) Fuzzy c-means clustering of regulated phosphosites with different kinetic profiles. Pie charts represent the distribution of profiles for heat (red) and cold (blue), while circle sizes correspond to the number of high membership profiles. Clusters are ordered according to similarities in their dynamic behavior for either up- or downregulation. B) Putative kinases associated with dynamic and static phosphosites based on KinomeXplorer predictions. Substrates for each kinase group are represented by bar plots. A relative enrichment of cyclin-dependent and MAP kinase substrates is observed among dynamic phosphosites, while a higher proportion of casein kinase 1/2 substrates is found for static phosphosites. C) Distribution of kinetic patterns among dynamic phosphosites associated with Cdk and MAPK kinase groups. Putative Cdk and MAPK substrates were found to be represented mostly in cluster 5 which correspond to a sustained dephosphorylation.

Several kinases and phosphatases were dynamically affected by changes in temperature and exhibited different kinetic profiles. For example, several sites of important kinases involved in stress response (cluster 2: Hog1 Y176), cell cycle regulation (cluster 6: Cdc28 Y19), nutrient sensing (cluster 8: Gcn2 S577) or cytokinesis (cluster 9: Cdc3 S503) were grouped in different clusters, suggesting distinct temporal regulatory activities. Based on this observation, we surmised that dynamic behaviors of kinase and phosphatase groups could be correlated based on their temporal profiles, and that substrates may exhibit similar trends. To test this proposal, we first associated dynamic and static phosphosites with assigned kinase groups based on predictions made by KinomeXplorer [35], a platform that integrates an improved NetworKIN algorithm for modeling kinase signaling networks by combining linear motif analysis with protein-protein interactions. We found that approximately 40 % of all dynamic phosphosites are associated with 3 main kinase groups represented by cyclin-dependent, mitogen-activated and AGC family kinases, and that a higher proportion of dynamic sites compared to static sites is observed for the first two groups (Figure 2.3B). These kinases are known to play multiple roles in the regulation cellular response to environmental conditions and integration of stress signals. The only group of kinases significantly under represented among dynamic phosphosites is casein kinases (Ycks). The relative proportion of enrichment or depletion of dynamic sites from other kinase groups is more difficult to establish as the numbers of affected phosphosites are small (< 10 sites).

Next, we regrouped dynamic phosphosites associated to specific kinases with their corresponding clusters to determine if phosphosites that were found to be phosphorylated by the same putative kinases were grouped in the same cluster. These analyses revealed that dynamic phosphosites attributed to specific kinases could be represented by different clusters (Supplementary Figure S2.7). This observation is not entirely unexpected since the phosphorylation status of any given site may be affected by several factors including the activity of other kinases and phosphatases, the subcellular location of protein substrates and the creation of binding sites modulating the interactions with proteins containing phosphobinding domains. While temporal profiles associated to specific kinases appeared to be complex, we also noted that several dynamic sites/clusters were more frequently represented in selected kinase groups (Figure 2.3C). For example, cluster 6 contains the cyclin-dependent kinase Cdc28, a major component of the cell cycle control system. The increase phosphorylation of Cdc28 at the

inhibitory site Y19 [45]is also correlated with a corresponding dephosphorylation of known Cdc28 substrates found in cluster 5 such as phosphatase Cdc14 (S429), transcription factor activator of CUP1 Expression Ace2 (S253), and MAP kinase Ste20 (S547, S562) [21]. Similarly, the increase activity of Hog1 (Y176) is also correlated by an increase phosphorylation of known substrates including the transcription factor Sko1 (T215) and Rck2 kinase (S46/S50) that were grouped under the same temporal profiles (cluster 2).

The observation that changes in phosphorylation profiles of kinases are associated with those of known substrates suggests that dynamic patterns could be used to identify putative kinase substrates. To explore this possibility, we focused on profiles related with changes in Cdc28 activity upon heat shock. First, we used STRING to identify dynamic phosphoproteins known to interact with Cdc28, based on interactions inferred from experimental data and assigned with the highest confidence (>0.9)[38]. Next, for these proteins we obtained information on sites phosphorylated by Cdc28 based on *in vivo* phosphorylation data from the PhosphoGrid database [46, 47]. These analyses identified 32 target phosphosites, of which 9 phosphosites were detected in our study as dynamic, and displayed similar patterns of dephosphorylation associated mainly with cluster 5 (Figure 2.4 and Supplementary Figure S2.8). It is noteworthy, that protein tyrosine phosphatase Mih1 (S82) which targets Y19 residue on Cdc28, showed a similar dephosphorylation profile. In addition to Cdc14 (S429), Ace2 (S253, S428), Ste20 (S547, S562), Cdc27 (T351) and Stb1 (S72, S89) that were previously known as Cdc28 substrates, these analyses uncovered new putative sites on Kar9 (T598), Msa2 (T5) along with a novel site on Ste20 (T573). To confirm putative Cdc28 substrates we also performed large-scale phosphoproteomics analyses on a yeast strain where the WT Cdc28 was replaced with an analog sensitive mutant Cdc28-*as1* expressed in the same strain background [21]. These experiments were carried out on six biological replicates with reverse SILAC labeling and confirmed the dephosphorylation of 2 out of 3 putative substrates upon Cdc28-*as1* inhibition with 1NM-PP1: Msa2 T5 (log_2FC: -4.68, -log_{10}(pValue): 2.48) and Ste20 T573 (log_2FC: -2.38, -log_{10}(pValue): 3.06). Unfortunately, the Kar9 T598 was not detected in these experiments due to its low abundance. The complete list of quantified phosphosites obtained from the inhibition of the analog sensitive mutant of Cdc28 is presented in Supplementary Table S2-6.

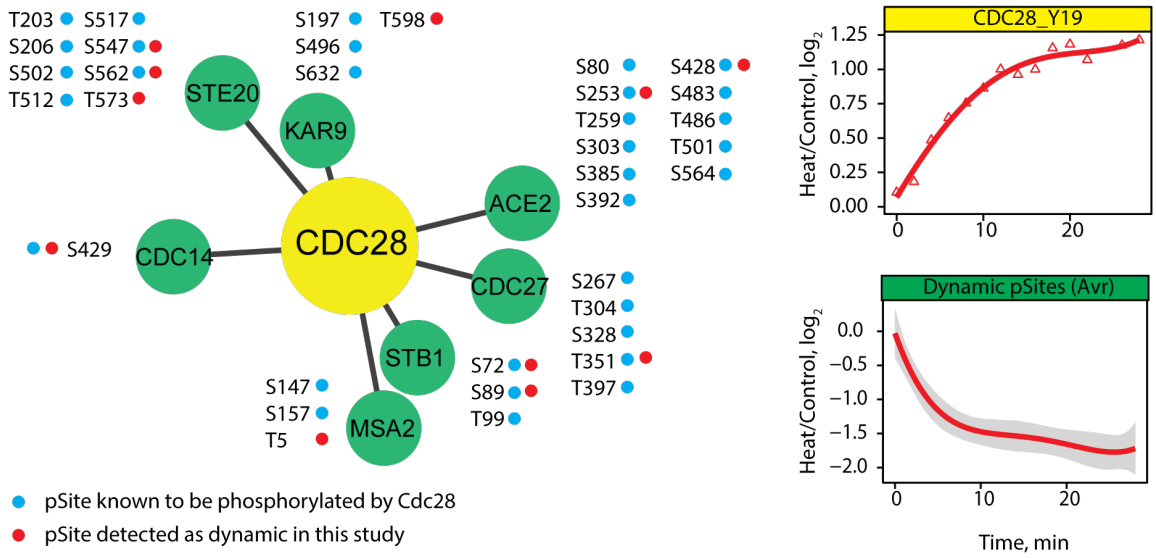

Figure 2.4. Cdc28 substrates display similar dynamic behavior.

An increased phosphorylation of Cdc28 at its inhibitory site Y19 was paralleled by a corresponding dephosphorylation on putative protein substrates. STRING was used to obtain high-confidence Cdc28 interactors among proteins with dynamic phosphosites, and known sites regulated by Cdc28 were inferred using PhosphoGRID. A total of eight dynamic phosphosites (red dots) with similar kinetic profiles were identified in our dataset (shaded area across averaged profile represents 95% confidence interval).

To gain further insights on the inference of kinase-substrate relationships based on dynamic profiles, motif analyses and protein-protein interactions, we also compared our dynamic phosphosites with those identified in a separate large-scale phosphoproteomics study performed on 116 gene deletion mutants of the non essential kinases or phosphatases, and 8 analog-sensitive kinase strains of some essential kinases (Supplementary Table S2-7) [20]. These analyses revealed that 43 % of our dynamic phosphosites from monophosphorylated peptides (134 phosphosites) were also found to be regulated in the system-wide perturbation of kinase and phosphatase study by Bodenmiller et al. (Supplementary Figure S2.9A) [20]. While approximately 2/3 of these sites were regulated by multiple kinases, we found that 42 phosphosites were associated to a single kinase (Fig S9B). Closer examination of regulated phosphosites common to both large-scale phosphoproteomics studies indicated an enrichment of some kinases in specific clusters (Supplementary Figure S2.9C). For example, putative Cdc28 substrates were identified in cluster 5 consistent with that observed previously using KinomeXplorer (Figure 2.3).

Our dataset also contained several phosphosites that showed rapid dephosphorylation upon heat shock followed by a recovery to basal level within 10 min (Figure 2.5). Among these are known examples of transient dephosphorylation of Msn2 and Msn4, two transcription factors that are activated upon cellular stress conditions, and rapidly undergo nuclear translocation [48]. The activation of Msn2/4 is associated with the rapid but transient dephosphorylation of several sites within the nuclear localization signal (NLS) [49]. Previous studies indicated that NLS of Msn2 is a direct target of cAMP-dependent protein kinase (PKA) that plays important roles in nutrient sensing [50]. Under heat shock we identified 3 sites on Msn2 (S201, S288, S633) and 4 sites on Msn4 (S263, S316, S488, S558), all located within PKA recognition motif.

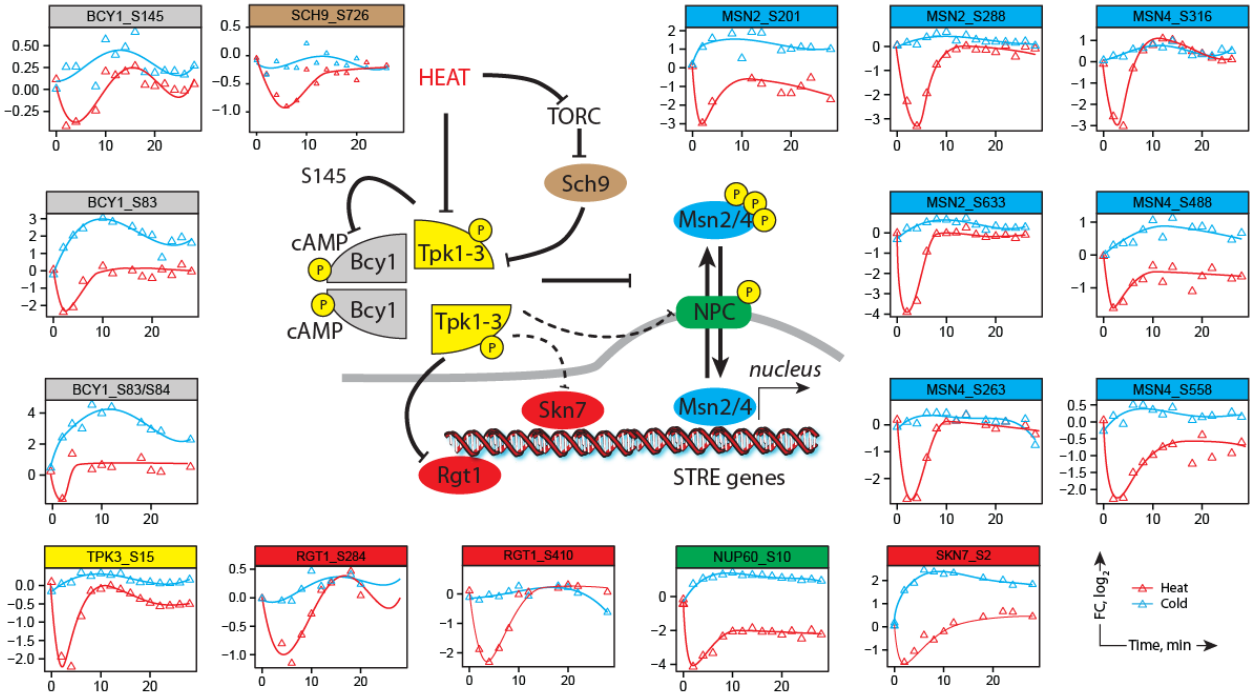

Figure 2.5. Dynamic profiles reveal functional association between kinases and putative substrates.

Schematic representation of cell signaling pathway associated with PKA and downstream substrates. Phosphorylation profiles are shown for each substrate site. The kinetic profiles of PKA (Tpk3 and Bcy1) are superimposable with those of known protein targets Msn2/4 and Rgt1. The correlation between temporal profiles was used to identify putative targets of PKA such as nucleoporin Nup60 and the transcription factor Skn7.

In this study, we observed the dephosphorylation of both PKA catalytic subunit Tpk3 (S15) and the regulatory subunit Bcy1 (S83, S84, S145) (Figure 2.5). The phosphorylation of Bcy1 at S145 by Tpk1-3 is required to establish a negative feedback loop in response to changes in nutrient concentrations [51]. Tpk3, Bcy1 and Msn2/4 all showed similar temporal phosphorylation

profiles, thus providing a dynamic link between these proteins. Upon heat shock, PKA is transiently deactivated which leads to rapid dephosphorylation of Msn2/4 favoring its nuclear translocation. The comparison of kinetic profiles similar to those of Msn2/4, Tpk3, and Bcy1 (cluster 1) also identified other putative PKA substrates including the nuclear pore protein Nup60 (S10), the transcription factors Skn7 (S2) and Rgt1 (S284, S410), the inhibitor of glycogen debranching Igd1 (S83) and a protein of unknown function associated with cell cycle regulation YPL247C (S12) (Figure 2.5). Rgt1 regulates the expression of HXT genes encoding glucose transporters, and is phosphorylated *in vitro* by all three isoforms of PKA at serine residues located within consensus sites [52]. Igd1 is also involved in glucose metabolism and was reported to act as an inhibitor of Gdb1p by enhancing the ability of yeast cells to store glucose as glycogen. The phosphorylation of Igd1 could regulate its interactions with Gdb1 [53]. The dephosphorylation of the nuclear response regulator and transcription factor Skn7 (S2) through the transient deactivation of Tpk3 might be required for optimal induction of heat-shock genes in response to oxidative stress [54].

We also observed the dephosphorylation of an upstream regulator of PKA activity - the yeast ortholog of mammalian PKB/Akt and target of rapamycin complex 1 (TORC1) effector, Sch9 protein kinase. Residue S726, which is located within the AGC-kinase domain, is a substrate of TORC1 and was dephosphosphorylated upon heat shock. Phosphorylation of this residue is lost upon rapamycin treatment, carbon or nitrogen starvation and is transiently reduced following application of osmotic, oxidative, or thermal stress [55, 56]. Consistent with this result, we also identified phosphorylation sites on Tco89 (S84) and Kog1 (S1045), two components of TORC1 that were dephosphorylated upon heat shock. It is noteworthy that PKA activity is modulated by changes in cAMP concentrations, and we observed an increase phosphorylation of residue T617 from adenylate cyclase Cyr1 upon heat shock. Residue T617 is located next to the Ras-associating domain of Cyr1 and its kinetic profile showed an opposite trend to that observed for the catalytic subunit Tpk3 (S15). Taken together, our results suggest that the combination of protein-protein interactions and phosphorylation dynamics provides a valuable approach to identify putative kinase substrates and prioritize large-scale phosphoproteomics data for subsequent experiments.

3.4.4 Differential regulation of signaling pathways upon heat shock and cold stress

We observed that a larger proportion of dynamic phosphosites were observed under heat shock compared to cold stress, indicating that cellular responses to these stimuli are inherently different. To study the differential regulation of signaling pathways activated under these environmental changes, we grouped all dynamic phosphosites into four categories based on their response to cold and heat. Accordingly, the behaviors of dynamic phosphosites were classified as bidirectional, temperature-independent or heat- and cold-specific to distinguish situations where profiles exhibited opposite, same response or no response to either cold or heat (Figure 2.6A). We found that 36 % of dynamic phosphosites are modulated in a bidirectional fashion in response to heat and cold (Figure 2.6A). Among these sites, we noted that 69 % displayed opposite trends in phosphorylation upon these stimuli, and could correspond to sites important for the regulation of protein activity. An example of this is represented by the neutral trehalase Nth1, an enzyme that hydrolyzes trehalose to glucose to provide energy and assist in recovery from stress. Earlier reports indicated that trehalose levels rise in response to heat shock and confer thermotolerance in the fission yeast *Schizosaccharomyces pombe* [57]. Importantly, trehalose levels must be tightly regulated, as cells lacking Nth1 exhibit impaired recovery from heat shock [58]. Our data suggest that phosphorylation of Nth1 might regulate its enzymatic activity to control intracellular levels of trehalose.

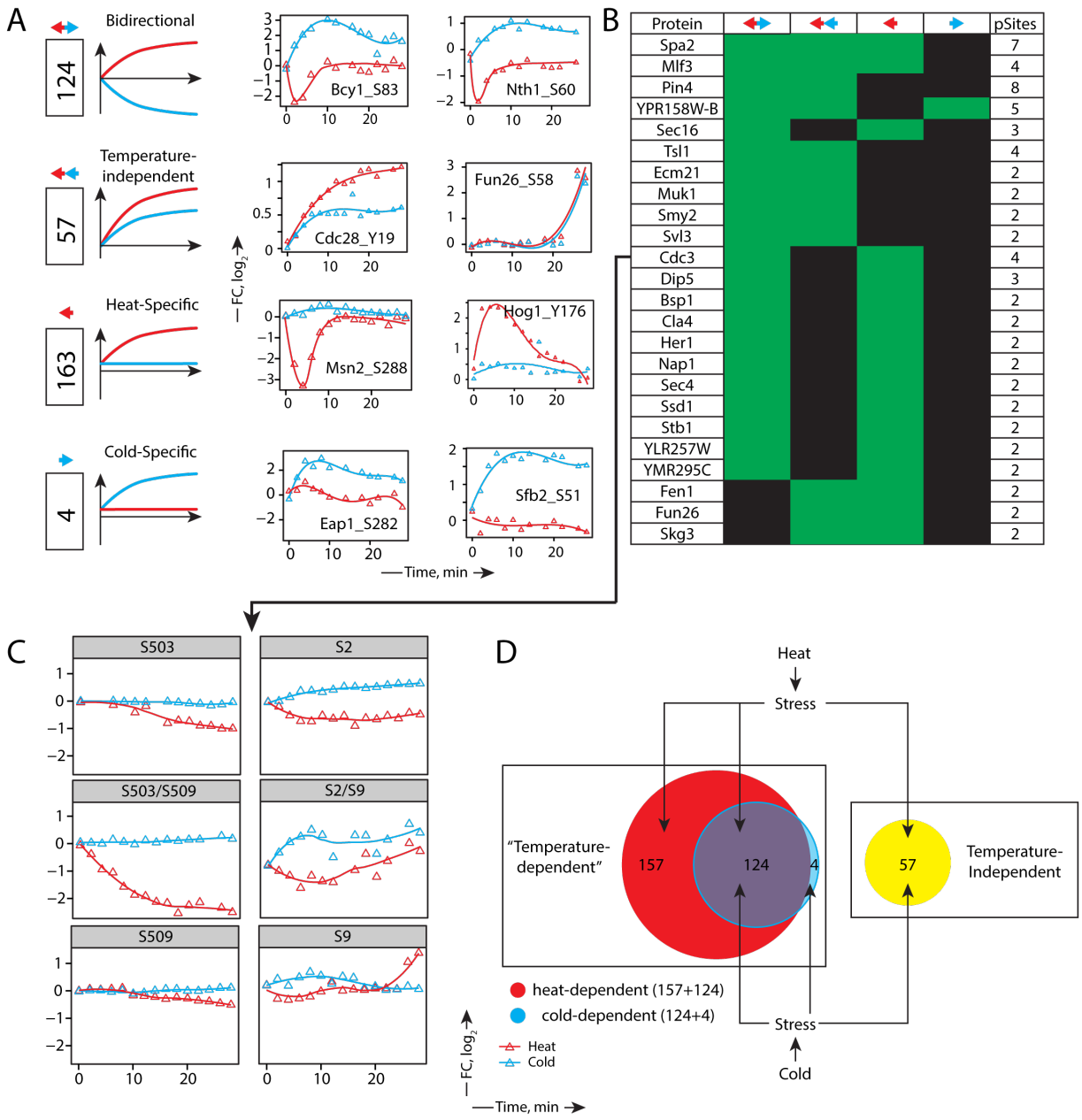

Figure 2.6. Cross-talk of signaling pathways upon heat and cold stresses.

A) Dynamic phosphosites are classified into four groups according to their response to heat (red) and cold (blue) along with representative examples. B) A total of 24 out of 270 dynamic proteins contained phosphosites from different groups highlighting a complex regulation of kinase/phosphatase network. C) Phosphorylation dynamics of septin Cdc3. Residues S503 and S509 are substrates of Cdc28, and their change in phosphorylation is known to regulate efficient ring disassembly (Tang & Reed, 2002). Dephosphorylation of both mono- and diphosphorylated forms of the corresponding peptide was observed upon heat shock, consistent with the inhibition of Cdc28 (see A). Dynamic changes on all phosphopeptide forms of S2 and S9 is also observed upon both heat shock and cold stress. D) Venn diagrams representing overlap between dynamic phosphosites associated with heat and cold stresses. Responses to heat and cold are partially redundant; both trigger temperature-independent and temperature-dependent changes.

Our population of phosphosites contained a subset representing 16% of all dynamic sites that react in a similar manner to both increase and decrease of temperature (Figure 2.6A). These phosphosites are probably involved in general stress response whereby signaling events trigger similar changes in cellular activities upon detection of abnormal temperature conditions. Among sites that showed a temperature-independent behavior, we noted the catalytic subunit of Cdc28, a master regulator of mitotic and meiotic cell cycles that has multiple roles in the regulation of cell cycle transcriptional programs, chromosome duplication and segregation, spindle dynamics, lipid biosynthesis, membrane trafficking, polarized cell growth, and morphogenesis. Inhibition of Cdc28 activity upon temperature stress via the phosphorylation on Y19 residue might be required to cause cell arrest and prevent cell proliferation until favorable cell growth conditions are restored [45, 59].

The largest group (46%) of dynamic phosphosites is represented under the category heat-specific response, and included proteins such as transcription factor Msn2 and Hog1 kinase (Figure 2.6A). The kinase Hog1 was previously shown to be activated upon thermal stress [60]. Transient changes in Hog1 activity may reflect a variation in the perceived turgor pressure upon thermal stress. It is noteworthy that cold stress near freezing conditions is also known to activate Hog1 and trigger glycerol production essential for freeze protection [16].

The last group typifying cold-specific response is represented by 4 phosphosites from eIF4E-associated protein Eap1, the component of the cleavage and polyadenylation factor I (CFI) Rna14, the transposon Ty1-PR2 Gag-Pol polyprotein YPR158W-B and the component of the COPII vesicle coat Sfb2 (Figure 2.6A). While Eap1 is known to bind eIF4E for protein translation, it may also affect the activity of GCN4 translation via a crosstalk mechanism involving TOR signaling [61]. The role of Eap1 phosphorylation is not known, though TOR activation results in the phosphorylation of the mammalian homolog eIF4E-binding protein to prevent its binding to eIF4E [62]. The second representative of this group is Sfb2, a component of the COPII coat involved in the anterograde transport of vesicles from the endoplasmic reticulum to the Golgi apparatus. However, the functional significance of Sfb2 phosphorylation on its activity remains unknown.

Phosphoproteins can harbor several dynamic phosphosites with different behavior in response to heat and cold, and our dataset contained 24 out of 270 dynamic phosphoproteins with multiple phosphosites from different categories (Figure 2.6B). One of such proteins is Cdc3, a component

of the septin complex that displayed both bidirectional (S2/S9) and heat-specific (S503/S509) dynamics. We observed both mono and diphosphorylated peptides for Cdc3 (Figure 2.6C). The septins comprise a family of filament-forming proteins ubiquitous in eukaryotic species. It has been suggested that phosphorylation of Cdc3 by the Cdc28 kinase on S503/S509 at the end of G1 may facilitate initiation of a new cell cycle by promoting disassembly of the obsolete septin ring from the previous cell cycle [63]. We observe dephosphorylation of both S503/S509 residues consistent with the inhibition of Cdc28 activity. While Cdc28 is inhibited under heat shock and cold stress, the dephosphorylation of Cdc3 appears to be heat-specific suggesting a more complex regulatory mechanism. Phosphorylation of S2/S9 residues follows an opposite trend in response to heat and cold, possibly suggesting the interaction of different kinases. NetworKIN predictions indicated that S2 can be phosphorylated by Rad53 while S9 is a putative substrate for SCH9/PKC1 kinases. Another interesting example of multisite phosphorylation is the RNA binding protein Pin4. This protein is involved in G2/M phase progression and is known to be phosphorylated in response to DNA damage [64]. We identified 8 phosphosites on Pin4 that are located within structural domains that likely affect its binding to RNA under thermal stress (Supplementary Figure S2.10). Altogether, these results indicate that phosphosites exhibit strikingly different behaviors in response to cold and heat, reflecting the cellular plasticity and signaling rewiring necessary for cell adaptation to adverse environment. Heat shock triggers a large number of specific phosphorylation events not observed under cold stress whereas a drop of temperature can trigger a signaling machinery common to heat shock to promote interconversion of metabolic intermediates necessary for cell survival (Figure 2.6D).

2.4.5 Significance of Cdc28 tyrosine 19 phosphorylation during the heat shock response

Our phosphoproteomic data indicated that several substrates of the Cdc28 kinase become hypophosphorylated in response to heat shock. This decrease in phosphorylation correlates well with the increased phosphorylation at the inhibitory site Y19 of Cdc28. In vertebrate cells, loss of the equivalent phosphorylation on Cdk1 induces premature mitotic entry [65], which suggests that Y19 phosphorylation in yeast could act by restraining cell cycle progression during the heat shock response. To test this possibility, we constructed a *cdc28-af* mutant defective for Y19 and T18 phosphorylation and determined its cell cycle profile after heat shock. It was necessary to

remove both T18 and Y19 phosphosites in Cdc28 since modification of the residue preceding the inhibitory tyrosine in CDKs can functionally compensate for the loss of tyrosine modification [65, 66]. *CDC28* and *cdc28-af* mutant cells were synchronously released from a G1 arrest into prewarmed medium, and samples were collected at regular intervals to determine kinetics of budding and mitotic spindle formation. The release experiments were conducted at 30 °C and 39 °C because yeast cells did not cycle effectively at 42 °C (Figure 2.7A and Supplementary Figure S2.11). Both *CDC28* and *cdc28-af* mutant cells formed buds and accumulated mitotic spindles with similar kinetics when released from a G1 arrest at 30 °C (Fig S11). In contrast, the appearance of cell cycle landmarks was advanced in the *cdc28-af* mutant released at 39°C relative to its wild-type counterpart (Figure 2.7B-C). Specifically, *cdc28-af* cells showed an early accumulation of metaphase spindles at mitotic entry (60 min post-release; Figure 2.7B-C) and faster kinetics of mitotic exit (as evidenced by an increased abundance of cells with G1/interphase-type microtubules arrays at the end of the experiment; Figure 2.7B) when compared to *CDC28* cells growing at 39 °C. These results are consistent with the known roles of Cdc28 in promoting bipolar spindle formation [67] and elongation [68] during mitosis. Altogether, our results indicate that the increased phosphorylation of Cdc28 Y19 and associated reduction in kinase activity observed during the heat shock response restrain cell cycle progression, most likely to allow time for cells to adapt to the cellular stress associated with increased temperatures and to promote effective cell division.

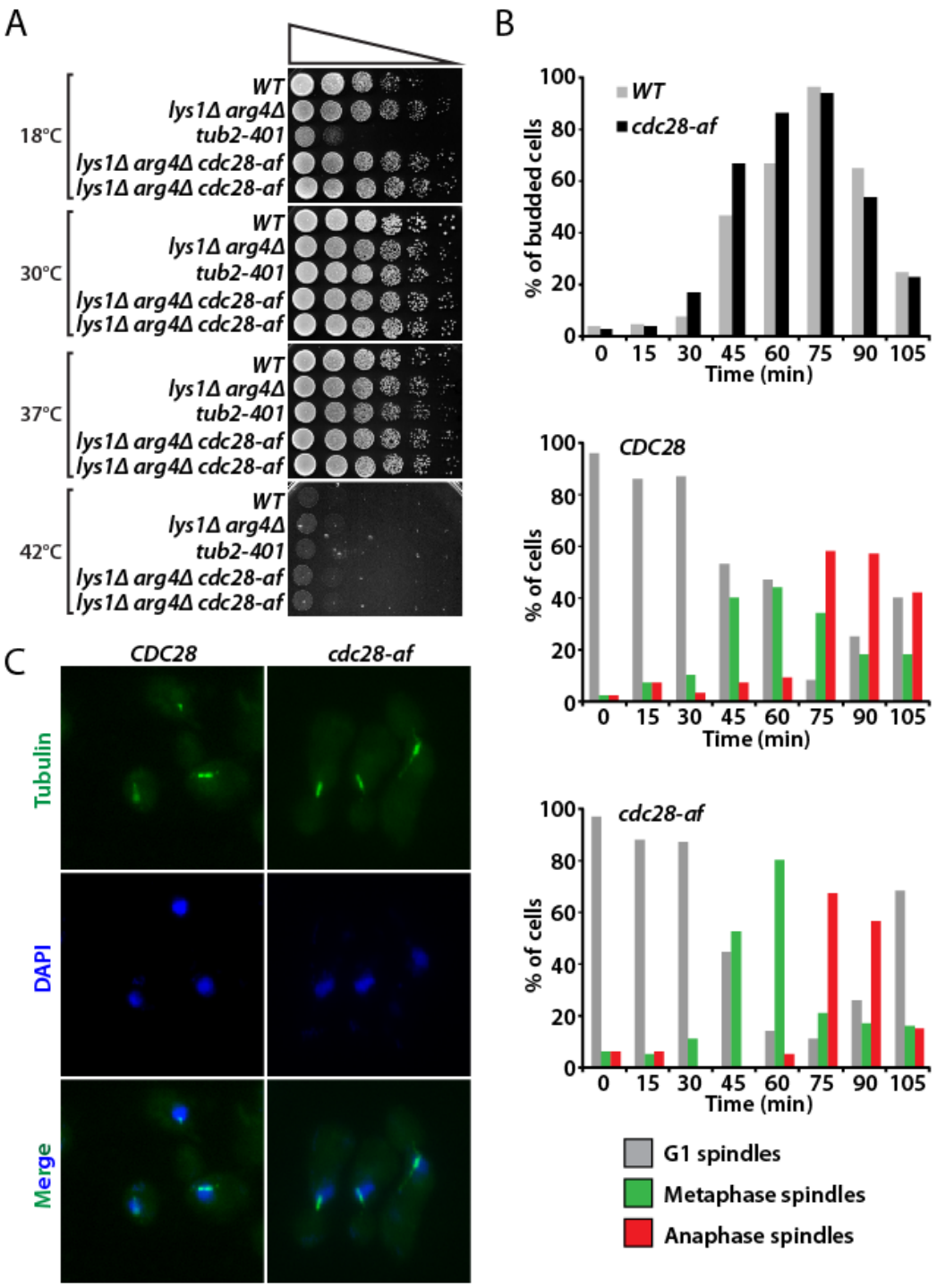

Figure 2.7. Cell cycle profile of cdc28-af mutants growing at elevated temperatures.

A) Growth properties of CDC28 and cdc28-af mutant cells exposed to various temperatures. Fivefold dilutions of yeast cells were spotted on YPD plates and grown at 18, 30, 37 and 42°C for 2–4 days. Strains included on plates are as follows: D1 (WT), YALB6 (lys1Δ arg4Δ), D253 (tub2-401, a cold-sensitive strain), D4591 and D4592 (two independent clones with the lys1Δ arg4Δ cdc28-af genotype). B) Budding index and spindle morphology of CDC28 and cdc28-af cells after release from a G1 arrest into fresh medium at 39°C. Samples of cells were taken at intervals to determine the kinetics of bud appearance (top graph), and microtubule morphology (middle and bottom graphs) in cultures of CDC28 and cdc28-af cells released synchronously into the cell cycle. At least 100 cells were counted at each time point. C) Micrographs of CDC28 and cdc28-af cells showing spindle morphology (tubulin) and nuclear mass position (DAPI) 60 min after G1 release at 39°C.

2.5 Discussion

All organisms have evolved adaptation mechanisms to survive adverse environmental conditions such as suboptimal growth temperatures. In *S. cerevisiae*, the response and adaptation to heat shock and cold stress are initiated by complex and rapid signaling pathways that affect a wide range of cellular processes including transcriptional programs, cell division and morphogenesis, protein folding and metabolic changes in nutrient flux. Previous transcriptional profiling studies on the heat shock response in yeast identified several differentially regulated genes involved in carbohydrate metabolism, protein folding and degradation, cytoskeletal reorganization, protein synthesis, ribosome synthesis and processing [3, 4]. While our quantitative proteomics data indicated that only ~2 % of proteins showed significant changes in protein abundance in the first 30 min upon heat shock, we noted that several proteins including HSP12, HSP26, HSP30, HSP42, HSP78, HSP82, and HSP104 were upregulated by at least 2-fold. We also observed that a subset of ~0.4 % of all quantified proteins including the mitochondrial electron transporter Cyc1 and Cdc25 that regulates RasGTPase activity and cAMP cellular levels were downregulated following heat shock (Supplementary Table S2-3). We found that approximately half of the differentially abundant proteins from our proteomics data were also regulated in previous transcriptomics studies [3], and supported the activity of important regulatory mechanisms involved in the response to environmental stress. However, the comparison of genes regulated upon heat shock with dynamic phosphoproteins identified in our study revealed an overlap of only 6% (119/1959), suggesting that phosphorylation dynamics are not necessarily correlated with gene transcription and protein expression (Supplementary Table S2-8). These results also underline the significance of protein phosphorylation as a primary response to heat shock.

In the present study, we developed a quantitative phosphoproteomics workflow that enabled the first large-scale profiling of early signaling events in yeast upon heat shock and cold stress. The ability to monitor changes in protein phosphorylation with high temporal resolution facilitated the identification of regulated phosphosites based on the shape of kinetic profiles rather than conventional approaches that typically rely on FC measurements. This provided an inherent advantage in the identification of sites that displayed small but tractable changes in phosphorylation. A temporal resolution of 2 min was selected to minimize the occurrence of

minima/maxima between measurements. In a recent study on osmotic shock response in yeast, we monitored changes in protein phosphorylation over a one minute period with 5 sec resolution, and identified only monotonous profiles [69]. Changes in phosphorylation including those associated with adaptation response likely take place over several minutes, and 2 min resolution was deemed optimal to detect these changes. The clustering of kinetic profiles enabled the grouping of new potential interactions between kinases and putative substrates, to further understand the integration of signaling pathways and the response to environmental stress.

Interestingly, we noted that an intricate network of kinases and phosphatases are rapidly activated upon changes in temperature. For example, deactivation of PKA subunit Tpk3 is taking place within 5 min upon heat shock and led to a transient dephosphorylation of several downstream substrates including Msn2/4 and Rgt1. The dephosphorylation of these transcription factors facilitates their nuclear import where they regulate the expression of genes associated to stress response element and different glucose transporters. Several other kinases and phosphatases displayed different temporal profiles as shown for Cdc28 and Mih1 which exhibited progressive and sustained changes in phosphorylation upon cell stimulation. The increased phosphorylation of Cdc28 at the inhibitory site Y19 was observed immediately upon changes of temperature, and was mirrored by a dephosphorylation of known protein targets including Cdc14, Ace2 and Ste20. Several of these substrates play key regulatory roles during the progression through the cell cycle. The functional significance of Cdc28 inhibition during heat shock was also determined using *Cdc28-af* mutants where elevated temperatures resulted in advanced cell cycle landmarks compared to its wild-type counterpart. These results suggest that the reduced Cdc28 activity observed during heat shock response slows down cell cycle progression and represents an adaptive response of yeast cells to this environmental stress.

We also noted that other proteins involved in cell cycle regulation also displayed important changes in phosphorylation. For example, Cdc14 is an important phosphatase that antagonizes Cdc28 activity during mitotic exit, and phosphorylation of Cdc14 S429 was recently reported to inhibit its activity during S phase [70]. During most of the cell cycle, Cdc14 is sequestered in the nucleolus where it associates with the Nucleolar silencing Establishing factor and Telophase regulator, Net1, also referred to as Cfi1 [71, 72]. In line with this, we identified 9 phosphosites on Net1, of which 2 sites (S447, S497) showed kinetic profiles similar to those of Cdc28

substrates, consistent with a previous report indicating that dephosphorylation of both Cdc14 and Net1 favors their association in the nucleolus [73] .

Cdc28 is a master regulator of mitotic and meiotic cell cycles and associates with G1 (Clns), S and G2/M (Clbs) phase cyclins to direct substrate specificity. Eukaryotic cells rely on positive feedback in genetic control networks and cell cycle checkpoints to ensure proper transition across cell cycle phases. The start checkpoint corresponds to a short time interval in late G1 phase during which the yeast commits to division. In this period the G1 cyclin Cln3 associates with Cdc28, and activates the transcription of about 200 genes by phosphorylating promoter bound protein complexes such as transcription factors Sbf and Mbf1, and the transcriptional inhibitor Whi5 [74, 75]. We also observed that several phosphosites on Whi5 (S154, S156, S161) displayed kinetic profiles consistent with a decrease in Cdc28 activity, though these sites were not predicted by KinomeXplorer. Residues S154 and S156 are located within a nuclear export sequence (NES), and their dephosphorylation promote the rapid nuclear translocation of Whi5 to inhibit SBF [76]. Furthermore, Srl3 (S212), a Whi5 paralog, also showed a dephosphorylation profile at a consensus CDK site that reflected the reduced Cdc28 activity. Altogether, kinetic profiles obtained on Cdc28 substrates suggest that heat shock affects cell cycle regulation by preventing cells to enter G1/S phase and commit to division.

Cell response to heat shock and cold stress was also reflected by an uneven distribution of dynamic phosphosites largely favoring the former stimulus. The observation that approximately 20 % of all dynamic phosphosites were observed upon cold stress is consistent with lower enzymatic activities and metabolic rates expected in yeast at temperatures below optimal growth conditions. In contrast to heat shock, we only observed a small number of kinases and phosphatases that exhibit a change in phosphorylation upon cold stress. Interestingly, we noted a 1.4-fold increase phosphorylation of Cdc28 at its inhibitory site Y19 during cold stress, but failed to observe a corresponding decrease in phosphorylation of Cdc28 substrates. This might suggest that a minimum activity threshold is required to detect changes in phosphorylation, or that other regulatory mechanisms are involved. It is noteworthy that yeast cells can initiate different responses under cold shock conditions (10–18 ℃) compared to near-freezing temperatures (<10 ℃) [77]. This possibly suggests that yeast can actively grow at 18 ℃, whereas growth is severely impeded at temperatures below 10 ℃. In spite of the low number of phosphosites regulated by the cold response, our quantitative phosphoproteomics analyses revealed that many

of these sites were associated with the accumulation of carbohydrate reserves trehalose and glycogen. Indeed, we observed several phosphosites on Nth1 (S20, S21, S60, S66, S83), Tsl1 (S147, S161) and GPH1 (T31) that displayed opposite trends in response to cold and heat, possibly suggesting that phosphorylation regulate the activity of the corresponding enzymes to control intracellular pools of trehalose and glycogen.

While the present study provided valuable insights into early signaling events regulating biological functions in yeast under heat and cold stresses, we anticipate that improvements in both MS sensitivity and metabolic labeling reagents (e.g. neutron-encoded amino acids [78]) will further expand phosphoproteome coverage and multiplexing capability of these experiments. The identification of putative substrates through the correlation their kinetic profiles with those of their corresponding kinases open interesting avenues for the selection of phosphosites of functional interest. Appropriate filters are required to select dynamic phosphosites displaying low variance and significant temporal changes. In the present study, we used polynomial fitting and selected only dynamic profiles with defined distribution ($N \geq 10$) and high correlation coefficients ($R^2 > 0.9$). Although the stringency of these selection criteria facilitated the selection of stimulus-specific profiles, we noted that phosphosites of functional relevance with fewer data points or higher variability of abundance can be excluded due to low intensity and/or poor ionization efficiency. This was the case for Hsf1 (S608, S655), a heat shock transcription factor that exhibits temperature-dependent phosphorylation to initiate transcriptional programs associated with heat shock elements (HSE) [79]. Also, the phosphorylation profiles of some protein substrates might differ from those of their kinases due to the combined activity of other kinases or phosphatases for the same sites. The occurrence of complex phosphorylation profiles is time-dependent, and phosphoproteomics experiments taking place over extended time periods are more likely to exhibit convoluted kinetic patterns. For example, Sic1 (T5) is a substrate and inhibitor of CDC28, and showed a dephosphorylation profile consistent with the change in Cdc28 activity for the first 20 min upon heat shock, but its return to basal levels at 28 min suggests a more complex regulation.

This contribution presents the first phosphoproteome dynamic study to investigate the response of yeast cells to rapid changes in temperature. Taken together, our data provide one of the most comprehensive phosphoproteomics study to identify differentially regulated signaling pathways upon heat shock and cold stress, and represent a unique resource to investigate cell biology

paradigms associated to the control and regulation of these environmental stresses. We also anticipate that the tools and approaches described in this study can be applied to other cell stimuli to gain further understanding of the evolution and organization of signaling machineries.

2.6 Acknowledgements

The authors would like to thank Dr. David Morgan (University of California at San Francisco) for providing the yeast strain cdc28as used in preliminary experiments, Dr. Éric Bonneil for technical assistance in MS analyses and Dr. Alain Verreault (Université de Montréal) for valuable comments during the course of this study. The authors acknowledge support from NSERC grant 311598, CIHR grant MOP-136788 and the Cancer Research Society. The Institute for Research in Immunology and Cancer (IRIC) receives infrastructure support from the Canadian Center of Excellence in Commercialization and Research, the Canadian Foundation for Innovation, and the Fonds de recherche du Québec - Santé (FRQS)

2.7 Supplementary material

2.7.1 Supplementary figures

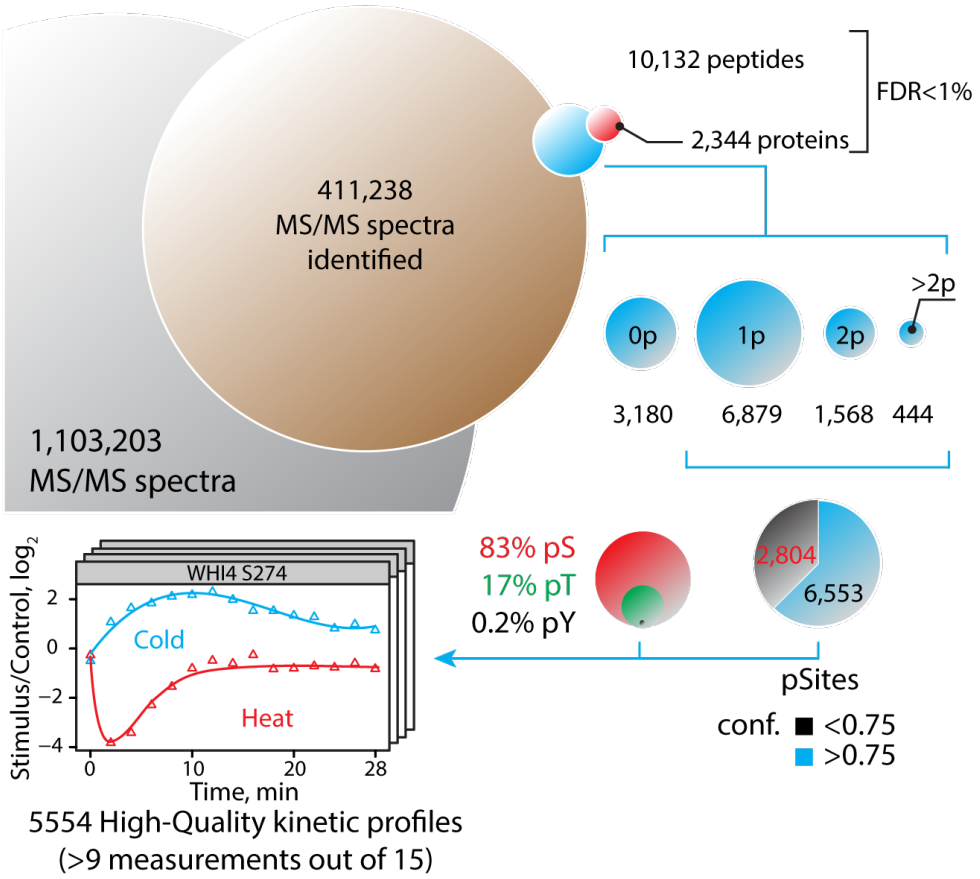

Supplementary Figure 2.1. Summary of phosphopeptide identification.

A total of 1,103,203 distinct MS/MS spectra were identified and assigned to 10,132 unique peptides from 2,344 proteins with a FDR < 1%. Phosphopeptides represented 73 % of all identified peptides, and 70% of all phosphosites (9,357) were assigned with high confidence (>0.75). A total of 5,554 dynamic profiles (≥ 10 out of 15 data points) were obtained from all high confidence assignments. Phosphorylation sites were distributed on Ser (83%) Thr (17%) and Tyr (0.2%) residues.

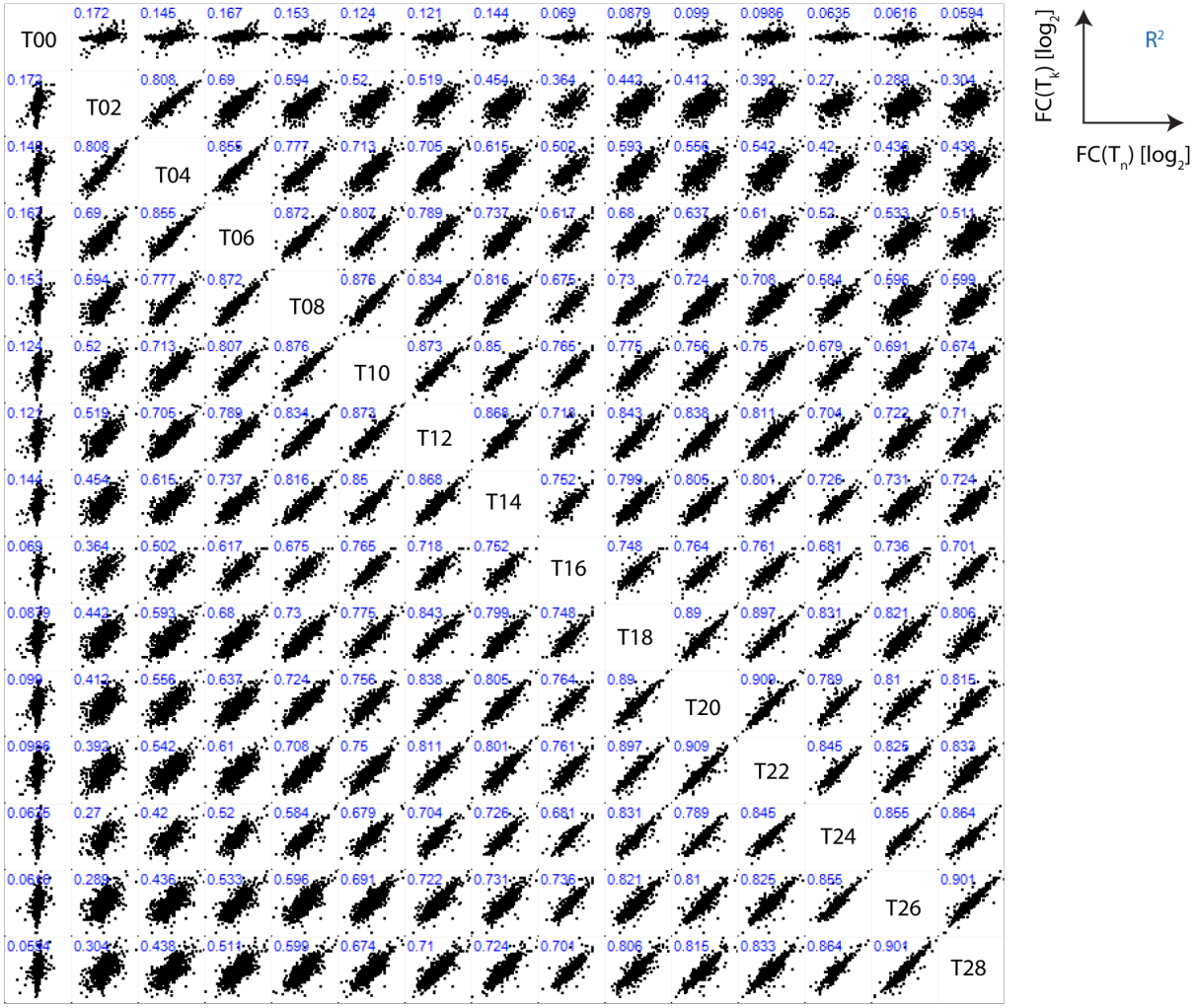

Supplementary Figure 2.2. Pair wise comparison of phosphopeptide abundance.

The comparison of SILAC ratios (H/L) is shown in a pair wise fashion for all time points corresponding to heat shock treatment. Phosphopeptide abundances of all SCX fractions are considered for each time point. R2 values obtained are shown on the top left corner of each graph.

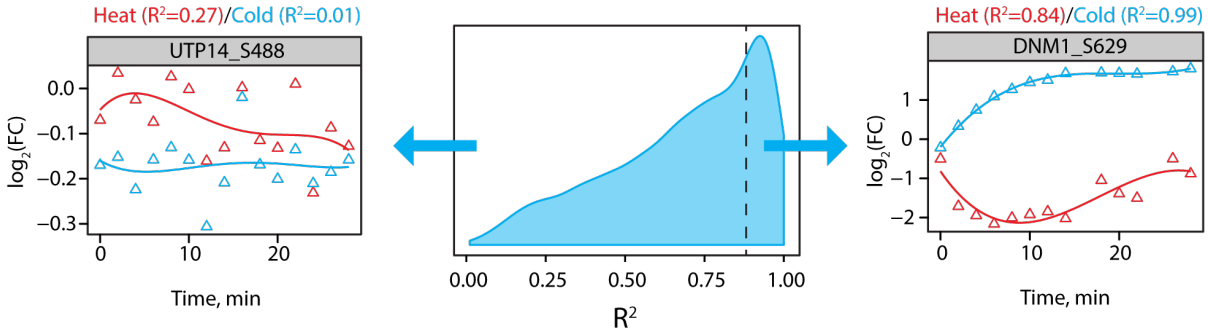

Supplementary Figure 2.3. Finding regulated kinetic profiles in the dataset.

In order to define subset of biologically regulated phosphosites, we performed fitting of all kinetic profiles using a polynomial model and selected only those with correlation coefficients (R2) > 0.9 (middle panel). Representative examples of phosphosites with R2 > 0.9 and R2 < 0.9 are displayed.

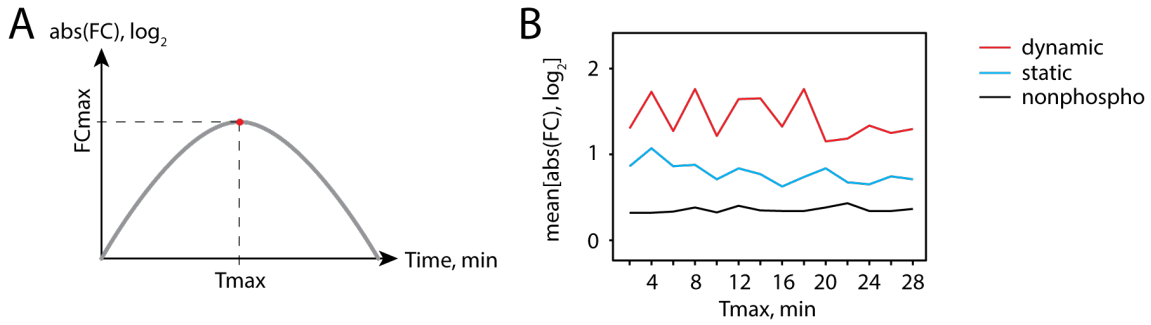

Supplementary Figure 2.4. Amplitude of fold change (FC) for dynamic sites.

A) From each profile the maximum amplitude (measured as absolute log2-transformed FC was determined over the stimulation period. B) Mean values of the maximum amplitude at individual time points showing that dynamic sites displayed higher fold change compared to static sites or non phosphorylated peptides.

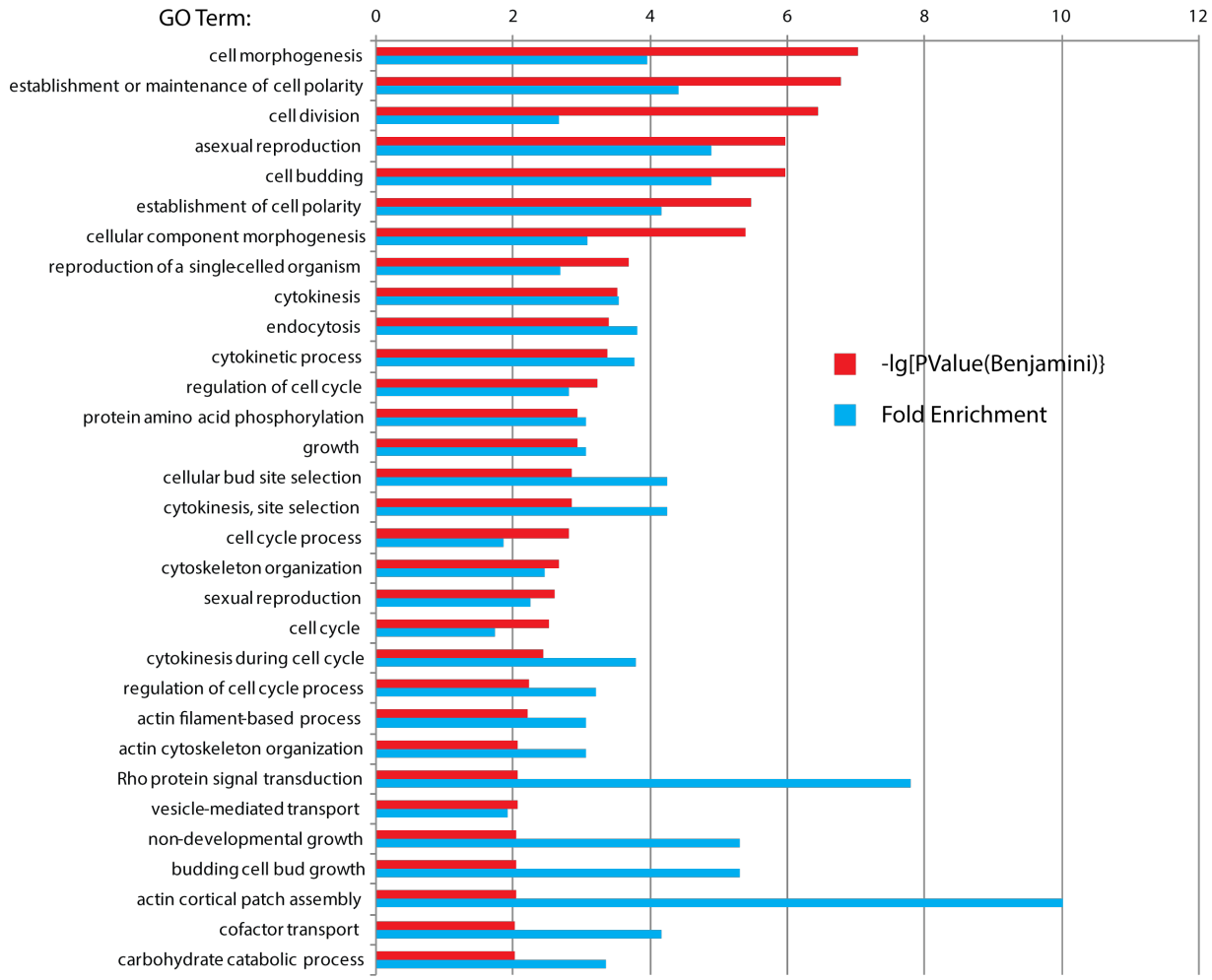

Supplementary Figure 2.5. GO enrichment analysis for phosphoproteins showing dynamic phosphorylation upon heat shock and cold stress.

Gene ontology enrichment analyses were performed using DAVID bioinformatics resources for proteins containing dynamic phosphorylation sites using the entire S. cerevisiae proteome as background. –Log[PValue(Benjamini)] correspond to the negative log10 of pValue corrected for multiple hypothesis testing using Benjamini criteria.

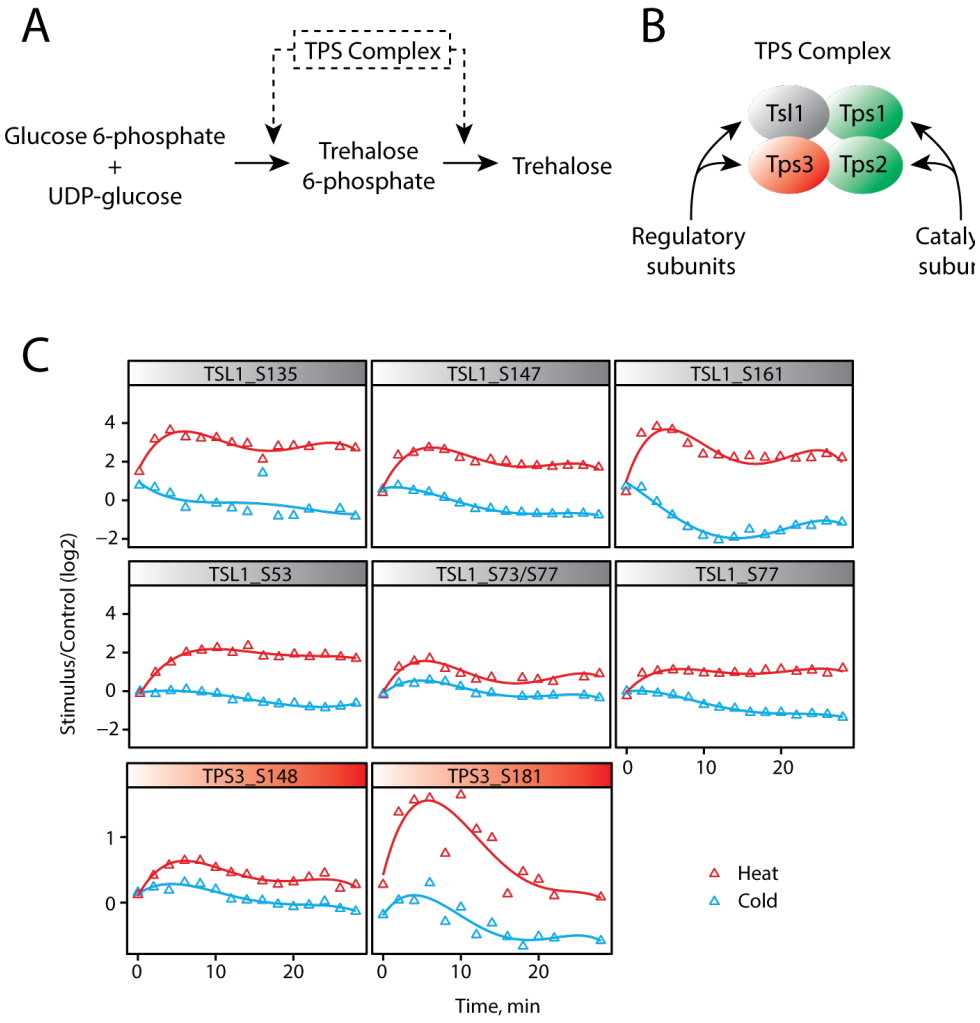

Supplementary Figure 2.6. Dynamic changes in protein phosphorylation on the trehalose -6-phosphate synthase (TPS) complex regulatory subunit Tsl1.

A) Trehalose biosynthesis involves a two step process whereby glucose 6-phosphate plus UDP-glucose are converted to trehalose 6-phosphate which is then converted to trehalose. Both steps are performed by the trehalose-6-phosphate synthase (TPS) complex. B) The yeast TPS complex comprises regulatory (Tsl1, Tps3) and catalytic (Tps1, Tps2) subunits. The Tps1 is associated with the conversion of glucose 6-phosphate into trehalose 6-phosphate while Tps2 subunit converts trehalose 6-phosphate into trehalose. Regulatory subunits Tps3 and Tsl1 have partially overlapping functions. C) Phosphorylation profiles of sites identified for the regulatory subunits Tsl1 and Tps3 following heat shock and cold stress.

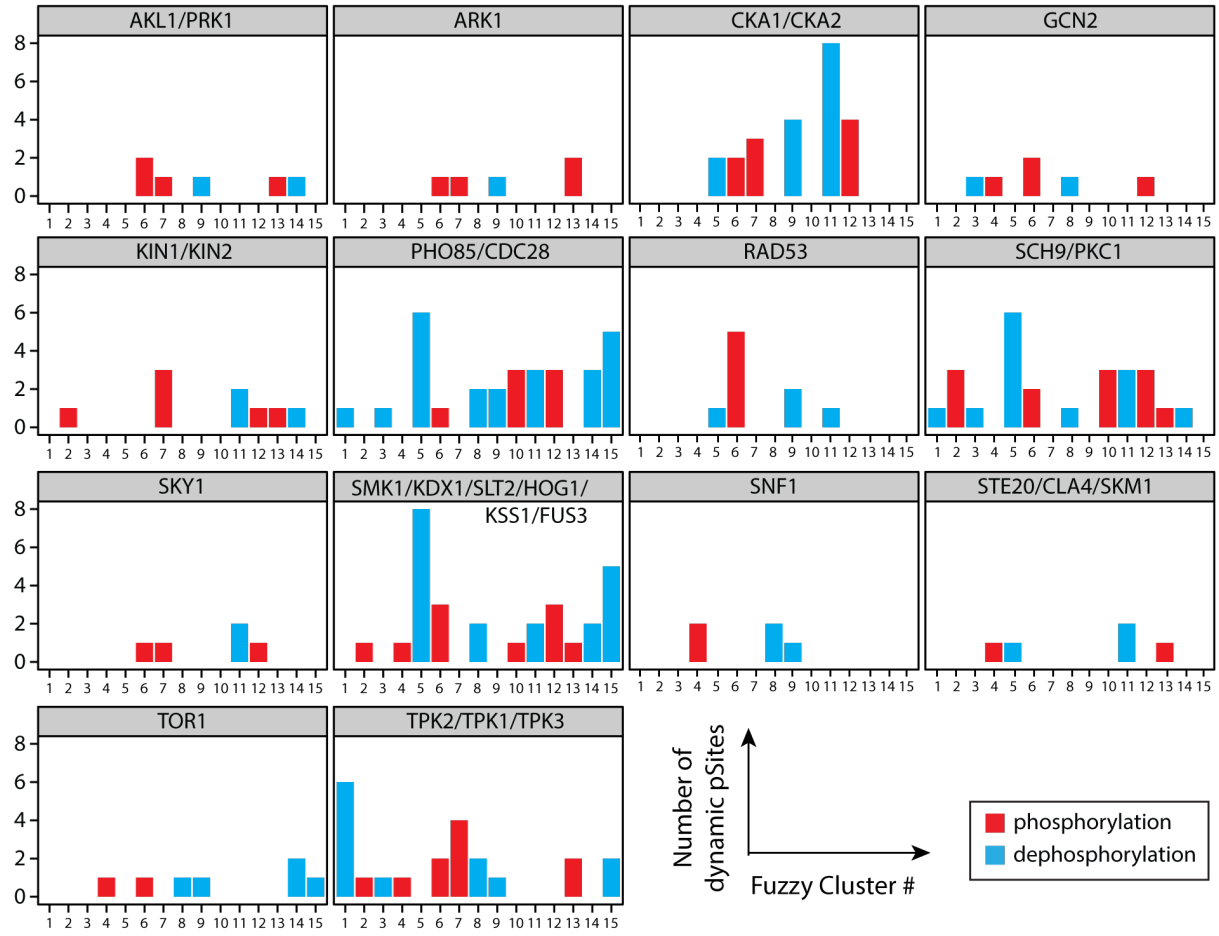

Supplementary Figure 2.7. Distribution of dynamic behaviors among putative substrates of different kinase groups.

We used KinomeXplorer to predict kinase groups associated with the phosphorylation of dynamic phosphosites detected in our study. Each panel represent the distribution of substrates for a particular kinase group for each fuzzy cluster (see Fig. 3), colors indicate whether the corresponding cluster represents an increase or a decrease in phosphorylation.

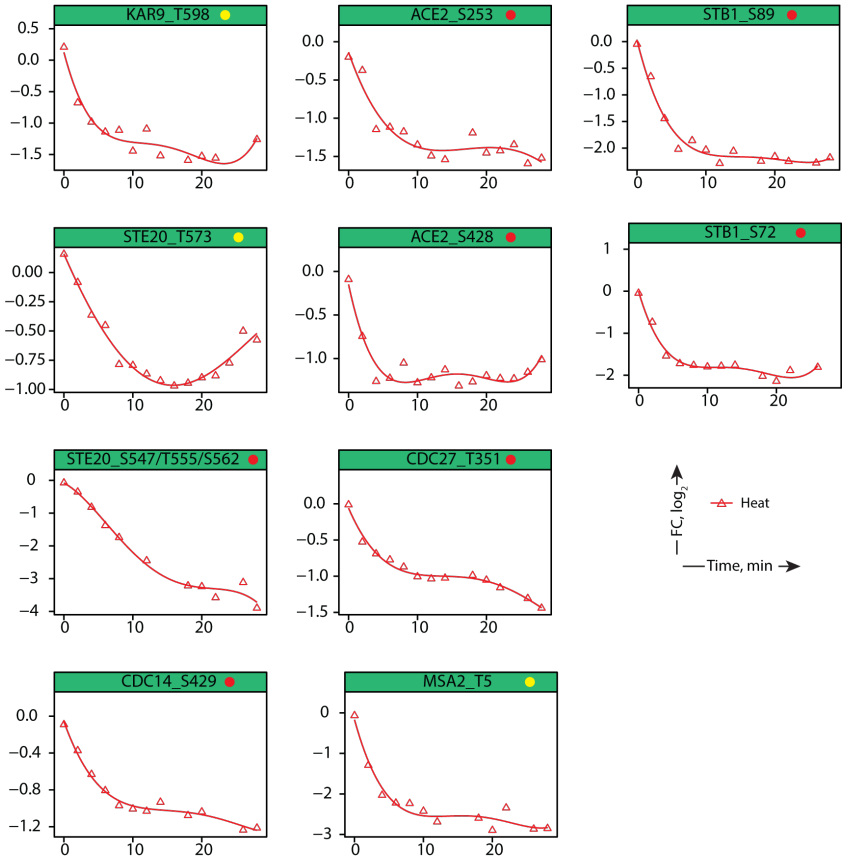

Supplementary Figure 2.8. Dynamic behavior of Cdc28 substrates.

An increase phosphorylation of Cdc28 at its inhibitory site Y19 was observed under in response to heat shock. STRING database was used to obtain high-confidence Cdc28 interactors among dynamic proteins detected in our study and PhosphoGRID database to infer known Cdc28-regulated phosphosites for these interactors. A total of 8 dynamic phosphosites (known substrates) were identified in our dataset, and all displayed similar dephosphorylation profiles (red dots). We detected similar dynamic profiles on phosphosites from other interactors, which were identified as putative substrates of Cdc28 (yellow dots).

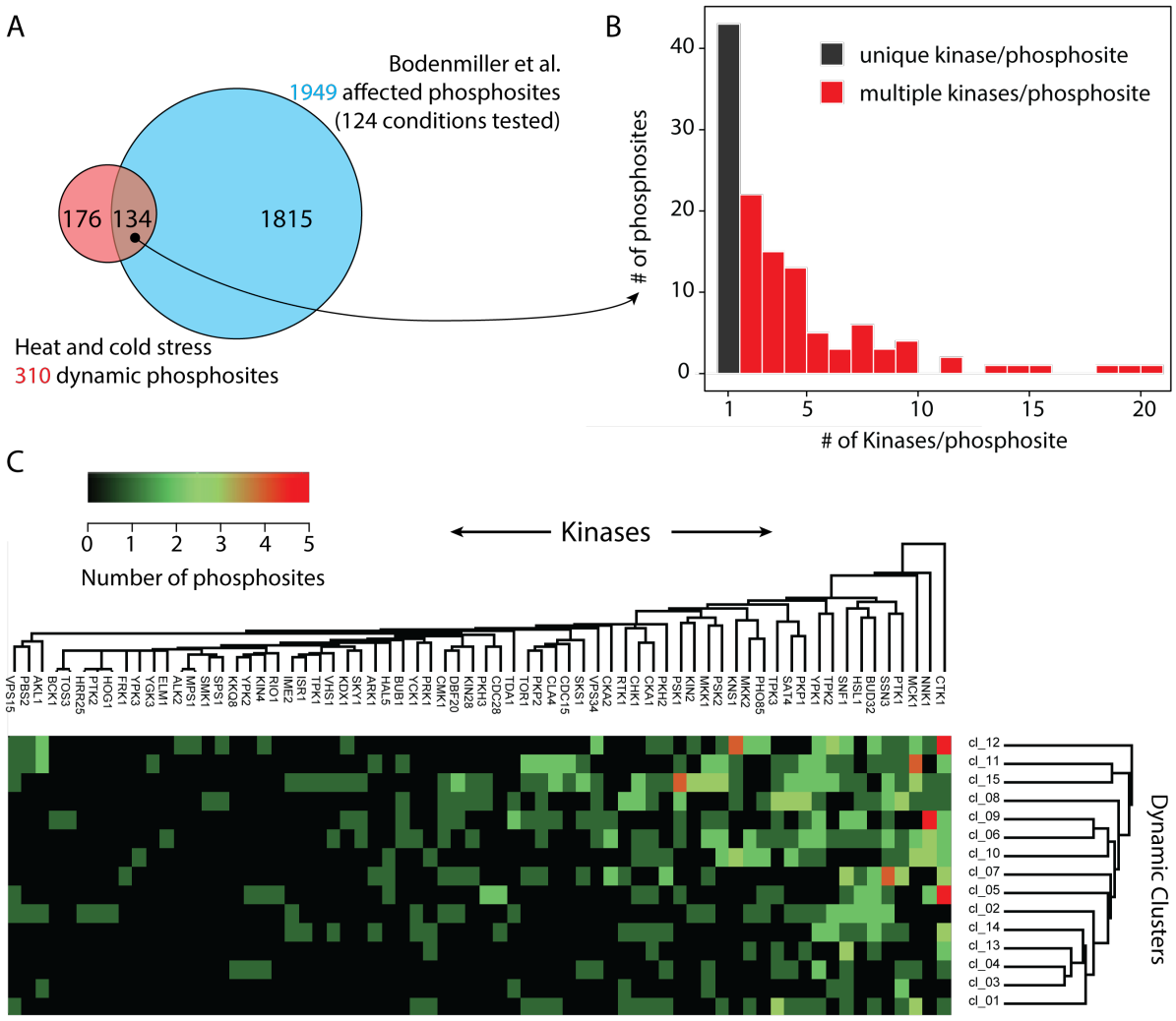

Supplementary Figure 2.9. Overlap of dynamic phosphosites with system-wide perturbations of kinases and phosphatases in yeast.

A) Comparison of dynamic phosphosites with those identified in large-scale phosphoproteomics study performed on 116 gene deletion mutants of the non essential kinases or phosphatases, and 8 analog-sensitive kinase strains of some essential kinases (Bodenmiller et al, 2010). Approximately 45% of dynamic phosphosites from monophosphorylated peptides (134 phosphosites) were also regulated in gene deletion or analog sensitive mutants. B) Distribution of dynamic phosphosites and their associated kinases. Majority of dynamic phosphosites are affected by more than one condition and associated with multiple kinases. C) Hierarchical clustering of kinases and their dynamic clusters. Heat map corresponds to grouping of individual kinases based on the dynamic behavior of the corresponding substrates.

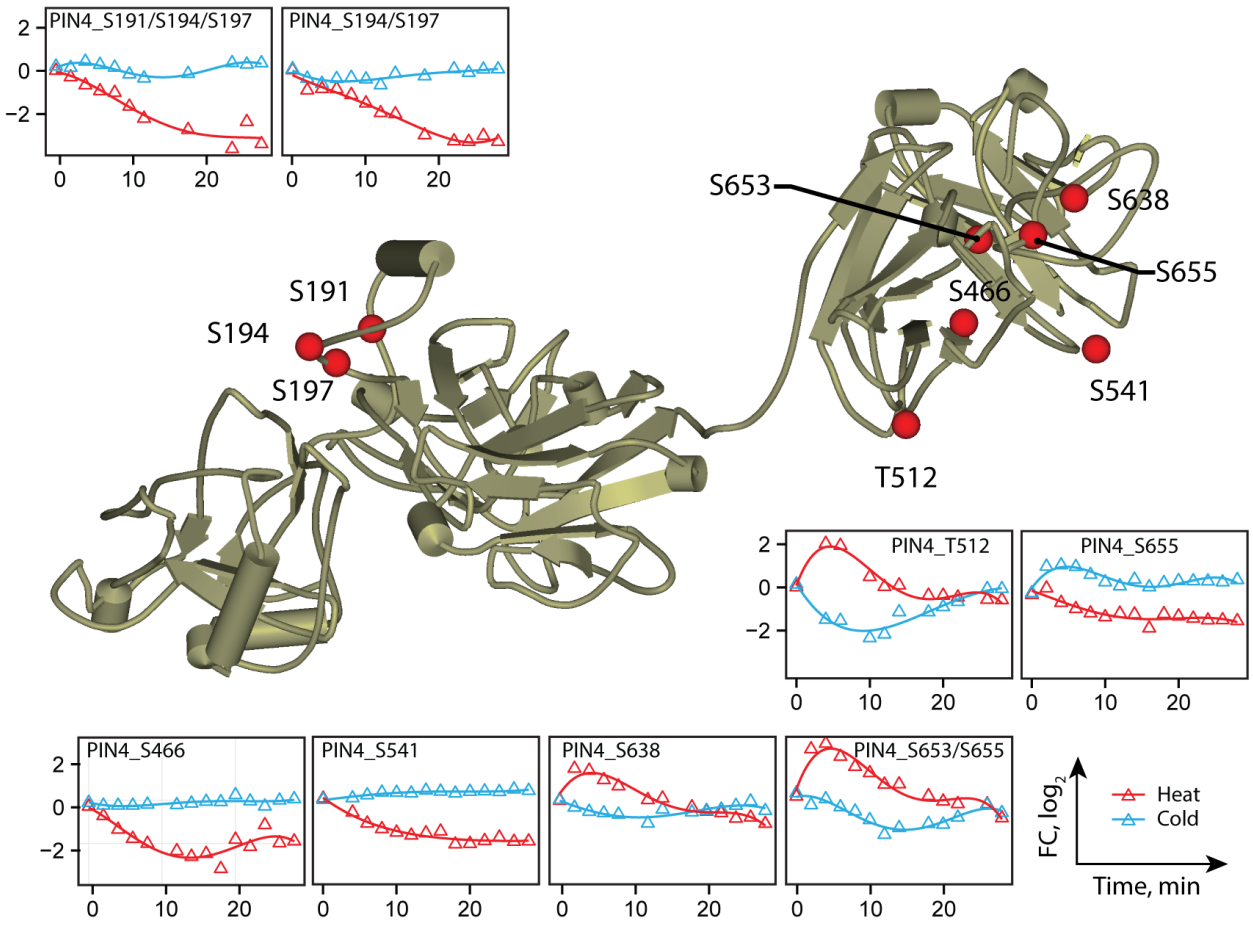

Supplementary Figure 2.10. Distribution of dynamic sites within Pin4 structure.

I-TASSER (Roy et al, 2010) was used to predict the structure of the RNA binding protein Pin4. Dynamic profiles of phosphosites are shown in response to heat and cold stresses. Changes in the phosphorylation of Pin4 could mediate its binding to RNA under changes of temperature.

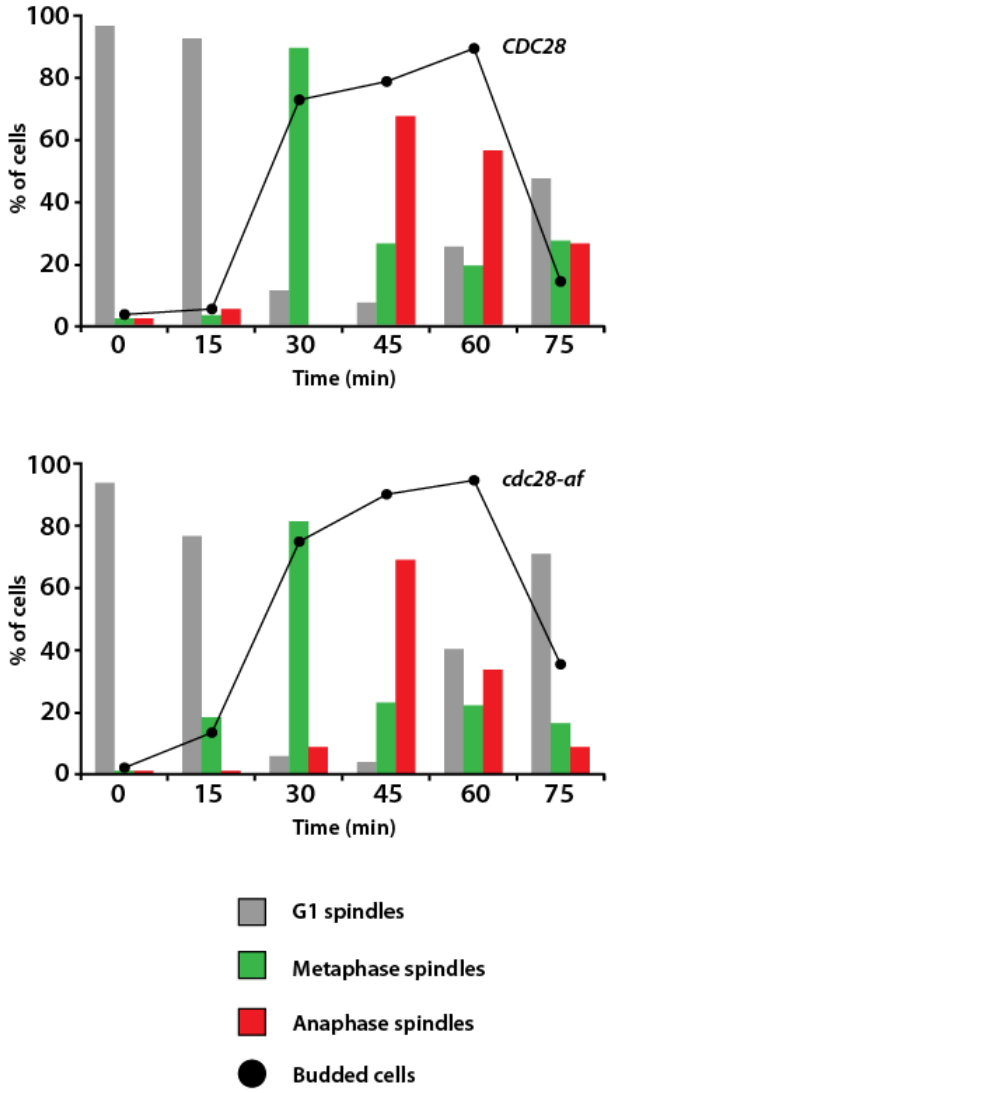

Supplementary Figure 2.11. Cell cycle profile of cdc28-af mutants growing at physiological temperature.

Graphs showing the budding index and spindle morphology of CDC28 (top) and cdc28-af cells (bottom) after release from a G1-arrest into fresh medium at 30 °C. Sample of cells were taken every 15 min to determine the budding index (lines), and microtubule morphology (bars) in cultures of CDC28 and cdc28-af cells progressing synchronously into the cell cycle. At least 100 cells were counted at each time point.

2.7.2 Supplementary tables

Supplementary Table S 2-1: All phosphopeptide profiles from heat and cold shock treatments (DVD-R).

Supplementary Table S 2-2: Dynamically regulated phosphopeptide profiles from heat and cold shock treatments (DVD-R).

Supplementary Table S 2-3: Protein identifications and quantifications from heat and cold shock treatments at 28 minutes. Quantification based on unmodified peptides (DVD-R).

Supplementary Table S 2-4: Gene Ontology enrichment of proteins containing dynamic phosphosites (DVD-R).

Supplementary Table S 2-5: Overview of the numbers of detected kinases and phosphoatases (DVD-R).

Supplementary Table S 2-6: All phosphosite identification and quantification data from treatments with Cdc28 inhibitor (DVD-R).

Supplementary Table S 2-7: Comparison of data from heat and cold treatments with phosphoproteomics results from Bodenmiller et al. (2010) (DVD-R).

Supplementary Table S 2-8: Comparison of phosphoprotoemics data from heat and cold treatments with transcriptomics data from Gasch AP et al. (2000) (DVD-R).

Supplementary Table S 2-9: MaxQuant parameters and experimental design templates (DVD-R).

2.8 References

1. Verghese, J., et al., *Biology of the heat shock response and protein chaperones: budding yeast (Saccharomyces cerevisiae) as a model system.* Microbiol Mol Biol Rev, 2012. **76**(2): p. 115-58.
2. Morano, K.A., C.M. Grant, and W.S. Moye-Rowley, *The response to heat shock and oxidative stress in Saccharomyces cerevisiae.* Genetics, 2012. **190**(4): p. 1157-95.
3. Gasch, A.P., et al., *Genomic expression programs in the response of yeast cells to environmental changes.* Mol Biol Cell, 2000. **11**(12): p. 4241-57.
4. Gasch, A.P. and M. Werner-Washburne, *The genomics of yeast responses to environmental stress and starvation.* Funct Integr Genomics, 2002. **2**(4-5): p. 181-92.
5. Kuhl, N.M. and L. Rensing, *Heat shock effects on cell cycle progression.* Cell Mol Life Sci, 2000. **57**(3): p. 450-63.
6. Rowley, A., et al., *Heat shock-mediated cell cycle blockage and G1 cyclin expression in the yeast Saccharomyces cerevisiae.* Mol Cell Biol, 1993. **13**(2): p. 1034-41.
7. Gancedo, J.M., *Control of pseudohyphae formation in Saccharomyces cerevisiae.* FEMS Microbiol Rev, 2001. **25**(1): p. 107-23.
8. Holly, S.P. and K.J. Blumer, *PAK-family kinases regulate cell and actin polarization throughout the cell cycle of Saccharomyces cerevisiae.* J Cell Biol, 1999. **147**(4): p. 845-56.
9. Raitt, D.C., F. Posas, and H. Saito, *Yeast Cdc42 GTPase and Ste20 PAK-like kinase regulate Sho1-dependent activation of the Hog1 MAPK pathway.* EMBO J, 2000. **19**(17): p. 4623-31.
10. Versele, M. and J. Thorner, *Septin collar formation in budding yeast requires GTP binding and direct phosphorylation by the PAK, Cla4.* J Cell Biol, 2004. **164**(5): p. 701-15.
11. Farrell, A. and D.O. Morgan, *Cdc37 promotes the stability of protein kinases Cdc28 and Cak1.* Mol Cell Biol, 2000. **20**(3): p. 749-54.
12. Hsieh, Y.Y., P.H. Hung, and J.Y. Leu, *Hsp90 regulates nongenetic variation in response to environmental stress.* Mol Cell, 2013. **50**(1): p. 82-92.
13. Aguilera, J., F. Randez-Gil, and J.A. Prieto, *Cold response in Saccharomyces cerevisiae: new functions for old mechanisms.* FEMS Microbiol Rev, 2007. **31**(3): p. 327-41.
14. Los, D.A. and N. Murata, *Membrane fluidity and its roles in the perception of environmental signals.* Biochim Biophys Acta, 2004. **1666**(1-2): p. 142-57.
15. Schade, B., et al., *Cold adaptation in budding yeast.* Mol Biol Cell, 2004. **15**(12): p. 5492-502.
16. Panadero, J., et al., *A downshift in temperature activates the high osmolarity glycerol (HOG) pathway, which determines freeze tolerance in Saccharomyces cerevisiae.* J Biol Chem, 2006. **281**(8): p. 4638-45.
17. Gruhler, A., et al., *Quantitative phosphoproteomics applied to the yeast pheromone signaling pathway.* Mol Cell Proteomics, 2005. **4**(3): p. 310-27.
18. Smolka, M.B., et al., *Proteome-wide identification of in vivo targets of DNA damage checkpoint kinases.* Proc Natl Acad Sci U S A, 2007. **104**(25): p. 10364-9.

19. Saleem, R.A., et al., *Integrated phosphoproteomics analysis of a signaling network governing nutrient response and peroxisome induction.* Mol Cell Proteomics, 2010. **9**(9): p. 2076-88.
20. Bodenmiller, B., et al., *Phosphoproteomic analysis reveals interconnected system-wide responses to perturbations of kinases and phosphatases in yeast.* Sci Signal, 2010. **3**(153): p. rs4.
21. Holt, L.J., et al., *Global analysis of Cdk1 substrate phosphorylation sites provides insights into evolution.* Science, 2009. **325**(5948): p. 1682-6.
22. de Godoy, L.M., et al., *Comprehensive mass-spectrometry-based proteome quantification of haploid versus diploid yeast.* Nature, 2008. **455**(7217): p. 1251-4.
23. Levy, E.D., S.W. Michnick, and C.R. Landry, *Protein abundance is key to distinguish promiscuous from functional phosphorylation based on evolutionary information.* Philos Trans R Soc Lond B Biol Sci, 2012. **367**(1602): p. 2594-606.
24. Ong, S.E. and M. Mann, *A practical recipe for stable isotope labeling by amino acids in cell culture (SILAC).* Nat Protoc, 2006. **1**(6): p. 2650-60.
25. Ratsima, H., et al., *Independent modulation of the kinase and polo-box activities of Cdc5 protein unravels unique roles in the maintenance of genome stability.* Proc Natl Acad Sci U S A, 2011. **108**(43): p. E914-23.
26. Kanshin, E., S.W. Michnick, and P. Thibault, *Displacement of N/Q-rich peptides on TiO2 beads enhances the depth and coverage of yeast phosphoproteome analyses.* J Proteome Res, 2013. **12**(6): p. 2905-13.
27. Rappsilber, J., Y. Ishihama, and M. Mann, *Stop and go extraction tips for matrix-assisted laser desorption/ionization, nanoelectrospray, and LC/MS sample pretreatment in proteomics.* Anal Chem, 2003. **75**(3): p. 663-70.
28. Ishihama, Y., J. Rappsilber, and M. Mann, *Modular stop and go extraction tips with stacked disks for parallel and multidimensional Peptide fractionation in proteomics.* J Proteome Res, 2006. **5**(4): p. 988-94.
29. Cox, J. and M. Mann, *MaxQuant enables high peptide identification rates, individualized p.p.b.-range mass accuracies and proteome-wide protein quantification.* Nat Biotechnol, 2008. **26**(12): p. 1367-72.
30. Cox, J., et al., *Andromeda: a peptide search engine integrated into the MaxQuant environment.* J Proteome Res, 2011. **10**(4): p. 1794-805.
31. Cox, J., A. Michalski, and M. Mann, *Software lock mass by two-dimensional minimization of peptide mass errors.* J Am Soc Mass Spectrom, 2011. **22**(8): p. 1373-80.
32. Nock, R. and F. Nielsen, *On weighting clustering.* IEEE Trans Pattern Anal Mach Intell, 2006. **28**(8): p. 1223-35.
33. Kumar, L. and E.F. M, *Mfuzz: a software package for soft clustering of microarray data.* Bioinformation, 2007. **2**(1): p. 5-7.
34. Schwammle, V. and O.N. Jensen, *A simple and fast method to determine the parameters for fuzzy c-means cluster analysis.* Bioinformatics, 2010. **26**(22): p. 2841-8.
35. Horn, H., et al., *KinomeXplorer: an integrated platform for kinome biology studies.* Nat Methods, 2014. **11**(6): p. 603-4.
36. Huang da, W., B.T. Sherman, and R.A. Lempicki, *Systematic and integrative analysis of large gene lists using DAVID bioinformatics resources.* Nat Protoc, 2009. **4**(1): p. 44-57.

37. Huang da, W., B.T. Sherman, and R.A. Lempicki, *Bioinformatics enrichment tools: paths toward the comprehensive functional analysis of large gene lists.* Nucleic Acids Res, 2009. **37**(1): p. 1-13.
38. Franceschini, A., et al., *STRING v9.1: protein-protein interaction networks, with increased coverage and integration.* Nucleic Acids Res, 2013. **41**(Database issue): p. D808-15.
39. Shannon, P., et al., *Cytoscape: a software environment for integrated models of biomolecular interaction networks.* Genome Res, 2003. **13**(11): p. 2498-504.
40. Cline, M.S., et al., *Integration of biological networks and gene expression data using Cytoscape.* Nat Protoc, 2007. **2**(10): p. 2366-82.
41. Smoot, M.E., et al., *Cytoscape 2.8: new features for data integration and network visualization.* Bioinformatics, 2011. **27**(3): p. 431-2.
42. Robellet, X., et al., *A high-sensitivity phospho-switch triggered by Cdk1 governs chromosome morphogenesis during cell division.* Genes Dev, 2015. **29**(4): p. 426-39.
43. Bilsland-Marchesan, E., et al., *Rck2 kinase is a substrate for the osmotic stress-activated mitogen-activated protein kinase Hog1.* Mol Cell Biol, 2000. **20**(11): p. 3887-95.
44. Ferreira, J.C., J.T. Silva, and A.D. Panek, *A regulatory role for TSL1 on trehalose synthase activity.* Biochem Mol Biol Int, 1996. **38**(2): p. 259-65.
45. Keaton, M.A., et al., *Differential susceptibility of yeast S and M phase CDK complexes to inhibitory tyrosine phosphorylation.* Curr Biol, 2007. **17**(14): p. 1181-9.
46. Stark, C., et al., *PhosphoGRID: a database of experimentally verified in vivo protein phosphorylation sites from the budding yeast Saccharomyces cerevisiae.* Database (Oxford), 2010. **2010**: p. bap026.
47. Sadowski, I., et al., *The PhosphoGRID Saccharomyces cerevisiae protein phosphorylation site database: version 2.0 update.* Database (Oxford), 2013. **2013**: p. bat026.
48. Jacquet, M., et al., *Oscillatory nucleocytoplasmic shuttling of the general stress response transcriptional activators Msn2 and Msn4 in Saccharomyces cerevisiae.* J Cell Biol, 2003. **161**(3): p. 497-505.
49. De Wever, V., et al., *A dual role for PP1 in shaping the Msn2-dependent transcriptional response to glucose starvation.* EMBO J, 2005. **24**(23): p. 4115-23.
50. Gorner, W., et al., *Acute glucose starvation activates the nuclear localization signal of a stress-specific yeast transcription factor.* EMBO J, 2002. **21**(1-2): p. 135-44.
51. Budhwar, R., A. Lu, and J.P. Hirsch, *Nutrient control of yeast PKA activity involves opposing effects on phosphorylation of the Bcy1 regulatory subunit.* Mol Biol Cell, 2010. **21**(21): p. 3749-58.
52. Kim, J.H. and M. Johnston, *Two glucose-sensing pathways converge on Rgt1 to regulate expression of glucose transporter genes in Saccharomyces cerevisiae.* J Biol Chem, 2006. **281**(36): p. 26144-9.
53. Walkey, C.J., et al., *The Saccharomyces cerevisiae fermentation stress response protein Igd1p/Yfr017p regulates glycogen levels by inhibiting the glycogen debranching enzyme.* FEMS Yeast Res, 2011. **11**(6): p. 499-508.
54. Raitt, D.C., et al., *The Skn7 response regulator of Saccharomyces cerevisiae interacts with Hsf1 in vivo and is required for the induction of heat shock genes by oxidative stress.* Mol Biol Cell, 2000. **11**(7): p. 2335-47.

55. Urban, J., et al., *Sch9 is a major target of TORC1 in Saccharomyces cerevisiae.* Mol Cell, 2007. **26**(5): p. 663-74.
56. Roelants, F.M., P.D. Torrance, and J. Thorner, *Differential roles of PDK1- and PDK2-phosphorylation sites in the yeast AGC kinases Ypk1, Pkc1 and Sch9.* Microbiology, 2004. **150**(Pt 10): p. 3289-304.
57. Ribeiro, M.J., et al., *Trehalose synthesis is important for the acquisition of thermotolerance in Schizosaccharomyces pombe.* Mol Microbiol, 1997. **25**(3): p. 571-81.
58. Lee, J., et al., *MAPK Hog1 closes the S. cerevisiae glycerol channel Fps1 by phosphorylating and displacing its positive regulators.* Genes Dev, 2013. **27**(23): p. 2590-601.
59. Booher, R.N., R.J. Deshaies, and M.W. Kirschner, *Properties of Saccharomyces cerevisiae wee1 and its differential regulation of p34CDC28 in response to G1 and G2 cyclins.* EMBO J, 1993. **12**(9): p. 3417-26.
60. Soufi, B., et al., *Global analysis of the yeast osmotic stress response by quantitative proteomics.* Mol Biosyst, 2009. **5**(11): p. 1337-46.
61. Matsuo, R., et al., *The yeast eIF4E-associated protein Eap1p attenuates GCN4 translation upon TOR-inactivation.* FEBS Lett, 2005. **579**(11): p. 2433-8.
62. Cosentino, G.P., et al., *Eap1p, a novel eukaryotic translation initiation factor 4E-associated protein in Saccharomyces cerevisiae.* Mol Cell Biol, 2000. **20**(13): p. 4604-13.
63. Tang, C.S. and S.I. Reed, *Phosphorylation of the septin cdc3 in g1 by the cdc28 kinase is essential for efficient septin ring disassembly.* Cell Cycle, 2002. **1**(1): p. 42-9.
64. Pike, B.L., et al., *Mdt1, a novel Rad53 FHA1 domain-interacting protein, modulates DNA damage tolerance and G(2)/M cell cycle progression in Saccharomyces cerevisiae.* Mol Cell Biol, 2004. **24**(7): p. 2779-88.
65. Krek, W. and E.A. Nigg, *Mutations of p34cdc2 phosphorylation sites induce premature mitotic events in HeLa cells: evidence for a double block to p34cdc2 kinase activation in vertebrates.* EMBO J, 1991. **10**(11): p. 3331-41.
66. Sorger, P.K. and A.W. Murray, *S-Phase Feedback-Control in Budding Yeast Independent of Tyrosine Phosphorylation of P34cdc28.* Nature, 1992. **355**(6358): p. 365-368.
67. Amon, A., et al., *Mechanisms that help the yeast cell cycle clock tick: G2 cyclins transcriptionally activate G2 cyclins and repress G1 cyclins.* Cell, 1993. **74**(6): p. 993-1007.
68. Rahal, R. and A. Amon, *Mitotic CDKs control the metaphase-anaphase transition and trigger spindle elongation.* Genes Dev, 2008. **22**(11): p. 1534-1548.
69. Kanshin, E., et al., *A cell-signaling network temporally resolves specific versus promiscuous phosphorylation.* Cell Rep, 2015. **10**(7): p. 1202-14.
70. Li, Y., F.R. Cross, and B.T. Chait, *Method for identifying phosphorylated substrates of specific cyclin/cyclin-dependent kinase complexes.* Proc Natl Acad Sci U S A, 2014. **111**(31): p. 11323-8.
71. Straight, A.F., et al., *Net1, a Sir2-associated nucleolar protein required for rDNA silencing and nucleolar integrity.* Cell, 1999. **97**(2): p. 245-56.
72. Visintin, R., E.S. Hwang, and A. Amon, *Cfi1 prevents premature exit from mitosis by anchoring Cdc14 phosphatase in the nucleolus.* Nature, 1999. **398**(6730): p. 818-23.
73. Azzam, R., et al., *Phosphorylation by cyclin B-Cdk underlies release of mitotic exit activator Cdc14 from the nucleolus.* Science, 2004. **305**(5683): p. 516-9.

74. Jorgensen, P. and M. Tyers, *How cells coordinate growth and division.* Curr Biol, 2004. **14**(23): p. R1014-27.
75. Skotheim, J.M., et al., *Positive feedback of G1 cyclins ensures coherent cell cycle entry.* Nature, 2008. **454**(7202): p. 291-6.
76. Costanzo, M., et al., *CDK activity antagonizes Whi5, an inhibitor of G1/S transcription in yeast.* Cell, 2004. **117**(7): p. 899-913.
77. Kandror, O., et al., *Yeast adapt to near-freezing temperatures by STRE/Msn2,4-dependent induction of trehalose synthesis and certain molecular chaperones.* Mol Cell, 2004. **13**(6): p. 771-81.
78. Hebert, A.S., et al., *Neutron-encoded mass signatures for multiplexed proteome quantification.* Nat Methods, 2013. **10**(4): p. 332-4.
79. Sorger, P.K. and H.R. Pelham, *Yeast heat shock factor is an essential DNA-binding protein that exhibits temperature-dependent phosphorylation.* Cell, 1988. **54**(6): p. 855-64.

Chapter 3

Time-resolved phosphoproteome analysis of paradoxical RAF activation reveals novel targets of ERK

Peter Kubiniok[1,2,#], Hugo Lavoie[1,#], Marc Therrien[1,3*] and Pierre Thibault[1,2,4,*]

[1] Institute for Research in Immunology and Cancer, Université de Montréal, C.P. 6128, Succursale centre-ville, Montréal, Québec, H3C 3J7, Canada.

[2] Department of Chemistry, Université de Montréal, C.P. 6128, Succursale centre-ville, Montréal, Québec, H3C 3J7, Canada.

[3] Department of Pathology and Cell Biology, Université de Montréal, C.P. 6128, Succursale Centre-Ville, Montréal, Québec H3C 3J7, Canada.

[4] Department of Biochemistry, Université de Montréal, C.P. 6128, Succursale centre-ville, Montréal, Québec, H3C 3J7, Canada.

[#] These authors contributed equally to this work

Manuscript: Published (April 2017 in Molecular and Cellular Proteomics, 16(4): 663–679)

Authors Contribution

All authors designed and participated in the study concept. P.K. performed all phosphoproteomics experiments after receiving training in cell culturing by H.L., P.K. analyzed phosphoproteomics data. All authors interpreted the data, H.L. and P.K. designed follow up experiments (In vitro kinase assays, point mutation of phosphorylation sites). P.K. and H.L. wrote a first draft of the manuscript which was finalized by P.T. and M.T. together.

3.1 Abstract

Small molecules targeting aberrant RAF activity, like Vemurafenib (PLX4032), are highly effective against cancers harboring the V600E BRAF mutation, and are now approved for clinical use against metastatic melanoma. However, in tissues showing elevated RAS activity and in RAS-mutant tumors, these inhibitors stimulate RAF dimerization, resulting in inhibitor resistance and downstream "paradoxical" ERK activation. To understand the global signaling response of cancer cells to RAF inhibitors, we profiled the temporal changes of the phosphoproteome of two colon cancer cell lines (Colo205 and HCT116) that respond differently to Vemurafenib. Comprehensive data mining and filtering identified a total of 37910 phosphorylation sites, 660 of which were dynamically modulated upon treatment with Vemurafenib. We established that 83% of these dynamic phosphorylation sites were modulated in accordance with the phospho-ERK profile of the two cell lines. Accordingly, kinase-substrate prediction algorithms linked most of these dynamic sites to direct ERK1/2-mediated phosphorylation, supporting a low off-target rate for Vemurafenib. Functional classification of target proteins indicated the enrichment of known (nuclear pore, transcription factors, RAS-RTK signaling) and novel (Rho GTPases signaling, actin cytoskeleton) ERK-controlled functions. Our phosphoproteomic data combined with experimental validation established novel dynamic connections between ERK signaling and the transcriptional regulators TEAD3 (Hippo pathway), MKL1 and MKL2 (Rho-SRF pathway). We also confirm that an ERK docking site found in MKL1 is directly antagonized by overlapping actin binding, defining a novel mechanism of actin-modulated phosphorylation. Altogether, time-resolved phosphoproteomics further documented Vemurafenib selectivity and identified novel ERK downstream substrates.

3.2 Introduction

Increased RAS-ERK signaling is critically connected with tumour initiation and progression [1]. Canonical pathway activation is initiated at the plasma membrane (PM) where ligand bound to receptor tyrosine kinases (RTKs) transduce the signal to enzymes that activate RAS (NRAS, KRAS or HRAS) by favouring its GTP loading [2]. Downstream of RAS, the RAF family of Ser/Thr kinases comprises three different homologues, ARAF, BRAF and CRAF involved in the regulation of the RAS-ERK signaling cascade [1, 3]. In quiescent cells, RAF is kept inactive in the cytoplasm in an auto-inhibited complex with 14-3-3 proteins. GTP-bound RAS directly associates with the RAF RAS-binding domain (RBD), which recruits RAF to the PM and relieves its auto-inhibition [3, 4]. Importantly, RAF activation also relies on the formation of homo and heterodimers that allosterically control kinase activity [5]. Upon activation, RAF signals downstream to MEK1/2 (MAP2K1/2), which in turn phosphorylates ERK1/2 (MAPK1/3) proteins leading to the phosphorylation of hundreds of cellular substrates on consensus PXS/TP motifs [6].

RAS and RAF oncogenic mutations render them constitutively active resulting in aberrant signaling to downstream effectors. This induces a sustained activation of downstream MEK and ERK in a growth factor-independent fashion, a hallmark of cancer cells signaling. The most frequent genetic lesions in *RAS* genes, the mutation of G12, G13 and Q61 residues, lock RAS proteins in the GTP-bound active state [2]. Similarly, BRAF mutations like V600E occur in the kinase catalytic domain and result in a conformational change rendering BRAF constitutively active [7, 8]. RAS mutations are one of the leading causes of cancer irrespective of tissue type [9] while BRAF V600E mutations are also found across several tumour types, but are especially frequent in melanoma (70%) and thyroid cancers (45%)[10-12].

In view of the frequent association of RAF with cancer signaling, several drug discovery programs have aimed at blocking its kinase activity [13]. Pharmacological inhibitors targeting oncogenic RAF such as the FDA-approved PLX4032 (Vemurafenib, Vectibix or Erbitux) can abrogate the activity of V600E mutant BRAF [14-16]. However, wild type (WT) RAF tumours bearing RAS mutations or showing elevated RTK signaling give rise to aberrant activation of RAF kinases upon RAF inhibitor treatment [17-19]. This undesired effect is caused by a RAS-dependent increase in RAF dimerization upon inhibitor binding which leads to the so-called

"paradoxical" activation of ERK signaling. The molecular basis of this phenomenon is the allosteric activation of drug-free RAF by drug-bound protomers across induced dimers [17-20]. Several cancer types therefore display poor response to RAF-specific inhibitors. This limits the use of ATP-competitive inhibitors like Vemurafenib (PLX4032) to the treatment of melanomas carrying the BRAF V600E mutation that have reduced RAS signaling [21]. Cancer cell lines (CCLs) derived from RAS- and RAF-mutant tumors thus behave in an opposite manner when exposed to RAF inhibitors. Although the "paradoxical" effect of RAF inhibitors is undesired in clinical settings, it represents a powerful tool to selectively induce pathway activation without the pleiotropic effects typically associated with RTK or phorbol ester stimulations.

We recently showed that dynamic profiling of phosphoproteomes enabled the identification of novel downstream effectors of well-studied signaling pathways with high confidence [22, 23]. This type of proteomics analysis facilitated the characterization of biological responses to a variety of stimuli like osmotic shock and thermal stress [22-24]. Phosphoproteome dynamics provides valuable information on the shape and extent of a biological response to unravel novel and unexpected kinase-substrate interactions [22]. In the specific context of the RAS-ERK signaling cascade, the identity of ERK substrates and the timing of pathway activation determine what biological response will be elicited (proliferation, differentiation, survival) [25]. Systems approaches that include treatment kinetics are therefore needed to derive an exhaustive repertoire of ERK substrates and to temporally resolve phosphorylation events.

While phosphoproteome analysis of RAS-ERK pathway blockade has recently been published [26], the proteome-wide consequences of "paradoxical" pathway activation have not yet been investigated. We posit that a dynamic understanding of this phenomenon could help decipher the complex response to RAF inhibitors and yield new insights on RAS-ERK pathway signaling. In the present study we report the application of high resolution temporal profiling coupled with metabolic labeling [27] to quantify changes in the phosphoproteome of HCT116 and Colo205 colon cancer cells following Vemurafenib treatment. Altogether, this approach enabled the identification of 37,910 phosphorylation sites, of which 660 were dynamically regulated. We used this rich dataset to understand the complex response to RAF inhibitors and to identify additional signaling nodes that act downstream of ERK.

3.3 Materials and methods

3.3.1 Alphascreen® SureFire® p-ERK 1/2 assay

The pERK Alphascreen® SureFire® (Perkin-Elmer; Waltham, MA) was used following manufacturer's instructions for the standard 2 plate assay protocol. For the time course experiments, a total of $3x10^4$ cells were plated in 96-well plates, incubated overnight and treated with variable concentrations of PLX4032 for 60 minutes or 3.3 μM PLX4032. Treatments were performed in biological triplicates. Plates were read on an EnVision plate reader (Perkin-Elmer; Waltham, MA).

3.3.2 Cell culturing of HCT116 and Colo205 cell lines

Cell lines were grown in double SILAC SD-Media (Thermo Fisher Scientific, Rockford, IL) containing 10%FBS, 164 μM Lysine (K) and 95μM Arginine (R) and 4.3 μM proline (Silantes, Munich, Germany) with additional nutrients consistent with Bendall *et al.* [28]. Cell plates were incubated at 37°C and 5% CO_2 in Panasonic incubator. Cells were counted using a Leica Microscope with 10x0.25 objectives.

Approximately $12.5x10^6$ cells were plated in 32 125x25mm petri dishes. Incubation with the Raf inhibitor Vemurafenib (PLX4032) (Selleck Chemicals Houston, TX) was performed by adding 1mL of PLX4032 or DMSO (vehicle) (Sigma Aldrich Co.) diluted in SILAC DMEM /10% FBS to reach a final concentration of 3.3μM in each petri dish. Cells were harvested every 5 min during the first hour of treatment with either PLX4032 (heavy label) or DMSO (light label). Cells were collected by adding 10mL of -80°C pre-cooled ethanol and final scraping. Heavy and Light cell pellets were combined in 10mL Falcon tubes. The workflow is shown in Figure 3.1C.

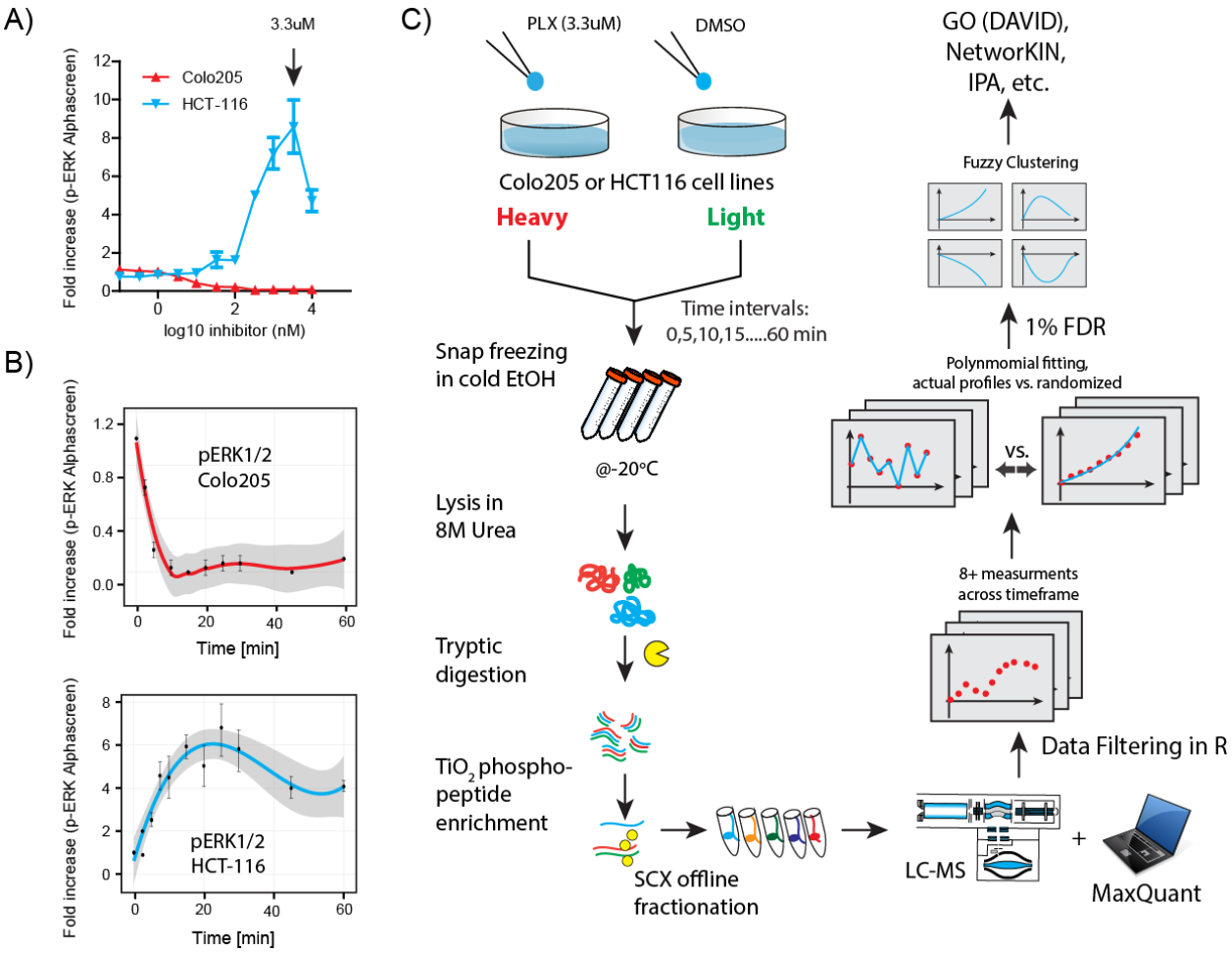

Figure 3.1. Experimental design and data analysis workflow for time-resolved phosphoproteome experiments.

A) Dose-dependent modulation of phospho-ERK1/2 following vemurafenib treatment in Colo205 and HCT116. B) Time course analysis of 3.3 µm vemurafenib treatment in Colo205 (top) and HCT116 (bottom) cell lines. C) Workflow of time-resolved phosphoproteome profiling. Cells were incubated with 3.3 µm vemurafenib (Heavy) or DMSO (Light) and collected every 5 min by mixing in cold ethanol to immediately preserve protein phosphorylation. Cells are centrifuged and lysed under denaturing conditions, and extracted proteins are digested with trypsin. Phosphopeptides are purified on TiO2 beads and fractionated off line on SCX spin columns prior to LC-MS/MS analyses. Phosphopeptide identification and quantitation are performed using MaxQuant, and only kinetic profiles containing at least eight time measurements were selected for further analysis. Polynomial fitting was used to define regulated phosphosites, and only phosphopeptide profiles with an FDR of <1% were selected and used for fuzzy c-means clustering and subsequent analyses.

3.3.3 Digestion and desalting of cell extracts

Heavy and Light cell pellets from each of the 15 time points were combined in 10mL Falcon tubes, separated by centrifugation at 700 rpm (Sorvall Legend RT centrifuge) and washed with 5 mL PBS. Cell lysis was performed by sonication for 15 seconds with Sonic dismembrator (Thermo Fisher Scientific; (Rockford, IL)) after adding 1 mL lysis buffer (8M Urea, 50mM

TRIS, pH 8, HALT phosphatase inhibitor from Thermo Fisher Scientific (Rockford, IL)). Cells were maintained at 0°C to prevent biological activities. Protein concentration was measured with Pierce BCA assay from Thermo Fisher Scientific (Rockford, IL). Protein disulfide bonds were reduced by incubating lysates in 5 mM Dithiothreitol (DTT, Sigma-Aldrich, St-Louis, MO) for 30 minutes at 56°C while shaking at 1000 rpm. Alkylation of cysteine residues was achieved by incubating iodoacetamide (IAA, Sigma-Aldrich) at a concentration of 15mM for 30 min at RT in the dark. Excess of IAA was deactivated by adding DTT up to 5mM for 15 minutes at room temperature.

All samples were diluted 5 times with 20 mM TRIS (Bioshop Burlington ON), 1mM CaCl, pH=8 and mixed with Trypsin (Sigma-Aldrich) (protein: trypsin 50:1 w:w) and incubated for 12 hours at 37°C. Trypsin stock, containing 2µg/µL Trypsin was kept at -80 °C and thawed only once. Desalting was performed in 60 mg SPE reverse phase cartridges (Oasis HLB 3cc cartridge, 60 mg, 30 µm particle size, Waters Mississauga, ON) previously conditioned with 3mL methanol, SPE Buffer (50% ACN, 1% FA) and finally 1% aqueous FA. Peptide samples were applied, desalted with 3mL 1% FA, eluted in 1mL SPE buffer and dried on a SpeedVac centrifuge (Thermo Fisher Scientific; Rockford, IL) at room temperature.

3.3.4 Phosphopeptide enrichment

Phosphopeptide enrichment was performed on 5µm titansphere bulk particles (Canadian Life Science, Peterborough, ON) according to recent protocols [29, 30]. This method provides the most efficient enrichment of phosphopeptides.

3.3.5 Offline strong cation exchange chromatography

To achieve high reproducibility and parallel sample fractionation, we used strong cation fractionation on homemade SCX spin columns packed with 18-22 mg of polysulfoethyl A (300Å Bulk material, Canada Life Science; Peterborough, ON). After equilibrating the SCX spin columns with each 100 µL of SCX Buffer A (10% ACN, 0.2%FA), Buffer B (1000 mM NaCl in 10% ACN, 0.2%FA) and finally 200 µL SCX Buffer A, peptides were resuspended in 100µL Buffer A, loaded on the SCX column and eluted in six salt step fractions of 100µL each (0, 30,

50, 80, 120 and 500 mM NaCl) in SCX Buffer A. In subsequent analyses, the last salt step fraction was not injected as they contained negligible amounts of peptides. Prior to LC-MS/MS analyses all fractions were dried on a SpeedVac centrifuge at room temperature (Thermo Fisher Scientific) and resuspended in 4% FA. All centrifugation steps were performed at 4°C except when indicated.

3.3.6 LC-MS/MS analysis

All LC-MS/MS analyses were performed on a Q-Exactive plus mass spectrometer using a homemade capillary LC columns (18 cm length, 150 µm ID, 360 µm OD). Capillary LC columns were packed with C18 Jupiter 3µm particles (Phenomenex, Torrance, CA) at 1000 psi. Precolumns of 5 mm were packed at 100 psi using the same material. LC separations were performed at a flow rate of 0.6 µL/min using a linear gradient of 5-40 % aqueous ACN (0.2% FA) in 150 minutes. MS spectra were acquired with a resolution of 70,000 using a lock mass (m/z: 445.120025) followed by up to 10 MS/MS data dependent scans on the most intense ions using high energy dissociation (HCD). AGC target values for MS and MS/MS scans were set to $1x10^6$ (max fill time 100 ms) and 5e4 (max fill time 120 ms), respectively. The precursor isolation window was set to m/z 1.6 with a HCD normalized collision energy of 24. The dynamic exclusion window was set to 30s.

3.3.7 Data processing and analysis

Raw data analysis of SILAC experiments was performed using Maxquant software 1.3.0.5 and the Andromeda search engine [31]. The false discovery rate (FDR) for peptide, protein, and site identification was set to 1%, the minimum peptide length was set to 6, and the ‘peptide requantification’ function was enabled. The option match between runs (3 min time tolerance) was enabled to correlate identification and quantitation results across different runs. Up to 2 missed cleavages per peptide were allowed. To adjust for any systematic quantification errors, SILAC ratios were normalized by time point. All additional parameters are reported in MaxQuant parameters.txt and experimentalDesign.txt provided in Supplementary Table S3-4. The Uniprot human proteome database (January 2014 containing 70584 entries) was used for all

searches. Protein groups were formed by MaxQuant, and all identified peptides were used to make pair-wise comparison between proteins in the database [31, 32]. Proteins containing an equal or overlapping set of peptides were merged together to form a protein group and ranked according to the highest number of peptides. All raw LC-MS/MS data and MaxQuant output files can be accessed from Peptide Atlas (http://www.peptideatlas.org/) using the identifier PASS00897. MaxQuant output files contain lists of all matched and unmatched spectra, all matched protein isoforms and peptides including scorings and more detailed information. In addition to an FDR of 1% set for peptide, protein and phosphosite identification levels, we used additional criteria to increase data quality. We selected only peptides for which abundance ratios (FC=PLX4032/Control) were measured in at least 8 out of 13 time points. Then we set a cut-off for maximum phosphosite localization confidence across experiments (time points) to 0.75 [33]. Next, we distinguished dynamic from static phosphosites by calculating a false discovery rate (FDR) based on curve fitting. This was achieved by fitting each profile to a polynomial order ranging from 1 to 8, and comparing the resulting profiles with those obtained from the same data following 5 rounds of randomization (Supplementary Figure 3.2). The coefficient of determination (R^2) was calculated for each profile of a given order, and compared against those from the randomized dataset. For each polynomial order, dynamic profiles were selected based on R^2 values below a FDR of 1%. Next, we used fuzzy C-means algorithm to cluster all dynamic profiles [34]. Analysis and visualization were performed in the R environment (http://www.r-project.org/) , clusters were obtained with the Mfuzz package [35]. Optimal setting of the "fuzzifier" parameter was 1.235 as estimated with the "mestimate" function. In order to find the optimal number of clusters, we performed repeated soft clustering for cluster numbers ranging from 2 to 30 and calculated the minimum centroid distance (minimum distance between two cluster centers produced by c-means clustering) [36]. Next, we determined the membership value of dynamic profiles, and selected only those with values greater or equal to 0.9 for high membership profiles.

Gene Ontology (GO) enrichment analyses were performed using the database DAVID version 6.7 [37]. Protein interaction networks were defined using the STRING database [38] and interacting proteins were visualized with Cytoscape version 2.8.3 [39]. Kinase substrate interactions were predicted using NetworKIN and KinomeXplorer [40]. A protein-protein interaction network was built in STRING version 9.1 for all proteins containing dynamic

phosphosites [38]. All interaction predictions were based on experimental evidences with a minimal confidence score of 0.9 (considered as a “highest confidence” filter in STRING). Structure rendering was done using PyMol (Schrödinger).

3.3.8 Protein purification and *in vitro* kinase assays

GST-TEV fusion of human MKL1 (sequence corresponding to accession 3TPQ_M), MKL2$^{46-162}$ (NP_054767.3) and TEAD3$^{1-436}$ (BC091488.1) were cloned between BamHI and XhoI in a pGEX4T1 plasmid engineered with a TEV cleavage site. The resulting plasmids were transformed in chimiocompetent *E. coli* BL21pLys and expression was induced overnight at 18°C with 1mM IPTG in 500ml of terrific broth (TB). Cells were harvested and lysed by one cycle of freeze-thawing on ice in 25 ml of buffer F (10mM Tris-HCl pH7.5, 150mM NaCl, 1mM EDTA, 1mM PMSF) supplemented with benzonase (Sigma-Aldrich). Lysates were then sonicated four times 10 seconds with a sonicator probe set at 80% power and cleared by centrifugation at 4°C for 20 minutes at 40, 000g in a Sorvall SS-34 rotor. The supernatant was adjusted to 0.05%Tween20 and incubated with 150 µl Glutathione-sepharose 4B (GE Healthcare; Little Chalfont, UK) at 4°C for 4 hours. Glutathione-sepharose column, washed with 20 bed-volumes of Buffer G (50mM Tris-HCl, pH7.5, 50mM NaCl, 0.1mM CaCl2, 2mM 2-mercaptoethanol, 0.05% Tween20) and eluted at room temperature in Buffer G with 25mM of reduced glutathione (pH was ajusted to 7.5 before elution). Recombinant protein concentration was established using the Bradford assay and protein purity was confirmed by SDS-PAGE followed by Coomassie staining. Proteins were stored at -80°C in Buffer G supplemented with 20% glycerol.

Active ERK was obtained from Carna Bio (Kobe, Japan) (04-143) and purified rabbit muscle actin was obtained from Cytoskeleton (AKL99). Actin was resuspended at 10mg/ml in Buffer H (5 mM Tris-HCl pH 8.0, 0.2 mM CaCl2, 0.2 mM ATP, 5% sucrose). G-actin was prepared by incubation with 50µM Latrunculin B for 1h at room temperature followed by sedimentation of F-actin in a Sorvall Discovery M150 SE at 100 000g for 1 hour at 4°C.

In vitro kinase assays were conducted in kinase A buffer (50mM HEPES pH 7.5, 10 mM MgCl2, 1 mM EGTA, 0.01% Brij-35, 2mM DTT, 1mM PMSF, 1X leupeptin and pepstatin) with 30 ng of active ERK and 2 µg of GST fusion protein. When required, the reactions were combined

with TEV cleavage of GST fusions by including 3 units of acTEV (Invitrogen; Carlsbad, CA) in the kinase reactions. Kinase reactions were initiated by addition of ATP (50μM final) + 5μCi of ATP[γ-32P] (Perkin Elmer; Waltham, MA) and were incubated at 37°C for 30min. Reactions were stopped at 95 C in the presence of Laemmli sample buffer. Kinase reactions were loaded on SDS-PAGE gels, proteins were stained with Coomassie G-250 and gels were finally dried and exposed to X-ray films.

For actin titration experiments, recombinant MKL1 was incubated overnight with different molar ratios of G-actin. The protein mixes were then subjected to kinase reaction in the presence of ERK2 and ATP as described above. All experiments were performed in biological triplicates and only the best western blots are depicted in the corresponding Figures.

3.4 Results

3.4.1 Dynamic changes in the phosphoproteome following Vemurafenib treatment

For this study, we chose two colon cancer cell lines that display elevated ERK signaling due to different genetic lesions. Colo205 cells harbor a *BRAF* V600E mutation but are otherwise WT for RAS, while HCT116 cells contain a *KRAS* G13D mutation but are WT for RAF [41]. These cell lines are widely used in the cancer research community and respond differently to RAF inhibitors. Indeed, phospho-ERK1/2 (pERK) is inhibited in Colo205 cells following incubation with RAF inhibitor while it is induced in HCT116 cells [20, 42]. We profiled the change in ERK1/2 activation for different concentration of the RAF inhibitor Vemurafenib, and determined that a concentration of 3.3 μM induced an 8-fold increase of pERK in HCT116 cells (Figure 3.1A). In contrast, the same concentration resulted in full pERK inhibition in Colo205 cells (Figure 3.1A). Time course measurements showed that the pERK response to Vemurafenib treatment was maximal after 20 min in both cell lines (Figure 3.1B).

To evaluate the downstream effects of this response, we monitored the global change in the phosphoproteome of both cell lines over a period of 60 min post stimulation with a temporal resolution of 5 min (Figure 3.1C). We used stable isotope labeling with amino acids in cell culture (SILAC) [43] where control (DMSO vehicle) and stimulated cells (3.3 μM Vemurafenib) were cultured in dialyzed FBS for more than 10 doublings with Light and Heavy Lys and Arg

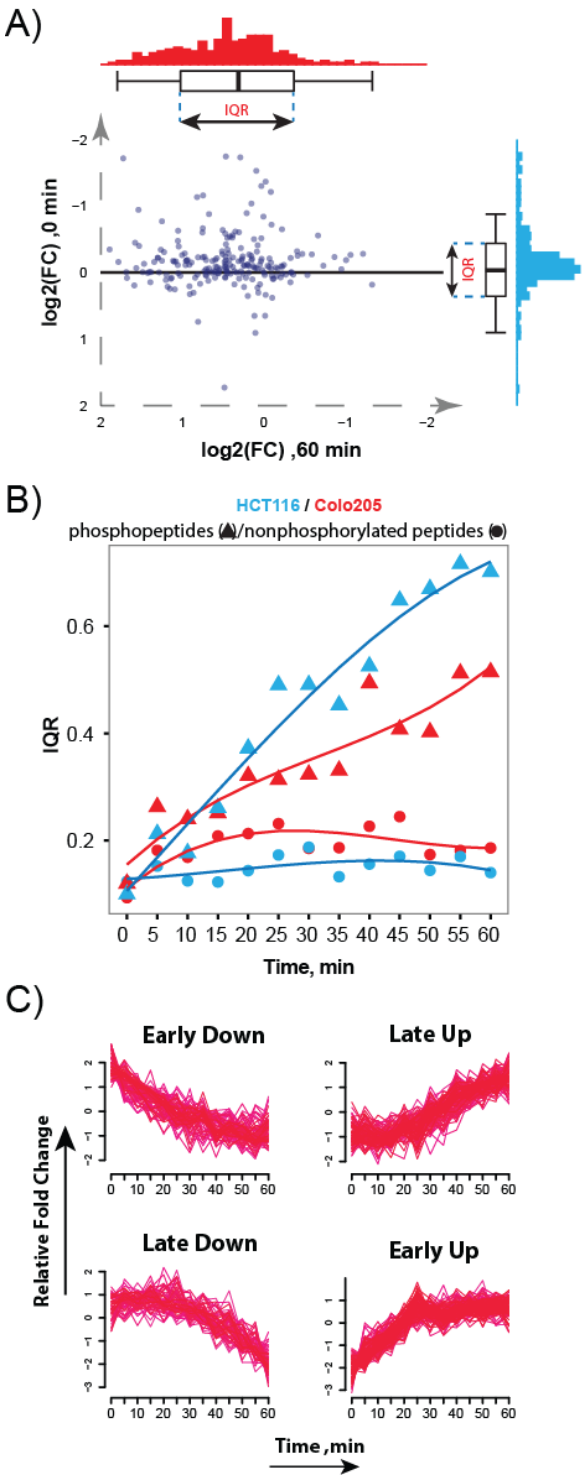

amino acids (see material and methods for additional details). Cells from each time point were harvested, rinsed with PBS, snap frozen in precooled ethanol at -80°C, and then combined in equal amounts. Prior to MS analyses, cell suspensions were washed with PBS to remove ethanol, lysed in urea, and proteins were reduced, alkylated and subsequently digested with trypsin. Phosphopeptides were enriched using TiO_2 microcolumns and fractionated off line into 6 SCX salt fractions prior to LC-MS/MS analysis. Phosphopeptide identification and quantification was performed using MaxQuant and processed in R (http://www.r-project.org/) to cluster phosphopeptide profiles and determine regulated phosphorylation sites.

These analyses enabled the identification of 28,711 and 20,931 phosphopeptides (localization confidence ≥ 75%) for HCT116 and Colo205 cells, respectively. In total, we identified 37,910 unique phosphopeptides, of which 10,300 were quantified across more than 8 time points (Supplementary Figure 3.1). To profile the global changes in the phosphoproteome, we determined the fold change (FC) in phosphopeptide abundance for the first hour after incubation with Vemurafenib (Figure 3.2A).

Figure 3.2. Phosphoproteome-wide effect of RAF inhibitors in HCT116 and Colo205 colon cancer cells.

A) Distribution of FC for dynamic sites of a given time point is represented by the IQR and is used to determine the global changes in phosphorylation upon inhibitor treatment. B) Phosphopeptides exhibited a progressive increase in IQR with time, reflecting the global effects of vemurafenib on the phosphoproteome. Notably, incubation of HCT116 cells with vemurafenib produced more pronounced effects compared with those observed for Colo205 cells. The distribution of FC for non-phosphorylated peptides remained largely unaffected for both cell types. C) 660 phosphopeptides showed time-dependent changes in abundance and clustered into four groups.

To define regulated phosphosites in the dataset, we first selected phosphopeptides quantified in more than 8 time points and performed fitting of all kinetic profiles with a polynomial model. Next, we distinguished dynamic from static phosphosites by calculating a false discovery rate (FDR) based on curve fitting. This was achieved by fitting each profile to a polynomial order ranging from 1 to 8, and comparing the resulting profiles with those obtained from the same data following 5 rounds of randomization (Supplementary Figure 3.2). The coefficient of determination (R^2) was calculated for each profile of a given order, and compared against those from the randomized dataset. For each polynomial order, dynamic profiles were selected based on R^2 values below a FDR of 1%, and prevented over fitting profiles to high polynomial order. Accordingly, these analyses identified 660 dynamic phosphopeptide profiles out of 10,300 profiles for polynomial order ≤ 4 (Supplementary Table S3-1). These dynamic profiles formed four distinct clusters according to the Mfuzz algorithm [35], and were either up-regulated or down-regulated and showed an early or a late response (Figure 3.2C). From the 660 dynamic profiles, we selected only those that have membership values equal or greater than 0.9, which resulted in 220 "high membership" profiles (Supplementary Table S3-2).

Dynamic data show progressive broadening of FC values observed for both cell lines with a gradual shift in the median distribution toward a decrease or an increase in phosphorylation for Colo205 and HCT116, respectively. The width of this distribution was calculated from the interquartile range (IQR) for the $\log_2$(FC) distribution of phosphopeptides at each time point and plotted over the entire cell stimulation period (Figure 3.2B). The resulting curve showed a progressive and linear increase in the phosphopeptides fold-change IQR with time, a trend that was markedly different from non-phosphorylated peptides which remained largely unaffected over the same time period (Figure 3.2B). Also, changes in protein phosphorylation were more pronounced for HCT116 compared to Colo205 as reflected from the variation of IQR with time. Interestingly, we observed a steady increase in IQR values during the first hour although phospho-ERK1/2 activation levels reached a maximum after 20 min post stimulation (Figure 3.1B).

3.4.2 RAS-ERK pathway modulation accounts for most dynamic phosphoproteome changes induced by Vemurafenib

Profiles within the "high-membership" dataset were used to contrast the response of the two cell lines, and to predict kinase activities following Vemurafenib inhibition. The grouping of profiles from both cell types identified five pairs of profiles with distinct patterns (Figure 3.3A).

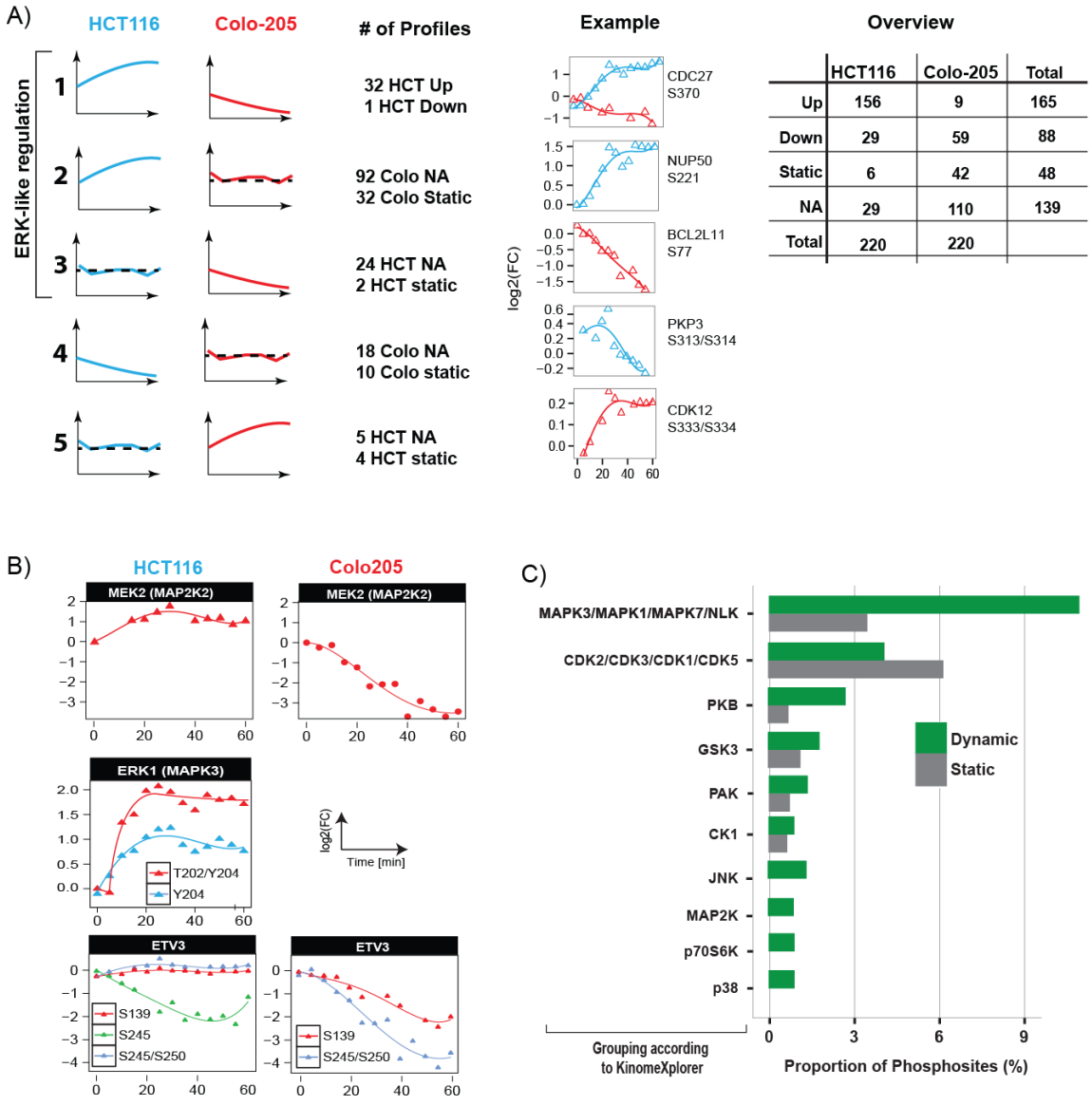

Figure 3.3. Phosphoproteome of HCT116 and Colo205 shows an opposite response to vemurafenib treatment.

A) Pairwise comparison of phosphopeptide profiles for HCT116 and Colo205 cell lines highlighting the most significant trends observed. The majority of observed dynamic phosphorylation events follow ERK-like regulation (groups 1–3). B) Core members of the RAS-ERK pathway (MEK and ERK) as well as downstream effectors (ETV3) show opposite regulation in each cell line. Singly phosphorylated ETV3_S245 decreases in abundance upon ERK activation due to an overall hyperphosphorylation of the doubly phosphorylated form of ETV3_S245/S250. C) Putative kinases associated with dynamic and static phosphosites based on NetworKIN predictions and KinaseXplorer grouping. Substrates for each kinase group are represented by bar graphs.

The first group is represented by opposite temporal changes in the two cell lines, and correspond to 33 down-regulated phosphosites identified in Colo205, and 32 were up-regulated in HCT116 (Figure 3.3A). The second and most populated group comprised 124 phosphopeptides up-regulated in HCT116, and were either not identified (92) or showed a static behavior in Colo205 (32) (Figure 3.3A). The third group corresponds to a more limited number of phosphopeptides that were dephosphorylated in Colo205 but were either not identified (24) or remained static in HCT116 (2) (Figure 3.3A). Groups 4 and 5 are discussed below.

The first three groups shown in Figure 3.3A represent 83% of the "high-membership" sites, and are directly or indirectly associated with RAS-ERK pathway activation (Figure 3.3A; ERK-like profiles). Consistent with this proposal, phosphopeptides comprising MEK2 (MAP2K2) and ERK1 (MAPK3) activation sites were clustered in groups 1 and 2, respectively (Figures 3.3A and 3.3B). A large proportion of dynamic phosphorylation sites thus behaved in accordance to the RAS-ERK pathway response whereby up-regulated phosphopeptides were largely dominated by profiles identified in HCT116 cells (156/165), while down-regulated phosphopeptides were mostly found in Colo205 (59/88). Also, the majority of the 220 dynamic phosphorylation sites of our "high-membership" dataset comprised proline-directed phosphorylation motifs (148/220), a hallmark of ERK-mediated events [6].

However, we noted that several sites of the "high membership" dataset were not fulfilling the ERK consensus motif, and could represent secondary or tertiary events occurring within the highly inter-connected kinase-substrate network downstream of ERK. To predict which kinase-substrate relationships were responsible for dynamic phosphorylation events in our dataset, we used the bioinformatic tool KinomeXplorer [40], a platform based on an improved NetworKIN algorithm that model kinase signaling networks by combining linear motif analysis with protein-protein interactions. The corresponding analysis is shown in Figure 3.3C where kinase groups are clustered according to KinomeXplorer. This analysis confirmed that a substantial enrichment of dynamic phosphorylation sites are predicted to be ERK-mediated (Figure 3.3C). In addition, putative substrates of JNK and p38 comprised a proline-directed consensus motif, and formed a subset of the dynamic sites (Figure 3.3C). This analysis also indicated that our "high-membership" dataset contained putative PKB, GSK3, PAK, CK1 and p70S6K substrates.

Interestingly, two AGC kinases (PKB and p70S6K) share a RXRXXS/T consensus motif with known ERK downstream effectors of the RSK family (p90RSK or RPS6KA)[44]. Concurrently, the RSK paralogs RPS6KA1, 3 and 4 were dynamically modulated on ERK-dependent sites in our dataset (Supplementary Table S3-1), and therefore, several dynamic phosphorylation on RXRXXS/T sites are likely to be secondary events associated with RSK proteins. Supporting this idea, several known RSK-modulated phosphosites (PDCD4_S457, BAD_S75, TBC1D4_S588) were identified in our dataset (Supplementary Tables S3-1 and S3-2) [45-47].

A small subset of 28 sites in HCT116 and 9 sites in Colo205 from our "high-membership" dataset did not correlate with pERK response and could potentially represent off-target events (Figure 3.3A; groups 4 and 5). A closer examination of these data revealed that several sites are located on peptides that contained multiply phosphorylated forms. The modulation of these phosphopeptides with a kinetic profile inconsistent with ERK activation/inhibition status are explained in part by the processivity of phosphotransfer whereby we observed an increase in the abundance of the multiphosphorylated peptides while the singly phosphorylated form decreased in abundance. The overall level of phosphorylation of a given peptide can therefore increase despite the fact that the monophosphorylated form disappeared over time. A case in point is ETV3 whose phosphorylation on S245 rapidly decreased while the doubly phosphorylated form (S245/S250) increased during the same time period in HCT116 (Figure 3.3B). It is noteworthy that 23 phosphopeptides from group 4 are singly-phosphorylated on a proline-directed motif, of which 13 contained a second putative proline-directed phosphorylation site (Supplementary Table S3-3). Altogether, these observations support the notion that most activity associated with Vemurafenib treatment corresponds to on-target effects with a limited number of secondary and tertiary signaling events associated with downstream ERK-modulated substrates. These observations are consistent with a recent phosphoproteomics study comparing RAF and MEK inhibitors activity [26].

3.4.3 Time-resolved phosphoproteome profiling identifies new ERK substrates

Our analysis established that dynamic phosphorylation sites were mostly associated with the regulation of the RAS-ERK pathway. We next wanted to exploit the kinetic information in our dataset in order to identify novel high-affinity downstream substrates of ERK. We posit that the

clustering of phosphopeptides as “Early” or “Late” could reflect ERK-substrate affinities. To perform this analysis, we grouped all high-membership phosphorylation sites from clusters “Early Down” and “Early Up” in both cancer cell lines and searched for ERK1/2 physical interactions with cognate proteins using the STRING databases [48]. This network was complemented with information on known and predicted ERK substrates derived from the BioGRID database [49] and the NetworKIN algorithm [50] respectively. This enabled the identification of 22 uncharacterized interactions between ERK and putative Early substrates (Figure 3.4; red and yellow nodes). The similarity of these putative ERK-mediated kinetic profiles was displayed as the average change in phosphorylation over time (Figure 3.4, top right).

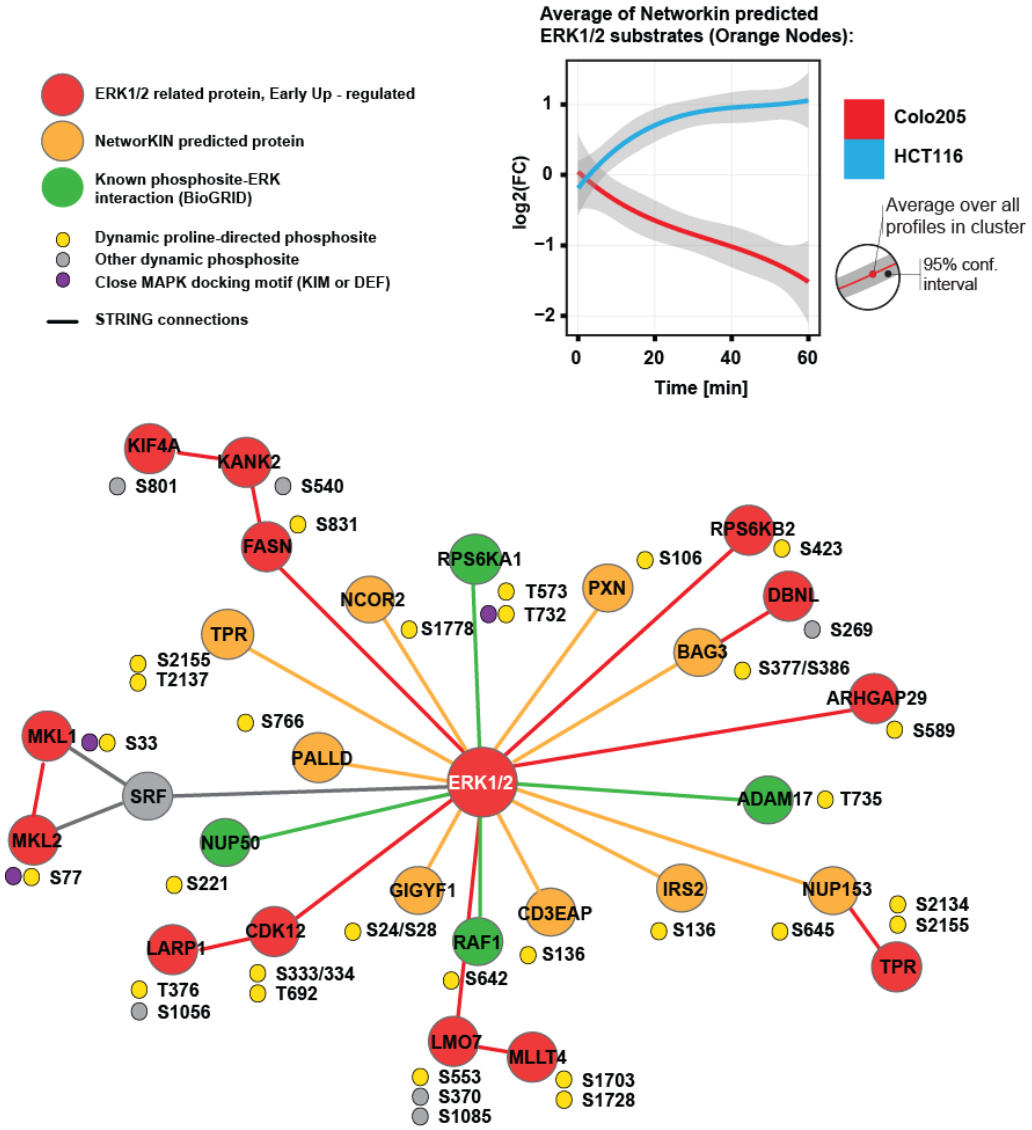

Figure 3.4. ERK substrate network modulated upon vemurafenib treatment (Refer to next page for figure legend).

Legend of ***Figure 3.4:***

STRING was used to obtain high confidence ERK1/2 interactors among proteins with dynamic phosphosites. This was complemented with known ERK1/2-regulated sites reported in BioGRID. Dynamic phosphosites were found in known interacting proteins (red dots, StringDB), in predicted direct interactors (yellow dots, Networkin algorithm), or in validated ERK substrates (green dots, BioGRID interaction database). Nodes represented in this high confidence ERK substrate network display similar dynamic behaviors upon vemurafenib treatment (top right, shaded area across averaged profile represents 95% confidence interval).

We complemented this interaction-based analysis with predictions of docking motifs to determine if ERK selectivity and processivity was also influenced by sequence motifs present in the corresponding substrates. We used ScanProsite [51] to identify KIM- (D-motif; variable consensus) [6] and DEF-motifs (F-X-F-P) [52] within 50 amino-acid distance of the high-membership ERK phosphorylation sites (Figure 3.4; blue dots)(Supplementary Figure 3.3A). We observed an enrichment of KIM- and DEF-motif consensus sequences in our dynamic set compared to static phosphoproteins although only a small subset of sequences (13) comprised these docking sites. Furthermore, six high-membership HCT116 phosphorylation sites that contained a docking motif were grouped in the Early cluster (Supplementary Figure 3.3B). In contrast, KIM or DEF-containing proteins were distributed in both Early and Late clusters in Colo205 cells (Supplementary Figure 3.3B). This result is not entirely unexpected since dephosphorylation of ERK substrates in Colo205 does not solely rely on ERK-substrate affinity but also on phosphatase-substrate interactions. Interestingly, the average kinetic profiles of Early phosphosites with KIM or DEF motifs showed a more rapid change in phosphorylation compared to those that did not contain these motifs (Supplementary Figure 3.3C). Examples of phosphosites for substrates with and without KIM or DEF motifs are shown in Supplementary Figures 3.3 D and 3.3E. It is noteworthy that bioinformatic searches for sequence determinants other than KIM- and DEF-motifs failed to identify relevant linear motifs in our datasets that could play a role in ERK-substrate interactions (data not shown).

3.4.4 Time-resolved phosphoproteome analysis identifies novel biological functions connected with RAS-ERK signaling

To decipher which cellular functions were regulated upon RAS-ERK pathway modulation by Vemurafenib we performed standard Gene Ontology (GO) enrichment analysis of our high-membership and dynamic datasets using DAVID [37, 53]. These analyses indicated the

enrichment of genes associated with "RAS/RTK signaling", "regulation of Rho signal transduction", "kinases/phosphatases" and "actin cytoskeleton organization" (Table 3.1). The dynamic gene set yielded similar GO term enrichment but also included the functional groups related to the regulation of "cell death/apoptosis", "mRNA transport/nuclear pore" and "RNA splicing" (Table 3.1). Although several of these GO terms were previously shown to connect with the RAS-ERK pathway, such as "mRNA transport/nuclear pore" [54], our analysis identified other less usual connections between ERK and "actin cytoskeleton organization" and "regulation of Rho signal transduction". We used GO terms enriched in our dataset (Table 3.1) combined with manual curation of gene lists to derive a systems level view of these novel RAS-ERK pathway connections (Figure 3.5).

Table 3.1. Gene Ontology terms (Biological Function) enriched amongst phosphorylated proteins that show time-dependent modulation after Vemurafenib treatment.

Comparison of the MFuzz "high-membership" dataset (Clustering Membership ≥ 0.9, total of 220 phosphorylation profiles) and "dynamic" dataset (Clustering Membership ≥ 0.0, total of 660 phosphorylation profiles) is shown.

Gene Ontology Term	pValue Mem≥0.9	pValue Mem≥0.0
RTK-Ras signaling	$9.82*10^{-3}$	$6.62*10^{-5}$
Regulation of Rho signal transduction	$9.40*10^{-3}$	$4.28*10^{-7}$
mRNA transport / Nuclear pore	NA	$3.94*10^{-3}$
RNA splicing	NA	$1.00*10^{-3}$
Kinases / phosphatases	$8.29*10^{-3}$	$7.52*10^{-4}$
Actin cytoskeleton organization	$9.29*10^{-3}$	$2.33*10^{-8}$
Regulation of cell death	NA	$7.78*10^{-5}$

These analyses revealed that several phosphosites occurred upstream of RAF and may represent negative feedback loops. Among those, we identified the time-dependent modulation of S642 in CRAF (RAF1) C-terminal tail, a target site of activated ERK involved in desensitizing CRAF to additional stimuli [55]. Upstream factors of canonical RTK-RAS signaling (RTKs ERBB2 and EGFR and the RAS-GEF SOS1) as well as the insulin receptor (InsR) signaling pathway (IRS1/2, GIGYF1/2) were also phosphorylated at proline-directed sites. Similarly, scaffolding proteins of the RAS-ERK cascade (GRB10, PXN and CNKSR1) were dynamically phosphorylated in response to Vemurafenib treatment (Figure 3.5). Interestingly, several of these

putative feedback sites were modulated early after Vemurafenib treatment, suggesting that phosphorylation of these sites is concurrent with the phosphorylation of downstream ERK effectors.

Our data also identified the modulation of *bona fide* signaling effectors of the RAS-ERK pathway such as RSK (RPS6KA1, 3 and 4) and p70-S6K (PRS6KB2) (Figure 3.5). Consistent with earlier reports [56], our phosphoproteomics study identified the phosphorylation by ERK of RPS6KA1 (S363, S732 and T573) and RPS6KB2 (S423) (Figure 3.5).

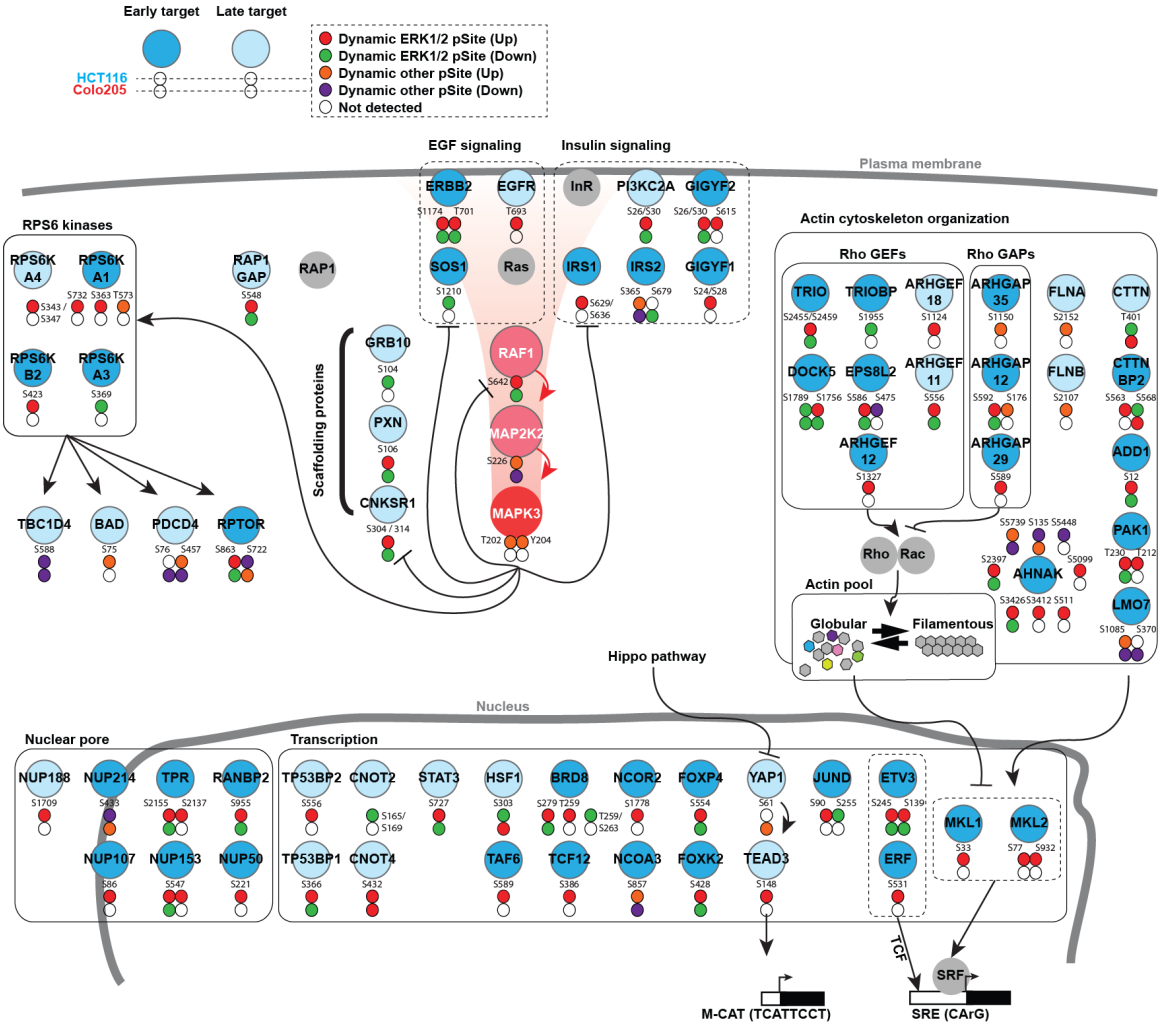

Figure 3.5. Depiction of RAS-ERK signaling pathway and primary and secondary connections to substrates identified by time-resolved phosphoproteome profiling. Primary and secondary targets dynamically modulated upon vemurafenib treatment.

Main functional groups depicted are "RPS6 kinases," "RTK signaling," actin cytoskeleton organization, nuclear pore, and "transcription". Key players of actin cytoskeleton regulation, including Rho GEF's and GAP's, are emphasized. The Hippo pathway target, YAP1, acts together with TEAD factors (here TEAD3) to control transcription at promoters containing M-CAT elements. TCF and MKL1/2 assemble with SRF on promoters comprising serum response elements (SREs). The MKL1/2 regulators LMO7 and FLNA/B included putative RSK (RPS6A) phosphosites that were dynamically modulated after vemurafenib treatment.

We also noted that Vemurafenib affected potential crosstalks with other signaling pathways. For example, several adaptor proteins of cAMP-dependent protein kinase (PKA) (AKAP1, 2, 11, 12 and 13) were dynamically phosphorylated on ERK target sites (Supplementary Figure 3.5) [57]. Another possible crosstalk identified by our analysis involved GO terms “Rho signaling” and “actin cytoskeleton organization”, which were amongst the main regulons modulated in response to Vemurafenib treatment. Several Rho GAPs (ARHGAP35, 12 and 29) and Rho GEFs (ARHGEF11, 12, 13 18, TRIO, TRIOBP, DOCK5 and EPS8L2) were dynamically modulated on ERK motifs (Figures 3.5A and B). We noted that the previously reported ERK target site T212 was concomitantly modulated in the Rho/Rac/CDC42 downstream effector PAK1 [58]. Several proteins involved in actin polymerization were also dynamically phosphorylated after Vemurafenib treatment (e.g. CTTN, CTTNBP2, FLNA and FLNB).

The phosphorylation of nuclear pore complex (NPC) subunits by ERK was reported in an earlier phosphoproteomic study [54]. Here, we identified the dynamic phosphorylation of NUP50, NUP107, NUP153, NUP188 and TPR and RANBP2 (Figures 3.5-3.6 and Supplementary Table S3-1). These proteins participate in several sub-structures of the nuclear pore and have distinct functions during translocation of biomolecules across the pore. ERK-dependent phosphorylation of NPC proteins was shown to affect the individual properties of the subunits. For instance, NUP50 phosphorylation on ERK sites located within FG repeats regulates its interaction with importin-beta and transportin [54]. Similarly, mutation of ERK sites in TPR resulted in cell cycle defects associated with the failure to recruit MAD1/2 to the NPC [59].

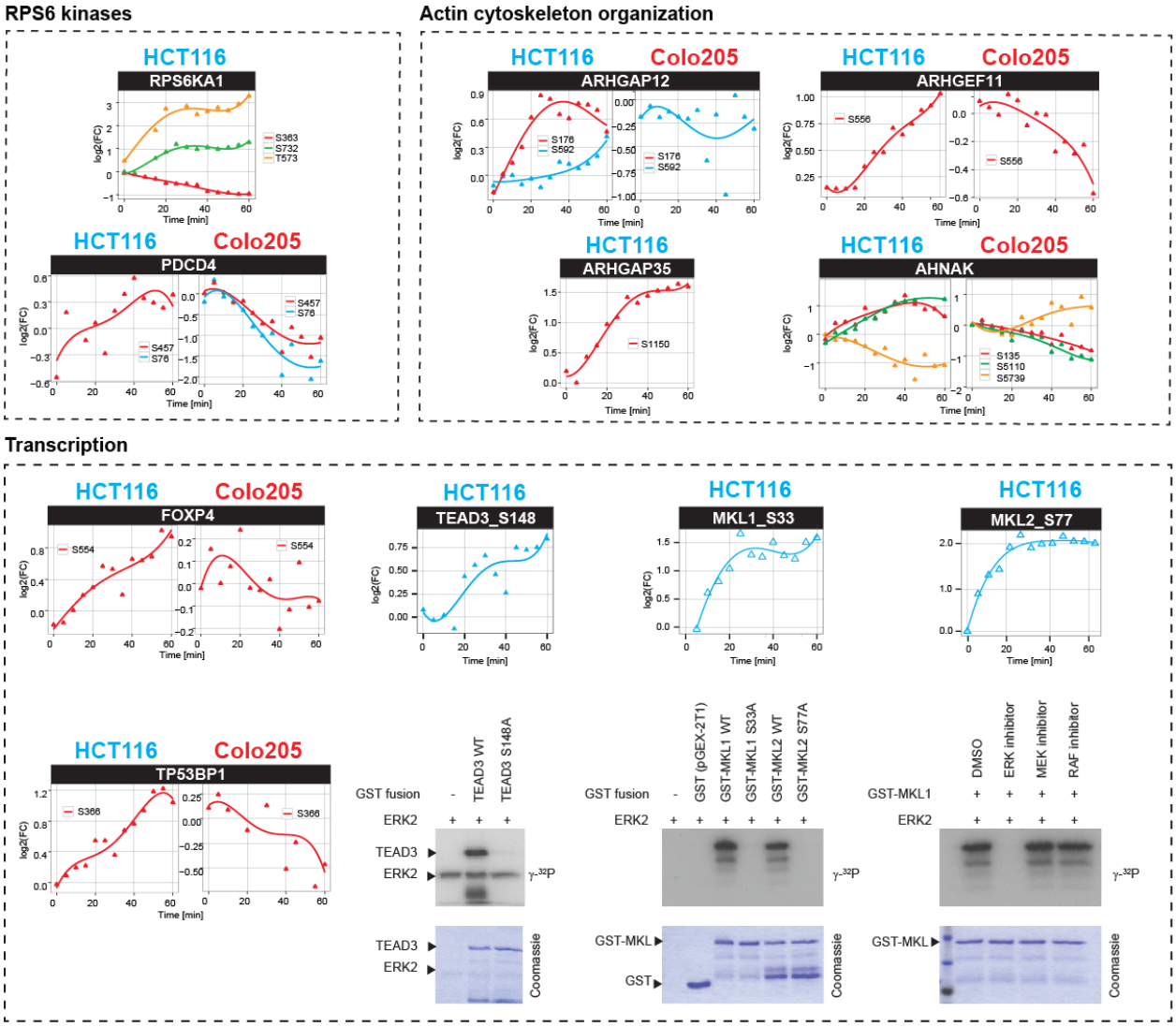

Figure 3.6. Kinetic profiles of selected phosphosites upon incubation with 3.3 µm vemurafenib and in vitro kinase assays.

Kinetic profiles are shown for selected phosphosites from RPS6 kinases, protein substrates from actin cytoskeleton organization, and transcription. In vitro kinase assays with radiolabeled ATP to confirm the direct phosphorylation of TEAD3_S148, MKL1_S33, and MKL2_S77 by recombinant active ERK2 (bottom right) are shown. In vitro phosphorylation of MKL1 using recombinant active ERK2 in the presence of ERK, MEK, or RAF inhibitors confirmed the site-specific phosphorylation of MKL1 by ERK (bottom right).

ERK activation is necessary for its migration into the nucleus where it phosphorylates specific regulatory proteins and transcription factors (TFs) to initiate transcription of immediate-early genes [60-62]. Accordingly, quantitative phosphoproteomics identified several known TFs phosphorylated by ERK such as ETV3_S245/S250, ERF_S531, JUND_S90/S255 and STAT3_S727 [63, 64] as well as putative substrates such as FOXP4_S554, TP53BP1_S366 and TEAD3_S148 (Figures 3.5-3.6). TEAD3 participates in the Hippo tumor-suppressor pathway,

which controls organ size and cell death. This pathway culminates in the phosphorylation and inactivation of the transcriptional co-activator YAP1, which itself relies on DNA-binding adaptors of the TEAD family to mediate a complex transcriptional response [65]. YAP1_S61 is a *bona fide* substrate of the Hippo pathway kinase LATS1 [66], and was found upregulated only in Colo205 cells. In contrast, TEAD3_S148, a proline-directed site, showed an increase in phosphorylation upon vemurafenib treatment only in HCT116 cells. Mammalian TEAD proteins (TEAD1-4) share a common domain architecture consisting of a TEA DNA-binding domain and a YAP1-interacting region [67]. TEAD3_S148 is located in the linker region between these two conserved portions of the protein. In order to assess direct phosphorylation of this site by ERK, we performed *in vitro* kinase assays. While WT TEAD3 was phosphorylated in the presence of active ERK2, ^{32}P incorporation was completely abrogated with TEAD3 S148A variant (Figure 3.6). This establishes a direct connection between RAS-ERK signaling and the Hippo pathway transcription factor TEAD3.

Among the transcription factors dynamically modulated upon Vemurafenib treatment, our attention was also attracted by the presence of megakaryoblastic leukemia 1 (MKL1) and 2 (MKL2). These were phosphorylated on S33 and S77 respectively; two orthologous phosphosites that comprise an upstream KIM-motif and that were not previously characterized (Figure 3.4 and Figure 3.5). Although these sites were not identified as ERK substrates based on STRING interactions, a previous report suggested the direct phosphorylation of MKL1_S454 by ERK as part of a negative feedback mechanism [68]. Interestingly, our phosphoproteomic analyses revealed the rapid phosphorylation of MKL1_S33 and MKL2_S77 upon Vemurafenib treatment while MKL1_S454 remained unchanged (Figure 3.6 and Supplementary Figure 3.4). Further experimental validation was obtained using *in vitro* kinase assays. GST-MKL fusion substrates were incubated with active ERK in the presence of radiolabeled ATP. *In vitro* reactions confirmed that active ERK specifically phosphorylated MKL1_S33 and MKL2_S77 since ^{32}P incorporation was abrogated in S33A and S77A mutant proteins (Figure 3.6).

3.4.5 MKL1 S33 defines a novel actin-dependent mechanism that modulates kinase-substrate interactions

Megakaryoblastic leukemia transcription factors MKL1/2 were grouped under the GO function "actin cytoskeleton organization", a term being highly enriched in our dataset. These proteins act as actin-dependent transcriptional coactivators of the serum-response factor (SRF), a known transcriptional regulatory hub acting downstream of the RAS-ERK pathway [69]. In resting cells, MKL1 transit between the nucleus and the cytosol, and its localization was reported to depend on the availability and binding of globular actin (G-actin) to RPEL motifs. In serum-starved conditions, MKL1 is bound to G-Actin and sequestered in the cytoplasm but is rapidly translocated to the nucleus in conditions that favor the polymerization of actin and the formation of stress fibers [70-73]. Structural analyses of MKL1-Actin interaction revealed that RPEL motifs and the two intervening spacers can each bind a G-actin monomer, forming a compact assembly of five G-actins with one MKL1 RPEL repeat [74-76] (Figure 3.7A).

Close inspection of MKL1 crystal structures revealed that KIM residues overlap with the G-actin binding site found in RPEL1 (Figures 3.7A and 3.7B, green)[71, 73]. Furthermore, MKL1 S33 is tightly packed against the second G-actin molecule that interacts with the linker connecting RPEL1 and RPEL2 (Figure 3.7A, yellow).

Based on these observations, we posit that the binding of G-actin to RPEL1 domain of MKL1 (Green) might control the access of ERK to the conserved KIM motif, thereby affecting the phosphorylation of MKL1 S33 (Figure 3.7C). Also, MKL1 S33 must be released from the second G-actin subunit (yellow) to facilitate its phosphorylation by ERK. To validate this proposal, we performed *in vitro* kinase assays on recombinant MKL1 harboring KIM-motif mutants R5A/R6A and L9A/L11A or RPEL1 mutant R16A/R17A (Figure 3.7D). These analyses confirmed that MKL1 phosphorylation by ERK was abrogated for the R5A/R6A and L9A/L11A MKL1 mutants, suggesting that the KIM motif is necessary for docking onto ERK to facilitate MKL1 S33 phosphorylation. In contrast, the R16A/R17A double mutant known to affect MKL1 binding to G-actin [74], did not affect ERK-dependent phosphorylation of S33 (Figure 3.7D).

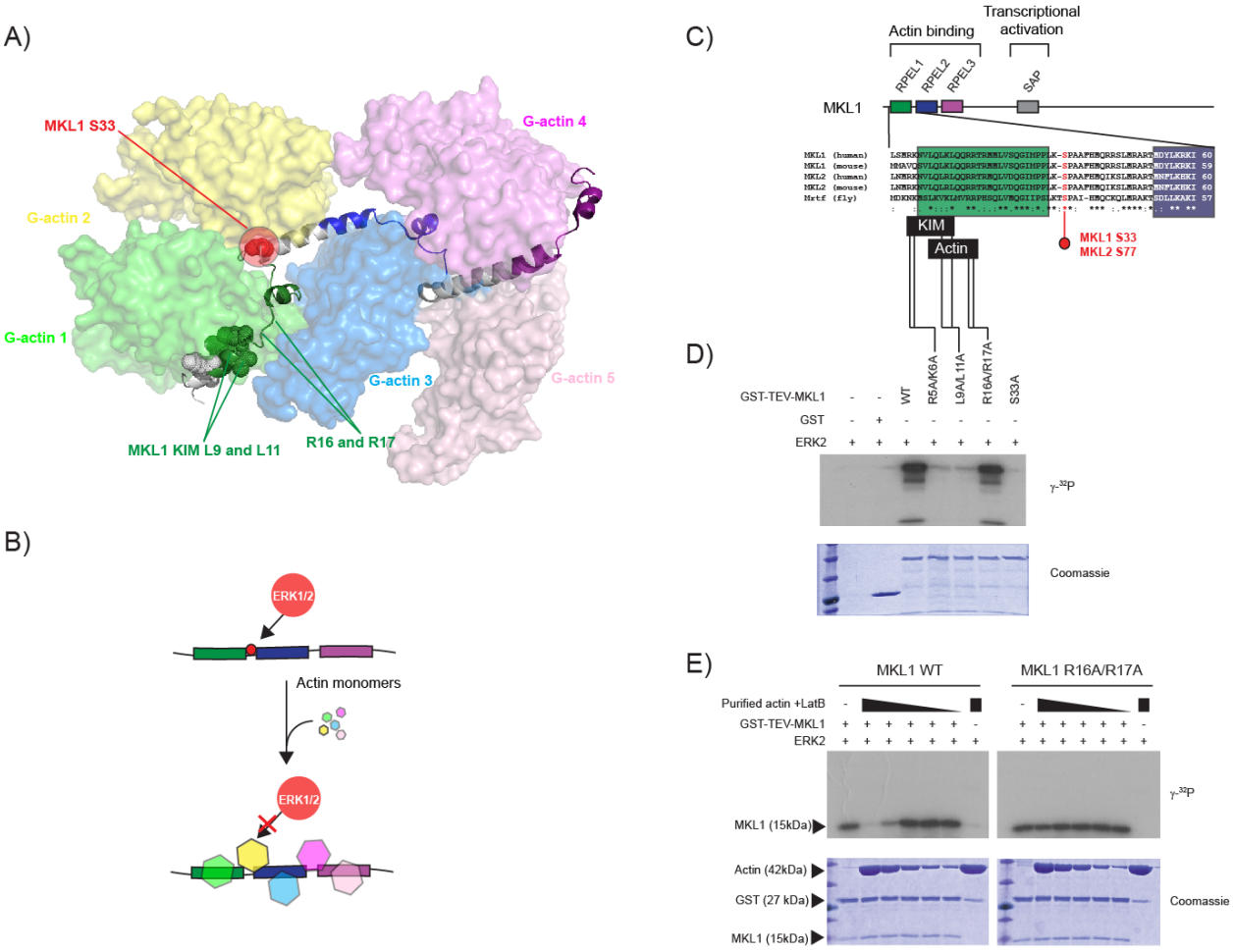

Figure 3.7. Phosphorylation of MKL1 is modulated by globular actin binding.

A) Structural representation of MKL1 (ribbon) with actin (surface) showing occlusion of MKL1 KIM motif and Ser-33 residue by G-actin. Protein Data Bank accession 3TPQ was used for structure rendering (76). B) Schematic representation of a model whereby actin binding to MKL1 prevents phosphorylation of MKL1 Ser-33 by ERK1/2. C) Sequence alignment of MKL1 showing the conservation of KIM motif and Ser-33 across species. Residue Ser-33 is located between the first two RPEL repeats required for monomeric actin binding. The putative kinase-interaction motif (KIM) for ERK as well as the actin-binding region of the first RPEL motif are also highlighted. D) In vitro kinase assays of wild type and alanine mutant GST-TEV-MKL1 with recombinant active ERK2. Mutation of residues Arg-5 and Lys-6 or Leu-9 and Leu-11 within the KIM motif is sufficient to prevent phosphorylation of Ser-33 by ERK2. E) In vitro phosphorylation assay of wild type and alanine mutant MKL1 in presence of recombinant active ERK2 and variable amounts of actin. Phosphorylation of MKL1_S33 by ERK2 is impeded at elevated actin concentrations (8:1 and 16:1 molar ratios), whereas the phosphorylation of R16A/R17A mutant MKL1 is resistant to actin titration.

To determine whether G-actin binding to MKL1 could affect its phosphorylation by ERK, we pre-incubated WT MKL1 overnight with various concentrations of G-actin, and performed *in vitro* ERK kinase assays (Figure 3.7E). These experiments revealed that phosphorylation of MKL1 was only observed at low G-actin concentration, suggesting that excess actin shielded MKL1 S33 and prevented its phosphorylation by ERK (Figure 3.7E, left panel). To rule out a

possible non-specific interaction due to protein crowding in the kinase assay, we conducted the same *in vitro* kinase assay using the MKL1 R16A/R17A double mutant (Figure 3.7E, right panel). In contrast to WT MKL1, the R16A/R17A double mutant was fully phosphorylated irrespective of G-actin concentration. These experiments support the notion that actin binding to MKL1 prevents S33 phosphorylation by ERK, and suggest an interplay between actin dynamics and MKL phosphorylation. In the course of preparing this manuscript, consistent findings were published by the group of Richard Treisman who validated S33 phosphorylation by ERK as well as the importance of the upstream KIM motif and the role of globular actin binding in blocking phosphorylation at this site [77]. However, we note that residue numbering differed between this publication (S98) and ours (S33) since different mRNA isoforms were used as references (S33 numbering corresponds to MKL1 isoform X1 (XP_016884377)).

3.5 Discussion

Mass spectrometry combined with metabolic labeling (e.g. SILAC) enabled the quantification of phosphoproteins on a systems-wide scale. The temporal profiling of protein phosphorylation facilitated the identification of RAS-ERK pathway substrates and secondary events in two colon cancer cell lines that respond differently to the RAF inhibitor Vemurafenib. By taking advantage of the opposite response to RAF inhibitors, our experimental strategy provided a quantitative view of ERK signaling dynamics without the pleiotropic effects of growth factors, serum or phorbol esters that can give rise to pathway crosstalks. Our quantitative phosphoproteomic analyses revealed that Vemurafenib has low off-target activity on kinases other than RAF or on phosphatases. This observation is consistent with a recent study comparing the proteome-wide effects of BRAF and MEK inhibitors when used alone or in combination [26].

The use of targeted RAF stimulation in combination with time resolved phosphoproteomics facilitated the deconvolution of early and late phosphorylation events, and associated downstream and upstream targets of ERK. Our analysis suggests that predicted direct ERK substrates (i.e. containing a proline-directed site) are in general rapidly phosphorylated upon RAF induction, as evidenced by the early phosphorylation of p90RSK proteins RPS6KA1 and RPS6KA3. A rapid induction was also observed for other well-known substrates such as nuclear pore complex subunits and transcription factors (e.g. ETV3, JUND, ERF). Rapid kinetics was

also observed for uncharacterized ERK downstream targets like several Rho GEFs and Rho GAPs. Nonetheless, *bona fide* ERK target sites were also associated with late events (e.g. STAT3, NUP188 and RPS6KA4). Therefore, substrate phosphorylation kinetics alone cannot distinguish direct from indirect ERK targets. Kinetic differences might however be explained by distinctive molecular features such as linear motifs (DEF- and KIM-motifs), three-dimensional structure elements, quaternary complexes formation and cellular co-localization that could account for changes in kinase–substrate affinities.

In addition to ERK targets, our study provided insights into the dynamic changes in phosphorylation of secondary events such as the phosphorylation of several RSK substrates. Interestingly, several known (TBC1D4, BAD, PDCD4) and predicted (FLNA and FLNB) RSK target sites, were identified as late events in our dynamic phosphoproteomic dataset (Supplementary Table S3-1 and S3-2). This observation is consistent with the view that RSK-dependent signaling events are subsequent to and thus downstream of ERK signaling. Although this will require more data, and analysis, it is likely that time-resolved phopshoproteomics will allow epistatic analysis of cell signaling networks.

Dynamic phosphoproteomics identified several known (e.g. STAT3, ETV3, ERF, JUND) and putative ERK substrates (e.g. TEAD3, TAF6, TCF12, FOXK2, FOXP4) involved in transcriptional regulation. In particular, we demonstrated for the first time that the transcription factor TEAD3 is directly phosphorylated by ERK at S148 in the linker region between TEA DNA-binding domain and YAP1-interacting region [67]. Our results are thus consistent with the presence of crosstalk between the RAS-ERK and the Hippo pathway that would implicate TEAD transcription factors. The phosphorylation of TEAD3 at S148 could modulate its interaction to DNA and/or to YAP1 either alone or through the recruitment of other binding partners. YAP1 is a downstream regulatory target in the Hippo signaling pathway and its binding to TEAD transcription factors is required to stimulate the expression of genes involved in tissue homeostasis [78]. Interestingly, a recent genetic screen in BRAF-mutant tumor cells identified YAP1 as a survival input mediating RAF and MEK inhibitors resistance in melanoma [79]. This, together with other evidence [80, 81] suggests a crosstalk between the Hippo and RAS-ERK pathways. The role of TEAD3 phosphorylation on S148 in this crosstalk would deserve to be investigated.

Our study also identified the RPEL motif of megakaryoblastic leukemia (MKL) transcription factors as putative ERK substrates. Using *in vitro* kinase assays we demonstrated that ERK directly phosphorylates MKL1_S33 and MKL2_S77 in the linker region between RPEL1 and RPEL2 domains. The phosphorylation of this orthologous site in both proteins relies on a canonical ERK KIM-motif that was only recently identified [77]. Our analysis showed that this motif facilitates the binding of ERK to MKL1 and enhance its phosphorylation. We also confirmed that accessibility to this KIM motif and to S33 is modulated by G-actin binding to the MKL1 RPEL repeats, consistent with results described in Panayitou et al. [77]. On the basis of these results, we proposed a novel mode of kinase-substrate regulation whereby G-actin binding can mask the docking and phosphorylation of MKL1/2 by ERK. Alternatively, unbound MKL1/2 can be more readily phosphorylated by ERK when actin dynamics is shifted to the formation of filaments. It will be interesting to determine if actin-dependent regulation of phosphosites applies more widely to other kinase-substrate pairs. Conversely, it was shown by gel filtration that S33 phosphorylation has an impact on the stoichiometry of actin binding by MKL1 RPEL motifs (S98 in Panayotou et al. 2016). Indeed, the WT protein binds to three molecules of actin while the phosphomimetic mutant binds to two actin molecules [77]. This result implicated ERK-dependent phosphorylation in the regulation of MKL1 nucleocytoplasmic shuttling by globular actin, whereby a reduction in actin binding upon S33 phosphorylation promotes nuclear import [77].

Interestingly, our analysis identified several Rho regulators presumably phosphorylated by ERK upon Vemurafenib treatment (ARHGAPs and ARHGEFs). It is unclear if these phosphorylation events in ARHGAPs and ARHGEFs affect their activity and downstream Rho activation status. Nevertheless, it is possible that these factors indirectly impinge on MKL1/2 activity by modulating the balance between globular and filamentous actin. Our analysis additionally identified LMO7 and FLNA as potential RSK substrates. These are two recently reported regulators of MKL1, further reinforcing the role of ERK in MKL1/2-dependent transcriptional control. LMO7 was shown to relieve actin-mediated repression of MKL while a recent study indicated that FLNA directly interacts with MKL1 [82, 83].

It is noteworthy that unlike another study conducted by Muehlich *et al.* [68], our data do not provide evidence for feedback phosphorylation sites T450 and S454 on MKL1/2 upon specific RAF-MEK-ERK activation. This might be explained either by the different stimulation periods

(e.g. 0-60 minutes of Vemurafenib treatment *vs.* up to 3 h by Muehlich *et al.*) or by the different stimulus used to trigger activation of the pathway. For instance, serum stimulation used by Muehlich *et al.* triggers a pleiotropic response that includes RAS and Rho activation while Vemurafenib acts specifically downstream of RAS to selectively turn on the RAF-MEK-ERK signaling pathway. Alternatively, feedback phosphorylation of MKL1 may require elevated ERK activation, which might not be achieved when paradoxical activation of the pathway is induced by Vemurafenib.

The novel link we and Panayiotou et al. (2016) established between ERK signaling and MKL1//2 regulation suggest that at least two ERK outputs converge on cofactors of serum-response factor (SRF) (Figure 3.5). The first one targets ETS-family proteins (e.g. ETV3 and ERF, identified in this study), together known as ternary complex factors (TCFs) that associate with SRF-bound promoters and are well-known ERK substrates [84]. The second one consists of MKL1/2 transcriptional co-activators. We thus suggest that TCFs might act in conjunction with an MKL1/2 axis downstream of ERK to modulate the transcription of SRF-bound elements (SREs; CArG) in promoters (Figure 3.5). This possible crosstalk between RAS-ERK and Rho-actin-MKL-SRF signaling is interesting on at least two accounts. Firstly, RAF mutations (BRAF or CRAF) are found in Noonan syndrome (NS) and cardio-facio-cutaneous syndrome (CFC) that belong to a group of syndromes called RASopathies but also in childhood-onset dilated cardiomyopathy. The clinical presentation of patients afflicted with these syndromes includes cardiac defects often associated with heart hypertrophy, which is also recapitulated in mouse models of NS [85, 86]. Myocardin family transcription factors including Myocardin itself (MYOCD), MKL1 and MKL2 are known to regulate a SRF-dependent transcriptional program involved in heart development [87-91]. It is thus possible that this RAS-ERK-MKL1/2 signaling axis contributes to some of the clinical manifestations observed in RASopathies. Secondly, several lines of evidence tie Rho signaling [92], MKL1 and SRF-dependent transcription with epithelial-mesenchymal transition (EMT) and metastasis [93]. The Rho-MKL1-SRF axis may therefore crosstalk with RAS-ERK signaling to modulate cancer cells invasiveness.

We anticipate that the global profiling of phosphorylation dynamics in response to cell stimuli will provide the foundation for the deconvolution of the cellular phosphoregulatory network. Phosphokinetic experiments such as those described here will also provide an important resource

to further rationalize direct/indirect interactions and off-target effects between substrates and their putative kinases.

3.6 Acknowledgements

The authors acknowledge support from NSERC grant 311598, CIHR grant MOP-119443. PT and MT hold Canada Research Chairs in Proteomics and Bioanalytical Spectrometry, and Intracellular Signaling, respectively. The Institute for Research in Immunology and Cancer (IRIC) receives infrastructure support from the Canadian Center of Excellence in Commercialization and Research, the Canadian Foundation for Innovation, and the Fonds de recherche du Québec - Santé (FRQS). Proteomics analyses were performed at the Center for Advanced Proteomic Analyses (CAPA), a Node of the Canadian Genomic Innovation Network supported by the Canadian Government through Genome Canada.

3.7 Supplementary material

3.7.1 Supplementary figures

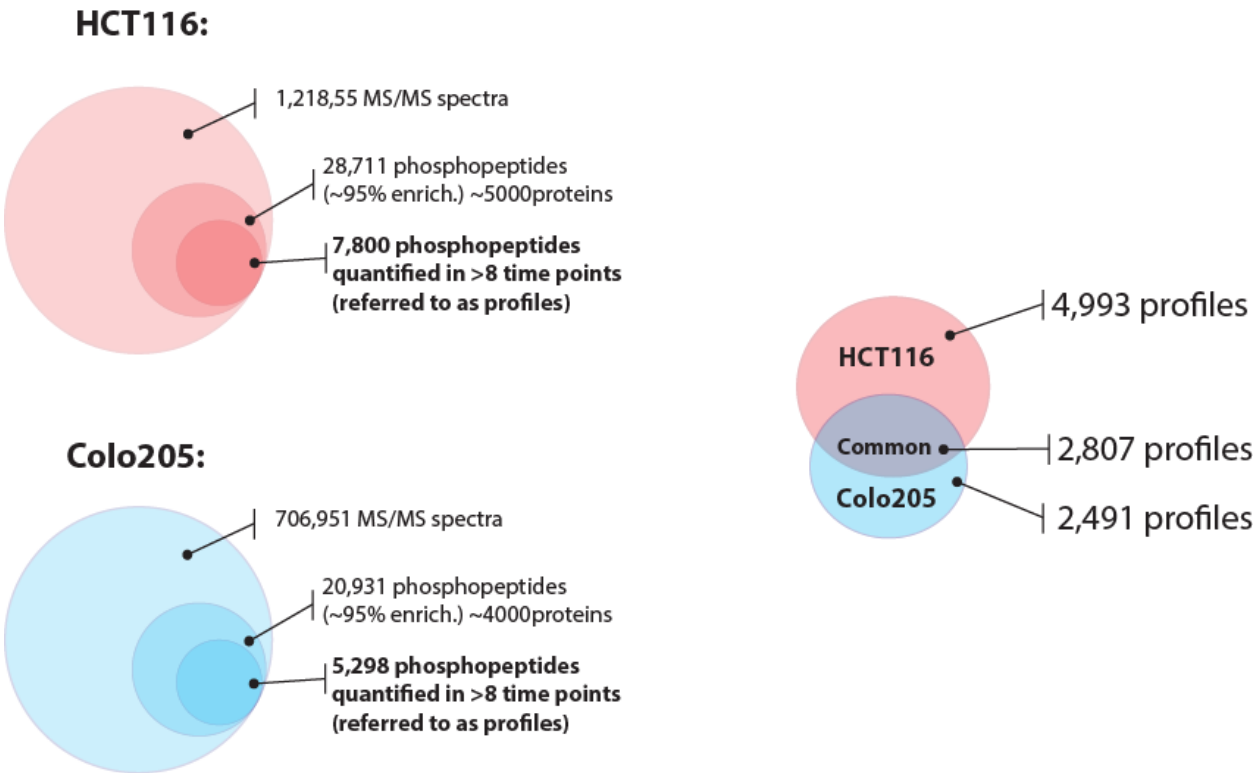

Supplementary Figure 3.1. Summary of phosphopeptide identification.

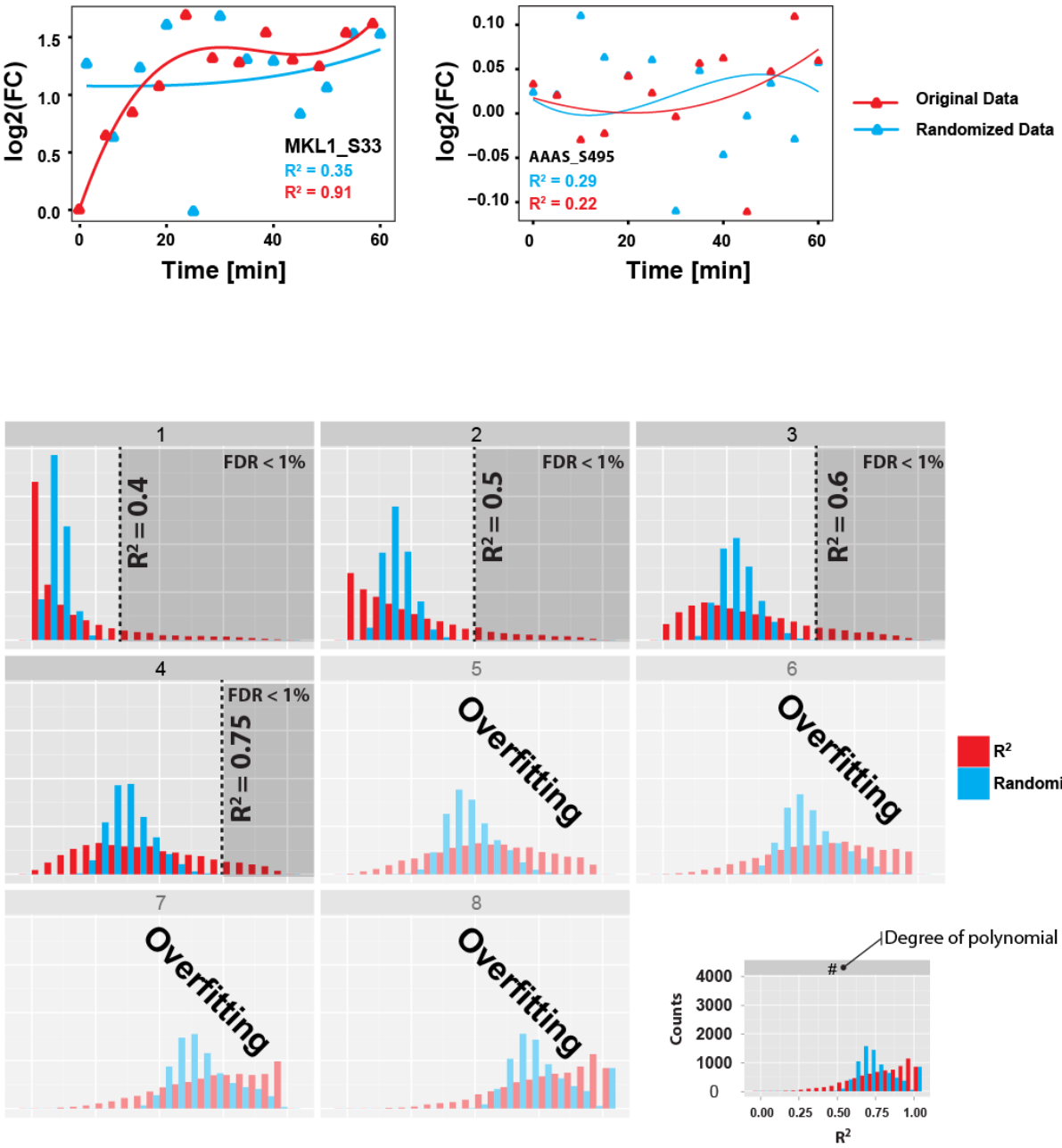

Supplementary Figure 3.2. Selection of dynamic phosphopeptide profiles using polynomial fitting.

Each profile was randomized 5 times and fitted with a polynomial of order 1-8. Original data were concomitantly fitted and the distribution for each polynomial (randomized vs. original data) was used to determine an FDR threshold. FDR of 1% was chosen at which a threshold of different R2 values for different polynoms are obtained. Finally, data were filtered by requiring that a given profile is fitted better than the R2 value of the threshold for each polynomial (order 1-5).

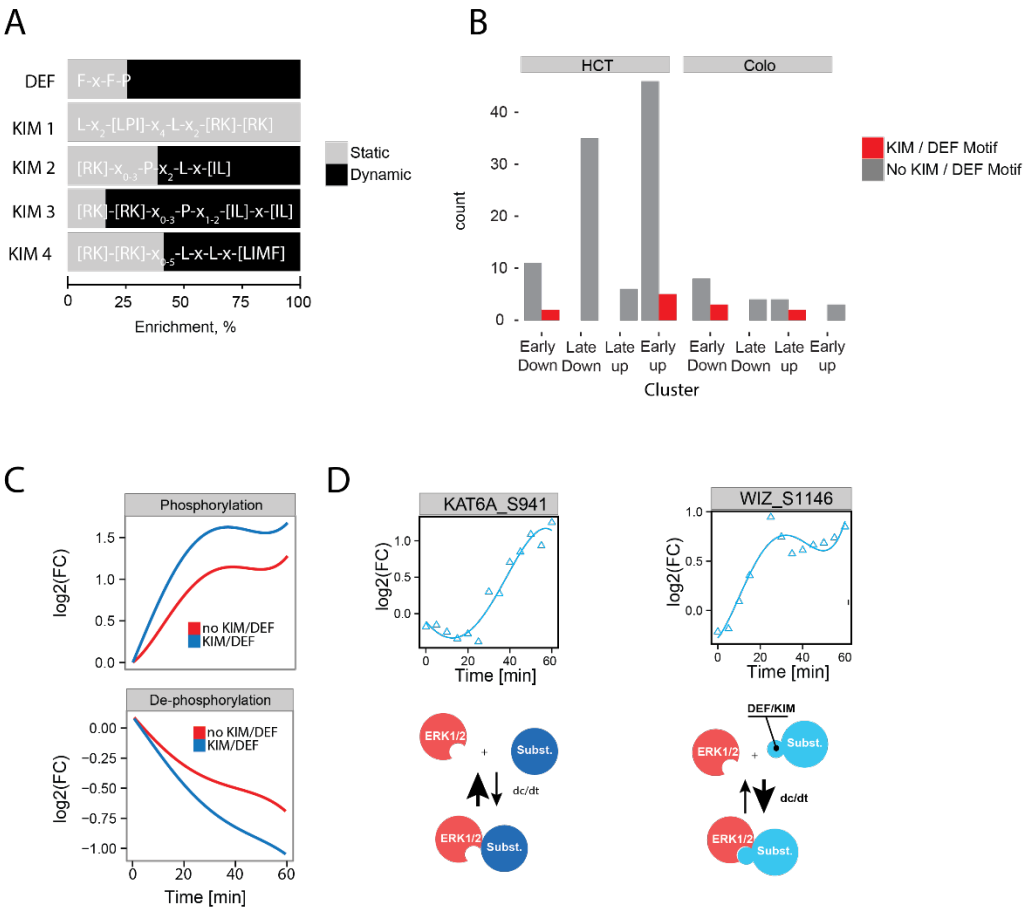

E

Gene_pSites	Cluster HCT116	Cluster Colo205	Motif	Distance	N-terminal
DOCK5_S1756	NA	Late Down	KaqrPksLqL	13	1
ETV3_S245	Early Down	NA	KRk..Pd.ImL	17	1
ETV3_S245/S250	NA	Early Down	KRk..Pd.ImL	17	0
AKAP1_S151	NA	Late Down	RRddstkLeLaL	21	0
ITPKB_S43/S49	NA	Early Down	FIFP	14	1
DOCK5_S1789	Early Down	NA	KaqrPksLqL	20	1
MKL1_S33	Early Up	NA	RRegstvLqLkL	25	0
MKL2_S77	Early Up	NA	RRegstvLqLkL	25	0
WIZ_S983	Early Up	NA	R...PgILsL	33	0
AHNAK_S3412	Early Up	NA	KK...Pd.Idl	35	1
AHNAK_S3426	Early Up	Early Down	KK...Pd.Idl	49	1
PLEKHM1_S432/S435	NA	Late Down	RpqaPspLdL	50	1
J3QS11_S87/S95	Early Up	NA	KR...PmsIpl	33	0

Supplementary Figure 3.3. Detection of ERK substrates that contain KIM and DEF docking sites.

A) Relative enrichment of KIM and DEF motifs among static and dynamic phosphosites. B) Distribution of KIM and DEF motifs across all four dynamic cluster groups. C) Averaged kinetic profiles of "early" phosphosites with and without KIM/DEF motifs. Profiles are separated according to up or down regulation. Phosphorylation on phosphosites in close proximity to KIM/DEF motifs generally responds quicker. D) Examples of phosphosites for substrates with and without KIM or DEF motifs. Substrates harboring KIM or DEF motifs tend to be phosphorylated more rapidly. E) List of all phosphosites with KIM/DEF motifs.

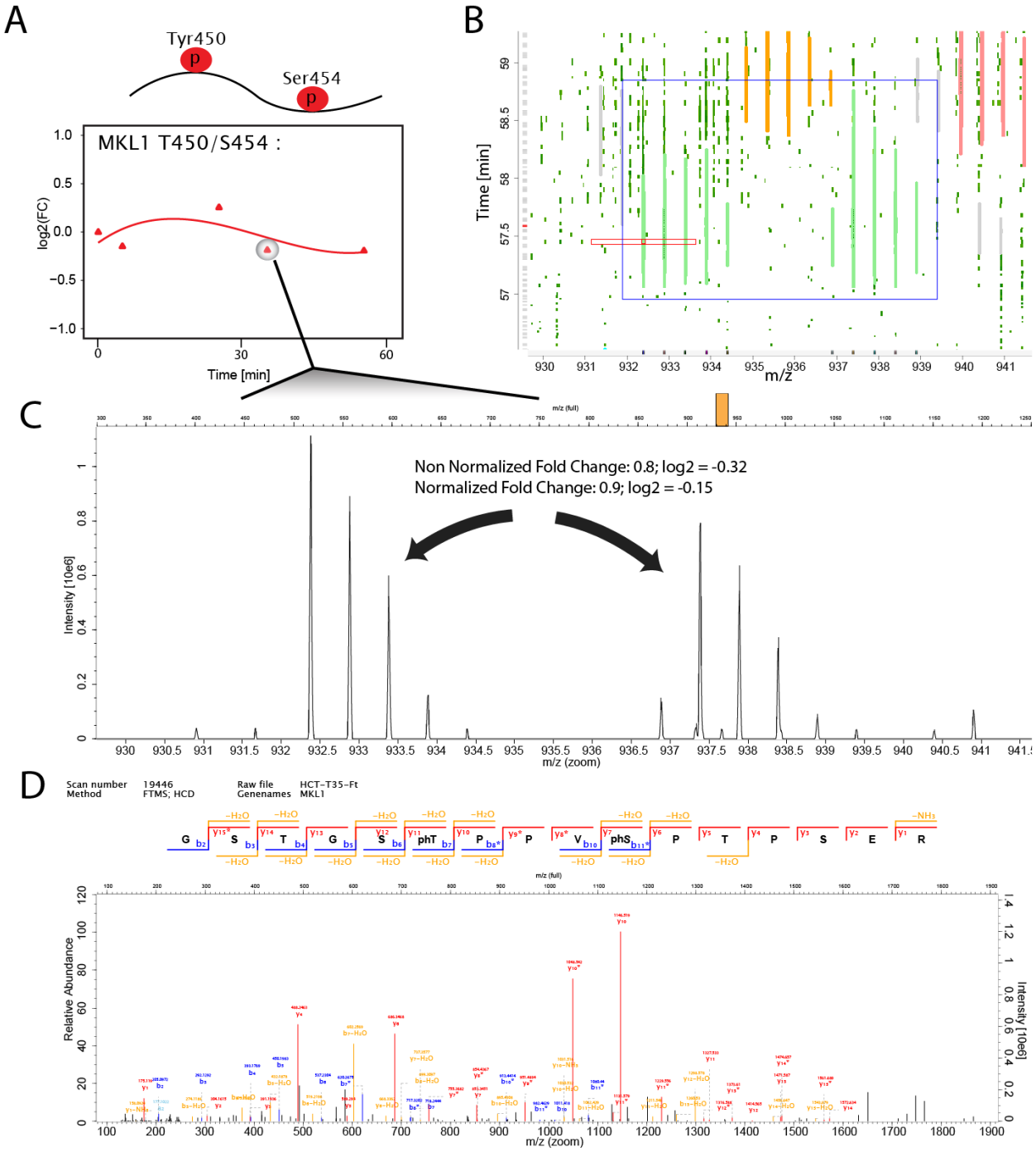

Supplementary Figure 3.4. MS verification showing that MKL1_T450/S454 phosphorylation is not changing over time.

A) Observed profile of MKL1_T450/S454 phosphorylation in HCT116. B) MaxQuant viewer showing the SILAC pair of the MKL1_T450/S454 peptide in the LC-chromatogram. C) Full MS spectra of the MKL1_T450/S454 SILAC pair close to the top of the elution peak. D) MS/MS verification of the MKL1_T450/S454 phosphopeptide.

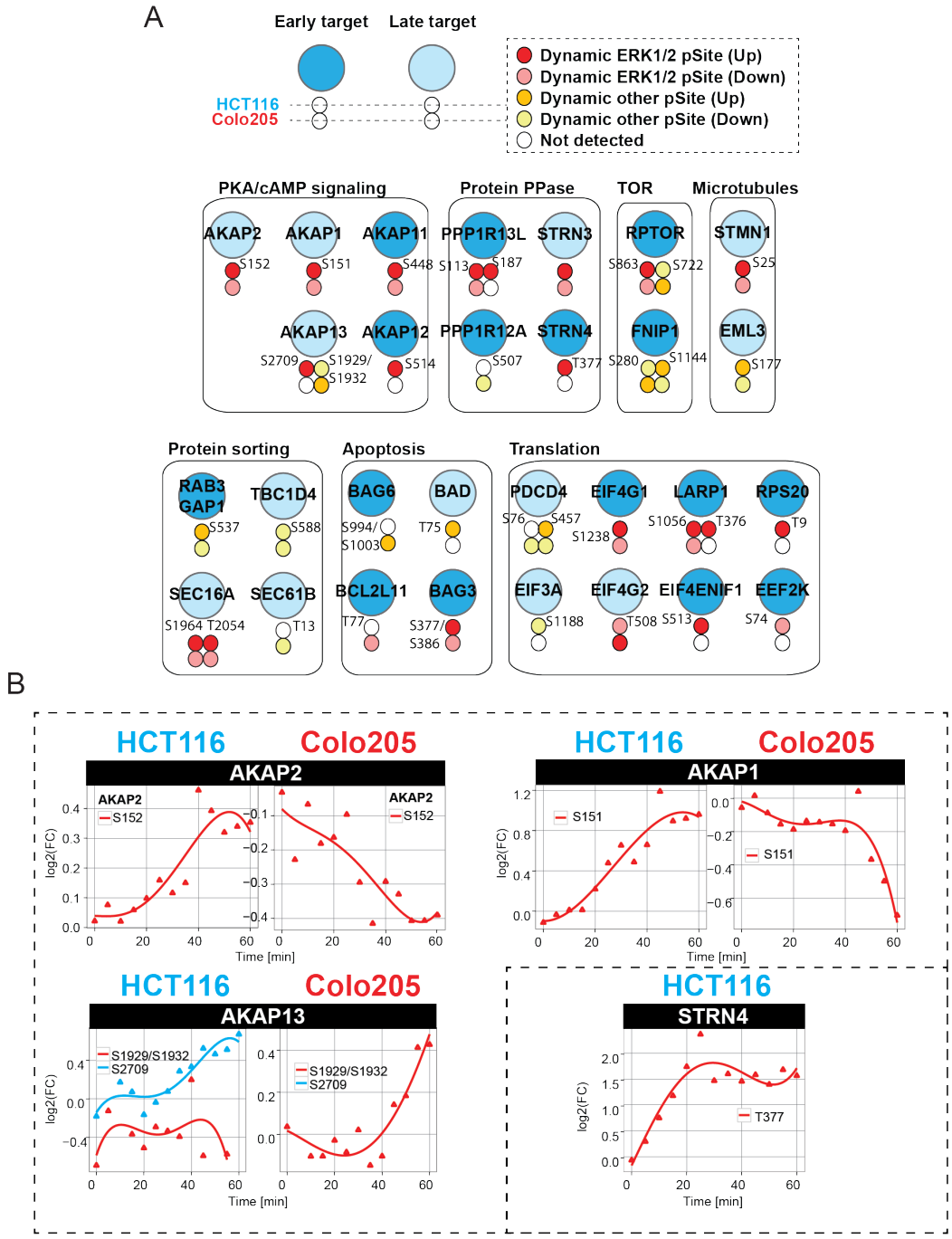

Supplementary Figure 3.5. ERK activity is regulating key cellular functions.

A) A subset of phosphosites dynamically modulated upon Vemurafenib treatment are involved in "PKA/cAMP signaling", "protein phosphatase complexes", "TOR signaling", "microtubules", "protein sorting", "apoptosis" and "translation". B) Kinetic profiles of representative substrates involved in "cAMP-dependent protein kinase (PKA) regulation" and in "protein phosphatase complexes" (STRN4).

3.7.2 Supplementary tables

Supplementary Table S 3-1: List of all identified phosphopeptide profiles (DVD-R).

Supplementary Table S 3-2: List of high membership dynamic phosphopeptide profiles (DVD-R).

Supplementary Table S 3-3: Phosphopeptides from group 4 with proline-directed phosphorylation motif (DVD-R).

Supplementary Table S 3-4: Maxquant parameters and experimental design (DVD-R).

3.8 References

1. Lavoie, H. and M. Therrien, *Regulation of RAF protein kinases in ERK signalling.* Nat Rev Mol Cell Biol, 2015. **16**(5): p. 281-98.
2. Malumbres, M. and M. Barbacid, *RAS oncogenes: the first 30 years.* Nat Rev Cancer, 2003. **3**(6): p. 459-65.
3. Wellbrock, C., M. Karasarides, and R. Marais, *The RAF proteins take centre stage.* Nat Rev Mol Cell Biol, 2004. **5**(11): p. 875-85.
4. Udell, C.M., et al., *Mechanistic principles of RAF kinase signaling.* Cell Mol Life Sci, 2011. **68**(4): p. 553-65.
5. Rajakulendran, T., et al., *A dimerization-dependent mechanism drives RAF catalytic activation.* Nature, 2009. **461**(7263): p. 542-5.
6. Peti, W. and R. Page, *Molecular basis of MAP kinase regulation.* Protein Sci, 2013. **22**(12): p. 1698-710.
7. Thevakumaran, N., et al., *Crystal structure of a BRAF kinase domain monomer explains basis for allosteric regulation.* Nat Struct Mol Biol, 2015. **22**(1): p. 37-43.
8. Wan, P.T., et al., *Mechanism of activation of the RAF-ERK signaling pathway by oncogenic mutations of B-RAF.* Cell, 2004. **116**(6): p. 855-67.
9. Pylayeva-Gupta, Y., E. Grabocka, and D. Bar-Sagi, *RAS oncogenes: weaving a tumorigenic web.* Nat Rev Cancer, 2011. **11**(11): p. 761-74.
10. Ascierto, P.A., et al., *The role of BRAF V600 mutation in melanoma.* J Transl Med, 2012. **10**: p. 85.
11. Davies, H., et al., *Mutations of the BRAF gene in human cancer.* Nature, 2002. **417**(6892): p. 949-54.
12. Xing, M., *BRAF mutation in thyroid cancer.* Endocr Relat Cancer, 2005. **12**(2): p. 245-62.
13. Holderfield, M., et al., *Targeting RAF kinases for cancer therapy: BRAF-mutated melanoma and beyond.* Nat Rev Cancer, 2014. **14**(7): p. 455-67.
14. Yang, H., et al., *RG7204 (PLX4032), a selective BRAFV600E inhibitor, displays potent antitumor activity in preclinical melanoma models.* Cancer Res, 2010. **70**(13): p. 5518-27.
15. Wang, S.F., et al., *Design, synthesis and biological evaluation of novel 5-phenyl-1H-pyrazole derivatives as potential BRAF(V600E) inhibitors.* Bioorg Med Chem, 2014. **22**(21): p. 6201-8.
16. Niehr, F., et al., *Combination therapy with vemurafenib (PLX4032/RG7204) and metformin in melanoma cell lines with distinct driver mutations.* J Transl Med, 2011. **9**: p. 76.
17. Heidorn, S.J., et al., *Kinase-dead BRAF and oncogenic RAS cooperate to drive tumor progression through CRAF.* Cell, 2010. **140**(2): p. 209-21.
18. Poulikakos, P.I., et al., *RAF inhibitors transactivate RAF dimers and ERK signalling in cells with wild-type BRAF.* Nature, 2010. **464**(7287): p. 427-30.
19. Hatzivassiliou, G., et al., *RAF inhibitors prime wild-type RAF to activate the MAPK pathway and enhance growth.* Nature, 2010. **464**(7287): p. 431-5.
20. Lavoie, H., et al., *Inhibitors that stabilize a closed RAF kinase domain conformation induce dimerization.* Nat Chem Biol, 2013. **9**(7): p. 428-36.

21. Yao, Z., et al., *BRAF Mutants Evade ERK-Dependent Feedback by Different Mechanisms that Determine Their Sensitivity to Pharmacologic Inhibition.* Cancer Cell, 2015. **28**(3): p. 370-83.
22. Kanshin, E., et al., *A cell-signaling network temporally resolves specific versus promiscuous phosphorylation.* Cell Rep, 2015. **10**(7): p. 1202-14.
23. Kanshin, E., et al., *Phosphoproteome dynamics of Saccharomyces cerevisiae under heat shock and cold stress.* Mol Syst Biol, 2015. **11**(6): p. 813.
24. Soufi, B., et al., *Global analysis of the yeast osmotic stress response by quantitative proteomics.* Mol Biosyst, 2009. **5**(11): p. 1337-46.
25. Sun, Y., et al., *Signaling pathway of MAPK/ERK in cell proliferation, differentiation, migration, senescence and apoptosis.* J Recept Signal Transduct Res, 2015: p. 1-5.
26. Stuart, S.A., et al., *A Phosphoproteomic Comparison of B-RAFV600E and MKK1/2 Inhibitors in Melanoma Cells.* Mol Cell Proteomics, 2015. **14**(6): p. 1599-615.
27. Ong, S.E. and M. Mann, *Stable isotope labeling by amino acids in cell culture for quantitative proteomics.* Methods Mol Biol, 2007. **359**: p. 37-52.
28. Bendall, S.C., et al., *Prevention of amino acid conversion in SILAC experiments with embryonic stem cells.* Mol Cell Proteomics, 2008. **7**(9): p. 1587-97.
29. Kanshin, E., S.W. Michnick, and P. Thibault, *Displacement of N/Q-rich peptides on TiO2 beads enhances the depth and coverage of yeast phosphoproteome analyses.* J Proteome Res, 2013. **12**(6): p. 2905-13.
30. Kanshin, E., S. Michnick, and P. Thibault, *Sample preparation and analytical strategies for large-scale phosphoproteomics experiments.* Semin Cell Dev Biol, 2012. **23**(8): p. 843-53.
31. Cox, J., et al., *Andromeda: A Peptide Search Engine Integrated into the MaxQuant Environment.* J Proteome Res, 2011. **10**(4): p. 1794-1805.
32. Cox, J. and M. Mann, *MaxQuant enables high peptide identification rates, individualized p.p.b.-range mass accuracies and proteome-wide protein quantification.* Nat Biotechnol, 2008. **26**(12): p. 1367-72.
33. Wiese, H., et al., *Comparison of alternative MS/MS and bioinformatics approaches for confident phosphorylation site localization.* J Proteome Res, 2014. **13**(2): p. 1128-37.
34. Nock, R. and F. Nielsen, *On weighting clustering.* IEEE Trans Pattern Anal Mach Intell, 2006. **28**(8): p. 1223-35.
35. Kumar, L. and E.F. M, *Mfuzz: a software package for soft clustering of microarray data.* Bioinformation, 2007. **2**(1): p. 5-7.
36. Schwammle, V. and O.N. Jensen, *A simple and fast method to determine the parameters for fuzzy c-means cluster analysis.* Bioinformatics, 2010. **26**(22): p. 2841-8.
37. Huang da, W., B.T. Sherman, and R.A. Lempicki, *Systematic and integrative analysis of large gene lists using DAVID bioinformatics resources.* Nat Protoc, 2009. **4**(1): p. 44-57.
38. Franceschini, A., et al., *STRING v9.1: protein-protein interaction networks, with increased coverage and integration.* Nucleic Acids Res, 2013. **41**(Database issue): p. D808-15.
39. Smoot, M.E., et al., *Cytoscape 2.8: new features for data integration and network visualization.* Bioinformatics, 2011. **27**(3): p. 431-2.
40. Horn, H., et al., *KinomeXplorer: an integrated platform for kinome biology studies.* Nat Methods, 2014. **11**(6): p. 603-4.

41. Forbes, S.A., et al., *COSMIC: exploring the world's knowledge of somatic mutations in human cancer.* Nucleic Acids Res, 2015. **43**(Database issue): p. D805-11.
42. Joseph, E.W., et al., *The RAF inhibitor PLX4032 inhibits ERK signaling and tumor cell proliferation in a V600E BRAF-selective manner.* Proc Natl Acad Sci U S A, 2010. **107**(33): p. 14903-8.
43. Ong, S.E. and M. Mann, *A practical recipe for stable isotope labeling by amino acids in cell culture (SILAC).* Nat Protoc, 2006. **1**(6): p. 2650-60.
44. Ubersax, J.A. and J.E. Ferrell, Jr., *Mechanisms of specificity in protein phosphorylation.* Nat Rev Mol Cell Biol, 2007. **8**(7): p. 530-41.
45. Geraghty, K.M., et al., *Regulation of multisite phosphorylation and 14-3-3 binding of AS160 in response to IGF-1, EGF, PMA and AICAR.* Biochem J, 2007. **407**(2): p. 231-41.
46. Bonni, A., et al., *Cell survival promoted by the Ras-MAPK signaling pathway by transcription-dependent and -independent mechanisms.* Science, 1999. **286**(5443): p. 1358-62.
47. Galan, J.A., et al., *Phosphoproteomic analysis identifies the tumor suppressor PDCD4 as a RSK substrate negatively regulated by 14-3-3.* Proc Natl Acad Sci U S A, 2014. **111**(29): p. E2918-27.
48. Chatr-Aryamontri, A., et al., *The BioGRID interaction database: 2015 update.* Nucleic Acids Res, 2015. **43**(Database issue): p. D470-8.
49. Szklarczyk, D., et al., *STRING v10: protein-protein interaction networks, integrated over the tree of life.* Nucleic Acids Res, 2015. **43**(Database issue): p. D447-52.
50. Linding, R., et al., *NetworKIN: a resource for exploring cellular phosphorylation networks.* Nucleic Acids Res, 2008. **36**(Database issue): p. D695-9.
51. Sigrist, C.J., et al., *New and continuing developments at PROSITE.* Nucleic Acids Res, 2013. **41**(Database issue): p. D344-7.
52. Jacobs, D., et al., *Multiple docking sites on substrate proteins form a modular system that mediates recognition by ERK MAP kinase.* Genes Dev, 1999. **13**(2): p. 163-75.
53. Huang da, W., B.T. Sherman, and R.A. Lempicki, *Bioinformatics enrichment tools: paths toward the comprehensive functional analysis of large gene lists.* Nucleic Acids Res, 2009. **37**(1): p. 1-13.
54. Kosako, H., et al., *Phosphoproteomics reveals new ERK MAP kinase targets and links ERK to nucleoporin-mediated nuclear transport.* Nat Struct Mol Biol, 2009. **16**(10): p. 1026-35.
55. Dougherty, M.K., et al., *Regulation of Raf-1 by direct feedback phosphorylation.* Mol Cell, 2005. **17**(2): p. 215-24.
56. Martin, K.A., et al., *Ribosomal S6 kinase 2 inhibition by a potent C-terminal repressor domain is relieved by mitogen-activated protein-extracellular signal-regulated kinase kinase-regulated phosphorylation.* J Biol Chem, 2001. **276**(11): p. 7892-8.
57. Wong, W. and J.D. Scott, *AKAP signalling complexes: focal points in space and time.* Nat Rev Mol Cell Biol, 2004. **5**(12): p. 959-70.
58. Sundberg-Smith, L.J., et al., *Adhesion stimulates direct PAK1/ERK2 association and leads to ERK-dependent PAK1 Thr212 phosphorylation.* J Biol Chem, 2005. **280**(3): p. 2055-64.

59. Rajanala, K., et al., *Phosphorylation of nucleoporin Tpr governs its differential localization and is required for its mitotic function.* J Cell Sci, 2014. **127**(Pt 16): p. 3505-20.
60. Joel, P.B., et al., *pp90rsk1 regulates estrogen receptor-mediated transcription through phosphorylation of Ser-167.* Mol Cell Biol, 1998. **18**(4): p. 1978-84.
61. Zhao, J., et al., *ERK-dependent phosphorylation of the transcription initiation factor TIF-IA is required for RNA polymerase I transcription and cell growth.* Mol Cell, 2003. **11**(2): p. 405-13.
62. Murphy, L.O., et al., *Molecular interpretation of ERK signal duration by immediate early gene products.* Nat Cell Biol, 2002. **4**(8): p. 556-64.
63. Vinciguerra, M., et al., *Differential phosphorylation of c-Jun and JunD in response to the epidermal growth factor is determined by the structure of MAPK targeting sequences.* J Biol Chem, 2004. **279**(10): p. 9634-41.
64. Deb, A., et al., *Protein kinase PKR is required for platelet-derived growth factor signaling of c-fos gene expression via Erks and Stat3.* EMBO J, 2001. **20**(10): p. 2487-96.
65. Zhao, B., et al., *TEAD mediates YAP-dependent gene induction and growth control.* Genes Dev, 2008. **22**(14): p. 1962-71.
66. Zhao, B., et al., *A coordinated phosphorylation by Lats and CK1 regulates YAP stability through SCF(beta-TRCP).* Genes Dev, 2010. **24**(1): p. 72-85.
67. Li, Z., et al., *Structural insights into the YAP and TEAD complex.* Genes Dev, 2010. **24**(3): p. 235-40.
68. Muehlich, S., et al., *Serum-induced phosphorylation of the serum response factor coactivator MKL1 by the extracellular signal-regulated kinase 1/2 pathway inhibits its nuclear localization.* Mol Cell Biol, 2008. **28**(20): p. 6302-13.
69. Shore, P. and A.D. Sharrocks, *The MADS-box family of transcription factors.* Eur J Biochem, 1995. **229**(1): p. 1-13.
70. Duggirala, A., et al., *cAMP-induced actin cytoskeleton remodelling inhibits MKL1-dependent expression of the chemotactic and pro-proliferative factor, CCN1.* J Mol Cell Cardiol, 2015. **79**: p. 157-68.
71. Mizuguchi, M., et al., *Transient alpha-helices in the disordered RPEL motifs of the serum response factor coactivator MKL1.* Sci Rep, 2014. **4**: p. 5224.
72. Ho, C.Y., et al., *Lamin A/C and emerin regulate MKL1-SRF activity by modulating actin dynamics.* Nature, 2013. **497**(7450): p. 507-11.
73. Smith, E.C., et al., *Induction of megakaryocyte differentiation drives nuclear accumulation and transcriptional function of MKL1 via actin polymerization and RhoA activation.* Blood, 2013. **121**(7): p. 1094-101.
74. Mouilleron, S., et al., *Molecular basis for G-actin binding to RPEL motifs from the serum response factor coactivator MAL.* EMBO J, 2008. **27**(23): p. 3198-208.
75. Mouilleron, S., et al., *Structure of a pentavalent G-actin*MRTF-A complex reveals how G-actin controls nucleocytoplasmic shuttling of a transcriptional coactivator.* Sci Signal, 2011. **4**(177): p. ra40.
76. Hirano, H. and Y. Matsuura, *Sensing actin dynamics: structural basis for G-actin-sensitive nuclear import of MAL.* Biochem Biophys Res Commun, 2011. **414**(2): p. 373-8.

77. Panayiotou, R., et al., *Phosphorylation acts positively and negatively to regulate MRTF-A subcellular localisation and activity.* Elife, 2016. **5**.
78. Yu, F.X., B. Zhao, and K.L. Guan, *Hippo Pathway in Organ Size Control, Tissue Homeostasis, and Cancer.* Cell, 2015. **163**(4): p. 811-28.
79. Lin, L., et al., *The Hippo effector YAP promotes resistance to RAF- and MEK-targeted cancer therapies.* Nat Genet, 2015. **47**(3): p. 250-6.
80. O'Neill, E., et al., *Role of the kinase MST2 in suppression of apoptosis by the proto-oncogene product Raf-1.* Science, 2004. **306**(5705): p. 2267-70.
81. Romano, D., et al., *Protein interaction switches coordinate Raf-1 and MST2/Hippo signalling.* Nat Cell Biol, 2014. **16**(7): p. 673-84.
82. Hu, Q., et al., *LMO7 mediates cell-specific activation of the Rho-myocardin-related transcription factor-serum response factor pathway and plays an important role in breast cancer cell migration.* Mol Cell Biol, 2011. **31**(16): p. 3223-40.
83. Kircher, P., et al., *Filamin A interacts with the coactivator MKL1 to promote the activity of the transcription factor SRF and cell migration.* Sci Signal, 2015. **8**(402): p. ra112.
84. Carlson, S.M., et al., *Large-scale discovery of ERK2 substrates identifies ERK-mediated transcriptional regulation by ETV3.* Sci Signal, 2011. **4**(196): p. rs11.
85. Rauen, K.A., *The RASopathies.* Annu Rev Genomics Hum Genet, 2013. **14**: p. 355-69.
86. Wu, X., et al., *Increased BRAF heterodimerization is the common pathogenic mechanism for noonan syndrome-associated RAF1 mutants.* Mol Cell Biol, 2012. **32**(19): p. 3872-90.
87. Sun, Y., et al., *Acute myeloid leukemia-associated Mkl1 (Mrtf-a) is a key regulator of mammary gland function.* Mol Cell Biol, 2006. **26**(15): p. 5809-26.
88. Cen, B., A. Selvaraj, and R. Prywes, *Myocardin/MKL family of SRF coactivators: key regulators of immediate early and muscle specific gene expression.* J Cell Biochem, 2004. **93**(1): p. 74-82.
89. Huang, J., et al., *Myocardin is required for cardiomyocyte survival and maintenance of heart function.* Proc Natl Acad Sci U S A, 2009. **106**(44): p. 18734-9.
90. Miano, J.M., et al., *Restricted inactivation of serum response factor to the cardiovascular system.* Proc Natl Acad Sci U S A, 2004. **101**(49): p. 17132-7.
91. Mokalled, M.H., et al., *Myocardin-related transcription factors are required for cardiac development and function.* Dev Biol, 2015. **406**(2): p. 109-16.
92. Lamouille, S., J. Xu, and R. Derynck, *Molecular mechanisms of epithelial-mesenchymal transition.* Nat Rev Mol Cell Biol, 2014. **15**(3): p. 178-96.
93. Medjkane, S., et al., *Myocardin-related transcription factors and SRF are required for cytoskeletal dynamics and experimental metastasis.* Nat Cell Biol, 2009. **11**(3): p. 257-68.

Chapter 4

Dynamic phosphoproteomics uncovers signaling pathways modulated by anti-oncogenic sphingolipid analogs

Peter Kubiniok[1,2,#], Brendan T. Finicle[3,#], Fanny Piffaretti[1,2] ,Alison McCracken[3], Michael Perryman[2], Stephen Hanessian[2], Aimee L. Edinger[3#] and Pierre Thibault[1,2,4#]

[1] Institute for Research in Immunology and Cancer, Université de Montréal, C.P. 6128, Succursale centre-ville, Montréal, Québec, H3C 3J7, Canada.

[2] Department of Chemistry, Université de Montréal, Quebec, Canada H3C 3J7

[3] Department of Developmental and Cell Biology, University of California Irvine, Irvine CA

[4] Department of Biochemistry, Université de Montréal, C.P. 6128, Succursale centre-ville, Montréal, Québec, H3C 3J7, Canada.

# These authors contributed equally to this work.

Manuscript: Submitted to Molecular and Cellular Proteomics, August 23rd, 2018

Authors Contribution

P.K. and P.T. designed the experimental setup. P.K. and F.P. conducted phosphoproteomics experiments. P.K. analyzed phosphoproteomics data. A.M. preformed CD98 transporter downregulation tests, B.F. performed immune fluorescence experiments. P.K., B.T., A.E. and P.T. interpreted data and discussed the storyline. P.K. and B.F. wrote the manuscript; the manuscript was finalized by P.T. and A.E..

4.1 Abstract

The anti-neoplastic sphingolipid analog SH-BC-893 starves cancer cells to death by down-regulating cell surface nutrient transporters and blocking lysosomal trafficking events. These effects are mediated by the activation of protein phosphatase 2A (PP2A). To identify putative PP2A substrates, we used quantitative phosphoproteomics to profile the temporal changes in protein phosphorylation in FL5.12 cells following incubation with SH-BC-893 or the specific PP2A inhibitor LB-100. These analyses enabled the profiling of more than 15,000 phosphorylation sites, of which 958 sites on 644 proteins were dynamically regulated. We identified 114 putative PP2A substrates including several nutrient transporter proteins, GTPase regulators (e.g. Agap2, Git1), and proteins associated with actin cytoskeletal remodeling (e.g. Vim, Pxn). To identify SH-BC-893-induced cell signaling events that disrupt lysosomal trafficking, we compared phosphorylation profiles in cells treated with SH-BC-893 or C2-ceramide, a non-vacuolating sphingolipid that does not impair lysosomal fusion. These analyses combined with functional assays uncovered the differential regulation of Akt and Gsk3b by SH-BC-893 (vacuolating) and C2-ceramide (non-vacuolating). Dynamic phosphoproteomics of cells treated with compounds affecting PP2A activity thus enabled the correlation of cell signaling with phenotypes to rationalize their mode of action.

4.2 Introduction

Oncogenic mutations selected during the tumorigenic process rewire the metabolic circuitry to meet the increased anabolic demands of cancer cells. Because oncogenic mutations constitutively drive growth and proliferation, cancer cells depend on a steady influx of nutrients via cell surface transporters and receptors and on the lysosomal degradation of internalized macromolecules into subunits that can be used for biosynthesis and/or the production of ATP [1]. Because cancer cells are constitutively anabolic, they are unable to tolerate nutrient stress that causes quiescence and catabolism in normal cells. Restricting nutrient access using sphingolipid-inspired compounds is an appealing therapeutic strategy to impede cancer cell proliferation and survival. Previous reports indicated that endogenous and synthetic sphingolipids starve many different cancer cell types to death by triggering the down regulation of multiple nutrient transporter proteins and/or blocking lysosomal fusion reactions [2-7].

In mammalian cells, ceramides can function as tumor suppressors, mediating signaling events associated with apoptosis, autophagic responses and cell cycle arrest [8]. Several sphingolipids activate protein phosphatase 2A (PP2A) and negatively regulate multiple signaling pathways that promote nutrient transporter expression [5, 9-13]. Although the mechanism underlying sphingolipid regulation of PP2A activity is not entirely clear, previous reports suggest that ceramides can bind to endogenous protein inhibitors of PP2A to enhance its catalytic activity [13]. Interestingly, while Fingolimod (FTY720, Gilenya), pyrrolidine analogs such as SH-BC-893, and ceramide all induce nutrient transporter down-regulation downstream of PP2A activation, only FTY720 and SH-BC-893 produce PP2A-dependent cytoplasmic vacuolation [5]. Ceramide, on the other hand, produces distinct effects from FTY720 and SH-BC-893 on the tubular recycling endosome, although whether these effects are PP2A-dependent is less certain [5, 14]. These observations suggest that these structurally-related molecules differentially activate PP2A, resulting in distinct patterns of dephosphorylation and different endolysosomal trafficking phenotypes.

To determine how PP2A activity induces nutrient transporter loss and cytosolic vacuolation, we profiled the dynamic changes in protein phosphorylation in the murine prolymphocytic cell line FL5.12 following incubation with SH-BC-893, the specific PP2A inhibitor LB-100, or C2-

ceramide. Metabolic labeling and quantitative phosphoproteomics [15-17] identified kinetic profiles that could be correlated with putative PP2A substrates. This approach identified 15,607 phosphorylation sites, of which 958 were dynamically regulated by the treatments. While 265 putative PP2A sites were common to both PP2A agonists, our analyses also revealed 467 sites uniquely regulated by either SH-BC-893 or C2-ceramide that provided further insights into the SH-BC-893-specific phenotype, vacuolation.

4.3 Materials and methods

4.3.1 Cell culture

FL5.12 cells were maintained in RPMI-1640 medium supplemented with 10% fetal bovine serum (FBS), 10 mM HEPES buffer, 55 µM 2-mercaptoethanol, 2 mM L-glutamine, 500 pg/mL murine recombinant IL-3, and antibiotics. HeLa cells were cultured in DMEM with 4.5 g/L glucose and L-glutamine supplemented with 10% FBS and antibiotics. For proteomic analyses FL5.12 cells were grown in triple SILAC SD-Media (Thermo Fisher Scientific, Rockford, IL) containing 10% FBS, 500 pg/mL murine recombinant IL-3, 164 µM Lysine (K), 95 µM Arginine (R), 4.3 µM proline (Silantes, Munich, Germany) with additional nutrients consistent with Bendall *et al.* [18]. Cells were incubated at 37°C and 5% CO_2. Cells were counted using a Leica microscope with a 10 x 0.25 objective. Approximately 500 million cells per SILAC channel were grown in 500 mL spinner flasks. Incubation with small molecules was performed by adding 1 mL of small molecule or DMSO (Sigma Aldrich Co.) diluted in SILAC RPMI 1640/10% FBS to reach the final concentration. Cells were harvested every 5 min during the first hour of treatment with either 5 µM SH-BC-893 (heavy label) or 50uM C2-ceramide (medium label) or 10 µM LB-100 (medium label) or DMSO (light label). Drug concentrations used for treatments are based on previously published references [5, 7, 19]. Cells were collected by pipetting 75 mL (25 mL per SILAC channel) of culture into 425 mL of -80°C pre-cooled ethanol.

4.3.2 Flow cytometry

For quantification of cell surface CD98, 400,000 FL5.12 cells were stained with either PE-conjugated rat IgG2a k isotype control (Biolegend, cat. no. 400508) or PE-conjugated rat anti-mouse CD98 (Biolegend, cat. no. 128208) in blocking buffer (PBS with 10% FBS and 0.05% sodium azide) for 30 min on ice. Cells were washed twice in ice-cold wash buffer (PBS with 2% FCS and 0.05% sodium azide), resuspended in wash buffer containing 1 µg/mL DAPI, and returned to ice. Analysis was restricted to live cells (DAPI-negative) and data normalized to the untreated control after background subtraction.

4.3.3 Vacuolation assay

Vacuoles were quantified as in Perryman et al. [20]. Briefly, FL5.12 cells were treated as indicated for 3 h then pelleted by centrifuging at 2,000 rpm for 3 min in a microfuge. The cell pellet was resuspended in 10 μL, and 3 μL of the cell suspension was examined under a 0.13 to 0.17 mm thick coverglass (VWR Micro cover glass, square, No.1, cat. no. 48366-045) on a microscope slide. FL5.12 cells were evaluated by differential interference microscopy (DIC) using a 100x oil-immersion objective with a Nikon TE2000-S fluorescence microscope. To calculate the vacuolation score, at least 10 different fields of view containing 5-12 cells per field were assessed. Scores were assigned to individual cells as follows: 0 = no vacuoles, 1 = very small vacuoles, 2 = multiple well-defined vacuoles, 3 = multiple large vacuoles. To calculate the vacuolation score, the following formula was used:

$$\text{score} = \frac{(3\times\%\ \text{cells in cat. } 3) + (2\times\%\ \text{cells in cat. } 2) + (1\times\%\ \text{cells in cat. } 1)}{3}$$

4.3.4 Fluorescence microscopy

To monitor F-actin, FL5.12 cells were fixed with 4% paraformaldehyde for 10 min, washed, and incubated in permeabilization and blocking buffer (PBS with 10% FBS, 0.3% saponin, and 0.05% sodium azide) containing Alexa Fluor 488 conjugated phalloidin (Cell Signalling Technologies, 1:100 dilution). Cells were then imaged on a Nikon Eclipse Ti spinning-disk confocal microscope using a 100x oil-immersion objective. Images were analyzed using ImageJ; fluorescence intensity was normalized between all images and displayed using the LUT "16 colors."

4.3.5 Immunoblotting

Cells were lysed in RIPA buffer containing protease (Pierce, Cat #88265) and phosphatase inhibitors (Sigma, Cat #4906845001). Protein concentration was quantified using a BCA protein assay (Thermo Scientific, Cat #23223). Samples were prepared in NuPAGE sample buffer (Invitrogen, Cat #NP0007) and 50 mM DTT, run on Invitrogen NuPAGE 4-12% Bis-Tris gels

(Cat #NP0336BOX), and transferred to BioTrace NT nitrocellulose membranes (Pall, Cat #66485). After transfer, membranes were dried at room temperature for 30 min, incubated in blocking solution (5% bovine serum albumin, 0.05% NaN3 in TBST) for 1 h, and then incubated overnight at 4°C in blocking solution containing primary antibody. Blots were washed three times in TBST (TBS with 0.1% Tween 20), incubated at RT for 1 h in blocking solution containing IRDye-conjugated secondary antibodies (1:10,000), and then washed three times in TBST. Blots were imaged using a LI-COR Odyssey CLx imaging system.

4.3.6 Digestion and desalting of cell extracts

Heavy, medium and light cells from each time point were combined in 500 mL collection tubes (Sorvall centrifuge bottles), separated by centrifugation at 1,200 rpm (Sorvall Legend RT centrifuge) and washed first with 35 mL PBS, then 5 mL PBS, and finally 3 times with 1 mL PBS while transferring from 500 mL collection tubes to 50 mL falcon tubes to 1.7mL Eppendorf tubes, respectively. Cell lysis was performed by sonication for 15 seconds with a sonic dismembrator (Thermo Fisher Scientific; Rockford, IL) after adding 1 mL lysis buffer (8M Urea, 50mM TRIS, pH 8, HALT phosphatase inhibitor (Thermo Fisher Scientific). Cells were maintained at 0°C to prevent protein degradation. Protein concentration was measured by BCA assay (Thermo Fisher Scientific). Protein disulfide bonds were reduced by incubating lysates in 5 mM dithiothreitol (DTT, Sigma-Aldrich, St-Louis, MO) for 30 min at 56°C while shaking at 1,000 rpm. Alkylation of cysteine residues was achieved by incubation with iodoacetamide (IAA, Sigma-Aldrich) at a concentration of 15 mM for 30 min at RT in the dark. Excess IAA was quenched for 15 min at RT by adding DTT to 5 mM. All samples were diluted 5 times with 20 mM TRIS (Bioshop Burlington ON), 1 mM $CaCl_2$, pH 8 and mixed with 2 µg/µL trypsin (Sigma-Aldrich) (protein: trypsin 50:1 w:w) and incubated for 12 h at 37°C. Trypsin was kept at -80 °C and thawed only once. Desalting was performed on 60 mg solid phase extraction (SPE) reverse phase cartridges (Oasis HLB 3cc cartridge, 60 mg, 30 µm particle size, Waters Mississauga, ON) previously conditioned with 3 mL methanol, SPE Buffer (50% acetonitrile, ACN, 1% formic acid, FA) and finally with 1% aqueous FA. Peptide samples were loaded, washed with 3 mL 1% FA, eluted in 1 mL SPE buffer and dried on a vacuum centrifuge (Thermo Fisher Scientific) at RT.

4.3.7 Phosphopeptide enrichment

Phosphopeptide enrichment was performed on 5 µm titansphere particles (Canadian Life Science, Peterborough, ON) according to published protocols [21, 22]. Loading of protein extracts on the titansphere beads, washing, and elution steps were performed using custom spin columns [23] made from 200 µl pipette tip containing a SDB-XC membrane (Empore, 3M) frit and filled with TiO_2 beads. Peptides were desalted in 50 µL of 1% FA and subsequently eluted from spin columns using 50 µL of 50% ACN 0.5% FA.

4.3.8 Offline strong cation exchange chromatography

To achieve high reproducibility and parallel sample fractionation in high throughput proteomics experiments, we used strong cation fractionation (SCX) on homemade spin columns packed with 18 to 22 mg (for cell lysate of 3 to 8 mg protein extract) of polysulfoethyl A 300Å particle, (Canada Life Science; Peterborough, ON). After equilibrating the SCX particles with each 100 µL of SCX Buffer A (10% ACN/0.2%FA v/v), Buffer B (1 M NaCl in 10% ACN/0.2%FA v/v) and finally 200 µL SCX Buffer A. Peptides were resuspended in 100 µL Buffer A, loaded on the SCX column and eluted in six salt step fractions of 100 µL each with 0, 30, 50, 80, 120 and 500 mM NaCl in SCX Buffer A. Prior to LC-MS/MS analyses all fractions were dried on a SpeedVac centrifuge at RT (Thermo Fisher Scientific) and resuspended in 4% FA. All centrifugation steps were performed at 4°C except where indicated.

4.3.9 Mass spectrometry analysis

LC-MS/MS analyses were performed on a Q-Exactive HF (SH-BC-893 vs. C2-ceramide experiments) or an Orbitrap tribrid Fusion (SH-BC-893 vs. LB-100 experiments) mass spectrometer using homemade capillary LC columns (18 cm length, 150 µm ID, 360 µm OD). Capillary LC columns were packed with C18 Jupiter 3 µm particles (Phenomenex, Torrance, CA) at 1,000 psi. Samples were directly injected on LC-columns and separations were performed at a flow rate of 0.6 µL/min using a linear gradient of 5-35 % aqueous ACN (0.2% FA) in 150 minutes. MS spectra were acquired with a resolution of 60,000 using a lock mass (m/z: 445.120025) followed by up to 20 MS/MS data dependent scans on the most intense ions using

high energy dissociation (HCD). AGC target values for MS and MS/MS scans were set to $1x10^6$ (max fill time 100 ms) and $5x10^5$ (max fill time 200 ms), respectively. The precursor isolation window was set to m/z 1.6 with a HCD normalized collision energy of 25. The dynamic exclusion window was set to 20 s.

4.3.10 Data processing and analysis

Raw data analysis of SILAC experiments was performed using Maxquant software 1.5.3.8 and the Andromeda search engine [24]. The false discovery rate (FDR) for peptide, protein, and site identification was set to 1%, the minimum peptide length was set to 6, and the 'peptide requantification' function was enabled. The option match between runs (2 min time tolerance) was enabled to correlate identification and quantitation results across different runs. Up to 2 missed cleavages per peptide were allowed. To adjust for any systematic quantification errors, SILAC ratios were normalized by time point. All additional parameters are reported in MaxQuant parameters.txt and experimentalDesign.txt provided in Supplementary Table S4-1. The Uniprot mouse proteome database (September 2015 containing 35,281 entries) was used for all searches. Protein groups were formed by MaxQuant, and all identified peptides were used to make pair-wise comparison between proteins in the database. Proteins containing an equal or overlapping set of peptides were merged together to form a protein group and ranked according to the highest number of peptides.

All raw LC-MS/MS data and MaxQuant output files can be accessed from PeptideAtlas Consortium via the FileZilla partner repository which can be accessed at the following location ftp://PASS01168:VH7449z@ftp.peptideatlas.org/ with the following password "VH7449z" and identifier "PASS01168". MaxQuant output files contain lists of all matched and unmatched spectra, all matched protein isoforms and peptides including scorings and more detailed information. In addition to an FDR of 1% set for peptide, protein and phosphosite identification levels, we used additional criteria to increase data quality. The Andromeda score threshold for the identification of phosphopeptides was set to 40 with a delta score to the second best match of 8, as optimized by Sharma K et a. (PMID 25159151). We selected only peptides for which abundance ratios (FC=Drug/Control) were measured in at least 6 time points. Then we set a cut-

off for maximum phosphosite localization confidence across experiments (time points) to 0.75. Next, we distinguished dynamic from static phosphosites by calculating an FDR based on curve fitting as recently described [17]. We further performed clustering analysis using the fuzzy means package [25] which is implemented to the R environment (https://cran.r-project.org/).

Gene Ontology (GO) enrichment analyses were performed using the database DAVID version 6.7 [26]. Protein interaction networks were defined using the STRING database and interacting proteins were visualized with Cytoscape version 2.8. A protein-protein interaction network was built in STRING version 9.1 for all proteins containing dynamic phosphosites. All interaction predictions were based on experimental evidences with a minimal confidence score of 0.7 (considered as a "high confidence" filter in STRING). Linear motif analysis was done using Motif-x [27, 28].

4.4 Experimental Design and Statistical Rationale

For time resolved phosphoproteomics experiments, FL5.12 cells were collected from one large cell culture (500mL) per SILAC channel. Time course experiments (SH-BC-893 and LB-100; SH-BC-893 and C2-ceramide) were conducted on different days. Sample processing for each time course experiment was performed in parallel and from the same batch of materials and chemicals to maximize reproducibility of peptide digestion, phosphopeptide enrichment and fractionation. All time points of each SCX fraction were consecutively loaded onto the LC-MS system to ensure similar peptide coverage for all time points. SCX fractions were injected with increasing salt concentration. All data were analyzed using the same FASTA file (Uniprot Mouse proteome, accessed September 2015, 35,281 entries) and MaxQuant version 1.5.8.3.

Microscopy experiments (e.g., phalloidin staining in Fig. 4.7A-C, vacuolation images in Fig. 4.1C, 4.7E, and 4.8A,C-E) were completed in 2-3 biological replicates performed on separate days to account for biological variation. Microscopy images representative of the >100 cells per condition per biological replicate were used in figures. For quantitation of cytoplasmic vacuolation (Fig. 4.8A,C-E), at least 400 cells per condition from three biological replicates were

performed and error bars show the 95% confidence interval. Statistical significance was evaluated with a Student's t test (two-tailed, paired), as described in each figure legend.

For flow cytometry experiments quantifying the surface levels of CD98 (Fig. 4.1B and 4.7D), at least three biological replicates were performed on different days to account for biological variation. Surface CD98 levels are normalized to vehicle within each experiment, and the normalized values are averaged. Variation is shown as standard error of the mean and statistical significance was assessed by Student's t test (two-tailed, paired), as described in the figure legends.

4.5 Results

4.5.1 SH-BC-893 and C2-ceramide produce distinct, PP2A-dependent alterations in endolysosomal trafficking

The synthetic sphingolipid SH-BC-893 is a structurally constrained analog of FTY720 (also known as Fingolimod) that fails to activate S1P receptors 1 or 3 yet retains anticancer properties [20, 29, 30]. Both SH-BC-893 and C2-ceramide (N-Acetyl-sphingosine, Figure 4.1A) suppress cell growth and survival in part by down-regulating nutrient transporter proteins through the activation of the cytosolic serine/threonine protein phosphatase PP2A [5, 7, 14, 29]. The cell surface antigen 4F2 heavy chain (solute carrier family 3 member 2, Slc3a2 or CD98) is a chaperone required for the surface expression of several associated light chains that transport amino-acids [31]. Incubation with either 2.5 μM SH-BC-893 or 50 μM C2-ceramide resulted in a 40% down regulation of 4F2hc that was reversed by the selective PP2A inhibitor LB-100 (Figure 4.1B). These observations are consistent with published studies in multiple cell types [5, 7, 14, 20, 29]. In addition to limiting cell surface CD98 expression, SH-BC-893, but not ceramide, prevented the fusion of endocytic vesicles and autophagosomes with lysosomes resulting in enlarged multivesicular bodies, MVB [5]; LB-100 reversed this effect (Figure. 4.1C). These results confirm that disruptions in endolysosomal trafficking that starve cancer cells to death [5] are PP2A-dependent in FL5.12 cells.

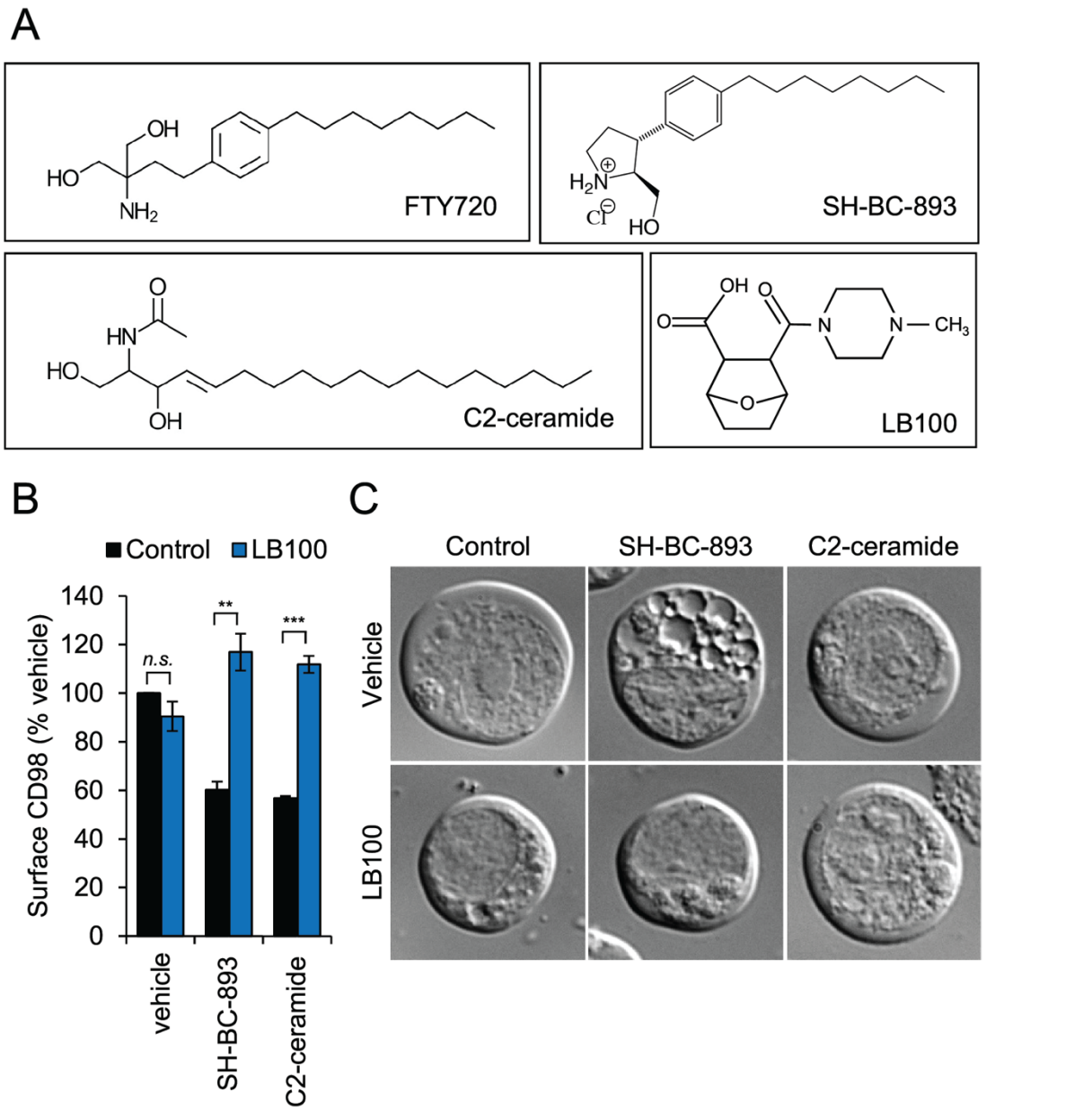

Figure 4.1. SH-BC-893 and C2-ceramide cause PP2A-dependent disruptions in endolysosomal trafficking.

A) Structures of the PP2A activators FTY720 (Fingolimod), C2-ceramide, SH-BC-893 and the PP2A inhibitor LB-100. B) Surface CD98 levels in FL5.12 cells pre-treated with LB-100 (100 μM) for 1.5 h prior to addition of DMSO vehicle, SH-BC-893 (5 μM), or C2-ceramide (50 μM) for 1 h. Using Student's t-test (n.s.) not significant; *,p ≤0.05;**, p≤0.01; and ***, p≤0.001 C) DIC microscopy of FL5.12 cells pre-treated with LB-100 (100 μM) for 1.5 h prior to addition of DMSO, vehicle, SH-BC-893 (5 μM), or C2-ceramide (50 μM) for 2 h.

4.5.2 Dynamic phosphoproteomics deconvolves signaling events associated with changes in PP2A activity

To investigate the molecular mechanisms underlying nutrient transporter loss and vacuolation, we profiled the temporal changes in protein phosphorylation in FL5.12 cells treated SH-BC-893, C2-ceramide, or LB-100 using quantitative phosphoproteomics and metabolic labeling (Figure 4.2). Changes in the phosphoproteome associated with SH-BC-893 or LB-100 treatment were analyzed in triple SILAC experiments.

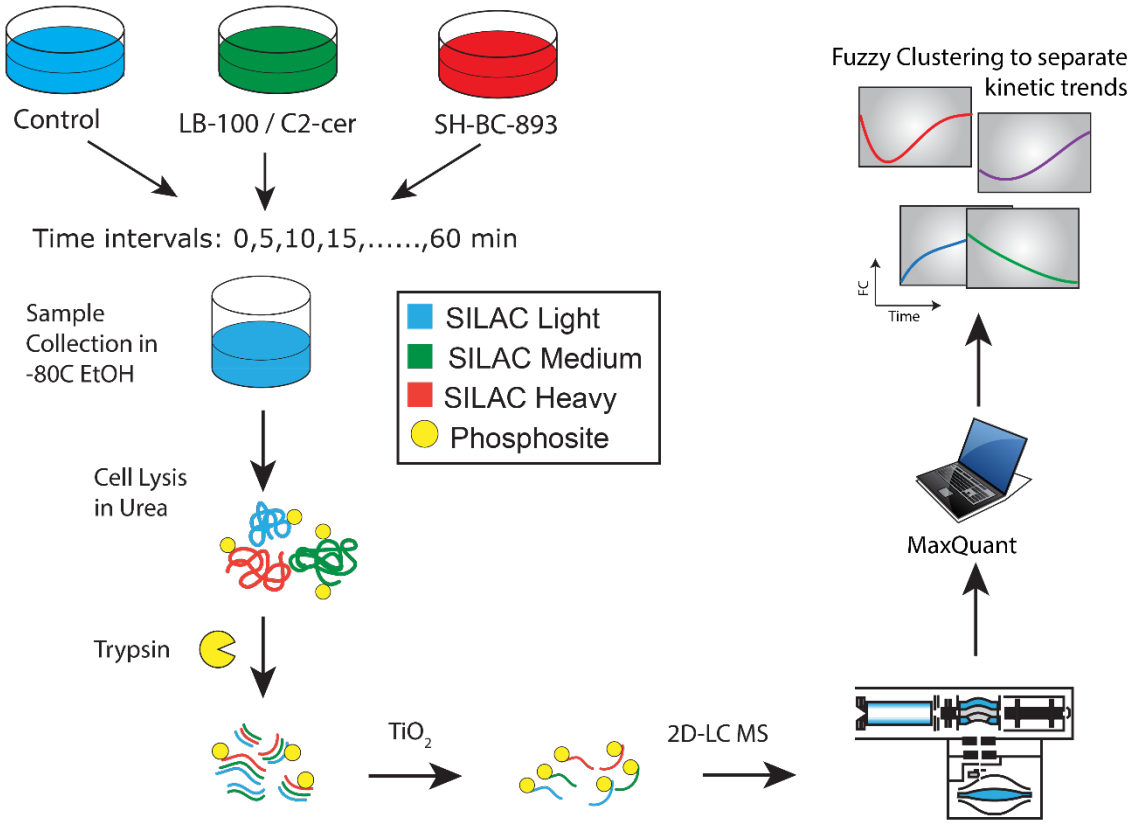

Figure 4.2. Triple SILAC phosphoproteomics workflow.

Light cells are treated with vehicle, medium cells were treated with C2-ceramide (50 μM) or LB-100 (10 μM), and heavy cells were treated with SH-BC-893 (5 μM). Cells were collected every 5 min from 0-60 min of stimulation by snap freezing in pre-cooled ethanol. Cells were lysed in urea, digested with trypsin and phosphopeptides were enriched using titanium dioxide. Strong cation fractionation (SCX) was performed prior to LC-MS/MS analysis. Phosphopeptide identification and quantitation was performed using MaxQuant, and only kinetic profiles of sites with localisation confidence > 0.75 and measured in at least 6 time points were selected for further analysis. Polynomial fitting was used to define regulated phosphosites, and only phosphopeptide profiles with FDR < 1% were selected and used for fuzzy c-means clustering and subsequent analyses.

LB-100 was selected for these studies as it is more selective towards PP2A than other serine/threonine protein phosphatase inhibitors such as calyculin A or okadaic acid which affect

both PP1 and PP2A [32, 33]. In a parallel set of experiments, C2-ceramide's effects on the phosphoproteome were compared to those of SH-BC-893 using a similar strategy. Unstimulated cells (^{0}Lys, ^{0}Arg, light), and cells treated with LB-100/C2-ceramide or SH-BC-893 (^{4}Lys, ^{6}Arg, medium or ^{8}Lys, ^{10}Arg, heavy) were collected every 5 min for 60 min, and combined together in pre-cooled ethanol (-80˚C) at each time point. Cells were centrifuged, lysed, and digested with trypsin prior to phosphopeptide enrichment on TiO_2 affinity media. The eluted phosphopeptides were subsequently fractionated on strong cation exchange (SCX) spin columns and analyzed by liquid chromatography tandem mass spectrometry (LC-MS/MS). Phosphopeptide identification and quantification was performed using MaxQuant [34, 35] and kinetic trends and clusters identified using R (http://www.r-project.org/). A total of 15,607 unique phosphopeptides were identified corresponding to an average phosphopeptide enrichment level of 85% for all experiments. SILAC experiments enabled the identification of 12,137 and 9,738 unique phosphopeptides on 2,949 and 2,550 proteins for LB-100/SH-BC-893 and C2-ceramide/SH-BC-893 experiments, respectively (Supplementary Table S4-2). On average, 70% of phosphosites were localized with high confidence (8,559 sites for LB-100/SH-BC-893 and 6,704 sites for C2-ceramide/SH-BC-893). Closer examination of these data revealed that 3,928 phosphosites in LB-100/SH-BC-893 and 2,919 phosphosites in C2-ceramide/SH-BC-893 experiments were quantified in at least 6 time points, and were classified as high-quality kinetic profiles (Supplementary Figures 4.1 and 4.2 and Supplementary Table S4-3). Of the 5,029 high quality profiles, 1,818 were common to both experiments (Supplementary Figure 4.3). A list of phosphopeptides corresponding to these profiles is presented in Supplementary Table S4-3 for both triple SILAC experiments. As described previously, curve fitting with a polynomial model and a false discovery rate (FDR) of 1% distinguished dynamic from static profiles [17]. These analyses identified 629 and 428 dynamic profiles corresponding to regulated phosphosites in LB-100/SH-BC-893 and C2-ceramide/SH-BC-893 experiments, respectively (Supplementary Table S4-4). A comparison of these regulated phosphosites revealed that only 54 phosphopeptides were common to all three conditions suggesting that many of the changes in cell signaling taking place were not regulated by all three stimuli (Supplementary Figure 4.3).

Phosphorylation events that vary in opposite directions in cells treated with SH-BC-893 and LB-100 are likely to be PP2A-dependent. The dynamic profiles showed a progressive broadening of

fold change (FC) values with a gradual shift in the median distribution toward a decrease or an increase in phosphorylation for cells treated with SH-BC-893 or LB-100, respectively. The width of this distribution was calculated from the inter quartile range (IQR) of the Log_2 (FC) distribution of phosphopeptides at each time point and plotted over the entire cell stimulation period (Figure 4.3A). The resulting curve showed a progressive increase in the IQR, in contrast to the trend observed from non-phosphorylated peptides that remained unaffected with time. Also, the extent of changes in protein phosphorylation was more pronounced for cells treated with LB-100 compared to those incubated with SH-BC-893.

Fuzzy clustering separated these dynamic profiles into those that displayed rapid or progressive increases or decreases in phosphorylation or showed an adaptation-like response (Figures 4.3B and C). From the 629 dynamic profiles identified in experiments comparing SH-BC-893 and LB-100 treatments, 384 were regulated by SH-BC-893, and are represented in Figure 4.3B. The majority of profiles in SH-BC-893-treated cells showed a progressive dephosphorylation (200 of 384 profiles), consistent with the expected agonist activity of this compound (Figure 4.3C). In contrast, profiles from cells treated with the PP2A inhibitor LB-100 displayed a progressive increase in phosphorylation with time (349 of 534 profiles). Fifty-two profiles in cells treated with SH-BC-893 exhibited adaptation characterized by a rapid dephosphorylation over the first 20 min post-stimulation followed by a recovery phase that extended over the remaining time period (Figure 4.3C). Interestingly, phosphosites that displayed transient dephosphorylation were more highly conserved than static sites ($p<0.001$) or dynamic sites that changed unidirectionally ($p<0.05$) suggesting that the adaptation cluster may define a subset of functionally important phosphorylation events (Supplementary Figure 4.4).

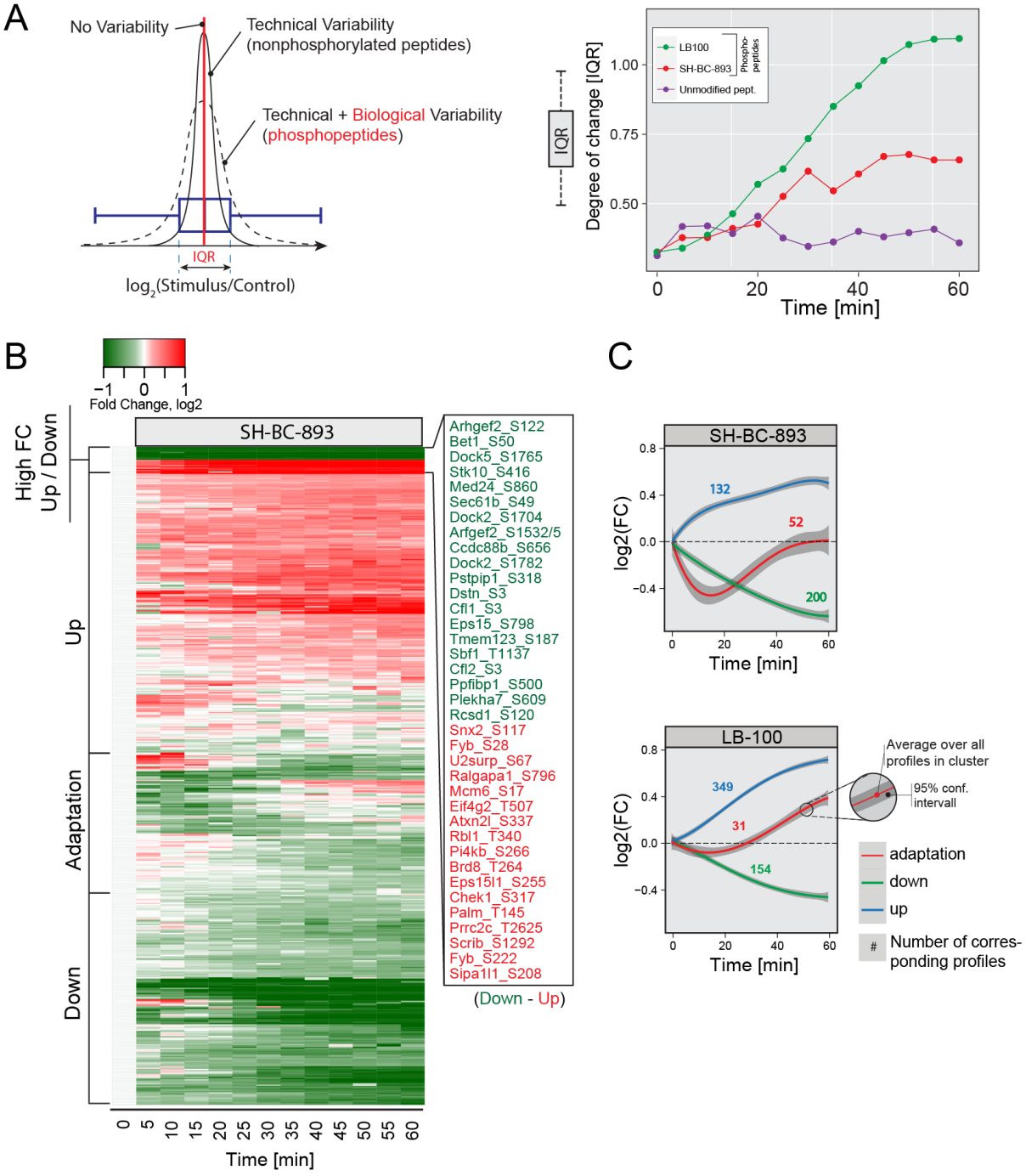

Figure 4.3. Phosphoproteomics results from the comparison of treatments with LB-100 (10 μM) and SH-BC-893 (5 μM).

A) Inter quartile range (IQR) shows the global change in phosphorylation upon treatment. Unmodified peptides (control) do not change over time while LB-100 and SH-BC-893 treatments show a progressive increase in IQR with time. B) Heatmap of all 390 phosphosites regulated by SH-BC-893. Different kinetic behaviors are indicated. C) Kinetic trends extracted from LB-100 and SH-BC-893 treatments using fuzzy means clustering, numbers correspond to profiles observed with a particular kinetic trend.

To identify putative PP2A substrates, we compared phosphorylation profiles that changed in opposite directions when FL5.12 cells were treated with LB-100 and SH-BC-893. Out of the 629 dynamic profiles identified in the triple SILAC experiment, 289 profiles were common to both treatments, and 114 of these profiles showed reciprocal (bidirectional) behavior (Figure 4.4A). We also noted that a subset of 175 profiles common to both LB-100 and SH-BC-893 displayed comparable trends that were either increasing or decreasing in phosphorylation with time, and were referred to as monodirectional. Linear motif analysis of monodirectional or bidirectional phosphopeptides with motif-X revealed that approximately half of phosphosites that displayed bidirectional profiles showed a SP or a RxxS motif while monodirectional sites were mainly represented by proline-directed phosphorylation (PxSP and SP motifs) (Figure 4.4B). To decipher which phosphorylation events are associated with changes in PP2A activity, we selected phosphosites that exhibited reciprocal trends with SH-BC-893 and LB-100 together with those uniquely regulated by SH-BC-893 (209 sites), and performed Gene Ontology (GO) enrichment using DAVID (Figure 4.4C). Proteins associated with guanosine triphosphate hydrolase (GTPase) regulators and actin filament reorganization were significantly enriched; GTPases and actin dynamics both play critical roles in regulating intracellular trafficking.

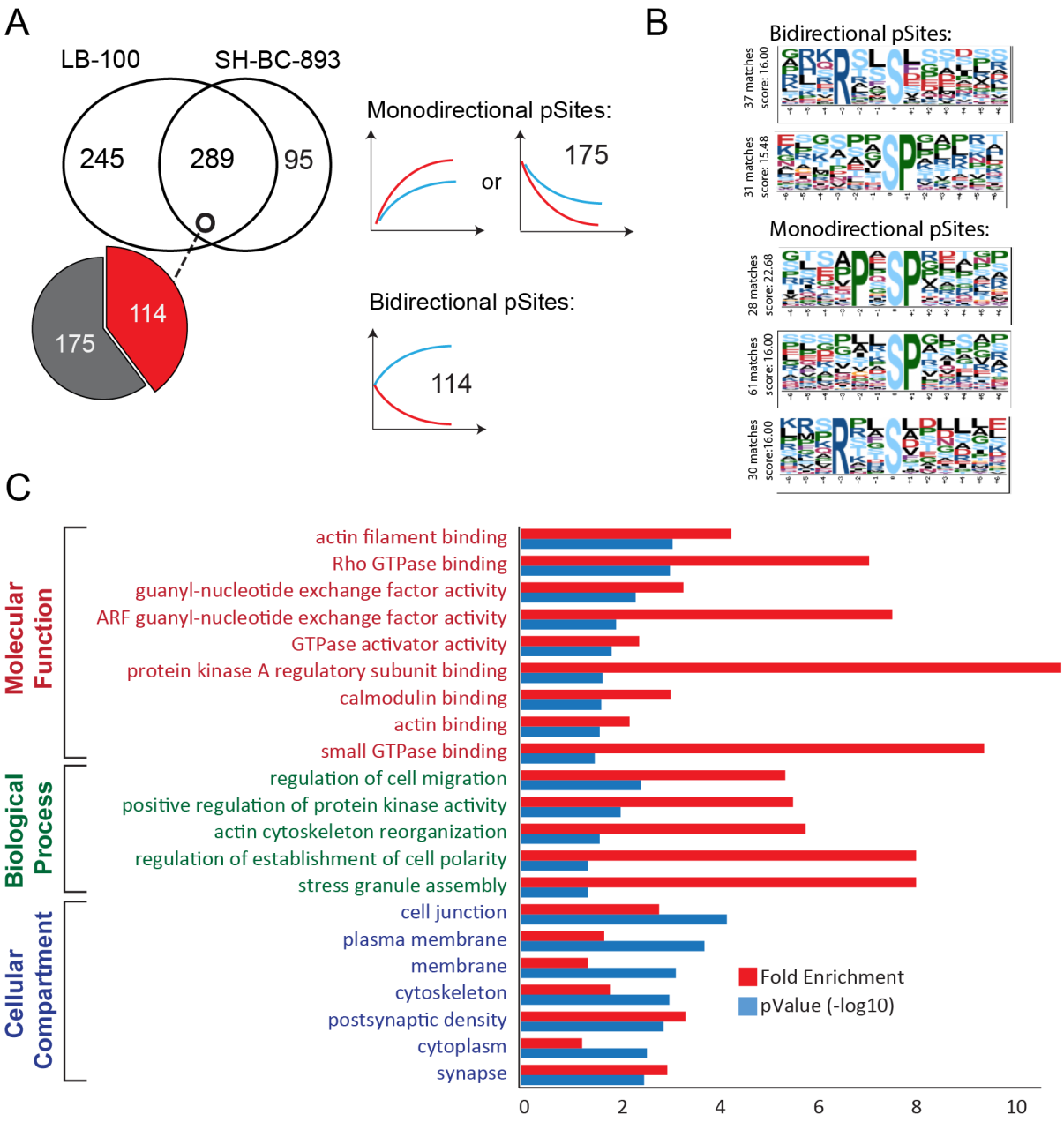

Figure 4.4. Comparison of dynamic phosphorylation sites following SH-BC-893 and LB-100 treatments.

A) Venn diagram showing that 292 phosphosites are common to both treatments while 253 and 98 phosphosites are uniquely regulated by LB-100 and SH-BC-893, respectively. Of the 292 common sites, 116 sites showed opposite (Bidirectional) tends and 176 sites are regulated in the same direction (Monodirectional). B) Phosphorylation motifs extracted from motif-x. Monodirectional phosphosites display PxSP and SP motifs. Bidirectional sites that show rapid changes in phosphorylation are present on Serine-rich peptides. C) Gene Ontology enrichment of proteins corresponding to the 214 bidirectional and unidirectional (for SH-BC-893) phosphosites.

A literature analysis was performed to determine whether dynamic profiles had been previously identified as PP2A interactors [36-38]. This analysis revealed that 30 proteins (37 phosphosites)

identified in our screen were common with PP2A-interactors identified in other reports [36-38] (Figure 4.5A, Supplementary Table S4-4). Closer examination of these data indicated that 15 of these proteins are interconnected through a protein-protein interaction network and that 6 of these members (Vim, Pxn, Pak2, Gsk3β, Cfl1, Arhgef2) are known regulators of cytoskeleton organization (Figure 4.5B). Phosphorylation profiles of these substrates are shown in Figure 4.5C. Previous reports have indicated that Vimentin (Vim) phosphorylation at several residues, including Ser42 and Ser430, is regulated by PP2A and functionally important [39, 40]; inactivation of vimentin leads to increased actin stress fiber assembly [41]. The cytoskeletal protein Paxillin (Pxn) that regulates the actin-membrane attachment showed a rapid dephosphorylation at site Ser83 upon the first 5 min of SH-BC-893 treatment followed by a recovery and a more gradual decrease in phosphorylation that extended over the entire stimulation period. The closely located phosphorylation sites Pxn Thr31 and Thr118 have previously been reported to regulate cell migration in a RhoA dependent manner [42, 43]. The cytoskeleton organizing kinase Pak2 showed strong dephosphorylation on Ser141. Furthermore, Arhgef2 Ser122 showed a rapid dephosphorylation upon SH-BC-893 treatment. This site is proximal to Ser143 previously described to impact F-actin based morphological changes [44]. The actin depolymerizing protein Cofilin1 (Cfl1) showed a progressive increase in phosphorylation at Ser3, a site whose phosphorylation inactivates the actin-depolymerizing activity of cofilin [45]. Similarly, SH-BC-893 induces phosphorylation of the glycogen synthase kinase 3 b (Gsk3b) on Ser9, a site that has previously been reported to regulate the reorganization of cytoskeleton forming microtubules [46]. With the exception of Cfl1 Ser3, all sites described above showed differential regulation upon SH-BC-893 and LB-100 treatments.

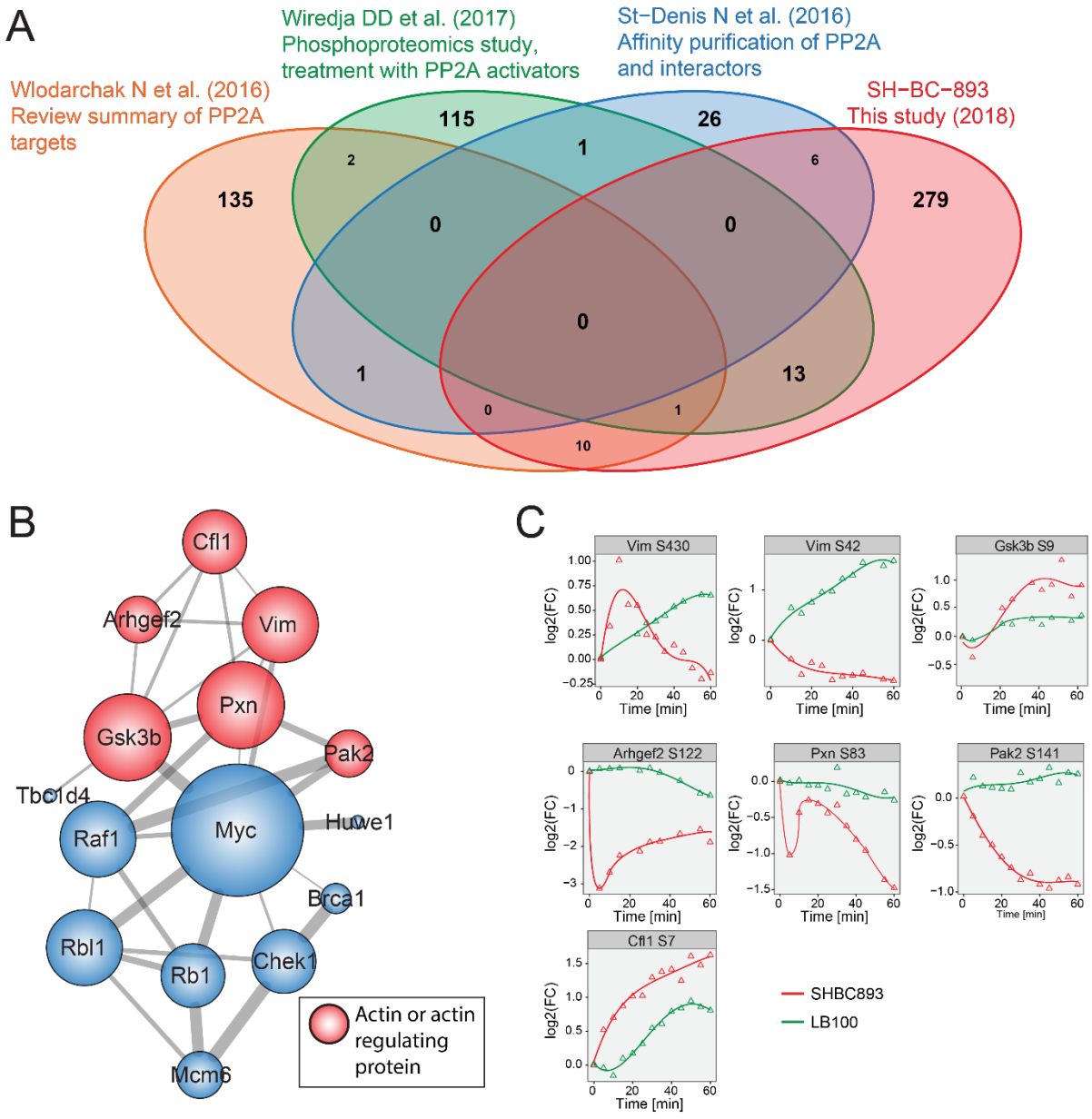

Figure 4.5. Identification of putative PP2A targets.

A) Comparative analysis of the list of candidate PP2A substrates identified from various proteomic studies. The comparison was done at the protein level since not all datasets reported the position of the phosphorylated sites. B) A network of phosphorylation sites identified as direct PP2A targets based on comparative literature review. Color coding indicates if the proteins are involved in actin reorganization. C) Dynamic profiles of sites from putative PP2A targets involved in actin reorganization.

4.5.3 Dynamic phosphoproteomics identifies distinct cell signaling events associated with C2-ceramide and SH-BC-893

While both SH-BC-893 and C2-ceramide down-regulate nutrient transporters in a PP2A-dependent manner, only SH-BC-893 promotes cytoplasmic vacuolation (Figure 4.1). Quantitative phosphoproteomics experiments performed on FL5.12 cells treated with SH-BC-893 or C2-ceramide enabled the identification of cell signaling events differentially associated with these compounds. Dynamic profiles again formed three distinct clusters according to fuzzy clustering, displaying rapid or progressive increases or decreases in phosphorylation or an adaptation-like response (Figure 4.6A and B). In total, we identified 428 dynamic profiles, of which 254 profiles were common to SH-BC-893 and C2-ceramide (Figure 4.6C). Approximately 80% of common profiles (203 of 254 profiles) showed a mono-directional trend where progressive changes in protein phosphorylation were similar both in magnitude and direction for these two compounds consistent with the fact that these agents produce largely overlapping phenotypes in cells. Interestingly, 51 of the 254 common profiles showed opposite trends, while 126 or 48 profiles were uniquely regulated by C2-ceramide or SH-BC-893, respectively. These differentially regulates sites could be responsible for divergent phenotypes such as vacuolation.

To correlate phosphorylation changes with the distinct vacuolation phenotypes associated with C2-ceramide and SH-BC-893, dynamic profiles were separated into three groups: 1) Common and mono-directional profiles, 2) Bi-directional profiles or dynamic profiles unique to SH-BC-893 and 3) Dynamic profiles unique to C2-ceramide. GO term enrichment analyses were performed to determine if these groups were related to specific cellular compartments and molecular functions. Results from the corresponding analyses are displayed in the radar plots of Figure 4.6D. The majority of profiles identified belong to group 1 (203 shared monodirectional profiles) and are likely to account for phenotypes induced by both C2-ceramide and SH-BC-893 (e.g., nutrient transporter down-regulation). These profiles correspond to substrates that are largely involved in the regulation GTPase activity and actin cytoskeleton organization. Profiles from group 2 that showed opposite trends or are specific to SH-BC-893 treatment (99 profiles) were associated with the GO terms: endosome, intracellular membrane bound organelle and plasma membrane. Amongst these we found 11 phosphorylation sites on 9 proteins involved in vesicle trafficking and lysosomal fusion (Supplementary Figure 4.5). This result is consistent

with findings that SH-BC-893 but not C2-ceramide inhibit lysosomal trafficking events [5]. Group 3 comprises 126 profiles that are unique to C2-ceramide treatment. Phosphorylated substrates associated with this group are mostly localized in the nucleus with functional GO terms enriched for DNA binding, Chromatin binding and “DNA-directed DNA polymerase activity”. A protein-protein interaction network of the corresponding phosphoproteins highlights several of the corresponding members and regroups proteins involved in DNA replication, DNA repair, nucleotide synthesis, and ribosome assembly (Supplementary Figure 4.6).

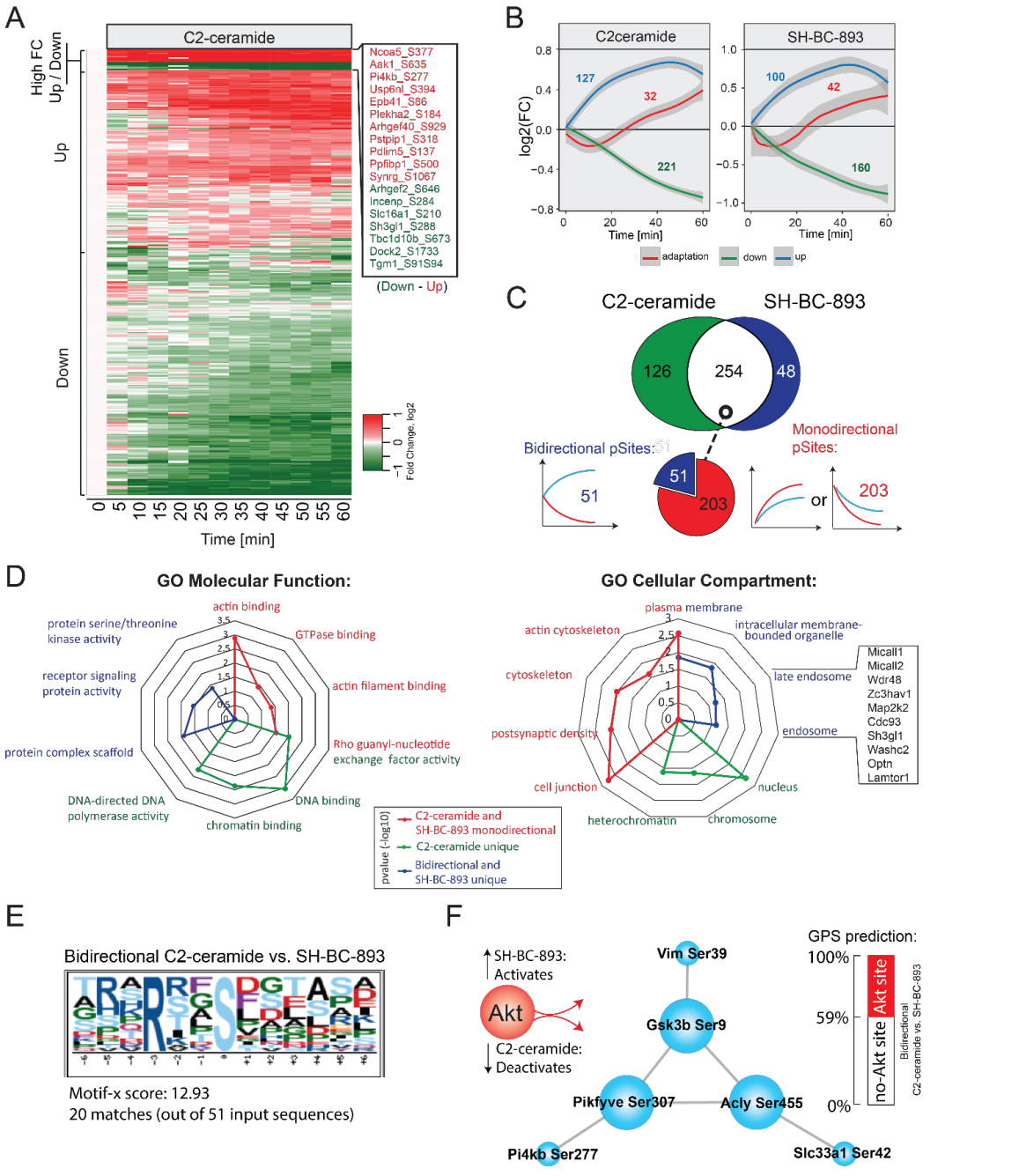

Figure 4.6. Dynamic phosphoproteomics identifies signaling events differently regulated by C2-ceramide and SH-BC-893 treatments.

A) Heatmap corresponding to 380 phosphorylation sites that were dynamically phosphorylated upon C2-ceramide treatment. Kinetic trends are indicated. B) Dynamic profiles extracted from C2-ceramide and SH-BC-893 treatments using fuzzy means clustering. Numbers correspond to profiles observed for a given cluster. C) Venn diagram of dynamic phosphosites showing that 254 phosphosites are common, 126 and 48 phosphosites are uniquely regulated by C2-ceramide and SH-BC-893, respectively. Of the 254 commonly regulated sites, 51 show opposite change in phosphorylation (bidirectional) and 203 are regulated in the same direction (monodirectional). D) Radar plot showing the enrichment of GO terms associated with specific groups highlighted in different colors. E) Motif-X analyses of bidirectional sites showing an over-representation of basophilic motifs. F) Network of putative Akt substrates and known interacting members.

Next, we analyzed dynamic profiles from each group with Motif-X to determine if a specific phosphorylation consensus sequence was over-represented in these datasets (Supplementary Figure 4.7A). These analyses indicated that a large proportion of dynamic profiles were represented by proline-directed and basophilic phosphorylation motifs. Further analyses performed with the kinase prediction software available from the Group-based Prediction System (GPS) [47] identified Akt as a putative kinase targeting dynamic basophilic motifs. Interestingly, bidirectional sites from group 2 comprised the largest proportion of putative Akt substrates from all groups (Figure 4.6E and Supplementary Figure 4.7B). Among the 21 putative Akt substrates from group 2, we identified 6 proteins (Vim, Slc33a1, Gsk3b, Pikfyve, Acly, Pi4kb) that are known to interact with each other, including 3 proteins (Gsk3b, Pikfyve, Acly) previously reported as Akt substrates [48-50] (Figure 4.6F). For convenience, Supplementary Figure 4.8 presents the kinetic phosphorylation profiles of several Akt substrates. Together, these results suggest that a subset of bidirectional sites are putative Akt substrates associated with vesicle trafficking and could account for the vacuolation phenotype observed only with SH-BC-893.

4.5.4 SH-BC-893 and C2-ceramide stimulate actin polymerization that is necessary for cytoplasmic vacuolation but not surface nutrient transporter loss

To gain a systems-level view of changes in protein phosphorylation observed for C2-ceramide and SH-BC-893, we used GO terms enriched in our datasets (Figure 4.6D, Supplementary Table S4-5) combined with manual curation of gene lists to generate a pictogram of regulated phosphosites (Supplementary Figure 4.9). Protein groups of interest included membrane transport, endocytosis/cell adhesion, actin reorganization, nutrient transport and GTPase regulation (GTPase activators, GAPs and guanidine nucleotide exchange factors, GEFs).

Because dynamic phosphorylation sites similarly affected by SH-BC-893 and C2-ceramide were clustered in proteins that modulate actin dynamics (Figure 4.6D), actin polymerization was monitored in SH-BC-893- or C2-ceramide-treated FL5.12 cells using fluorescently-conjugated phalloidin. Both SH-BC-893 and C2-ceramide robustly increased F-actin formation in the cell

cortex and in a cytosolic, likely endosomal, compartment (Figure 4.7A). Similar effects were observed in murine embryonic fibroblasts (MEFs) and in HeLa cells (data not shown). Consistent with a role for PP2A activation in this phenotype, the PP2A inhibitors LB-100 and calyculinA (CalyA) blocked actin polymerization at both locations (Figure 4.7B). The actin polymerization inhibitor Latrunculin A (LatA) also prevented actin polymerization with SH-BC-893 and C2-ceramide (Figure 4.7C). However, while LB-100 blocked CD98 down-regulation induced by SH-BC-893 or ceramide (Figure 4.1B), LatA did not suggesting that the loss of surface transporters depends on PP2A activation but not actin polymerization (Figure 4.7D). This result was unexpected, as actin polymerization is essential for nutrient permease downregulation by sphingolipids in yeast [51]. Interestingly, LatA reversed vacuolation by SH-BC-893 (Figure 4.7E). The actin polymerization stimulator Jasplakinolide did not promote vacuolation on its own (data not shown). Together, these data suggest that both C2-ceramide and SH-BC-893 stimulate actin polymerization in a PP2A-dependent manner and that actin polymerization is necessary but not sufficient to produce cytoplasmic vacuolation.

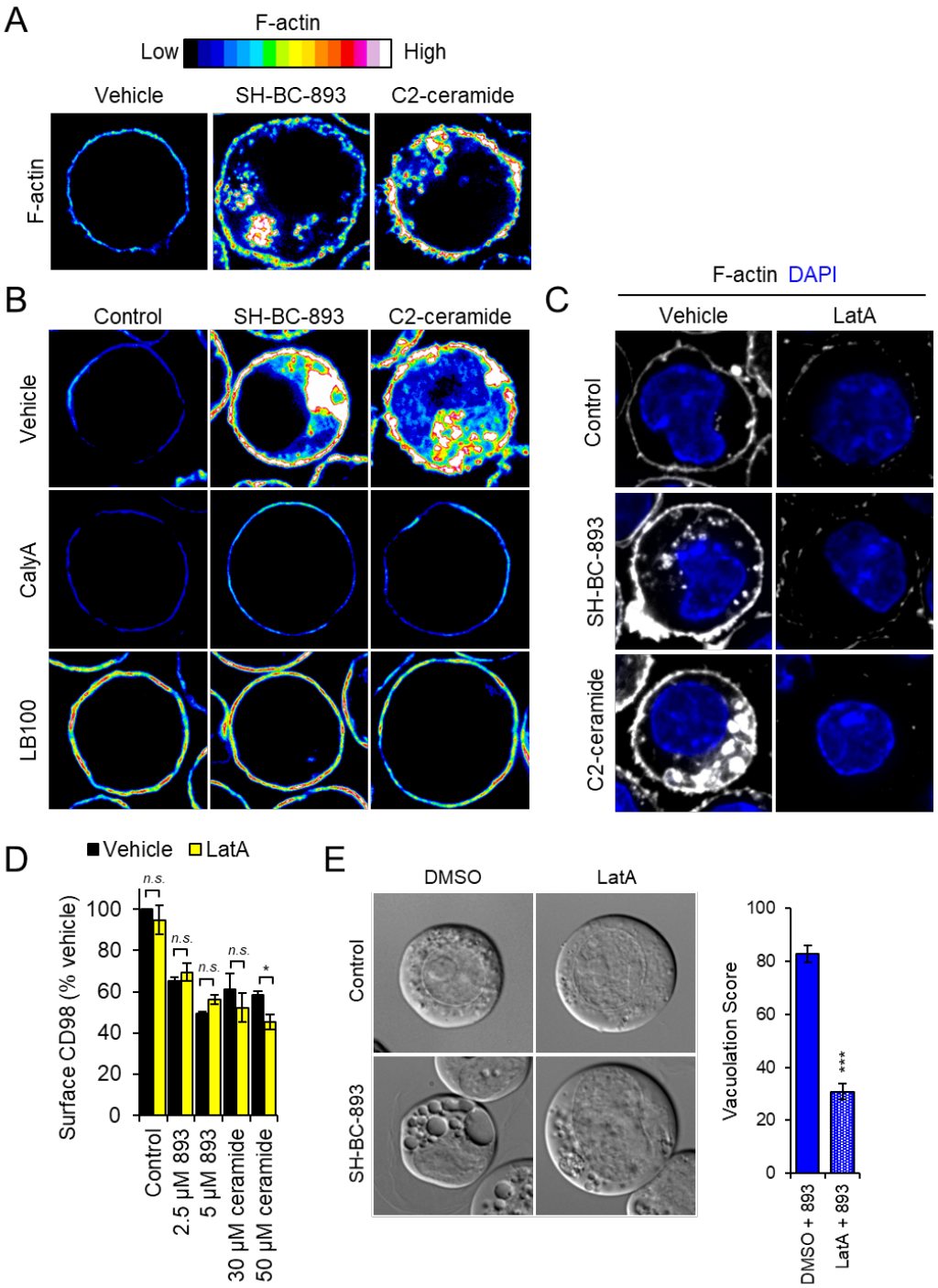

Figure 4.7. C2-ceramide and SH-BC-893 promote actin polymerization.

A) FL5.12 cells treated with SH-BC-893 (10 µM) or C2-ceramide (50 µM) for 1 h and then stained for F-actin with Alexa Fluor 488-conjugated phalloidin. B) Same as in A), except cells pre-treated with vehicle or PP2A inhibitors calyculinA (calyA, 5 nM) or LB100 (10 or 100 µM) for 1.5 h prior to SH-BC-893 addition. C) Same as in A), except cells pre-treated with vehicle or actin polymerization inhibitor latrunculinA (LatA, 1 µM) for 30 min prior to SH-BC-893 (2.5 µM) or C2-ceramide (30 µM) addition. D) FL5.12 cells pre-treated (30 min) with LatA (1 µM) were treated with SH-BC-893 (2.5 or 5 µM) or C2-ceramide (30 or 50 µM) for 1 h and surface CD98 quantified by flow cytometry. E) FL5.12 cells pre-treated with LatA (30 min, 1 µM) were treated with SH-BC-893 (5 µM) for 2 h and imaged by DIC microscopy to visualize vacuoles. $n = 2$ in D). $n \geq 30$ cells per condition in E). In E), using two-tailed t-test to compare 893-treated cells to combination of LatA and 893, *** = $p \leq 0.001$.

4.5.5 Ceramide inhibits SH-BC-893-induced vacuolation by inactivating Akt

The finding that ceramide results in the dephosphorylation of more proteins than SH-BC-893 suggested that, rather than failing to induce vacuolation, ceramide may dephosphorylate and inactivate a proteins necessary for vacuolation. In support of this model, co-addition of C2-ceramide inhibited cytoplasmic vacuolation by SH-BC-893 in FL5.12 cells (Figure 4.8A). Similar results were obtained in HeLa cells and murine prostate cancer epithelial cells (Supplementary Figure 4.10A and not shown). As highlighted in Supplementary Figure 4.8, multiple Akt substrates were dephosphorylated in cells treated with C2-ceramide but not SH-BC-893. That the effect of C2-ceramide was dominant was confirmed in Figure 4.8B and Supplementary Figure 4.10, B,C by monitoring the Akt-dependent phosphorylation of PRAS40 at threonine 246 [52]. These observations suggested that C2-ceramide may block vacuolation by inactivating Akt. Consistent with this model, the allosteric Akt inhibitor MK2206 reduced both Akt activity and vacuolation in FL5.12 cells treated with SH-BC-893 (Figures 4.8B,C); similar results were obtained in mPCE prostate cancer cells (Supplementary Figures 4.10C,D). The deletion of Rictor, an mTORC2 component necessary for Akt activation [53], also blocked vacuolation in the presence of SH-BC-893 again suggesting that Akt activity is essential for this phenotype (Figure 4.8D). Together, these data suggest that C2-ceramide does not vacuolate cells because Akt inactivation prevents the manifestation of this phenotype.

Two Akt substrates that are dephosphorylated in the presence of C2-ceramide but not SH-BC-893, Pikfyve and Pik4b, regulate late endocytic trafficking [54, 55]. Gsk3b also localizes to MVBs and lysosomes and may regulate their function [56]. Consistent with its phosphorylation by Akt, GSK3b Ser9 phosphorylation increases with SH-BC-893 but decreases with C2-ceramide (Supplementary Figure 4.8). Because Ser9 phosphorylation inhibits Gsk3b activity [57], Gsk3b inhibition may contribute to vacuolation. To test this, SH-BC-893 or C2-ceramide was combined with the Gsk3b inhibitor CHIR99021 and vacuolation monitored. While CHIR99021 did not vacuolate on its own or induce vacuolation in C2-ceramide-treated cells, CHIR99021 enhanced vacuolation of FL5.12 cells by SH-BC-893 (Figure 4.8E). This effect was much more dramatic in HeLa cells where CHIR99021 also sensitized cells to SH-BC-893

induced death despite its complete lack of toxicity as a single agent (Supplementary Figures 4.10E,F). These data suggest that SH-BC-893, but not C2-ceramide, vacuolates cells because Akt continues to inhibit Gsk3b.

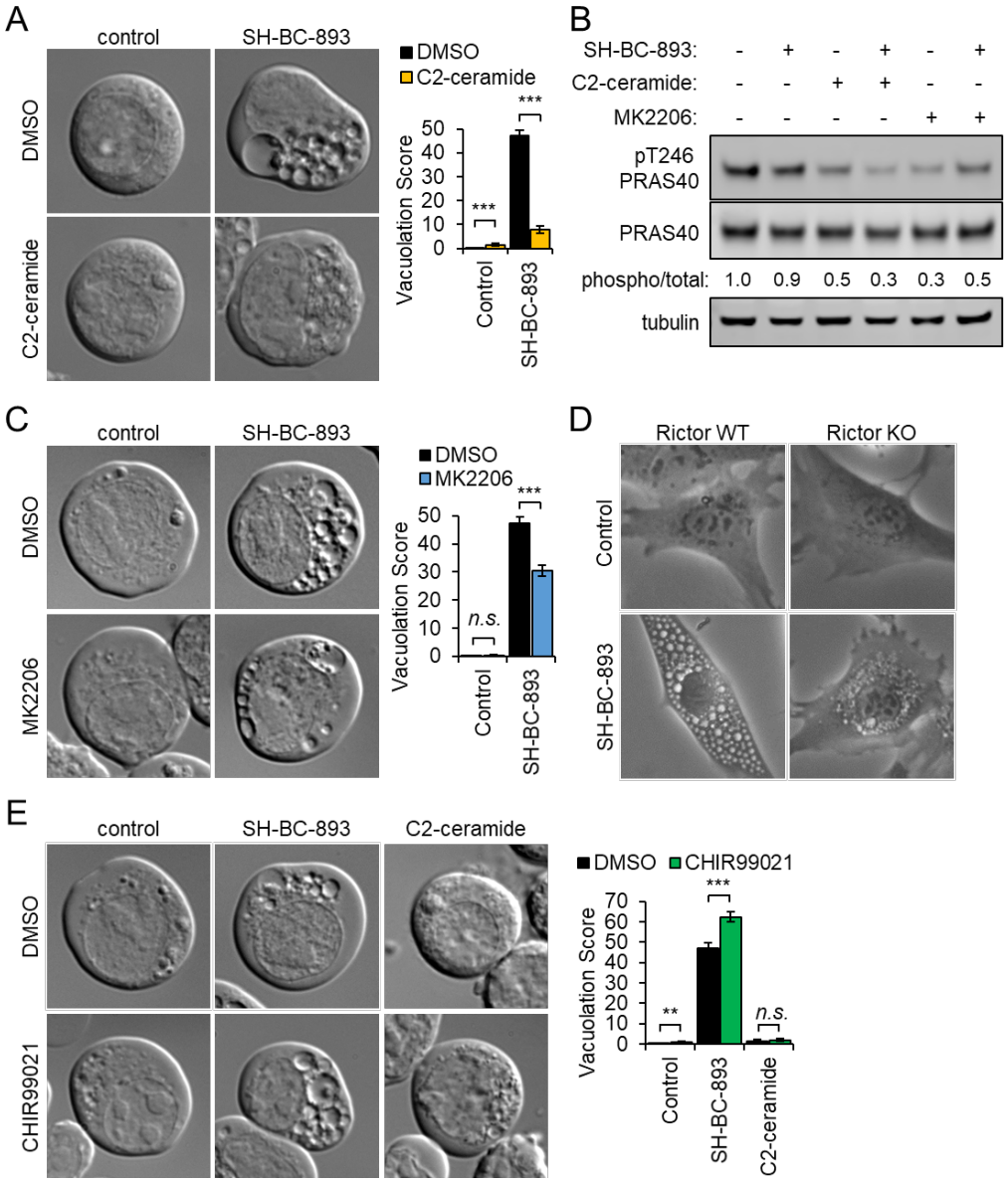

Figure 4.8. Ceramide inhibits vacuolation by reducing Akt activity.

A) FL5.12 cells were treated for 3 h with SH-BC-893 (2.5 μM) and/or C2-ceramide (50 μM) as indicated and imaged by DIC microscopy. B) Western blot measuring the phosphorylation of the AKT substrate PRAS40 (total and phospho-Thr246) in FL5.12 cells treated for 30 min with SH-BC-893 (5 μM), C2-ceramide (50 μM), and/or MK2206 (1 μM) as indicated. C) FL5.12 cells treated for 3 h with SH-BC-893 (2.5 μM) and/or AKT inhibitor MK2206 (1 μM) as indicated and visualized as in (A). D) Rictor WT and KO murine embryonic fibroblasts (MEFs) treated for 6 h with vehicle or SH-BC-893 (5 μM) then visualized by phase contrast microscopy. E) FL5.12 cells treated for 3 h with SH-BC-893 (2.5 μM) or C2-ceramide (50 μM) and the Gsk3b inhibitor CHIR99021 (10 μM) as indicated; visualized as in (A). In (A,C,E), ≥ 400 cells per condition were analyzed from a total of three independent experiments; using a two-tailed t-test to compare either SH-BC-893 or C2-ceramide to the vehicle control (in E) or SH-BC-893 alone to the combination of SH-BC-893 with C2-ceramide (A), MK2206 (C), or CHIR99021 (E), *n.s.* = not significant, ** = $p \leq 0.01$, or *** = $p \leq 0.001$.

4.6 Discussion

In this study, quantitative phosphoproteomics was used to identify phosphoproteins that responded differentially to pharmacological compounds that modulate PP2A activity and to correlate the PP2A-dependent phenotypes that affect intracellular trafficking and nutrient transporter loss. Time-resolved phosphoproteome analyses of FL5.12 cells treated with the PP2A agonist SH-BC-893 or the PP2A inhibitor LB-100 enabled the identification of putative PP2A substrates and phosphorylation events specific to each compound. These analyses confirmed that SH-BC-893 affected PP2A activity as approximately 75% of phosphorylation sites (289 out of 384 sites) were also targeted by LB-100. A more detailed analysis of the dynamic changes in protein phosphorylation common to LB-100 and SH-BC-893 revealed that 40% of these profiles displayed the expected reciprocal response and could represent putative PP2A substrates. A significant proportion of these targets are involved in the regulation of cell migration and actin cytoskeleton organization, including previously known PP2A substrates such as Vim, Pxn, Pak2, and Arhgef2.

Gene ontology analysis of phosphoproteins that were dynamically regulated monodirectionally by SH-BC-893 and C2-ceramide suggested that changes in actin dynamics contribute to the intracellular trafficking defects observed in sphingolipid-treated cells (Figure 4.6D) and led to the discovery that both SH-BC-893 and C2-ceramide promote PP2A-dependent actin polymerization at the cell cortex and in the cytoplasm (Figures 4.7A,B). Given that actin polymerization plays an important role in sphingolipid-induced nutrient transporter internalization in yeast [51], it was surprising that actin polymerization was not necessary for down-regulation of nutrient transporter proteins by SH-BC-893 and C2-ceramide (Figures 4.7C,D). Moreover, rather than contributing the shared phenotype, loss of surface nutrient transporters, actin polymerization was necessary for a phenotype observed uniquely in SH-BC-893-treated cells, vacuolation (Figure 4.7E). As vacuolation contributes to the anti-neoplastic activity of SH-BC-893 *in vitro* and *in vivo* [5], the molecular mechanism underlying this phenotype is of significant interest.

The differential ability of SH-BC-893 and C2-ceramide to produce vacuolation (Figure 4.1C) led us to hypothesize that cell signaling events responsible for vacuolation would be encompassed in phosphosites that varied in opposite manner in SH-BC-893- and C2-ceramide-treated cells. A basophilic phosphorylation motif typical of Akt substrates was enriched among these differentially regulated dynamic sites; multiple Akt substrates were dephosphorylated in C2-ceramide-, but not SH-BC-893-treated, cells (Figure 4.6F and Supplementary Figure 4.8). It has been widely reported that ceramide reduces the phosphorylation and activity of Akt [58]. In contrast, Akt Ser473 phosphorylation was maintained in SH-BC-893-treated cells not just in this study (Supplementary Figure 4.10A,B), but also in vivo in autochthonous prostate tumors [5]. Differential regulation of Akt activity by SH-BC-893 and C2-ceramide might result if these sphingolipids activate PP2A through distinct mechanisms. Alternatively, as SH-BC-893 is water soluble to >60 mM while C2-ceramide is poorly soluble in aqueous solutions, these compounds may activate PP2A in different subcellular compartments. Membrane-localized C2-ceramide may activate plasma-membrane localized PP2A more effectively than SH-BC-893; Akt is activated by kinases found at the plasma membrane [59]. It is also possible that SH-BC-893 and C2-ceramide differentially regulate the phosphorylation of the PP2A regulatory subunit B56β (Ppp2r5b) by Clk2 thereby affecting the interaction between Akt and PP2A [60, 61]. Regardless of the mechanism underlying differential Akt activation by these sphingolipids, the reduction in vacuolation when Akt was inhibited by MK2206, Rictor deletion, or C2-ceramide demonstrate that Akt activity is necessary for SH-BC-893-induced vacuolation (Figures 4.8A-D and Supplementary Figures 4.10A-D). In summary, these phosphoproteomics studies led to the unexpected discovery that C2-ceramide was dominant over SH-BC-893 in vacuolation assays (Figure 8A and Supplementary Figure 4.10A) and the conclusion that, rather lacking an activity possessed by SH-BC-893, ceramide fails to vacuolate cells because it inactivates Akt.

A detailed mechanistic understanding of how Akt activity supports vacuolation will require additional studies. However, the almost 2-fold increase or decrease in the phosphorylation of the Akt substrate Gsk3b phosphorylation at its inhibitory site Ser9 with SH-BC-893 or C2-ceramide, respectively (Supplementary Figure 4.8), and the accentuation of vacuolation by the Gsk3b inhibitor CHIR99021 (Figure 4.8E and Supplementary Figure 4.10E) suggest that Gsk3b may suppress vacuolation by positively regulating MVB function. Because CHIR99021 was not

sufficient to induce vacuolation in C2-ceramide treated cells (Figure 4.8E), it is likely that additional Akt substrates besides Gsk3b contribute to the vacuolation phenotype. Consistent with published studies showing that vacuolation contributes to the anti-neoplastic effects of SH-BC-893 [5], inhibition of Gsk3b also sensitized cells to SH-BC-893-induced death (Supplementary Figure 4.10F). Gsk3b inhibitors are currently being developed for treatment of acute myeloid leukemia and breast cancer. Considering these findings, there may be a strong rationale for combining Gsk3b inhibitors and SH-BC-893 in cancer treatment. In conclusion, global, kinetic phosphoproteomic screens utilizing PP2A-activating sphingolipids helped to elucidate signaling pathways necessary for cellular starvation by sphingolipids, and highlighted a key role for Akt and Gsk3b signaling in regulating lysosomal trafficking events.

4.7 Acknowledgements

This work was funded in part by the Natural Sciences and Engineering Research Council (NSERC) (P.T. 311598; S.H. 04726), grants to A.L.E. from the NIH (R01 GM089919, R21 CA178230), CDMRP (W81XWH-15-1-0010), the American Cancer Society (RSG-11-111-01-CDD), and the UCI CORCL. The Institute for Research in Immunology and Cancer (IRIC) receives infrastructure support from the Canadian Center of Excellence in Commercialization and Research, the Canadian Foundation for Innovation, and the Fonds de recherche du Québec - Santé (FRQS). Proteomics analyses were performed at the Center for Advanced Proteomic and Chemogenomics Analyses (CAPCA), a Node of the Genomic Technology Platform supported by the Canadian Government through Genome Canada. Imaging was performed in the Optical Biology Core at UCI which is supported in part by NIH P30 CA062203. The authors would like to thank David Sabatini (Whitehead Institute, MIT) for generously providing Rictor knockout MEFs.

4.8 Supplementary material

4.8.1 Supplementary figures

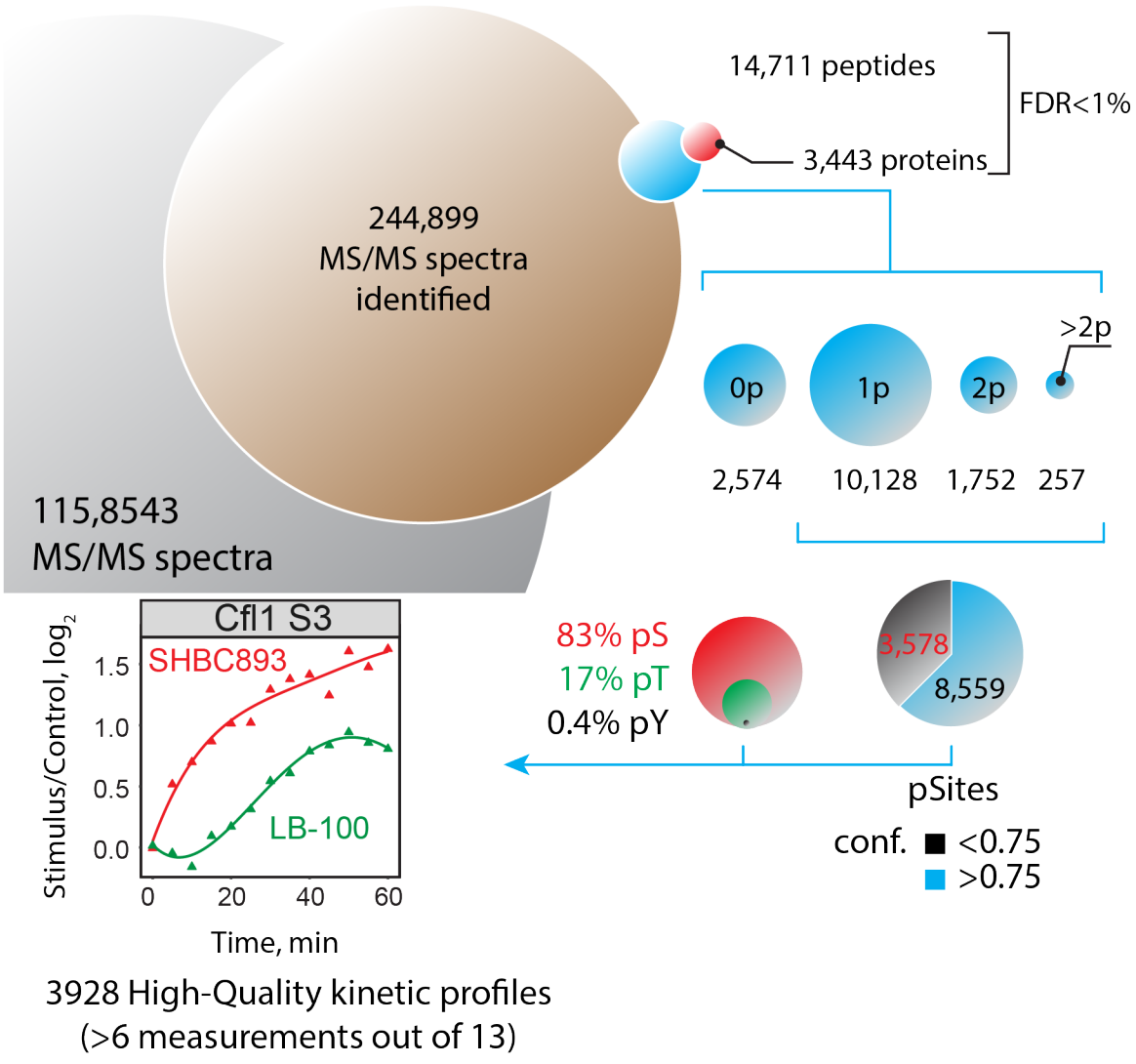

Supplementary Figure 4.1. Summary of statistics of triple SILAC phosphoproteomics experiment comparing LB-100 and SH-BC-893-treated FL5.12 cells.

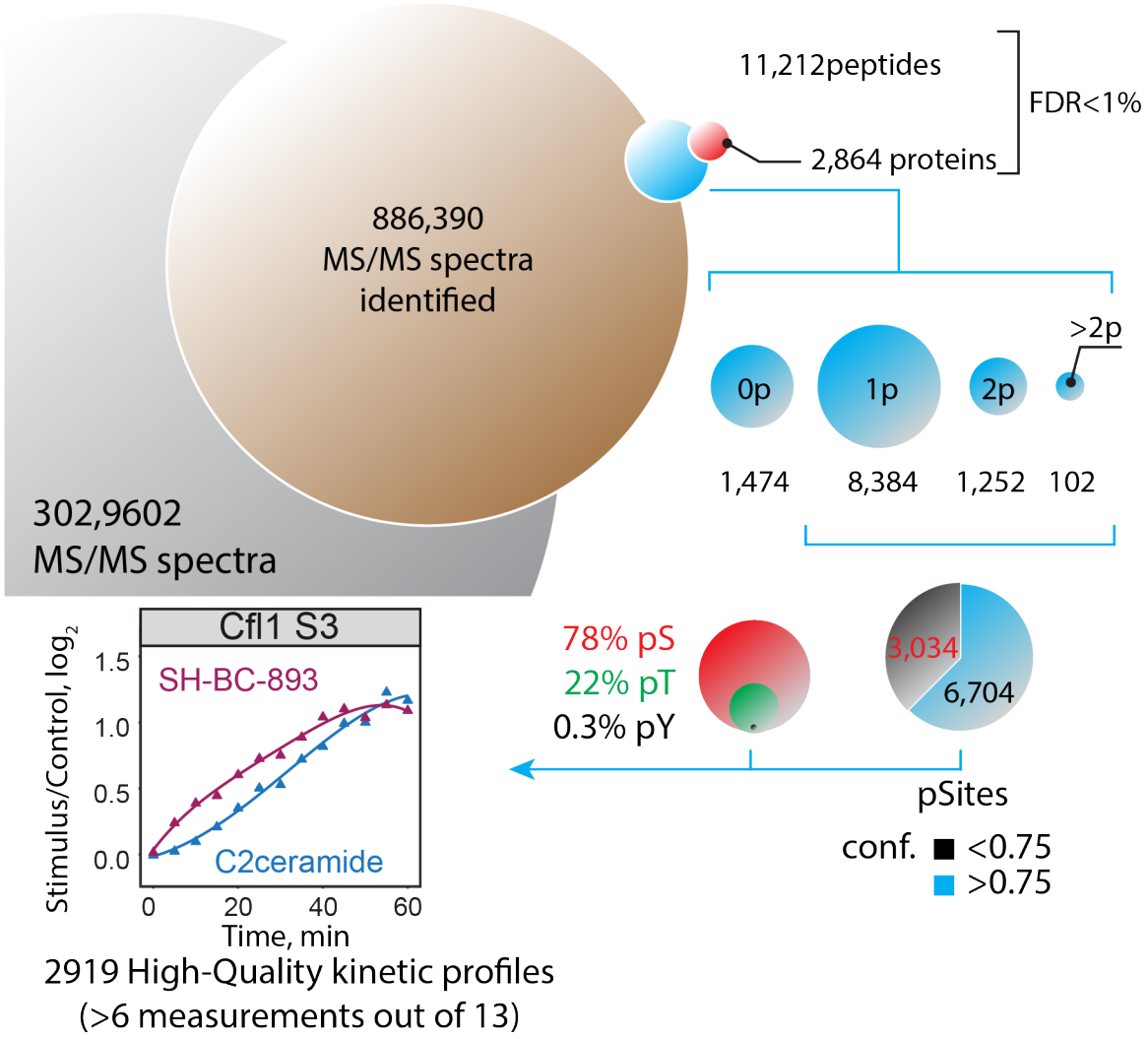

Supplementary Figure 4.2. Summary of statistics of triple SILAC phosphoproteomics experiment comparing C2-ceramide and SH-BC-893-treated FL5.12 cells.

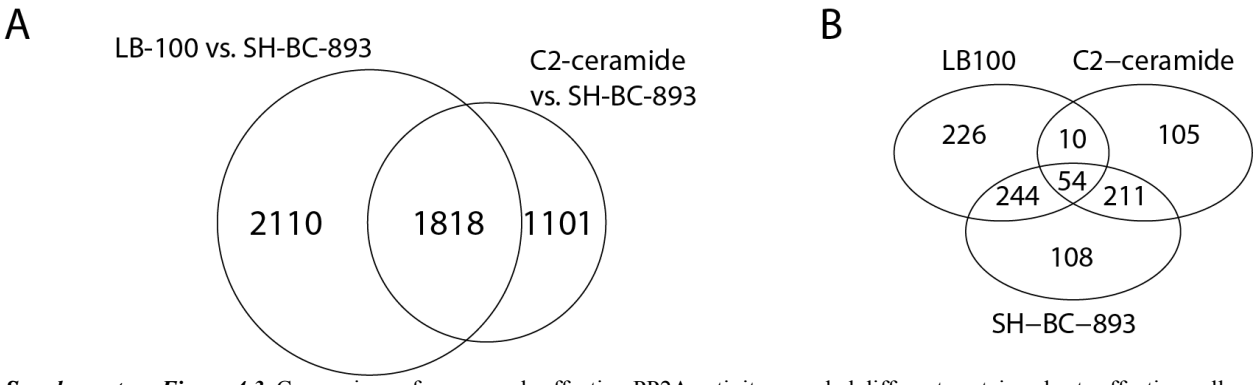

Supplementary Figure 4.3. Comparison of compounds affecting PP2A activity revealed different protein subsets affecting cell signaling.

A) Overlap of high quality kinetic profiles obtained from both triple SILAC experiments comparing either SH-BC-893 and LB-100 or SH-BC-893 and C2-ceramide. 1860 profiles were common to both experiments. B) Overlap of dynamically regulated phosphosites.

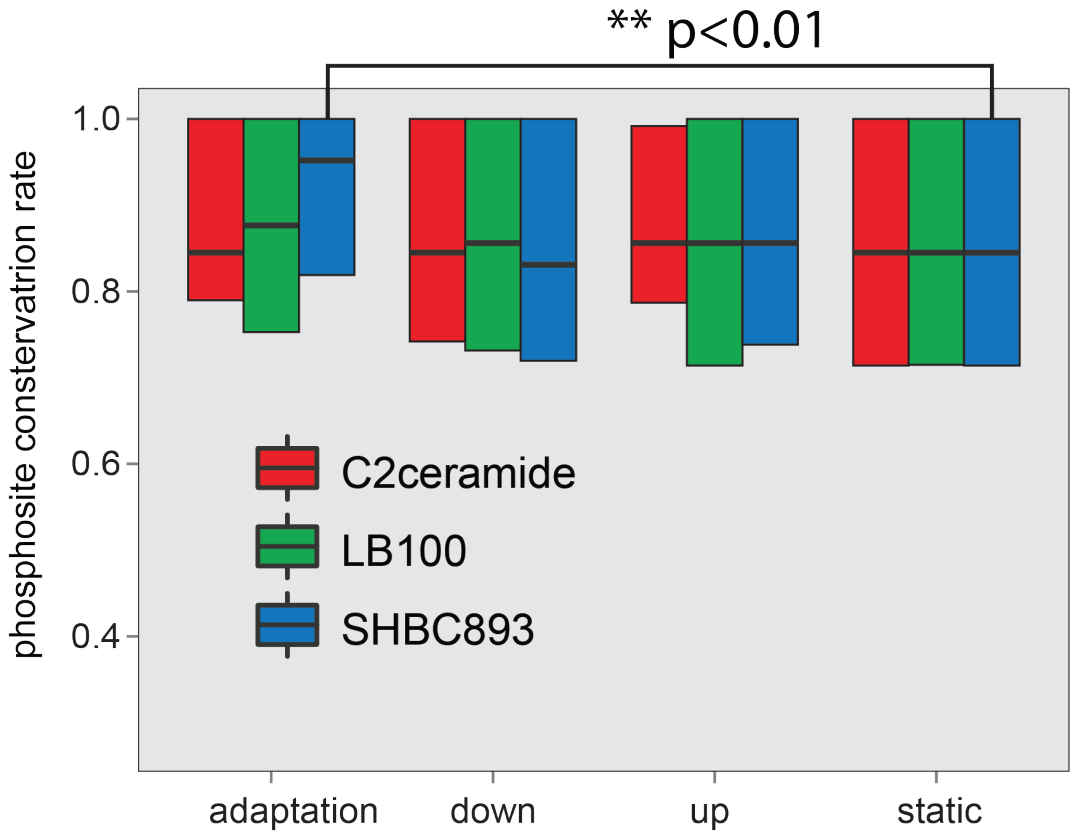

Supplementary Figure 4.4. Conservation rate analysis.

Conservation of phosphorylation sites was compared based on grouping of the kinetic profiles observed for different treatments. Phosphorylation sites showing adaptation-like behavior upon treatment with SH-BC-893 are more conserved across species.

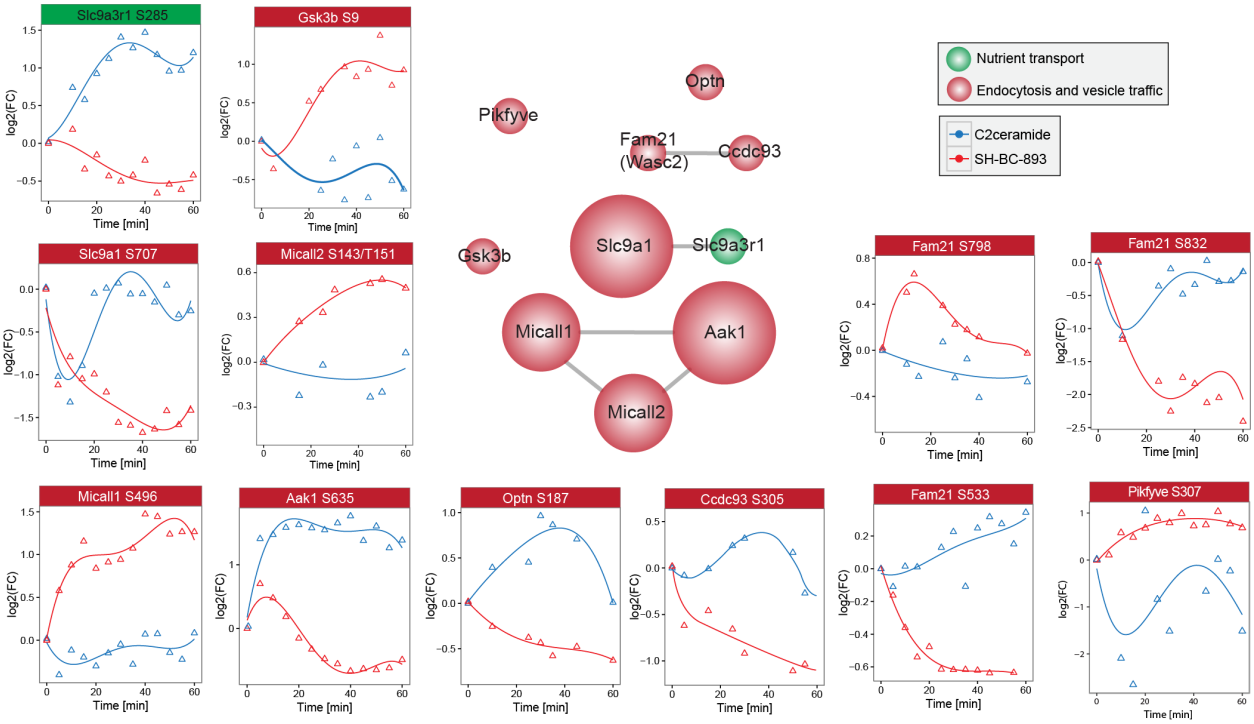

Supplementary Figure 4.5. Proteins from endosomes, late endosomes or intracellular membrane-bound organelles are differentially phosphorylated upon treatment with sphingolipids.

Partial network and kinetic profiles of phosphorylation from proteins following cell treatment with SH-BC-893 and C2-ceramide.

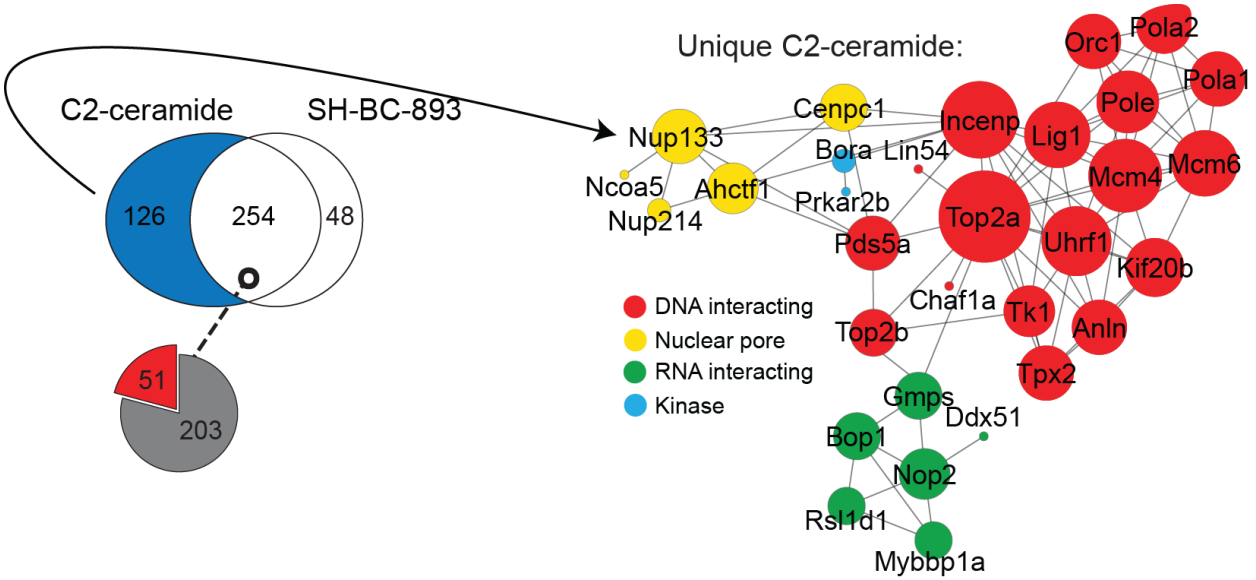

Supplementary Figure 4.6. Network of proteins that are uniquely phosphorylated upon C2-ceramide treatment.

Supplementary Figure 4.7. Consensus motif of phosphorylation sites observed in dynamic profiles from C2-ceramide and SH-BC-893 phosphoproteomic experiments.

A) Motif-X analyses of phosphorylation sites from three groups of dynamic profiles. B) Relative proportion of Akt sites within each group predicted from GPS 3.0 (http://gps.biocuckoo.org/).

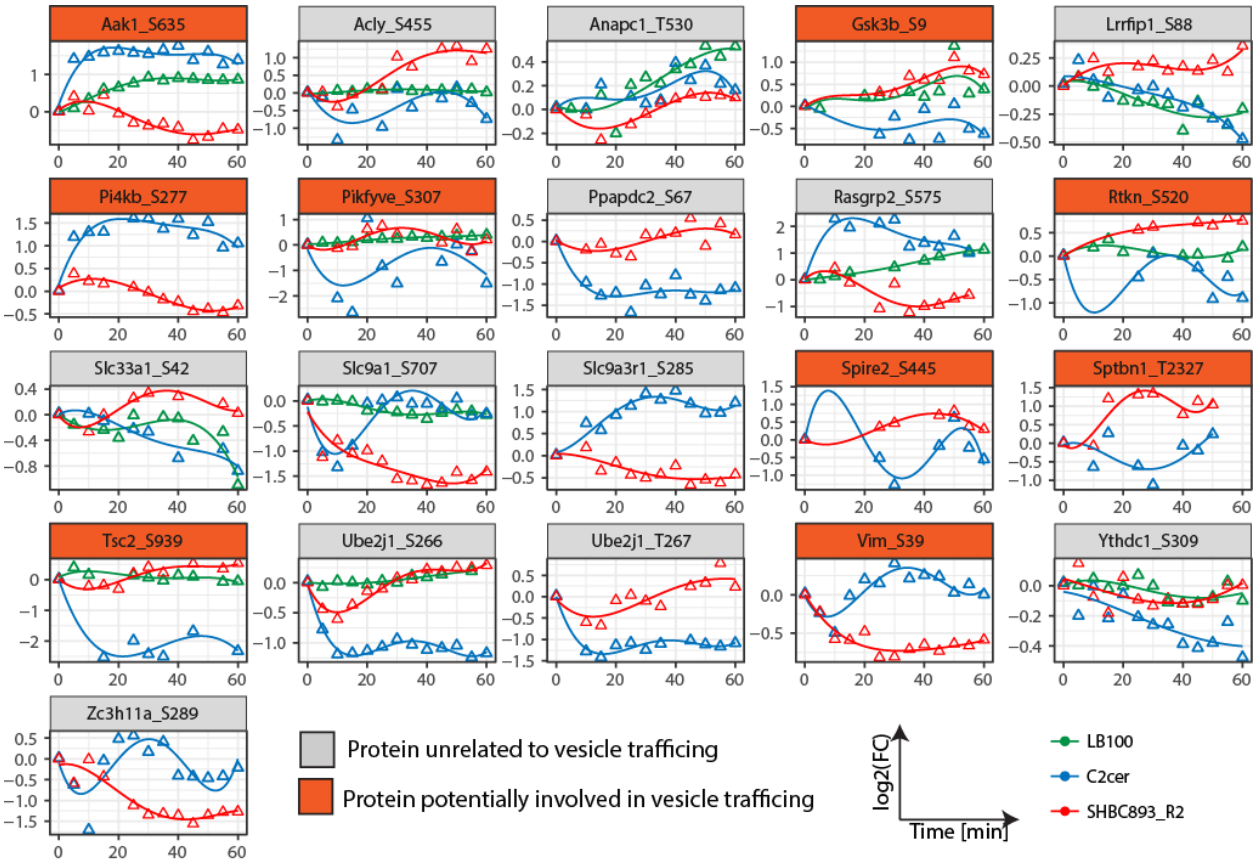

Supplementary Figure 4.8. Dynamic profiles of putative Akt substrates associated with vesicle trafficking.

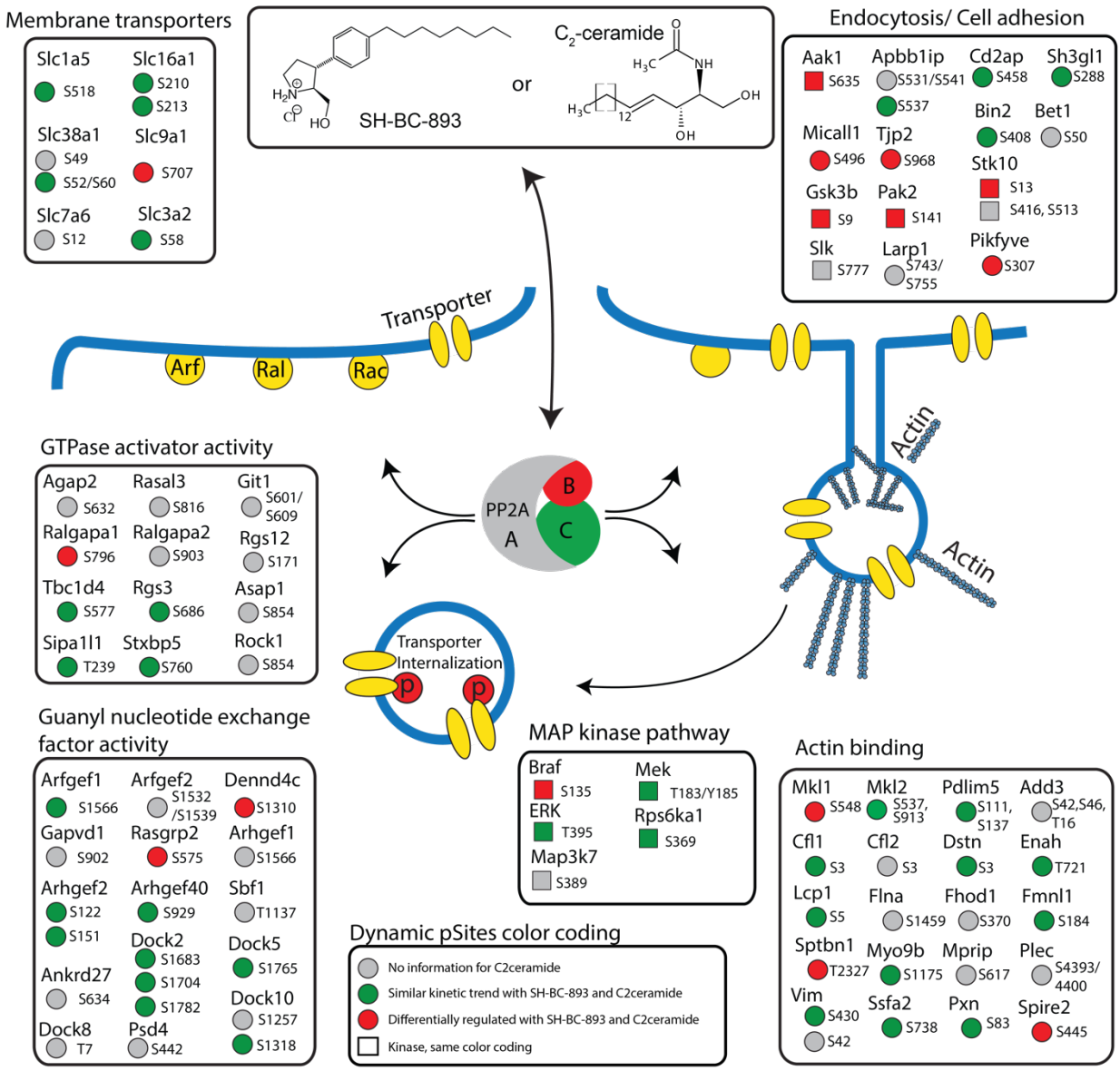

Supplementary Figure 4.9. Pictogram of proteins that are dynamically phosphorylated upon SH-BC-893 and C2-ceramide treatment.

Only proteins associated to the main GO term molecular functions (Membrane transport, GTPase and GEF regulation, Actin binding, Endocytosis) are shown. Color coding indicates differences and similarities observed between C2-ceramide and SH-BC-893 treatments.

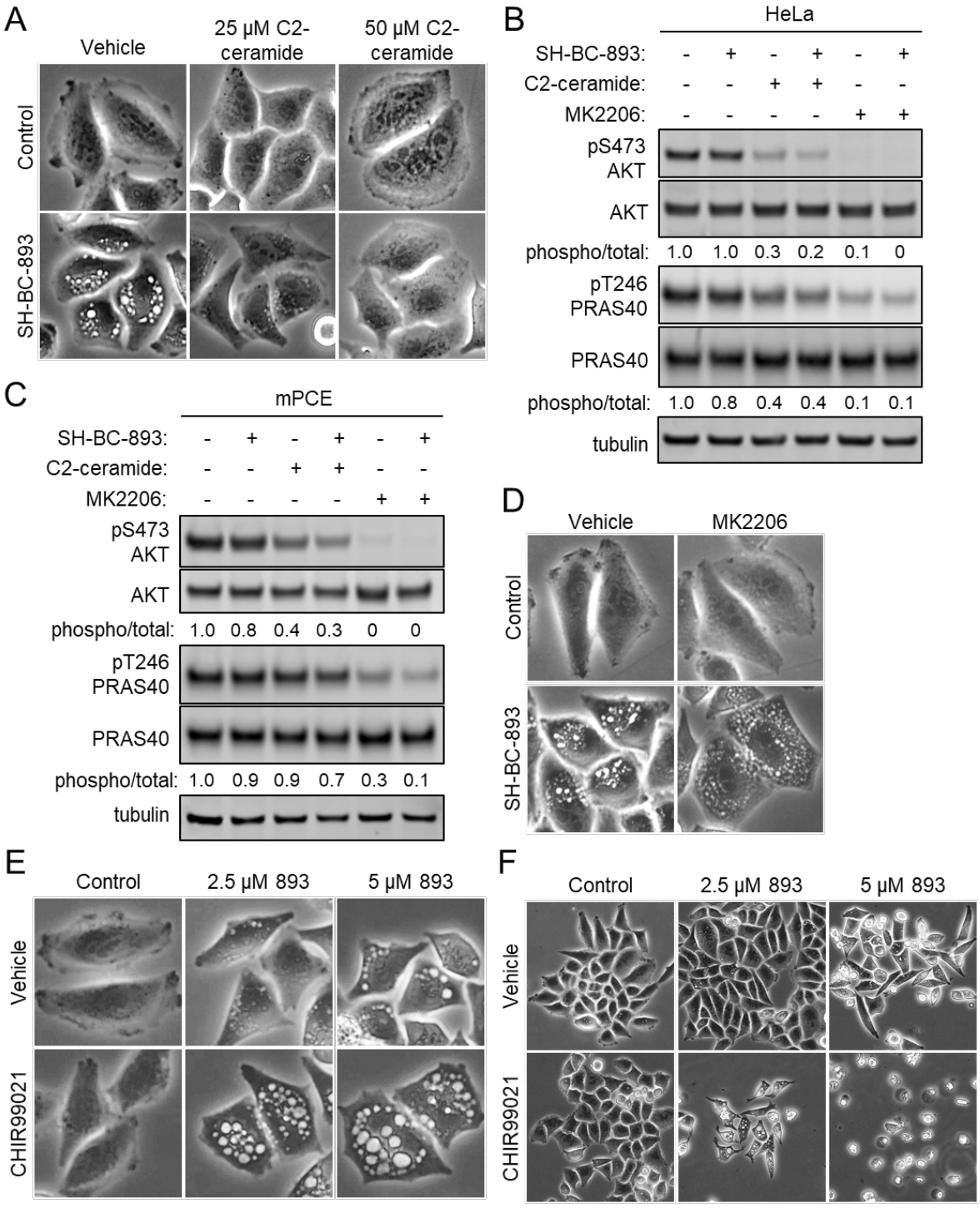

Supplementary Figure 4.10. Ceramide inhibits vacuolation in multiple cell lines by reducing Akt activity.

A) HeLa cells treated for 3 h with SH-BC-893 (5 μM) and the indicated concentrations of C2-ceramide were imaged by phase contrast microscopy to visualize vacuoles.(B) Western blot for AKT (total and phospho-Ser473), PRAS40 (total and phospho-Thr246) and tubulin (loading control) in HeLa cells treated for 30 min with SH-BC-893 (5 μM), C2-ceramide (50 μM), and/or MK2206 (1 μM). C) As in (B), except with mouse prostate cancer epithelial cells (mPCE). D) HeLa cells treated for 6 h with SH-BC-893 (5 μM) and/or the AKT inhibitor MK2206 (1 μM) were visualized as in (A). E) HeLa cells were treated for 6 h with indicated concentrations of SH-BC-893 or C2-ceramide and/or CHIR99021 (10 μM) as indicated and visualized as in (A). F) As in E, except at 24 h.

4.8.2 Supplementary tables

Supplementary Table S 4-1: MaxQuant search paramters (DVD-R).

Supplementary Table S 4-2: List of all identified phosphopeptide profiles (DVD-R).

Supplementary Table S 4-3: List of high quality phosphopeptide profiles (DVD-R).

Supplementary Table S 4-4: List of all dynamically regulated phosphoprofiles (DVD-R).

Supplementary Table S 4-5: Gene Ontology enrichment of phosphorylation sites from the comparison of C2-ceramide and SH-BC-893 based on grouping described in 4.5.4 (DVD-R).

4.9 References

1. Selwan, E.M., et al., *Attacking the supply wagons to starve cancer cells to death.* FEBS Lett, 2016. **590**(7): p. 885-907.
2. Barthelemy, C., et al., *FTY720-induced endocytosis of yeast and human amino acid transporters is preceded by reduction of their inherent activity and TORC1 inhibition.* Sci Rep, 2017. **7**(1): p. 13816.
3. Guenther, G.G., et al., *Loss of TSC2 confers resistance to ceramide and nutrient deprivation.* Oncogene, 2014. **33**(14): p. 1776-87.
4. Hyde, R., et al., *Ceramide down-regulates System A amino acid transport and protein synthesis in rat skeletal muscle cells.* FASEB J, 2005. **19**(3): p. 461-3.
5. Kim, S.M., et al., *Targeting cancer metabolism by simultaneously disrupting parallel nutrient access pathways.* J Clin Invest, 2016. **126**(11): p. 4088-4102.
6. Romero Rosales, K., et al., *Sphingolipid-based drugs selectively kill cancer cells by down-regulating nutrient transporter proteins.* Biochem J, 2011. **439**(2): p. 299-311.
7. Guenther, G.G., et al., *Ceramide starves cells to death by downregulating nutrient transporter proteins.* Proc Natl Acad Sci U S A, 2008. **105**(45): p. 17402-7.
8. Morad, S.A. and M.C. Cabot, *Ceramide-orchestrated signalling in cancer cells.* Nat Rev Cancer, 2013. **13**(1): p. 51-65.
9. Chalfant, C.E., et al., *Long chain ceramides activate protein phosphatase-1 and protein phosphatase-2A. Activation is stereospecific and regulated by phosphatidic acid.* J Biol Chem, 1999. **274**(29): p. 20313-7.
10. Dobrowsky, R.T., et al., *Ceramide activates heterotrimeric protein phosphatase 2A.* J Biol Chem, 1993. **268**(21): p. 15523-30.
11. Edinger, A.L., *Controlling cell growth and survival through regulated nutrient transporter expression.* Biochem J, 2007. **406**(1): p. 1-12.
12. Habrukowich, C., et al., *Sphingosine interaction with acidic leucine-rich nuclear phosphoprotein-32A (ANP32A) regulates PP2A activity and cyclooxygenase (COX)-2 expression in human endothelial cells.* J Biol Chem, 2010. **285**(35): p. 26825-31.
13. Oaks, J. and B. Ogretmen, *Regulation of PP2A by Sphingolipid Metabolism and Signaling.* Front Oncol, 2014. **4**: p. 388.
14. Finicle, B.T., et al., *Sphingolipids inhibit endosomal recycling of nutrient transporters by inactivating ARF6.* J Cell Sci, 2018. **131**(12).
15. Kanshin, E., et al., *A cell-signaling network temporally resolves specific versus promiscuous phosphorylation.* Cell Rep, 2015. **10**(7): p. 1202-14.
16. Kanshin, E., et al., *Phosphoproteome dynamics of Saccharomyces cerevisiae under heat shock and cold stress.* Mol Syst Biol, 2015. **11**(6): p. 813.
17. Kubiniok, P., et al., *Time-resolved Phosphoproteome Analysis of Paradoxical RAF Activation Reveals Novel Targets of ERK.* Mol Cell Proteomics, 2017. **16**(4): p. 663-679.
18. Bendall, S.C., et al., *Prevention of amino acid conversion in SILAC experiments with embryonic stem cells.* Mol Cell Proteomics, 2008. **7**(9): p. 1587-97.
19. Dai, C., et al., *Targeting PP2A activates AMPK signaling to inhibit colorectal cancer cells.* Oncotarget, 2017. **8**(56): p. 95810-95823.
20. Perryman, M.S., et al., *Effects of stereochemistry, saturation, and hydrocarbon chain length on the ability of synthetic constrained azacyclic sphingolipids to trigger nutrient*

transporter down-regulation, vacuolation, and cell death. Bioorg Med Chem, 2016. **24**(18): p. 4390-7.
21. Kanshin, E., S.W. Michnick, and P. Thibault, *Displacement of N/Q-rich peptides on TiO2 beads enhances the depth and coverage of yeast phosphoproteome analyses.* J Proteome Res, 2013. **12**(6): p. 2905-13.
22. Kanshin, E., S. Michnick, and P. Thibault, *Sample preparation and analytical strategies for large-scale phosphoproteomics experiments.* Semin Cell Dev Biol, 2012. **23**(8): p. 843-53.
23. Ishihama, Y., J. Rappsilber, and M. Mann, *Modular stop and go extraction tips with stacked disks for parallel and multidimensional Peptide fractionation in proteomics.* J Proteome Res, 2006. **5**(4): p. 988-94.
24. Tyanova, S., T. Temu, and J. Cox, *The MaxQuant computational platform for mass spectrometry-based shotgun proteomics.* Nat Protoc, 2016. **11**(12): p. 2301-2319.
25. Kumar, L. and E.F. M, *Mfuzz: a software package for soft clustering of microarray data.* Bioinformation, 2007. **2**(1): p. 5-7.
26. Huang da, W., B.T. Sherman, and R.A. Lempicki, *Systematic and integrative analysis of large gene lists using DAVID bioinformatics resources.* Nat Protoc, 2009. **4**(1): p. 44-57.
27. Chou, M.F. and D. Schwartz, *Biological sequence motif discovery using motif-x.* Curr Protoc Bioinformatics, 2011. **Chapter 13**: p. Unit 13 15-24.
28. Schwartz, D. and S.P. Gygi, *An iterative statistical approach to the identification of protein phosphorylation motifs from large-scale data sets.* Nat Biotechnol, 2005. **23**(11): p. 1391-8.
29. Chen, B., et al., *Azacyclic FTY720 Analogues That Limit Nutrient Transporter Expression but Lack S1P Receptor Activity and Negative Chronotropic Effects Offer a Novel and Effective Strategy to Kill Cancer Cells in Vivo.* ACS Chem Biol, 2016. **11**(2): p. 409-14.
30. Fransson, R., et al., *Design, Synthesis, and Anti-leukemic Activity of Stereochemically Defined Constrained Analogs of FTY720 (Gilenya).* ACS Med Chem Lett, 2013. **4**(10).
31. Broer, S. and A. Broer, *Amino acid homeostasis and signalling in mammalian cells and organisms.* Biochem J, 2017. **474**(12): p. 1935-1963.
32. Cohen, P., S. Klumpp, and D.L. Schelling, *An improved procedure for identifying and quantitating protein phosphatases in mammalian tissues.* FEBS Lett, 1989. **250**(2): p. 596-600.
33. Ishihara, H., et al., *Calyculin A and okadaic acid: inhibitors of protein phosphatase activity.* Biochem Biophys Res Commun, 1989. **159**(3): p. 871-7.
34. Cox, J. and M. Mann, *MaxQuant enables high peptide identification rates, individualized p.p.b.-range mass accuracies and proteome-wide protein quantification.* Nat Biotechnol, 2008. **26**(12): p. 1367-72.
35. Cox, J., et al., *Andromeda: a peptide search engine integrated into the MaxQuant environment.* J Proteome Res, 2011. **10**(4): p. 1794-805.
36. St-Denis, N., et al., *Phenotypic and Interaction Profiling of the Human Phosphatases Identifies Diverse Mitotic Regulators.* Cell Rep, 2016. **17**(9): p. 2488-2501.
37. Wiredja, D.D., et al., *Phosphoproteomics Profiling of Nonsmall Cell Lung Cancer Cells Treated with a Novel Phosphatase Activator.* Proteomics, 2017. **17**(22).
38. Wlodarchak, N. and Y. Xing, *PP2A as a master regulator of the cell cycle.* Crit Rev Biochem Mol Biol, 2016. **51**(3): p. 162-84.

39. Ando, S., et al., *Domain- and sequence-specific phosphorylation of vimentin induces disassembly of the filament structure.* Biochemistry, 1989. **28**(7): p. 2974-9.
40. Eriksson, J.E., et al., *Specific in vivo phosphorylation sites determine the assembly dynamics of vimentin intermediate filaments.* J Cell Sci, 2004. **117**(Pt 6): p. 919-32.
41. Jiu, Y., et al., *Vimentin intermediate filaments control actin stress fiber assembly through GEF-H1 and RhoA.* J Cell Sci, 2017. **130**(5): p. 892-902.
42. Iwasaki, T., et al., *Involvement of phosphorylation of Tyr-31 and Tyr-118 of paxillin in MM1 cancer cell migration.* Int J Cancer, 2002. **97**(3): p. 330-5.
43. Chen, H.Y., et al., *Brk activates rac1 and promotes cell migration and invasion by phosphorylating paxillin.* Mol Cell Biol, 2004. **24**(24): p. 10558-72.
44. Callow, M.G., et al., *PAK4 mediates morphological changes through the regulation of GEF-H1.* J Cell Sci, 2005. **118**(Pt 9): p. 1861-72.
45. Arber, S., et al., *Regulation of actin dynamics through phosphorylation of cofilin by LIM-kinase.* Nature, 1998. **393**(6687): p. 805-9.
46. Wakatsuki, S., F. Saitoh, and T. Araki, *ZNRF1 promotes Wallerian degeneration by degrading AKT to induce GSK3B-dependent CRMP2 phosphorylation.* Nat Cell Biol, 2011. **13**(12): p. 1415-23.
47. Xue, Y., et al., *GPS 2.0, a tool to predict kinase-specific phosphorylation sites in hierarchy.* Mol Cell Proteomics, 2008. **7**(9): p. 1598-608.
48. Cross, D.A., et al., *Inhibition of glycogen synthase kinase-3 by insulin mediated by protein kinase B.* Nature, 1995. **378**(6559): p. 785-9.
49. Hill, E.V., et al., *Regulation of PIKfyve phosphorylation by insulin and osmotic stress.* Biochem Biophys Res Commun, 2010. **397**(4): p. 650-5.
50. Osinalde, N., et al., *Nuclear Phosphoproteomic Screen Uncovers ACLY as Mediator of IL-2-induced Proliferation of CD4+ T lymphocytes.* Mol Cell Proteomics, 2016. **15**(6): p. 2076-92.
51. Dickson, R.C., *Roles for sphingolipids in Saccharomyces cerevisiae.* Adv Exp Med Biol, 2010. **688**: p. 217-31.
52. Kovacina, K.S., et al., *Identification of a proline-rich Akt substrate as a 14-3-3 binding partner.* J Biol Chem, 2003. **278**(12): p. 10189-94.
53. Sarbassov, D.D., et al., *Phosphorylation and regulation of Akt/PKB by the rictor-mTOR complex.* Science, 2005. **307**(5712): p. 1098-101.
54. Kim, G.H., et al., *PIKfyve inhibition interferes with phagosome and endosome maturation in macrophages.* Traffic, 2014. **15**(10): p. 1143-63.
55. Clayton, E.L., S. Minogue, and M.G. Waugh, *Mammalian phosphatidylinositol 4-kinases as modulators of membrane trafficking and lipid signaling networks.* Prog Lipid Res, 2013. **52**(3): p. 294-304.
56. Taelman, V.F., et al., *Wnt signaling requires sequestration of glycogen synthase kinase 3 inside multivesicular endosomes.* Cell, 2010. **143**(7): p. 1136-48.
57. Sutherland, C., I.A. Leighton, and P. Cohen, *Inactivation of glycogen synthase kinase-3 beta by phosphorylation: new kinase connections in insulin and growth-factor signalling.* Biochem J, 1993. **296 (Pt 1)**: p. 15-9.
58. Chavez, J.A. and S.A. Summers, *A ceramide-centric view of insulin resistance.* Cell Metab, 2012. **15**(5): p. 585-94.
59. Manning, B.D. and A. Toker, *AKT/PKB Signaling: Navigating the Network.* Cell, 2017. **169**(3): p. 381-405.

60. Rodgers, J.T., R.O. Vogel, and P. Puigserver, *Clk2 and B56beta mediate insulin-regulated assembly of the PP2A phosphatase holoenzyme complex on Akt.* Mol Cell, 2011. **41**(4): p. 471-9.
61. Kuo, Y.C., et al., *Regulation of phosphorylation of Thr-308 of Akt, cell proliferation, and survival by the B55alpha regulatory subunit targeting of the protein phosphatase 2A holoenzyme to Akt.* J Biol Chem, 2008. **283**(4): p. 1882-92.

Chapter 5

Conclusion and Future Perspectives

5.1 Conclusion

Protein phosphorylation is one of the most prominent post-translational modification regulating the functioning of cells. Protein phosphorylation is carried from one protein to another on pre-defined routes to regulate molecular machineries. These intracellular routes, or pathways, transmit information that is crucial for the functioning of cells and, if deregulated, can have unpredictable outcomes. Understanding signaling pathways, and identifying their precise member proteins has been of major interest in cancer research in the past decades. Various techniques including mass spectrometry based phosphoproteomics and biochemical assays such as western blots have been used to generate maps of signaling cascades. Defining the boundaries of these cascades mostly relies on known phosphorylation motifs that can be used to predictively associate kinases to their substrates. Our persisting interest in phosphorylation pathways and the development of new methodologies led to the hypothesis that signaling routes could be disentangled based on kinetic profiling of the phosphoproteome. Accordingly, the aim of my thesis was to develop mass spectrometry methodologies that allow the monitoring of phosphoproteome kinetics post-stimulation, with vast phosphoproteome coverage. Monitoring phosphorylation reactions at high temporal resolution was anticipated to provide insights on intracellular signaling routes.

Within the scope of this thesis, I developed and applied methodologies allowing to profile the phosphoproteome at high temporal resolution. Phosphoproteome profiling was used to generate datasets following perturbations of yeast and mammalian cancers cells. These data proved to be of high statistical reliability and allowed the characterization of distinct signaling pathways from untargeted stimulation (such as temperature shocks) as wells as from targeted perturbations of cells with anti-oncogenic drugs.

In a first study, I combined triple SILAC labeling with previously-optimized phosphoproteomics workflows [1, 2] and followed the temperature stress response of the yeast phosphoproteome within the first thirty minutes of stimulation at a temporal resolution of three minutes [3]. To investigate the phosphoproteome with high temporal resolution, snap freezing technologies were implemented to preserve timepoints prior to mass spectrometry based proteomics analysis. Data

analysis revealed that phosphorylation was a major regulator of the temperature stress response as over 5% of the yeast phosphoproteome appeared to be dynamically regulated. Temporal profiling unraveled 15 specific kinetic trends of which many could be associated to stimulation-specific pathways. Intriguingly, time-resolved data could be used as a predictive tool to link kinase activity to their substrates. The most noteworthy observation was a rapid increase in phosphorylation on Tyr 19 of the cell cycle-regulating kinase Cdc28 following heat shock. Phosphorylation of Tyr 19 on Cdc28 has been shown to inactivate the kinase activity [4], and consistently, known substrates of Cdc28 showed a rapid decrease in phosphorylation with similar dynamic characteristics. Temporal information was then used to reveal functional association between the protein kinase A (PKA) and putative substrates. The ability to derive enzyme-substrate relationships from dynamic datasets was considered an important feature that could potentially aid to precisely define the signaling events perturbed by anti-oncogenic drugs in future studies.

Hence, the developed time resolved phosphoprotoemics techniques were applied to study the phosphoproteome response of human colon cancer cells treated with the BRAF kinase inhibitor Vemurafenib in my second publication [5]. Colon cancer cells that respond paradoxically to treatment with Vemurafenib were investigated to understand the underlying mechanisms that drive the death of these cancers. The resulting dataset enabled the generation of a precise signaling network of the BRAF-RAS-MEK-ERK cascade. Temporal information allowed the distinction between early and late signaling events linking kinase substrates to later feedback mechanisms. Only the increased depth of phosphoproteome coverage in this dataset enabled the accurate definition of the MAP kinase network, which at present, is the most comprehensive one available [6]. Novel members of the MAPK signaling network were associated to the MAP kinase ERK by using *in vitro* kinase assays. Those confirmed the predicted kinase–substrate relationships. This dataset also unveiled that the anti-oncogenic drug Vemurafenib increases phosphorylation on the transcription factors MKL1/2 in colon cancer cells harboring somatic BRAF mutations. The increased phosphorylation was shown to be blocked by the binding of globular actin to the MKL1/2 RPEL motifs. Consistently, it was recently published that MKL1/2 phosphorylation at these sites reduces their affinity for actin and has thus profound functional consequences on these transcription activators [7]. As kinetic information proved to be supportive to profile drug induced perturbations of the cellular signaling machinery, expanding

the application of temporally-resolved proteomics to study novel, anti-oncogenic compounds became obvious.

In a third study I profiled the phosphoproteome response of hematopoietic mouse cells to treatment with the anti-oncogenic sphingolipid-derived compound SH-BC-893 and its natural analogue C2-ceramide. Compound SH-BC-893 causes cell starvation through induction of nutrient transporter loss at the cell surface and vacuolation; C2-ceramide phenocopies SH-BC-893 except that it does not induce vacuolation. These phenotypes have previously been found to occur after PP2A activation with both compounds [8-10]. Interestingly, time-resolved phosphoproteomics, deployed to unravel the molecular events leading to starvation phenotypes depicted activation and deactivation of PP2A post-incubation with sphingolipids. Comparison of sphingolipid responses to those of the specific PP2A inhibitor, LB100, highlighted that sphingolipids specifically increase the affinity of PP2A to phosphogroups on GTPase- and actin-regulating proteins. The observed targeted activation of PP2A leading to de-phosphorylation of these proteins suggests that GTPases and actins are key events that mediate cell starvation. Using fluorescence microscopy we found that actin reorganization, induced through sphingolipid activity, was inhibiting the cellular nutrient import machineries. Comparison of phosphoproteomes following C2-ceramide and SH-BC-893 treatment was further used to generate maps of proteins likely causing vacuolar fusion reactions. Altogether, this dataset depicts that specific activation of PP2A with sphingolipids results in cell starvation through targeted dephosphorylation of actin regulators and GTPases.

Throughout the above summarized studies, temporal profiling of the phosphoproteome yielded a precise picture of the cellular events taking place post-stimulation. It allowed to decipher kinase substrate networks based on kinetic trends and enabled the definition of molecular machineries associated with targeted stimulation. Accordingly, this tool improved our current view on intracellular signaling cascades by taking snapshots of the phosphoproteome status at predefined time points following stimulation. The biggest asset and novelty from this approach was that up to fourteen timepoints were taken in intervals as small as 3 minutes. This appeared advantageous for the precise definition of phosphorylation kinetics, in comparison to other studies were only few timepoints were taken at large intervals. Only dynamic profiling of phosphorylation events allowed to link regulated phosphorylation sites to molecular events as those described above.

An additional characteristic that emerged from temporally resolved data is that statistics defining regulation of a phosphosite became more intuitive. While experiments based on the observation of a single timepoint use t-test based fold change cutoffs to define if a phosphorylation site is significantly changing or not, time-resolved data allowed the assessment of significance based on curve fitting of dynamic profiles. Using the datasets presented in this thesis, I generated bioinformatic workflows allowing the distinction of dynamic and static phosphorylation sites based on polynomial fitting and false discovery rates. This allowed the unbiased extraction of low and high amplitude changes while discriminating for profiles containing a large number of outliers.

In conclusion, experimental design, analytical reproducibility and bioinformatics analysis provided the means to generate the high-quality datasets enabling the unraveling of key signaling events on a systems biology level.

5.2 Perspectives

Time-resolved phosphoproteomics have been deployed to gain further insights into the dynamics of intracellular signaling pathways. It was found to be well-suited to study drug response signaling as well as overall perturbations of the cellular system. Future improvements could be made on the analytical workflow and bioinformatics analyses. Furthermore, the knowledge obtained from the datasets should be expanded by performing targeted follow up studies. All three perspectives are discussed below.

5.2.1 Simplifying the analytical workflow

SILAC has proven to be a reliable technique to quantify phosphosites with high precision. The downsides, however, are its limited multiplexing capacities as only up to three SILAC channels can be used per MS run, making the acquisition of kinetic data time consuming. In a triple SILAC experiment, each time point is one sample where a control and up to two stimulations can be compared. During MS analysis of these samples, quantification of low abundance peptides across all timepoints becomes highly unlikely, resulting in less complete kinetic information. MS run time and in between run reproducibility could be greatly improved by the use of labeling techniques with higher multiplexing capacities and would circumvent the disadvantages encountered from SILAC labeling. In the past years, several techniques that allow for accurate quantification and pooling of up to 10 stimulations have been developed. The most frequently used multiplexing strategy is tandem mass tagging (TMT). TMT allows the analysis of highly multiplexed samples by chemically labeling peptides post digestion [11, 12]. While this MS/MS based quantification strategy has been found to cause ratio suppression due to the quantification in the low mass range, novel approaches including ion mobility spectrometry or MS^3 quantification can diminish these issues, making it applicable for kinetic studies [13, 14]. The use of TMT for temporal profiling of the phosphoproteome would allow to obtain all time measurements for almost all phosphopeptides that are identified. In turn, much fewer observations where only few timepoints are measured would occur, allowing for even higher coverage of the dynamic proteome than achieved with SILAC. In addition, the MS run time would be drastically decreased, making the analysis of numerous stimulations more feasible.

While implementing a TMT workflow to follow phosphoproteome dynamics, one has to carefully consider that peptide labeling and pooling of timepoints is performed post digestion. Compared to SILAC where cells are pooled at the time each sample is collected, the later pooling and labeling of peptides with the TMT approach will induce a larger margin of error for quantification. This error would have to be assessed prior to performing any large scale experiment and sample handling would have to be iteratively improved.

5.2.2 Improving bioinformatics analysis of phosphoproteome data

Data filtering and assessment of kinetics have been optimized over the course of the three studies presented in the thesis. However, interpretation of data to extract biologically relevant information has been the most time consuming and confusing part of data analysis. The most frequently used tools were Gene Ontology enrichment [15, 16] to unravel molecular mechanisms and STRING database [17] to predict protein-protein interactions. Both tools are highly biased towards the already studied information and thus do not allow for breakthrough discoveries. Especially when novel boundaries of signaling routes are intended to be defined as anticipated from kinetic data, biased analysis is the least useful. Development of informatics tools that would find the boundaries of pathways solely based on kinetic information could be of great help. For example, recent work published from Pierre Thibault's laboratory makes use of machine learning algorithms to find phosphorylation networks in an unbiased manner from peptide sequence information [18]. Similar tools using the additional kinetic information would be of high interest to be developed for all kinds of kinetic experiments.

5.2.3 Building up on the knowledge obtained from dynamic phosphoproteome datasets

Phosphoprotoemic datasets, especially those with kinetic information, harbor a vast amount of information that is difficult to assess and to expand. In most cases, expansion of knowledge is based on the very biased selection of observations that are of particular interest to the hypothesis or the scientist themselves. Accordingly, follow up studies on findings that could be useful for the general community have to be carefully selected. Unbiased follow up experiments that would link the big picture phosphoproteomic data to biochemical mechanisms would be preferred.

From all experiments conducted in this thesis, the most unsolved question that remains is the mechanism by which anti-oncogenic sphingolipids starve cancer cells to death. Phosphorylation on molecular machineries associated with GTPase regulation and actin cytoskeleton reorganization were found to be impaired later to sphingolipid treatment. We found these processes to affect nutrient access to cancer cells later to PP2A activation. However, concrete effects of single phosphorylation sites that were observed to change in abundance following treatments remain uninvestigated. Prospective experiments should focus to characterize selected phosphorylation sites through expression of point mutants in cancer cells. Phosphorylation sites that are of high interest for further assessment include Arhgef2 Ser122 and Micall1 Ser430. As highlighted in chapter 4, Arhgef2 is a well-studied guanylyl exchange factor that drives endocytosis and actin reorganization, phenotypes that could regulate nutrient access to cancer cells [19-22]. Micall1 was further suggested to drive cytoplasmic vacuolation, a phenotype that plays a crucial role in the survival of cancer cells [23, 24]. Mutagenesis of these selected phosphorylation sites would prove the findings from the phosphoproteomics experiments and add to the knowledge about regulation of nutrient homeostasis.

Moreover, understanding the biochemical mechanism of action of sphingolipids including the cancer killing drug SH-BC-893 should become a priority of future research. SH-BC-893 bears extremely high potential to serve the treatment of a variety of cancers as it significantly impacts tumor growth [24]. Understanding the mechanism of action of these drugs would be of high impact for the scientific and medical community and aid the process to render SH-BC-893 clinically usable. While the phosphoproteomic data greatly enhanced the current understanding of PP2A activation by SH-BC-893 and C2-ceramide, not all observed alterations of the phosphoproteome appeared to depend on PP2A activation, indicating functional off-target effects. Chemical proteomics and genomics could complete the picture of SH-BC-893's mechanism of action and provide the information necessary to assess the drug's applicability to real life. Both chemo-proteomics and chemo-genomics are orthogonal techniques that assess protein binders and genetic interactors of small molecules, respectively. Together, crispr-cas9 based chemogenomics as described by Bertomeu *et al*. (2018), and affinity-based enrichment of drug binders as described by Klaeger *et al*. (2017), could link the observed phosphoprotoemics data to biochemical interactions taking place upon drug treatment [25, 26]. Aiming for a complete understanding of the mechanism of action by which SH-BC-893 starves cancer cells

should be the next step to investigate this novel therapeutic approach. Implementation of these techniques would not only be useful for the study of SH-BC-893 in particular, but the developed assays would also display a complete platform that could be used together with phosphoproteomic profiling to perform drug discovery on a larger scale.

5.3 References

1. Kanshin, E., S. Michnick, and P. Thibault, *Sample preparation and analytical strategies for large-scale phosphoproteomics experiments.* Semin Cell Dev Biol, 2012. **23**(8): p. 843-53.
2. Kanshin, E., S.W. Michnick, and P. Thibault, *Displacement of N/Q-rich peptides on TiO2 beads enhances the depth and coverage of yeast phosphoproteome analyses.* J Proteome Res, 2013. **12**(6): p. 2905-13.
3. Kanshin, E., et al., *Phosphoproteome dynamics of Saccharomyces cerevisiae under heat shock and cold stress.* Mol Syst Biol, 2015. **11**(6): p. 813.
4. Gould, K.L. and P. Nurse, *Tyrosine phosphorylation of the fission yeast cdc2+ protein kinase regulates entry into mitosis.* Nature, 1989. **342**(6245): p. 39-45.
5. Kubiniok, P., et al., *Time-resolved Phosphoproteome Analysis of Paradoxical RAF Activation Reveals Novel Targets of ERK.* Mol Cell Proteomics, 2017. **16**(4): p. 663-679.
6. Unal, E.B., F. Uhlitz, and N. Bluthgen, *A compendium of ERK targets.* FEBS Lett, 2017. **591**(17): p. 2607-2615.
7. Panayiotou, R., et al., *Phosphorylation acts positively and negatively to regulate MRTF-A subcellular localisation and activity.* eLife, 2016. **5**: p. e15460.
8. Selwan, E.M., et al., *Attacking the supply wagons to starve cancer cells to death.* FEBS Lett, 2016. **590**(7): p. 885-907.
9. Chen, B., et al., *Azacyclic FTY720 Analogues That Limit Nutrient Transporter Expression but Lack S1P Receptor Activity and Negative Chronotropic Effects Offer a Novel and Effective Strategy to Kill Cancer Cells in Vivo.* ACS Chem Biol, 2016. **11**(2): p. 409-14.
10. Guenther, G.G., et al., *Ceramide starves cells to death by downregulating nutrient transporter proteins.* Proc Natl Acad Sci U S A, 2008. **105**(45): p. 17402-7.
11. Werner, T., et al., *High-resolution enabled TMT 8-plexing.* Anal Chem, 2012. **84**(16): p. 7188-94.
12. Liu, P., et al., *Quantitative Comparisons of Large Numbers of Human Plasma Samples Using TMT10plex Labeling.* Methods Mol Biol, 2017. **1619**: p. 319-337.
13. Pfammatter, S., E. Bonneil, and P. Thibault, *Improvement of Quantitative Measurements in Multiplex Proteomics Using High-Field Asymmetric Waveform Spectrometry.* J Proteome Res, 2016. **15**(12): p. 4653-4665.
14. Ting, L., et al., *MS3 eliminates ratio distortion in isobaric multiplexed quantitative proteomics.* Nat Methods, 2011. **8**(11): p. 937-40.
15. Huang da, W., B.T. Sherman, and R.A. Lempicki, *Bioinformatics enrichment tools: paths toward the comprehensive functional analysis of large gene lists.* Nucleic Acids Res, 2009. **37**(1): p. 1-13.
16. Huang da, W., B.T. Sherman, and R.A. Lempicki, *Systematic and integrative analysis of large gene lists using DAVID bioinformatics resources.* Nat Protoc, 2009. **4**(1): p. 44-57.
17. Szklarczyk, D., et al., *The STRING database in 2017: quality-controlled protein-protein association networks, made broadly accessible.* Nucleic Acids Res, 2017. **45**(D1): p. D362-D368.
18. Kanshin, E., et al., *Machine Learning of Global Phosphoproteomic Profiles Enables Discrimination of Direct versus Indirect Kinase Substrates.* Mol Cell Proteomics, 2017. **16**(5): p. 786-798.

19. Cheng, I.K., et al., *GEF-H1 over-expression in hepatocellular carcinoma promotes cell motility via activation of RhoA signalling.* J Pathol, 2012. **228**(4): p. 575-85.
20. Chiang, H.S., et al., *GEF-H1 controls microtubule-dependent sensing of nucleic acids for antiviral host defenses.* Nat Immunol, 2014. **15**(1): p. 63-71.
21. Pathak, R. and C. Dermardirossian, *GEF-H1: orchestrating the interplay between cytoskeleton and vesicle trafficking.* Small GTPases, 2013. **4**(3): p. 174-9.
22. Callow, M.G., et al., *PAK4 mediates morphological changes through the regulation of GEF-H1.* J Cell Sci, 2005. **118**(Pt 9): p. 1861-72.
23. Shubin, A.V., et al., *Cytoplasmic vacuolization in cell death and survival.* Oncotarget, 2016. **7**(34): p. 55863-55889.
24. Kim, S.M., et al., *Targeting cancer metabolism by simultaneously disrupting parallel nutrient access pathways.* J Clin Invest, 2016. **126**(11): p. 4088-4102.
25. Klaeger, S., et al., *The target landscape of clinical kinase drugs.* Science, 2017. **358**(6367).
26. Bertomeu, T., et al., *A High-Resolution Genome-Wide CRISPR/Cas9 Viability Screen Reveals Structural Features and Contextual Diversity of the Human Cell-Essential Proteome.* Mol Cell Biol, 2018. **38**(1).

Appendix - Scientific Contributions

Publications

1. **Peter Kubiniok**, Alison McCracken, Tricia Nguyen, Lorenzo Sernissi, Stephen Hanessian, Aimee L. Edinger and Pierre Thibault, Chemoproteomics techniques to profile drug targets of synthetic and natural anti-oncogenic sphingolipids (Manuscript in preparation)

2. **Peter Kubiniok#**, Brendan Finicle#, Fanny Piffaretti , Alison McCracken, Michael Perryman, Stephen Hanessian, Aimee L. Edinger and Pierre Thibault, **(# co-first authors)**, Dynamic phosphoproteomics uncovers signalling pathways modulated by anti-oncogenic sphingolipids (Manuscript submitted to Molecular and Cellular Proteomics, August 23rd, 2018)

3. Seong M. Kim, Tricia T. Nguyen, Archna Ravi, **Peter Kubiniok**, Brendan T. Finicle, Vaishali Jayashankar, Leonel Malacrida, Jue Hou, Jane Robertson, Dong Gao, Jonathan Chernoff, Michelle A. Digman, Eric O. Potma, Bruce J. Tromberg, Pierre Thibault and Aimee L. Edinger, PTEN deficiency and AMPK activation promote nutrient scavenging and analbolism in prostate cancer cells, Cancer Discovery, Mar 23 2018

4. **Peter Kubiniok#**, Hugo Lavoie#, Therrien M and Pierre Thibault, **(# co-first authors)**, Time-resolved phosphoproteome analysis of paradoxical RAF activation reveals novel ERK downstream events , Molecular and Cellular Proteomics, Jan 2017

5. Evgeny Kanshin#, **Peter Kubiniok#**, Yogitha Thattikota, Damien D'Amours and Pierre Thibault **(# co-first authors)**, Phosphoproteome dynamics of Saccharomyces cerevisiae under heat shock and cold stress, Molecular Systems Biology, Jun 3 2015.

Conference contributions (selected highlights)

1. **Peter Kubiniok**, Alison McCracken, Brendan Finicle, Lorenzo Sernissi, Stephen Hanessian, Aimee Edinger and Pierre Thibault, Chemical proteomics unravel protein targets and binding sites of sphingolipid like small molecules with anticancer properties, at the HUPO 2018, October 1-3, 2018, Orlando, FL, USA

2. **Peter Kubiniok**, Alison McCracken, Michael Perryman, Stephen Hanessian, Aimee L. Edinger and Pierre Thibault, Chemoproteomics techniques to profile drug targets in cell lysates, at the CNPN meeting, April 18-20, 2017, Montreal, QC, Canada

3. **Peter Kubiniok**, Alison McCracken, Michael Perryman, Stephen Hanessian, Aimee Edinger and Pierre Thibault, Chemo-proteomics unravel how Sphingolipid derived small molecules alter protein phosphatase 2A activity and starve cancer from the inside and out, at the Proteomic Forum, April 2-5, 2017, Potsdam, Germany

4. Seong M. Kim*, Archna Ravi*, Tricia T. Nguyen*, **Peter Kubiniok**, Jue Hou, Brendan Finicle, Leonel Malacrida, Michelle Digman, Bruce J. Tromberg, Pierre Thibault, and Aimee L. Edinger Prostate cancer cells convert cell corpses into biomass via micropinocytosis, Post ASMS meeting Montreal, Oct. 18,2016, QC, Canada

5. **Peter Kubiniok**, Alison McCracken, Michael Perryman, Stephen Hanessian, Aimee Edinger and Pierre Thibault, Profiling changes in the phosphoproteome of hematopoietic cells in response to a novel class of anti-oncogenic sphingolipid derived small molecules at HUPO, September 18-22, 2016, Taipei, Taiwan

6. **Peter Kubiniok**, Alison McCracken, Michael Perryman, Stephen Hanessian, Aimee Edinger and Pierre Thibault, Profiling changes in the phosphoproteome of hematopoietic cells in response to a novel class of anti-oncogenic sphingolipid derived small molecules at ASMS (American Society for Mass Spectrometry) conference, June 5-9 2016, San Antonio, TX, USA

7. **Peter Kubiniok**, Alison McCracken, Michael Perryman, Stephen Hanessian, Aimee Edinger and Pierre Thibault, Profiling changes in the phosphoproteome of hematopoietic cells in response to a novel class of anti-oncogenic sphingolipid derived small molecules at CNPN, April 12-13, 2016, Toronto, ON, Canada

8. **Peter Kubiniok**, Hugo Lavoie, Therrien M and Pierre Thibault, Time-resolved phosphoproteome analysis of paradoxical RAF activation, at ASMS (American Society for Mass Spectrometry) conference, May 31-June 4, 2015, St. Louis MO, USA

9. **Peter Kubiniok**, Evgeny Kanshin and Pierre Thibault, Phosphoproteome dynamics using quantitavie mass spectrometry methodologies, at the CNPN (Canadian National Proteomics Network) conference, April 14-16 2015, Montreal, QC, Canada